

Design and Development of Imaging Platforms for Phenotypic Characterization of Early Zebrafish

Zur Erlangung des akademischen Grades eines
DOKTORS DER INGENIEURWISSENSCHAFTEN (Dr.-Ing.)

bei der Fakultät für Maschinenbau des
Karlsruher Instituts für Technologie (KIT)

angenommene

DISSERTATION

von

Dipl.-Ing. Daniel Marcato

Tag der mündlichen Prüfung: 05.02.2018

Hauptreferentin: Prof. Dr. Dr.-Ing. Dr. h. c. Jivka Ovtcharova IMI

Korreferenten: Prof. Dr. Uwe Strähle ITG

apl. Prof. Dr. Christian Pylatiuk IAI

Selbstständigkeitserklärung

Hiermit erkläre ich, dass ich die vorliegende Arbeit selbständig angefertigt und keine anderen als die angegebenen Quellen und Hilfsmittel benutzt habe. Die wörtlich und inhaltlich übernommenen Stellen wurden als solche kenntlich gemacht und die Satzung des Karlsruher Instituts für Technologie (KIT) zur Sicherung guter wissenschaftlicher Praxis in der aktuell gültigen Fassung vom 27. November 2014 wurde beachtet.

Weder diese noch andere Arbeiten wurden ganz oder in Teilen außerhalb der Fakultät in noch anhängigen oder erfolglos beendeten Promotionsverfahren von mir verwendet.

Karlsruhe, 02. Juli 2018

Daniel Marcato

Zusammenfassung

Der Zebraäbrbling hat sich in den letzten Jahrzehnten als ein beliebter und vielversprechender Modellorganismus herausgestellt. Mit seiner Hilfe werden zunehmend die grundlegenden biologischen Funktionsweisen von Wirbeltieren untersucht und anhand der Erkenntnisse neue Therapien und Medikamente für Krankheiten entwickelt. Zusätzlich hat sich die Verhaltensforschung als Gebiet mit hohem Potential für neue Entdeckungen entpuppt, da es hier möglich ist, deutlich feinere Unterscheidungen und Effekte nachzuvollziehen als es bei stark abgegrenzten Endpunkten wie Verformungen oder Toxizität der Fall ist.

Im frühen Stadium bis fünf Tage nach Befruchtung zeigen die Embryonen und Larven des Zebraäbrblings einige charakteristische Verhaltensweisen, die durch künstliche Stimulation hervorgerufen werden können. Noch in der Eischale bei einem Alter von nur 30 bis 42 Stunden nach der Befruchtung reagieren die Embryonen auf einen Lichtblitz mit erhöhter Bewegung, der sogenannten Photomotor Response. Bei wiederholtem Belichten bleibt diese Reaktion aus, was als ein typisches Verhaltensmuster interpretiert werden kann. Werden die Embryonen jedoch Chemikalien oder Mutationen ausgesetzt, kann sich dieses Muster verändern und es können Rückschlüsse über die Funktionsweise der verursachenden Methoden gewonnen werden. Als zusätzliche Verhaltensweisen lassen sich die beiden Schreckreaktionen auf Vibration und Berührung nutzen. Bereits in der Eischale lassen sich die Embryonen durch Berührung zum Bewegen bringen. Sobald sie in einem Alter von ca. drei Tagen nach Befruchtung geschlüpft sind, wird die Reaktion als C-Krümmung bezeichnet, da die Larve eine charakteristische Biegung entlang ihrer Körperachse einnimmt bevor sie davonschwimmt. Dasselbe gilt für die Vibrationsreaktion ab einem Alter von ca. fünf Tagen nach Befruchtung.

Um diese Verhalten sinnvoll nutzen zu können sind automatisierte Lösungen notwendig, die die Vorbereitung, die Abläufe und die Analyse soweit vereinfachen, dass kaum noch menschliches Eingreifen notwendig ist. Nur so kann der notwendige Durchsatz und die Reproduzierbarkeit gewährleistet werden um statistisch aussagekräftige Effekte nachzuweisen. Aus diesem Grund wurden drei unabhängige mechatronische Systeme entwickelt, die je eines der drei genannten Verhaltensmuster automatisiert auslösen, aufzeichnen und

analysieren können. Dazu waren neben der Hard- und Softwareentwicklung auch biologische Vorgehensweisen notwendig um die Systeme zu validieren und sie bereits in ersten biologischen Untersuchungen einzusetzen.

Für das PMR System wurde ein hochautomatisierter Versuchsablauf entwickelt, der anhand eines Roboters die Embryonen zur Vorbereitung sortiert und anschließend in einem automatisierten Mikroskop mit vollständig eigenentwickelter Steuerungssoftware die Aufzeichnung der Reaktion gewährleistet. Anschließend können die Rohdaten in Form von Videos automatisiert analysiert werden um numerische Daten aus den Bildreihen zu extrahieren.

Das Vibrationssystem umfasst einen neuentwickelten Vibrationserreger in Form eines modifizierten Lautsprechers, der es erlaubt, mehrere Proben parallel zu untersuchen. Dazu wurde der Erreger ausgiebig charakterisiert um zu gewährleisten, dass die erzielten Beschleunigungswerte sowie die Impulsdauer und Frequenz den angestrebten Werten von 14 g, 1 ms und 500 Hz entsprechen. Durch den Einsatz von Beschleunigungssensoren wurden die Erreger kalibriert und die Steuerungssoftware an die Ergebnisse so angepasst, dass ein einheitlicher Effekt zwischen den Erregern gewährleistet ist. Die Implementierung einer Hochgeschwindigkeitskamera erlaubt die Aufzeichnung der Reaktion bei bis zu 1000 Bildern pro Sekunde, was aufgrund der äußerst schnellen Reaktionszeit der Larven im Millisekundenbereich notwendig ist um den vollen Umfang der Reaktion abzubilden.

Um Hochdurchsatzversuche zur Berührung der Larven zu ermöglichen, wurde das erste automatisierte System entwickelt, welches durch den Einsatz einer motorisiert positionierbaren Nadel einen computergesteuerten Berührungsvorgang ermöglicht. Ein berührungsempfindliches Mehrachsensystem wurde so konstruiert, dass der Nutzer über eine grafische Oberfläche das System fernsteuern kann und so die subjektiven und unnötig langwierigen Aspekte von manuellen Versuchsaufbauten umgangen werden können. Das System wurde mit einer digitalen Objekterkennung so erweitert, dass auch autonome Versuche möglich wurden.

Die Systeme wurden im Rahmen von mehreren biologischen Untersuchungen am ITG ausgiebig getestet. Mit Hilfe des PMR Systems wurde eine mehrere hundert Proben umfassende Sammlung von Cannabinoid-ähnlichen Substanzen auf ihre neuroaktive Wirkung untersucht. So konnten charakteristische Reaktionsmuster identifiziert werden, die nun dabei helfen können, das Verständnis über die Struktur- und Wirkungszusammenhänge zu erhöhen. An den beiden Schreckreaktionen konnte die unterschiedliche Wirkung von Anästhetika auf Phänokopien von genetisch veränderten Zebrabärblingen nachgewiesen werden, was die Einsatzfähigkeit für chemische sowie genetische Versuche substantiiert.

Acknowledgements

The following dissertation is the product of work carried out at the Institute for Applied Computer Science as well as the Institute of Toxicology and Genetics at the KIT from March 2014 to August 2017. Combining computer science with a direct biological application resulted in a highly interdisciplinary project that would not have been possible without a number of people involved.

First of all I want to thank Prof. Dr. Uwe Strähle for giving me the opportunity to focus on the technological side of zebrafish research at the ITG and Prof. Dr. Georg Bretthauer for accepting and supporting me as a PhD student at the IAI. Many thanks to Prof. Dr. Dr.-Ing. Dr. h. c. Jivka Ovtcharova at the IMI for taking over the role as primary reviewer and evaluating the technology driven focus of this work.

Due to the special arrangement with me being part of both the IAI and ITG I call myself lucky to have had not just one but two direct supervisors that always found the time to listen when I needed to talk. I am incredibly grateful for Prof. Dr. Christian Pylatiuk and Ravindra Peravali being the phenomenal mentors they are. Their never-ending support, guidance, constructive feedback and motivation in situations when I doubted my abilities are the reason why I was able to always find a solution to whatever problem I had. Furthermore I want to thank the other members of my thesis advisory committee, with Dr. Robert Geisler, Dr. Thomas Dickmeis and especially Prof. Dr. Ralf Mikut giving me invaluable input during my time at KIT.

I also want to thank all colleagues, students and trainees who I had the pleasure to meet and work with at the BIF-IGS, IAI, ITG and KIT in general. Especially Anjana Hariharan, Dr. Johannes Stegmaier, Helmut Breitwieser, Dr. Rüdiger Alshut, Paul Scheickl, Jonas Mertens, Eduard Gursky, Sara Nasrat, Mark Schutera, Marcel Vogt, Dr. Markus Reischl, Dr. Maryam Shahid, Nadine Borel, Dr. Sandra Schneider, Richard Fodor and Stefan Vollmanshauser had huge impact on my work not only from a professional perspective but a personal one as well. Luckily Dr. Martin Koos is really good at imagining moving needles and Dr. Silla Hansen knows me so well that I was able to start the PhD in the first place.

Last but not least I want to thank all of the personal friends that I made along the way and my family for supporting me no matter what I do and always lifting my spirits. Freundemensa will be deeply missed - especially Fridays. Thanks to my parents and sister for caring so much about me - I hope I could make you proud.

Lena, thank you for your love, trust, support and encouragement no matter where we have been in this world. I am looking forward to discovering even more with you.

Contents

List of Figures	I
List of Tables	IV
List of Abbreviations	V
1 Introduction	1
1.1 The Need for Model Organisms	1
1.2 Zebrafish in Science	2
1.2.1 Development and Morphology	4
1.2.2 Early Behaviors	6
1.3 Screening Approaches	8
1.3.1 Existing Solutions for Zebrafish Analysis	9
1.4 Aim of Thesis	14
2 Materials and Methods	19
2.1 Lab Procedures	19
2.1.1 Zebrafish Housing and Husbandry	19
2.1.2 Equipment and Chemicals	21
2.1.3 Sample Preparation	23
2.2 Digital Technologies	27
2.2.1 C# and the .NET Framework	28
2.2.2 Matlab	31
2.2.3 Arduino	33
2.2.4 Computer-aided Design and 3D Printing	36
2.2.5 Data Compression	37
2.2.6 Computer Hardware Setup	39
3 Photomotor Response	41
3.1 Sample Handling	42

3.2	Data Acquisition	44
3.3	Data Analysis	52
3.4	Validation Screens	62
3.4.1	Initial Validation Screen	62
3.4.2	Cannabinoid Library Screen	63
3.5	Conclusions	65
4	Vibrational Startle Response	75
4.1	State of the Art	76
4.2	System Requirements	77
4.3	Setup	79
4.3.1	Accelerometer	79
4.3.2	Vibrational Exciter	83
4.3.3	Exciter Calibration	92
4.4	Software	96
4.4.1	Vibration Analysis Tool	102
4.5	Assays and Results	104
4.6	Conclusions	109
5	Touch Response	111
5.1	State of the Art	111
5.2	System Requirements	112
5.3	Mechanical Setup	113
5.4	Software	120
5.5	Assays and Results	131
5.6	Conclusions	134
6	Summary and Outlook	135
	Bibliography	141
	Appendix	155
A	Arduino DUE Benchmark Code	155
B	Arduino Nano LED Signalling Code	156
C	Camera Recording Loop Code	156

List of Figures

Figure 1.1	Homology of various model organisms	2
Figure 1.2	Number of publications per year for search term “zebrafish”	3
Figure 1.3	Male and Female zebrafish	5
Figure 1.4	Embryonic Zebrafish Development	6
Figure 1.5	Popular well plate formats	9
Figure 1.6	Overview over Noldus’ DanioVision observation chamber	11
Figure 1.7	ViewPoint ZebraBox system	13
Figure 1.8	Occurrences of behaviors on timeaxis after fertilization	15
Figure 2.1	EZRC tanks	20
Figure 2.2	Effect of fill level in PMR well	24
Figure 2.3	Effect of agarose in 60 mm dish	25
Figure 2.4	Agarose cutter tool for 60 mm dish	26
Figure 2.5	Cutter tool for 12-well plates	27
Figure 2.6	CLR diagram	28
Figure 2.7	Arduino Sketch Flowchart	34
Figure 2.8	I ² C bus representation	35
Figure 2.9	SPI bus representation	36
Figure 3.1	PMR control behavior	42
Figure 3.2	IR egg sorter	43
Figure 3.3	PMR IR LED ring	45
Figure 3.4	Resolution comparison of chorions between different optical setups	45
Figure 3.5	PMR Microscope setup	46
Figure 3.6	PMR control software flowchart	47
Figure 3.7	PMR application GUI	49
Figure 3.8	PMR config file	50
Figure 3.9	PMR settings GUI	51
Figure 3.10	Data analysis GUI	52

Figure 3.11	Circular Hough transformation accumulation matrix	53
Figure 3.12	Schematic of Circular Hough transformations	54
Figure 3.13	Weighted Circular Hough transformation accumulation matrix	55
Figure 3.14	Comparison of detection results for the egg detection algorithms	56
Figure 3.15	Masking square ROIs for circular objects	57
Figure 3.16	Illustration of frame differencing	58
Figure 3.17	Comparison of normalization algorithms	58
Figure 3.18	Final PMR control software flowchart	60
Figure 3.19	PMR score analysis tool	61
Figure 3.20	PMR validation screen results for WT	67
Figure 3.21	PMR validation screen results for Isoproterenol	68
Figure 3.22	PMR validation screen results for Apomorphine	69
Figure 3.23	PMR validation screen results for Diazepam	70
Figure 3.24	Two general cannabinoid compound classes	71
Figure 3.25	PMR results for selected cannabinoid compounds	72
Figure 3.26	Cannabinoid dose response results	73
Figure 4.1	C-bend in zebrafish	76
Figure 4.2	Overview of the mini shaker by Brüel & Kjær	77
Figure 4.3	Signal pulse	79
Figure 4.4	ADXL345 on a breakout board	81
Figure 4.5	Arduino DUE Serial Ports	81
Figure 4.6	C code for direct pin manipulation	83
Figure 4.7	Acoustic speaker	84
Figure 4.8	Speaker frequency analysis	85
Figure 4.9	Volume dependent accelerometer data	86
Figure 4.10	Petri dish holder design	86
Figure 4.11	Bolt holder design for improved alignment	87
Figure 4.12	Backlight illumination sheet	88
Figure 4.13	Final speaker assembly	89
Figure 4.14	Overview of the final system assembly	90
Figure 4.15	Wiring diagram for relays and signal LEDs	92
Figure 4.16	Voltage levels at various output volumes	93
Figure 4.17	Speaker calibration results	95
Figure 4.18	Vibration control software flowchart	96

Figure 4.19	Vibration system GUI	97
Figure 4.20	Vibration experiment configuration file	98
Figure 4.21	Flowchart of the vibration experiment process	99
Figure 4.22	Pseudo code for audio signal generation	100
Figure 4.23	Camera frame rate analysis	101
Figure 4.24	Camera recording algorithm flowchart	102
Figure 4.25	Vibration analysis tool performance analysis	103
Figure 4.26	Development of the vibrational startle response	104
Figure 4.27	Sensitivity of the larvae to vibrational stimuli	106
Figure 4.28	Waking behavior analysis via vibration response	107
Figure 4.29	Cannabinoids on vibration response	108
Figure 5.1	End switch holder for linear actuator	114
Figure 5.2	Spring loaded needle to sense the well bottom	115
Figure 5.3	Needle holder for touch experiments	116
Figure 5.4	Magnetic connector for safety purposes	117
Figure 5.5	Camera holder for touch experiments	118
Figure 5.6	Touch system overview	119
Figure 5.7	Touch system control application flowchart	121
Figure 5.8	Touch system application GUI	121
Figure 5.9	Diagonal movement schematic	123
Figure 5.10	Touch system 2D movement algorithm flowchart	125
Figure 5.11	Touch system object detection algorithm flowchart	125
Figure 5.12	Two binarization thresholds for object detection	126
Figure 5.13	Touch system object detection pipeline	127
Figure 5.14	Needle pathfinding	128
Figure 5.15	Effect of needle speed on the touch responsiveness	132
Figure 5.16	Waking behavior analysis via touch response	133

List of Tables

Table 1.1	Selection of behavioral endpoints in zebrafish	7
Table 1.2	Companies offering solutions for zebrafish research	10
Table 2.1	Devices and equipment used for sample preparation	22
Table 2.2	Commercial compounds used for screenings	22
Table 2.3	External C# libraries and frameworks	31
Table 2.4	External Matlab solutions and tools	32
Table 2.5	Equipment used to build PCs	39
Table 3.1	Equipment used for PMR acquisition	47
Table 3.2	Overview of features between PMR systems	66
Table 4.1	Selection of accelerometers	80
Table 4.2	Weight of parts for vibrational setup	89
Table 4.3	Overview of features between vibration systems	110
Table 5.1	Overview of typical industrial robot configurations	113

List of Abbreviations

ABS	Acrylonitrile Butadiene Styrene
API	Application Programming Interface
ASCII	American Standard Code for Information Interchange
CAD	Computer-aided Design
DMSO	Dimethyl Sulfoxide
dpf	Days Post Fertilization
EEPROM	Electrically Erasable Programmable Read-only Memory
EMS	Ethylmethanesulfonate
ENU	N-Ethyl-N-Nitrosourea
EZRC	European Zebrafish Resource Center
GABAA	γ -aminobutyric acid type A
GlyT1	Glycine Transporter 1
GPIO	General Purpose Input/Output
GUI	Graphical User Interface
hpf	Hours Post Fertilization
IC	Integrated Circuit
IDE	Integrated Development Environment
KIT	Karlsruhe Institute of Technology
LED	Light Emitting Diode
LSB	Least Significant Bit
MCU	Microcontroller Unit
MVVM	Model-View-ViewModel
NFPS	N[3-(4'-fluorophenyl)-3-(4'-phenylphenoxy)propyl]sarcosine
PCB	Printed Circuit Board
Propofol	2,6-Diisopropylphenol

PSU	Power Supply Unit
PTU	1-Phenyl-2-Thiourea
ROI	Region of Interest
SDK	Software Development Kit
SMD	Surface-mounted Device
TTL	Transistor-Transistor Logic
UART	Universal Asynchronous Receiver Transmitter
USB	Universal Serial Bus
WPF	Windows Presentation Foundation
WT	Wildtype
XAML	Extensible Application Markup Language
XML	Extensible Markup Language

1. Introduction

Modern biology strives to improve the understanding of how living systems (and especially the human body) work, how diseases harm us and which mechanisms can be utilized to make humans live longer and healthier. To do this, however, increasingly difficult and detailed questions have to be answered and new methods need to be established that can help doing this. The solutions are oftentimes highly interdisciplinary with the border between biology, chemistry, mechanical engineering and computer science being quite blurry. This is why this project is combining ideas and procedures from all of these fields in an effort to provide novel insights into the biology of zebrafish (*Danio rerio*) by introducing new technological solutions for automated behavioral analysis of their early developmental stages up to 5 days post fertilization (dpf). The motivation in using zebrafish is that they offer the opportunity to be used as a model organism for humans. The following sections explain why this is an important advancement in biology and how zebrafish can be used in order to gain a better understanding of fundamental processes in vertebrates.

1.1. The Need for Model Organisms

With a growing understanding of the complexity of the biology of living systems, scientists have to find ways to experiment on not just *in-vitro* systems like cells in a petri dish but have to take the symbiosis of all the metabolic pathways that happen in an *in-vivo* system into account. Direct experiments on humans, however, are ethically challenging, difficult to monitor and very expensive. This makes them economically unfeasible, which means that alternative organisms have to be used that represent the targeted organism as closely as possible while having the advantages of being easier to handle and to examine. The obvious choice when targeting humans are other mammalian models like mice, rats or apes because they are bound to be highly similar to us. This close relationship is confirmed in figure 1.1. Their large homology to the human genome (>80% of genes in these organisms have an orthologue in humans [1]) results in strikingly similar organ development, metabolism and brain functionality with the early developmental stages closely resembling the ones seen in human embryos.

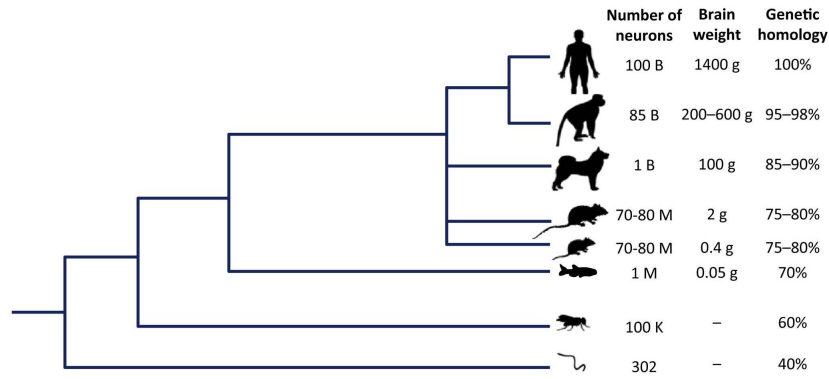


Figure 1.1: Graph showing a phylogenetic tree indicating the homology of various model organisms compared to humans [2]. The model organisms represent apes, dogs, rats, mice, zebrafish, fruit flies and nematodes. Image reproduced with permission from Elsevier.

Such a large analogy, however, might not always be necessary. In the past, even invertebrates like fruit flies (*Drosophila melanogaster*) and nematodes (*Caenorhabditis elegans*) with much lower homology have been successfully used to gain significant insight into the working principles of gene functions and disease pathways [3]. The advantages of studies on invertebrates like these are the reduced cost for maintenance and handling as well as their rapid reproduction cycle. However, there are obvious drawbacks like the clearly different anatomy or the lack of an adaptive immune system, which make them far from ideal model-organisms for humans.

1.2. Zebrafish in Science

The tropical freshwater fish *Danio rerio* or “zebrafish” is widely regarded as one of the most promising model organisms [4] for humans. They are mainly used to study vertebrate development [5], their nervous system as well as individual gene functions [6]. Its rising popularity in the scientific community [2] is based on several advantages compared to the traditional mammalian models. These include an already fully sequenced genome, highly fecund fish (a single female can lay up to 200 – 300 eggs per week), rapid embryonic development (with larvae hatching after just two days) and their small transparent eggs (their diameter ranges from approximately 0.7 mm [7] right after fertilization to around 1 mm at 24 hpf [8]) that are fertilized outside of the mother’s body.

Zebrafish have become increasingly popular since the mid of the 20th century, with the number of publications on zebrafish research growing steadily. As evident in figure 1.2, the growth accelerated in the 1980s when new technologies for genetic manipulation like

cloning [9], mutagenesis [10] or transgenesis [11] emerged and could be applied successfully to zebrafish. With this, zebrafish offer the unique advantage of combining favorable traits of the invertebrate model-organism species with the ones of vertebrates.

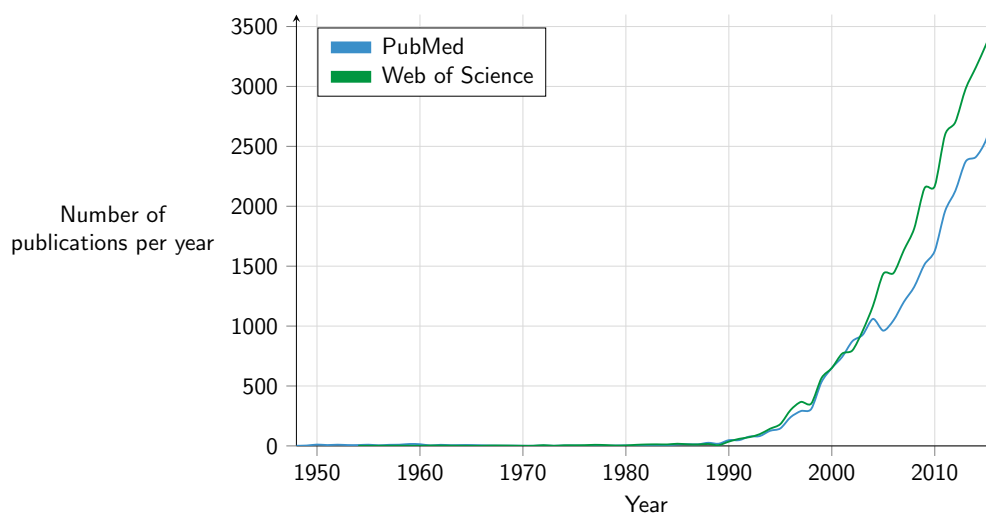


Figure 1.2: Number of publications per year from 1950 to 2016 for search term “zebrafish” in the databases of PubMed and Web of Science. A large increase since the 1990s shows the increasing popularity of zebrafish as a model organism.

Zebrafish are mainly used in either toxicological, genetic or pharmaceutical research. While toxicological and pharmaceutical screens aim at characterizing known or unknown compounds and the effects they have on a living organism, genetic studies are typically more specific and aim at gaining new insights into the functionality of individual genes or signaling pathways. A common method in the field of toxicology is the LC50 (Lethal Concentration 50%) assay in which compounds such as nanoparticles are tested for their dose dependent toxicity. Groups of specimens are exposed to various concentration levels and their survival rate is measured. With this, the LC50 can be calculated as the theoretical concentration at which 50% of the individuals in an examined group would die. The LC50 is then used as an indication marker of the toxicity of a compound and aids in assessing safe levels for water pollution or consumer products. Pharmaceutical studies on the other hand are closely related to toxicological ones in terms of being aimed at finding out more about the effects compounds can have, but are ultimately supposed to help finding bioactive molecules that can be utilized as therapeutic drugs to fight or prevent diseases. They report first indications for potential candidates that can then be evaluated further and also provide information on what the range for an effective dose might be. In genetics the interest is not solely targeted on identifying individual candidates out of a pool of compounds, but rather

in understanding how biological systems are built and function. In order to do this the genome can for example be randomly modified via mutagens like radiation or chemicals like Ethylmethanesulfonate (EMS) or N-Ethyl-N-Nitrosourea (ENU). The organism is then raised and the phenotype examined for changes to the control specimen. This method is called a forward genetic screen. It is based on a top-down approach in which researchers learn about the origin of a certain phenotype by introducing mutations all over the genome and then looking for changes in the resulting phenotype. Because the exact mutation is unknown in this approach, all that is known in the end is the resulting phenotype while the genes responsible for it can then be identified once an interesting mutation is found. The complementary strategy in which the gene is known but the phenotype not is called a reverse genetic screen. Here, an uncharacterized but known sequence of interest is modified to find out its role on the development of a phenotype. The targeted deactivation of a gene that results in the loss of its protein expression capabilities is called a “knockout”. Gene deactivation can be induced by for example a deletion of the sequence or the insertion of additional DNA fragments that render the sequence inactive. Such knockouts are currently used in for instance the Zebrafish Mutation Project undertaken by the Sanger Institute in England, which aims at creating knockouts for every protein-coding gene in the zebrafish genome and annotating their functionality [12].

But zebrafish cannot only be used to study compounds or individual gene functionality. They can also help to understand more fundamental mechanisms in vertebrates. Next to breakthroughs in the understanding of signaling pathways [13, 14] there have also been fascinating discoveries regarding the zebrafish’s ability to regenerate tissue. When a zebrafish heart is cut for example, the fish is able to repair the wound and regrow the missing tissues [15]. Even a damaged spinal cord does not mean that the fish has to stay paralyzed as opposed to humans. The damage can be repaired by secreting special growth factors that lead to a regeneration of the damaged neurons [16].

1.2.1. Development and Morphology

In their adult form zebrafish can grow to be approximately 40 mm long when held in captivity [17] and have a lifespan of around 42 months. For research purposes, however, they are often disposed of early after around 24 months when their reproductivity decreases significantly. The typical wildtype (WT) fish show five dark stripes of pigmentation along their main body axis from head to tail, hence the name. However, various subspecies and mutants can have completely different pigmentation patterns [18] or even none at all [19].

Adult female and male fish can usually be distinguished from each other by their size, shape and color. While male fish have a more slender shape, the females are typically larger in size and have a rounded, whitish belly in which they carry the unfertilized eggs. In figure 1.3 it is clearly visible how male fish can also have slight golden or yellow hues on their ventral side.



Figure 1.3: Male (top) and female (bottom) zebrafish [20] showing obvious differences in their coloration and overall shape. Image courtesy of Dr. Sarah Zala (Vetmeduni Vienna).

Females lay their eggs outside of their bodies where they are then fertilized by the male sperm. Once the fertilization occurred, the embryonic development undergoes very analogous steps to what is observable in human embryos, but the timeframe is much shorter. Starting in a single cell stage they reach gastrulation after approximately 5.25 hpf [7] and hatch after just 48 hpf from their protective shell called the chorion as outlined in figure 1.4. For optimal and consistent growth conditions the water temperature has to be maintained at 28.5 °C [21]. During their early developmental stages the embryos stay almost completely transparent. Even though the early pigmentation in typical wildtype strains starts shortly after 24 hpf, it can be suppressed by adding 1-phenyl-2-thiourea (PTU) at a standard concentration of 200 μ M [22] to the fishwater. This allows for imaging in standard light microscopes and enables researchers to make detailed observations on the developing organism from the outside without the need for harming either the mother or the embryo itself.

When the larvae hatch, however, they will not be nurtured by their parents and are not yet fully developed. They are only able to feed by themselves without relying on nutrients from the yolk at a time point after 5 dpf at which they are also actively and freely swimming. Freshly hatched they remain mostly dormant and lie inactively on the bottom of their container. Only after inflating their swim bladder with air from the surface [23] can they keep their neutral buoyancy and are able to maintain their vertical position in the water.

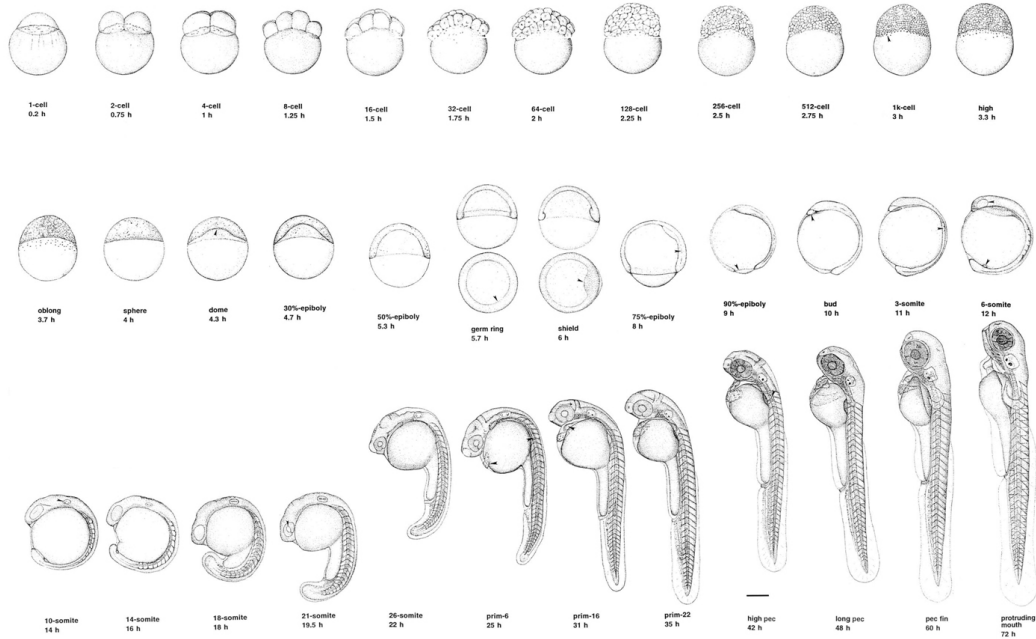


Figure 1.4: Schematics of the developmental stages of a typical zebrafish embryo after fertilization [7]. The chorion that surrounds the embryo until they hatch after ≈ 48 hpf is omitted. Image courtesy of John Wiley & Sons, Inc.

Zebrafish possess all of the known classes of senses like taste, touch, smell, balance, vision and hearing [24]. The lateral line for example is a mechanosensory system on the surface of the fish's skin that responds to water displacements and vibrations. It is comprised of several receptors called neuromasts and starts developing after 18 hpf when a first neurogenic placode can be observed on the head side of the fish [25]. The visual system seems to be very similar to that of other vertebrates [26] and responds to light intensity changes as early as 68 hpf [27]. It will reach adult like performance at just 4 dpf [24].

When assessing the developmental stages there are several established endpoints to choose from [28]. They range from general viability (or coagulation) and growth (body length) to the morphology of brain, jaw, heart, fins, somites or of the tail to the overall body shape (curvature) and cardiovascular function. Even characteristic behaviors like locomotion and touch are commonly used.

1.2.2. Early Behaviors

Zebrafish share not just large parts of their morphology with humans, but also brain functionality and neuroanatomy [29]. This makes them highly interesting for various kinds of neuroscience research, like gaining a better understanding of neurological disorders such as Alzheimer's, dementia or depression and finding therapeutic drugs via pharmacological

approaches. Since fish are quite small and easily obtainable in their early stages, performing screens is typically favored to be performed as early as possible. Most of the time this translates to a timeframe up to 5 dpf as this complies with the European Directive 2010/63/EU on the protection of animals used for scientific purposes [30, 31]. During their early developmental stages, the fish already show numerous behavioral features that are listed in table 1.1 that offer the potential to be utilized for neurophenotyping.

Table 1.1: Selection of behavioral endpoints in early zebrafish. [29]

Name	Description
Mauthner Reflex	Mauthner cells mediated startle response
Coiling	Embryonic body contraction inside the chorion
Photomotor response (PMR)	Embryonic reaction to a sudden light flash [32]
Rest behavior	Sleep related floating in water
Rheotaxis	The fish will try to swim against an applied current mimicking an upstream swim
Fleeing	Flight behavior towards other fish or stimuli
Thigmotaxis	Tendency to stay at the edge of the enclosure
Prey capture	Involves identification of prey and capture
Phototaxis	Light seeking for larval fish; light avoidance in adult fish
UV avoidance	Also see Phototaxis

These can be used as endpoints for various experiments in order to examine the physiological as well as neurological development or the effects chemical compounds have on a developing vertebrate. The major advantage that behavioral screens possess is the fact that they allow for identification of much more subtle effects than traditional morphological endpoints can offer. Instead of only looking into the toxicity of a compound by checking for coagulation for example, behavior makes it possible to look into much smaller concentrations and see if an effect can be observed much earlier. All this can be done without actually having to kill animals and potentially even being able to rescue and reuse them for additional follow-up experiments. In theory, a single embryo could even be followed through a pipeline of multiple behavioral assays in order to form a comprehensive phenotypical characterization. Out of the available catalogue of potential behaviors, the nonvisual [33] photomotor response and the Mauthner cell mediated startle responses seem especially interesting as they represent involuntary reactions of the fish to a precisely defined stimulus. While most

other behaviors tend to require long data acquisition times before any meaningful deductions can be made, the startle responses are rather quick and can be evoked deliberately and repeatably by applying artificial stimuli.

1.3. Screening Approaches

As already discussed in section 1.2.1 there are several endpoints available for use in chemical screens such as coagulation or bodily deformations. A widespread application for this is the so-called fish embryo test (FET) that was established by the OECD in their guidelines for the testing of chemicals [34]. In this, the developing embryos are exposed to various chemical compounds over a time span of 96 h in order to mimic hazards like industrial wastewater and assess the environmental risks associated with it. The embryos are screened every 24 h for coagulation, lack of somite formation, lack of detachment of the tail bud from the yolk sac and lack of heartbeat [35]. The heart is of special interest to researchers due to its potential to be used to study not just developmental mechanisms [36] but also use features like heartbeat for drug discovery [37] as well. Instead of solely relying on the heart rate as an indicator though, modern systems [38] allow for more detailed analysis by for example measuring the fractional shortening in order to find circulation defects that could be caused by either mutation, developmental irregularities or chemical compounds.

Performing chemical screens like the FET with a large number of compounds, however, can obviously become a very tedious task or even impossible to complete with just manual observations. To solve this issue, high-throughput screening solutions are supposed to increase the number of samples that can be analyzed to a level humans cannot reach. Increasing throughput has always been of interest for researchers and was initially obtained by decreasing sample size. This also leads to minimization of compound usage and a speed up of preparation steps. In order to streamline the required lab procedures, new equipment has been established in the course of the 20th century like the popular 96-well microtiterplate format and its descendants that are shown in figure 1.5. The most recent evolution was the introduction of 384-well microtiterplates that can hold even more samples while maintaining the same physical dimensions of the plate.

However, in most modern pharmaceutical companies and even research institutions the quota for samples that are supposed to be analyzed is approaching several hundreds if not thousands of samples per day [40]. The numbers obviously depend on the sort of analysis that is supposed to be carried out, with whole organism based screens consisting of fewer samples than single cell screens, simply because they are still more elaborate to set up and

prepare. With an increasing number of compounds to test, automated high-throughput solutions are evidently becoming increasingly important and actually crucial in order to cope with demand. Methods dealing with large numbers of zebrafish have been previously reported by e.g. Peravali et al. [41] and Spomer et al. [42] that show just how well the zebrafish is suited for approaches like this.

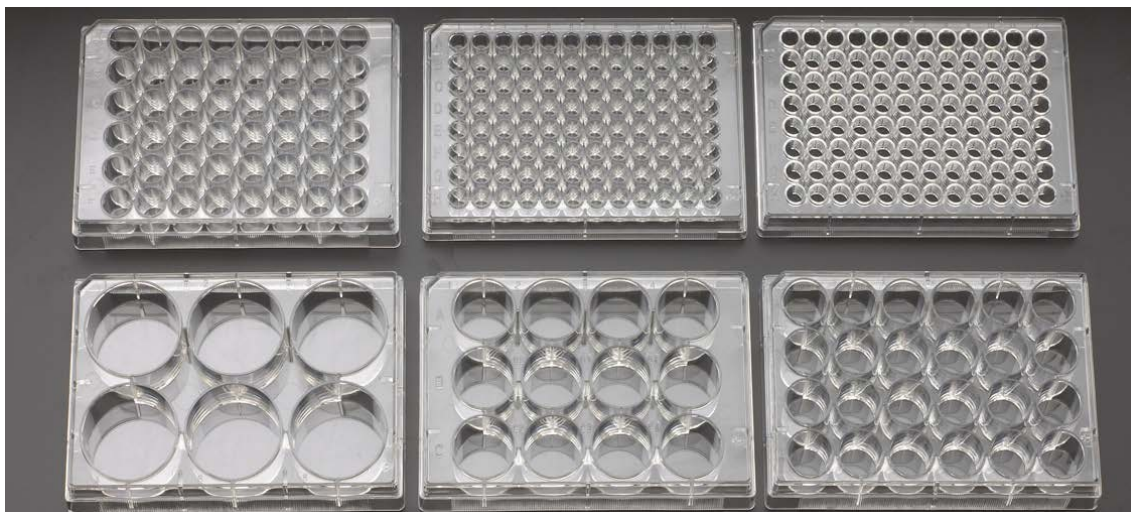


Figure 1.5: Popular well plate formats: 48, two versions with 96, 6, 12 and 24 wells per plate (from top left to bottom right) [39]. These are typically offered in variations with different well bottom shapes (e.g. flat or round bottom) or opacities. Modern addition to this lineup is the 384-well microtiterplate which is not pictured. Image courtesy of CELLTREAT Scientific Products.

1.3.1. Existing Solutions for Zebrafish Analysis

With its rise in popularity the zebrafish has also attracted a number of industrial companies to develop products for the growing research community. There are numerous products available, ranging from single software packages to machines or hardware setups to entirely outsourced analysis services and pipelines. Table 1.2 shows a number of companies and what their offered products can be categorized into.

The most established and widely known systems in this list are made by Noldus Information Technology and Viewpoint. Both are European companies that specialize in setups for behavioral analysis of not just zebrafish but rodents as well.

The DanioVision is Noldus' hardware solution for behavioral analysis of zebrafish [43] and is pictured in figure 1.6. It houses a digital camera with a 1280x960 pixel resolution and maximum frame rate of 60 frames per second. The device is designed as a multipurpose observation chamber that houses the camera plus lighting, well plate mounting hardware and power supply unit. Additionally, there are optional modules that can be added to the

base configuration to expand its functionality. Noldus offers an external temperature control unit and a separate tapping device that is supposed to evoke vibrational startle response. A large sliding opening seals the inside from any ambient light entering the system from the outside, so that experiments can be performed in darkness as well. The well plate holder guarantees correct positioning and alignment. As illumination they provide two individual light sources. One is an infrared backlight and the other a controllable and adjustable white light source.

Table 1.2: A selection of companies offering solutions for zebrafish research in sectors like hard- and software as well as services. Most of them offer solutions from not just one but multiple sectors at the same time.

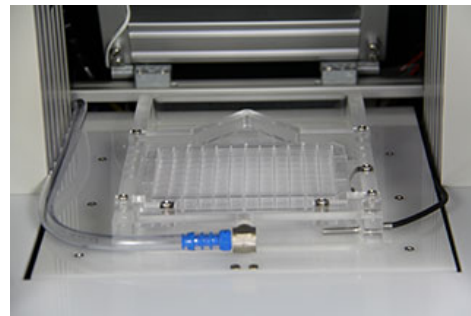
Company	Category		
	Service	Software	Hardware
Noldus		•	•
Viewpoint		•	•
Loligo Systems		•	•
ZF Biolabs	•		
Teleos Therapeutics	•		
CleverSysInc		•	
xyZ Fish	•	•	
Phylonix	•		
MDE Research		•	•
A-MS Systems	•		

The device is controlled via the EthoVisionXT software platform that is designed to allow for tracking and analysis of image data. It is intended to specifically work for zebrafish embryos inside and outside of the chorion and can be used to track the locomotion of up to 96 individual larvae in a 96-well plate. Additionally, features for heartbeat detection and startle response analysis are included. It is not limited to zebrafish though and offers capabilities to be used for rodents or fruit flies as well. Noldus also offers an additional video analysis tool for zebrafish called DanioScope that can be used in combination with a normal microscope instead of the sophisticated DanioVision. It is capable of measuring embryo activity, cardiovascular conditions, morphology and gut and blood flow [44] from video recordings made on a ZEISS SteREO Discovery.V8 microscope. Activity of multiple

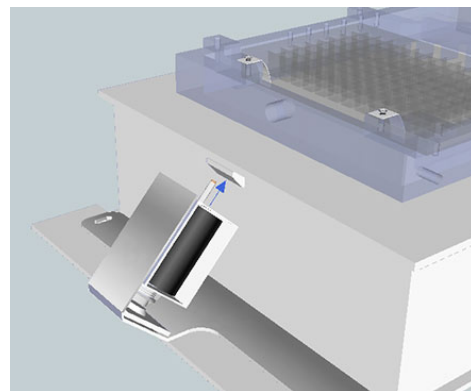
embryos can be measured simultaneously with automatic object detection. However, the software is not capable of following, for example, a floating egg that changes its position over the course of the video. This would require manual user correction and shows a weak spot of the systems. Truly autonomous image or video analysis is not featured yet, while the recording hardware is based on dated technology with moderate frame rates at standard resolution.



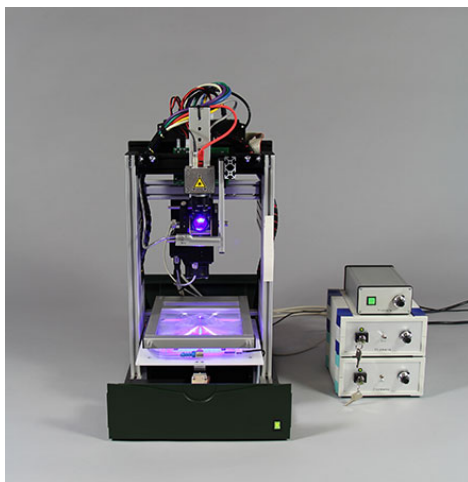
(a) DanioVision [43]



(c) 96-well plate holder [46]



(d) Tapping module [47]



(b) DanioVision without lid [45]



(e) Temperature module [48]

Figure 1.6: Overview over Noldus' DanioVision observation chamber that is used to image the fish in various experiments and is able to have its functionality extended by adding modules for stimulus application or externally controlled heating. Images courtesy of Noldus Information Technology bv.

Viewpoint offers a comparable system to the DanioVision called the ZebraBox which is shown in figure 1.7. It has a similar form factor with a compact observation chamber suitable for single well plates or petri dishes. It is advertised as “the first ever high throughput monitoring enclosure to analyze zebrafish behaviors” [49] and can be customized via various modules to the desired test conditions ranging from PMR to vibration to the response to electrical shocks. An optional and external temperature control unit keeps the temperature at a defined value using a warm water circulation system. The base model includes an IR sensitive camera capable of recording 1024x768 pixels at 60 frames per second. This can be upgraded to a high frame rate camera that allows acquisition of the full well plate with either 300 fps at 2048x1400 pixels or 1000 fps at a resolution of 2048x500 pixels for startle response recording. The decrease in vertical resolution causes the field of view to shrink, so that at 1000 fps only a third of the well plate can be recorded (one row on a 12-well plate) [50]. The vibration module utilizes an acoustic speaker that is horizontally connected to the well plate holder to give vibrational stimuli. However, there is no sensory feedback for the applied forces but the empirically chosen amplification settings for the pulse. The PMR module applies a light flash to all wells of the well plate simultaneously. With a fixed camera, this leads to a resolution for a single well of approximately $\frac{1024}{12} = 85$ pixels horizontally and $\frac{768}{8} = 96$ pixels vertically when the standard camera is used. The ZebraLab software package allows the control of the ZebraBox hardware. It can track and record the behavior of 192 zebrafish larvae at the same time, while adult zebrafish can be analyzed in shoals of up to 20 individuals [51]. To increase throughput the ZebraLab software allows the control of four ZebraBoxes connected to the same computer in parallel.

Another approach for companies is, instead of selling individual hardware systems that have to be operated by the end-user, to offer their expertise and systems as commercial services. This allows research institutions and private companies to profit from zebrafish screens without having to maintain costly zebrafish facilities. This is especially helpful for smaller companies for which the fixed costs of running a zebrafish lab would not be viable. While companies like ZF Biolabs offer to provide customers with actual embryos and larvae, others like Phylonix offer to actually perform a number of different screens tailored to the needs of their customer including assays to address FDA Guidelines for Drug Safety [52].

Due to the involved systems being intended for a highly specialized purpose, however, they usually require significant investments. A single device of the standard versions of the above mentioned hardware systems for example, will cost approximately 30 000 €, with additional features like high frame rate cameras increasing the aforementioned figure significantly.

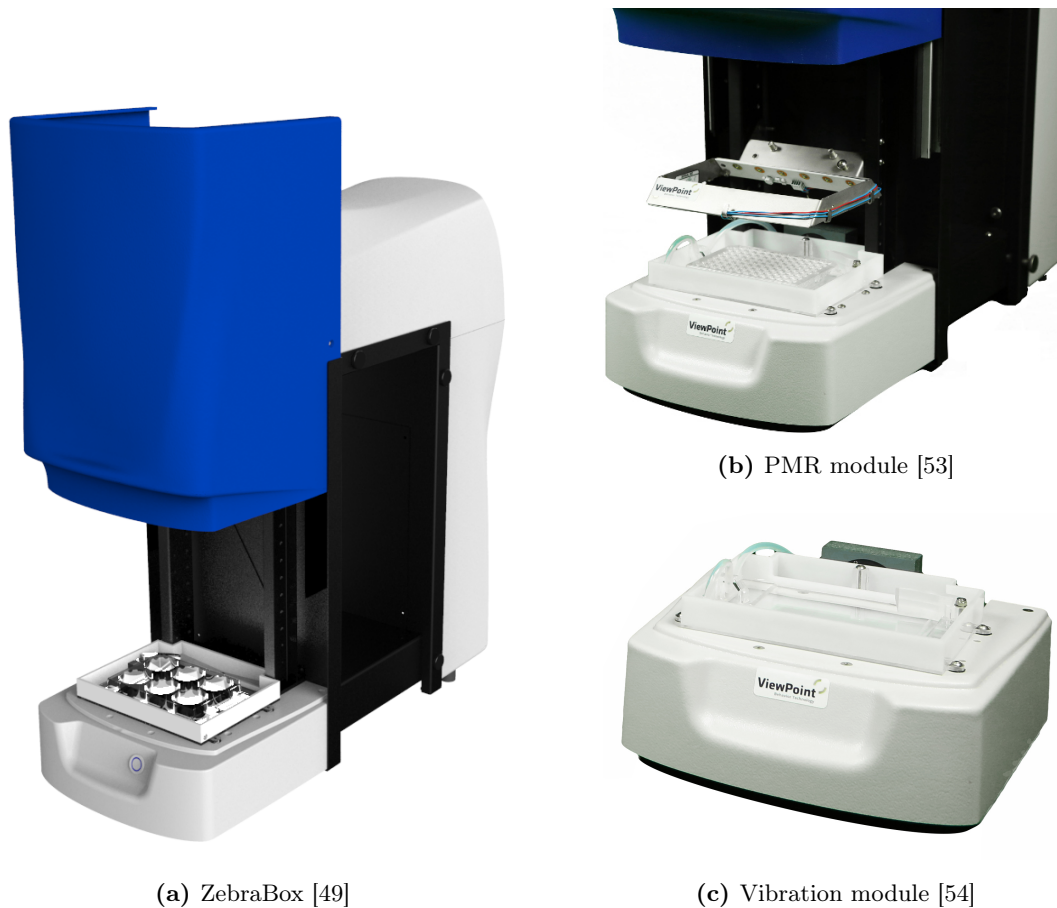


Figure 1.7: ViewPoint’s ZebraBox system offers a modular construction that allows to extend the base functionality by adding various modules, each dedicated to a certain type of assay like for example PMR or vibration response. Images courtesy of ViewPoint.

The high cost and often times even lack of specific functionality of systems like this have triggered research teams all over the world to develop and establish their own solutions for zebrafish analysis [55], ranging from comprehensive automated solutions for sample preparation and imaging [56, 57] to systems that also include compound delivery and incubation [58] to systems targeting specific behaviors like PMR [59, 32], heartbeat detection [60] or startle responses [61, 62]. Even the initial plate preparation does already benefit from increasingly automated solutions [63] with some using advanced image analysis [64] to distinguish phenotypes and sort the embryos accordingly. Technological systems, however, can always be improved to, for instance, deliver clearer images with less noise at higher frame rates and resolutions. Besides there has been no known undertaking to combine systems like these into a single comprehensive behavioral analysis pipeline for early zebrafish that could help to gain a deeper understanding of how chemical or genetic effects can manifest themselves at not just a single time point but over the course of several days.

1.4. Aim of Thesis

This thesis is aimed at introducing novel systems for the behavioral analysis of early zebrafish in an endeavor to improve the way they are used by researchers today. The focus is on providing automated solutions for the phenotypic characterization of some of their prominent behaviors at early stages. With this, a comprehensive platform of multiple behaviors will be available for the first time to researchers to use in their efforts to better understand neural signaling pathways. All systems are supposed to offer new opportunities in the way researchers interact with the fish by increasing the throughput compared to the manual execution of experiments and raising the level of repeatability by minimizing variable factors. The proposed systems have first been conceptualized and the required hard- and software was then implemented to result in fully functional devices that can directly be used in biological experiments. For this, their performance was evaluated by showing their functionality in actual chemical and genetic screens that already emphasize their potential to be viable options for novel studies on zebrafish behavior.

In the end, three independent systems were developed utilizing three different stages of the fish's development, which can lead to a comprehensive overview over the changes the embryos and larvae are going through during their early development from single-cell stage to a basically free-swimming fish. The behaviors appear in succession (see figure 1.8) and are thus relatively independent of each other, ensuring unbiased read-outs for each of them.

With PMR being an already established protocol, the main goal was to find and demonstrate a solution that could be easily introduced in any laboratory interested in doing similar behavioral zebrafish research by relying on often already existing hardware like a standard inverted microscope. Also there was no comprehensive pipeline available that combines automated sample handling, imaging and analysis in order to minimize the number of tedious manual tasks and any excess exposure to light. For the vibration assay, no cost-effective high-throughput systems are known that are capable of delivering precisely defined stimuli and thus an entirely new approach to screening larvae for their vibrational startle response was established. Touch, being one of the earliest stimuli the embryos can respond to, has always been of huge interest for zebrafish researchers. So far, however, there was no automated solution at all and every known assay has been relying on rather non-scientific methods like manually touching the larvae with pipettes or needles [65]. This is why a completely new system has been developed from the ground up to offer consistent and reproducible stimuli to a multitude of fish plus the ability to increase the number of touch stimuli that can be performed in a given timeframe.

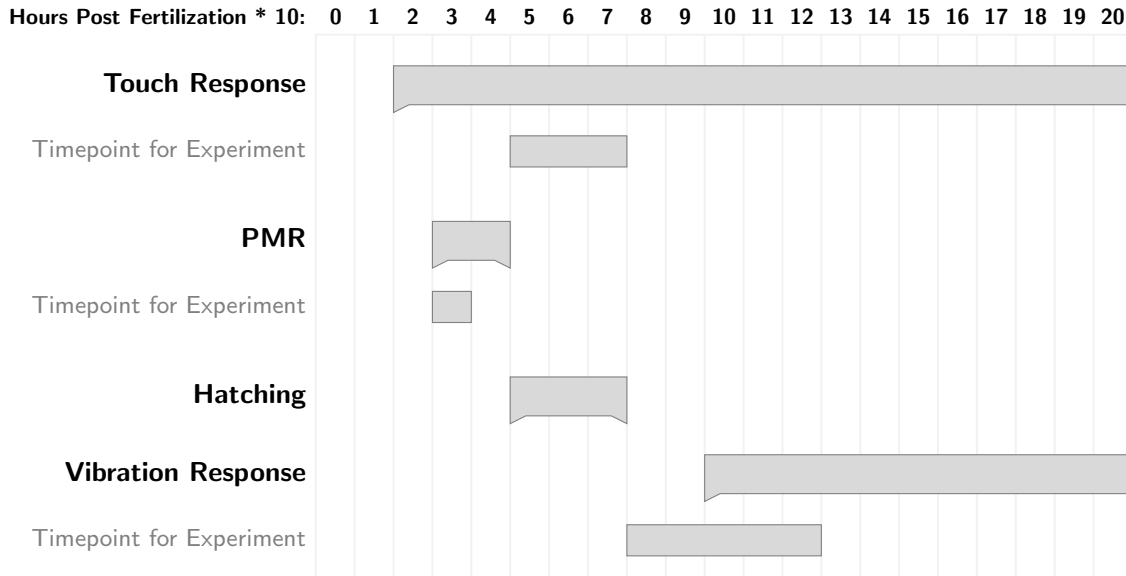


Figure 1.8: Overview of the occurrences of behaviors after fertilization with touch and PMR being the first observable behaviors starting at around 20 hpf. The time points to perform the corresponding experiments at are also pictured. For the touch response a time point after hatching is used, so that the fish movement is not constrained to the inside of the chorion, allowing for more detailed imaging and analysis.

Major challenges in the development of these systems were the need for high-speed cameras and their implementation for the ability to resolve the fast moving objects, signal generation as well as signal analysis and image analysis for object detection. For each system several such objectives had to be solved, although some of the solutions could be transferred between the vibration and touch systems and are thus not restricted to solely one of them. The following list gives an overview of the specific objectives that had to be solved and implemented to develop each system.

- Photomotor Response Platform
 - Configuring an already existing Nikon microscope with movable XY-stage and controllable shutter
 - Recording in darkness required an IR lighting solution that could illuminate the individual wells of a 96-well plate uniformly
 - Implementing the camera’s SDK in order to be able to record images and save them as videos and also offer a live preview to the user
 - Improving an already existing analysis tool [33, 66] by making it more robust and able to handle multiple videos plus integrating it in the workflow

- Establishing a routine for visualization and statistical analysis of the processed data
- Custom software was required to control stage, shutter and lighting to perform a PMR experiment in an automated fashion
- Vibration Response Platform
 - Finding a cost-effective vibrational exciter capable of delivering the desired accelerations, durations and waveforms
 - Creating sine wave signals digitally before emitting them as analogue signals via an amplifier to the desired exciter
 - Establishing a high frame rate recording setup capable of recording motions lasting only milliseconds
 - Due to large file sizes at high frame rates the resulting videos had to be encoded in order to not waste valuable storage space
 - With inherent differences in the output of the exciters, a method to characterize them had to be found and implemented
 - With weight being an issue, a light but still fully functional illumination setup had to be found and implemented
 - The individual parts had to be connected and a pipeline established to automate experiments
 - Automating the analysis by implementing an external tracking tool and adjusting it to work on the generated data sets
- Touch Response Platform
 - Developing a suitable excitation mechanism that is capable of delivering a physical touch stimulus without the risk of harming the animal
 - Using the same high frame rate camera as for the vibration response, with slight performance advances in displaying the live preview as well as encoding the resulting videos
 - For the chosen mechanism of excitation an accurate and simultaneous positioning of multiple motorized axes had to be developed and implemented
 - Developing an easy to use software to automate the touch excitation
 - Developing a proof-of-concept object detection via a real-time image analysis pipeline in order to increase the degree of automation

Since the systems are supposed to be used by individuals with different technological backgrounds, the goal was to simplify the usage and make the procedures so robust that anybody is able use them and that they are easy to debug in case of errors. Thus, simple GUIs, easy to follow procedures and error messages for all systems were essential.

The resulting devices and analysis pipelines were then tested in various sample screens with neuroactive compounds like anesthetics or genetic mutants. For PMR, a large cannabinoid derivative library with more than 250 compounds was screened. Each compound was tested for its individual activity at a fixed concentration of 100 μM and some selected candidates were then analyzed for their dose response at several different concentration steps. On the vibration system, different waking behaviors for anesthetics were shown, thus proving the validity of the system. The touch system was characterized for different parameters like various degrees of stimulation and is ready to be used to perform larger screens with it.

2. Materials and Methods

The topic at hand is a highly interdisciplinary one, applying computer science and mechatronics to biological and chemical questions. In order to help to understand the subsequent chapters about the individual systems, how they were built and how the experiments using them were set up, an overview on the used lab procedures, devices, technologies and computer programs is presented here.

2.1. Lab Procedures

To be able to replicate the performed experiments, the zebrafish strains, their housing and husbandry as well as the used devices and chemicals need to be explained. Additionally, the sample handling and plate preparation has a large effect on the efficiency of the experiments which is why the necessary steps are also illustrated. By introducing novel tools and methods the sample handling could be significantly improved to result in faster preparation, better detection and less exposure for the zebrafish.

2.1.1. Zebrafish Housing and Husbandry

Essential for any high-throughput screening approach is a sufficient number of test objects. Luckily new zebrafish descendants can be regularly acquired in large numbers by crossing female with male zebrafish. For an optimal yield and easy extraction of fertilized and healthy eggs the fish need to be handled according to established guidelines, like the ones proposed by Reed et al. [67]. The KIT houses Europe's largest fish facility for experimental purposes in the European Zebrafish Resource Center (EZRC) with a capacity of more than 300 000 fish. The fish are kept in large racks filled with tanks in dedicated fish rooms like the one shown in figure 2.1.

A continuous water system is used in which each tank is continuously provided with fresh water and the overflowing water being recycled and then recirculated. This helps to drain the tanks from any toxins or floating waste but increases the need for regular monitoring of the water parameters. There is an exchange between recycled water and fresh water

of about 7.5% every 24h. The water itself is set to have a pH between 6.8 and 7.2 at a temperature of 27 °C. Additionally the total number of ions is measured as conductivity and is supposed to be at approximately $250 \mu\text{S cm}^{-3}$. There is no artificial addition of salts or minerals, with the water being generated by mixing purified water with groundwater from the KIT well. The fish are fed at least twice a day with adolescent specimens getting one additional feeding step. To mimic a natural environment, the fish get to experience a 14h/10h day and night cycle with a timer controlled lighting system. This ambient light functions as a trigger for the fish to mate, with fish generally resting in darkness and starting to breed when the lights turn back on. Such a behavior can be used to generate precisely timed eggs that all have very similar fertilization starting points. When doing experiments with early fish this can be very important as the embryos develop very fast and the developmental stages are required to be similar in between the specimens of a single batch in order to achieve comparable results.

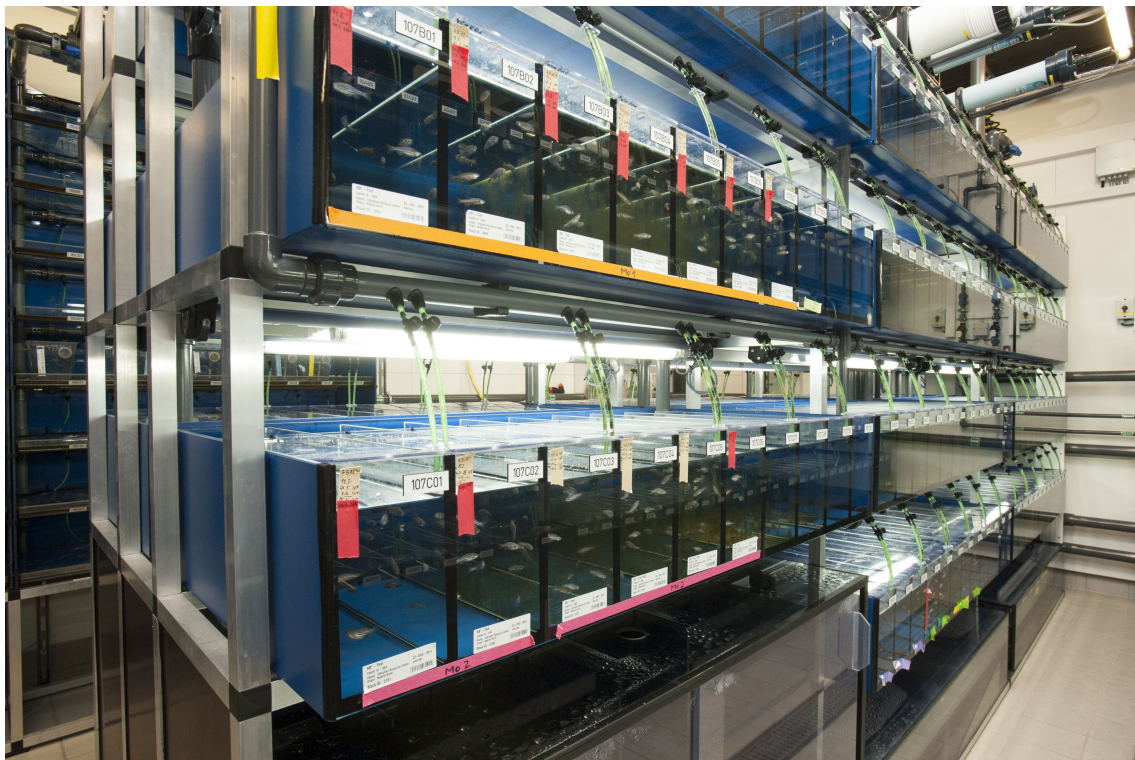


Figure 2.1: Racks with individual tanks housing adult zebrafish at KIT’s European Zebrafish Resource Center (EZRC) [68]. Image courtesy of Martin Lober (Karlsruhe Institute of Technology).

To generate eggs, the typical procedure involves the separation of a male and female fish in a plastic container the day prior to the intended birth date of the eggs. A single pair does usually only generate around 100 to 200 eggs per day, which often is not enough for a meaningful experiment and the reason why multiple pairs need to be set up. It might also

happen that a pair does not lay any eggs at all, which can have various reasons like a too frequent crossing and too little rest in between, user error with a wrong determination of the fish's gender, the fish's diet or health status. This is why for each crossing multiple pairs are set up to ensure a sufficient amount of eggs. The fish are taken from their main tank with a large net and then released into a transparent plastic container. Additional containers are filled with fish water and individual females placed inside them. A mesh insert is placed on top of each female, while ensuring they have sufficient room to swim freely underneath. Individual males are then placed on the top side of this added divider. The fish are kept like this overnight and are put back together the next morning once the lights go on. With both fish on top of the divider they are then able to mate but also limited in their range of motion so that they cannot eat their own eggs once laid. They are left alone for approximately 1 h to give them enough time to excrete the eggs and fertilize them. Afterwards the fish are put back into their tank and the eggs collected with a finely pored net. They are then transferred to petri dishes filled with fish water and put into the incubator to develop. In the afternoon the state of development is verified and unfertilized, coagulated or retarded embryos are discarded. A typical female can lay roughly every three days, which is why a rotational system is often put in place with multiple shoals of fish from a number of tanks that get crossed one after the other. This ensures sufficient time in between crossings, so that the individual fish can rest and recover.

As zebrafish strain the AB line was used as wildtype control with an F2 generation as parents of the used eggs and larvae. The AB line originates from lines A and B that were bought from a pet shop in the United States by George Streisinger and is one of the most commonly used laboratory strains next to the Tübingen line that was established by Christiane Nüsslein-Volhard, the wild-type India Calcutta line or India line [69]. The age of the used parent fish varied between six months and two years.

2.1.2. Equipment and Chemicals

In order to prepare solutions or other samples for testing, several commercial lab devices and other equipment was used that is listed in table 2.1. Two scales were used depending on the desired precision and sensitivity. Both dark incubators were set to 29 °C to provide optimal growth conditions for the embryos. Multiple well plates were chosen depending on the use case with larger wells used for hatched fish to be able to freely swim or black plates being used to ensure isolation of individual wells in terms of light exposure.

Table 2.1: Devices and equipment used for sample preparation.

Type	Manufacturer	Model
Scale	Mettler-Toledo	BD202
Scale	RADWAG	AS 82/220-R2
Pipettes	Eppendorf	Research plus 10-1000 μ l
Incubator	VWR	Incu-Line IL 115
Incubator	Lovibond	ET 618-4
Vortex	VWR	444-1372
96-well plate	PerkinElmer	CellCarrier-96 Black
12-well plate	Greiner Bio-One	Cellstar
Petri dish	Greiner Bio-One	Petri Dish 94x16 mm
Petri dish	Greiner Bio-One	Cellstar Cell Culture Dishes 60x15 mm
Falcon Tube	Greiner Bio-One	Cellstar Tubes 15-50 ml
Eppendorf Cup	Eppendorf	Tubes 1.5 ml

The preparation of experiments involving the use of chemical compounds was done with either novel agents synthesized by the “Compounds-Platform” (ComPlat) at KIT or commercially available ones that are listed in table 2.2. NFPS and Propofol were kindly supplied by Julia Dallman (University of Miami). Solutions were prepared by either dissolving or diluting the source compounds to the desired concentrations. Dilutions were always prepared fresh on the day of the experiments to ensure no degradation. As solvent DMSO was used and dilutions adjusted to result in a final DMSO concentration of less than 1%.

Table 2.2: Commercial compounds used for screenings.

Name	Source	Model
Diazepam	Ratiopharm	10 mg ml ⁻¹
Apomorphine	Sigma Aldrich	A4393-250MG
Isoproterenol	Sigma Aldrich	I5627-5G
NFPS	Sigma Aldrich	SML0897
HU-210 Cannabinoid	Sigma Aldrich	S-024-1ML
DMSO	Carl Roth	A994.2
Propofol	Sigma Aldrich	W505102

2.1.3. Sample Preparation

Samples were prepared differently for each of the systems. While PMR was carried out on rather unusual black 96-well plates with a transparent flat bottom, the vibration system was set up to use 60 mm petri dishes and the touch system was designed to work with standard 12-well plates. This means that the preparation steps differ from one another and are explained individually.

2.1.3.1. PMR Sample Preparation

For the PMR system multiple zebrafish embryos inside their chorion have to be transferred to the flat-bottom wells of a black 96-well plate. The black plate is necessary to isolate each well and keep the light from diffusing into neighboring wells which would cause the embryos to get accustomed to light and their responses to become inconclusive. The flat bottom ensures that all embryos are in the same focal plane compared to a round bottom well in which the center is lower than the circumference.

At an age of roughly 28 hpf the fish are transferred to the individual wells with around 14 embryos per well either via the egg sorter robot that was originally developed by Alexander Pfriem [63] and later substantially improved by Helmut Breitwieser [70] or by pipetting them manually, depending on the number of wells to fill. Either way, the well plate is put onto a modified version of the egg sorter robot afterwards to guarantee a uniform volume in all wells for further processing. The robot is then repurposed to draw excess water from the individual wells, so that the following dilution steps are more precise and easier to perform. To do this the robot was calibrated so that a specific height of its suction tip results in the desired volume to remain in the well. First, a calibration curve was established by completely filling all 96-wells of a reference well plate and then removing the excess volume from each of the wells using the same tip height on all of them. The plate is then weighed to calculate the remaining volume for each well. Doing this for various tip heights results in a linear trendline that can then be used to calculate the corresponding height for any desired volume.

Since the surface tension of water causes a capillary effect and formation of a lens-like surface, only images at a total volume of less than 270 μl per well had a small enough number of illumination artifacts. This effect is pictured in figure 2.2, where the overexposure at high volumes is obvious. Less volume seems to be even more favorable in terms of artifacts but can cause problems with the oxygen supply for the embryos. This is why a “large” volume was preferred.

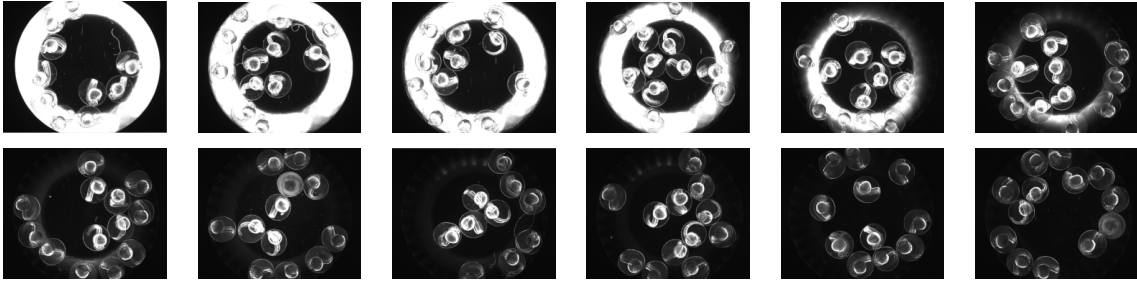


Figure 2.2: Overview of the effect the fill level in PMR wells has on the image quality. From top left to bottom right the volume decreases from 360 to 250 μl in 10 μl steps. A high fill level causes lens effects due to the surface tension of water that introduce illumination artifacts to the images. This effect becomes unnoticeable between 270 and 260 μl .

An empirically chosen volume of 265 μl was established as the standard volume for the performed experiments. To allow the addition of compounds to the wells and reach defined concentration levels, the compounds have to be diluted accordingly. Allowing the added compound volume to be an arbitrary 100 μl , the final dilution step has to result in a 2.65 times higher concentrated dilution than the desired final concentration in the well is supposed to be. To reach a 100 μM concentration for example the added dilution needs to be 265 μM as explained in equation 2.1.

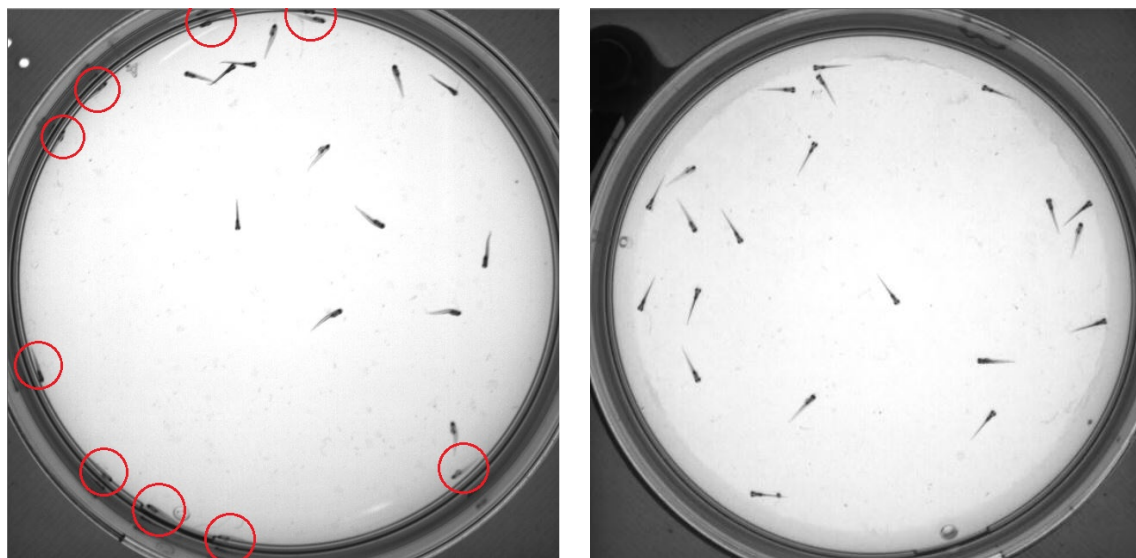
$$\begin{aligned}
 & \overbrace{(265 \mu\text{l} - 100 \mu\text{l}) * 0 \mu\text{M}}^{\text{Fishwater}} + \underbrace{100 \mu\text{l} * x}_{\text{Compound dilution}} = \overbrace{265 \mu\text{l} * 100 \mu\text{M}}^{\text{Final concentration}} \\
 & x = 265 \mu\text{M}
 \end{aligned} \tag{2.1}$$

With this, the dilutions can easily be prepared beforehand and can be added to the well with a consistent volume which streamlines the lab procedure. After exposing the embryos to the compounds they are wrapped in aluminum foil in order to not expose them to any excess light and then put into the incubator for the desired exposure time.

Once multiple plates are supposed to be screened, however, the above mentioned procedure of manually pipetting eggs into wells becomes quite tedious and, therefore, also prone to mistakes. In this case it is recommended to use the egg sorter robot system in its original functionality which was extended to also be capable of doing the sorting under solely IR lighting conditions. Depending on the number of wells and number of eggs to sort, it might become necessary to change the source petri dishes from time to time in order to keep the system running.

2.1.3.2. Vibration Response Sample Preparation

Thigmotaxis is the tendency of animals to stay close to the edge or walls in a chamber or tank. It is a natural sign of anxiety or caution and is also present in fish at the relevant age for vibration experiments. When fish are positioned close to the walls of a well, however, it becomes challenging to distinguish them from the background. This is an unfortunate limitation of using standard well plates or petri dishes and can cause severe deficiencies in the detection rate. Because of this, a simple yet effective solution was found that helps to mechanically keep the fish away from the walls while keeping the optical properties of the dish the same. In [71] the use of an agarose ring is demonstrated that limits the effective area in which the fish can move to the center of a well. This idea was adopted and proved to work reliably in larger petri dishes as well. Figure 2.3 gives an indication on how much the zebrafish detection can be improved by introducing the agarose ring.



(a) Petri dish without agarose, red circles indicate larvae that are challenging to detect (b) Petri dish with added ring made of agarose gel

Figure 2.3: Effect of an agarose ring in a 60 mm dish on the detection of thigmotaxis driven zebrafish larvae. The larvae still tend to go to the wall (now made of agarose gel) but because of the gel's transparency they can still be easily detected.

A custom tool to create the required cutout with a diameter of 47.75 mm was designed and 3D printed. It consists of two parts that slide into each other with an outer ring that is meant to center the tool on the dish and an inner ring with a much smaller wall thickness that acts like a blade to cut the gel. Figure 2.4 shows the CAD view of the custom tool as well as the printed parts.

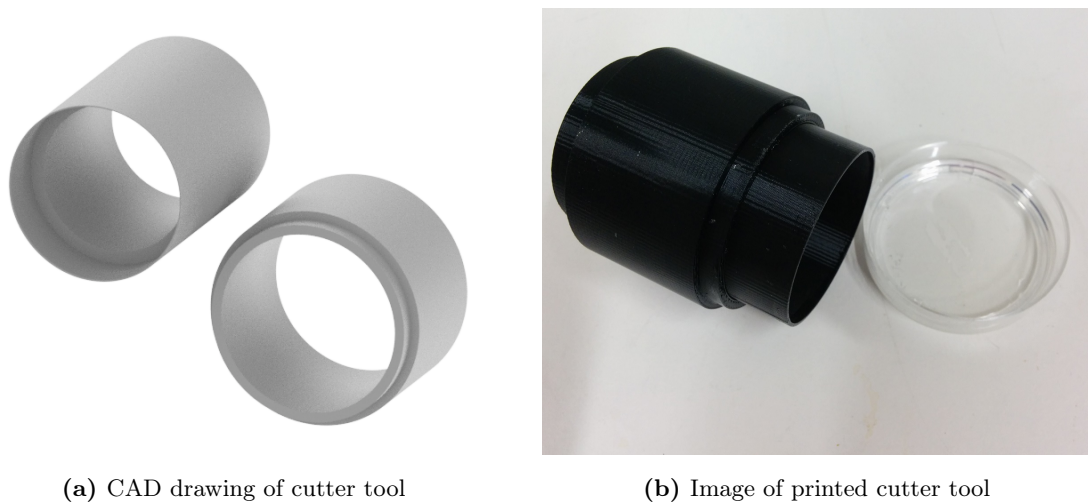


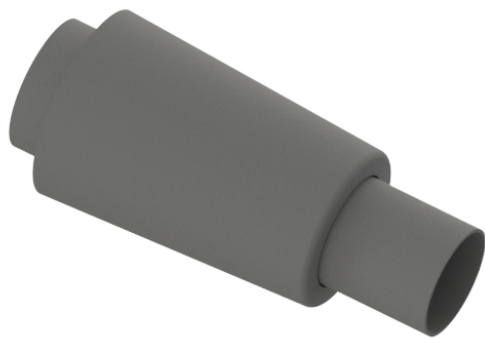
Figure 2.4: The cutter tool is used to remove the inner area from an agarose gel filled petri dish so that only an outer ring remains.

To prepare a petri dish for an experiment, the agarose solution has to be mixed accordingly, left to solidify and then the ring has to be cut out of the solid gel. Good transparency of the gel while still maintaining its retaining qualities was reached by using a 0.5% (w/v) ratio. In 100 ml of fishwater 0.5 g of agarose powder were dissolved by heating it to 100 °C in a standard kitchen microwave. Evaporated water was added again afterwards. The dishes were then filled with 4 g of this solution and put in a 8 °C fridge to cool. Once the dishes were needed, the ring was cut and the excess agarose removed. Before adding actual larvae to the prepared dish it is important to allow for the dish to heat up to at least ambient temperature.

Since the vibration system is set up to work with an additional weight of 5 g per petri dish, the fish and corresponding volume are added while being placed on a scale. This ensures proper stimulation and comparability between experiments. Exposing the fish to chemical compounds is typically done in regular sized petri dishes prior to transferring them to the smaller ones. Therefore, compound concentrations and dilution steps need to be calculated according to the total volume in the media the fish are exposed in. Usually the water in a dish is adjusted to a fixed volume and a corresponding dilution then added. For example a 2 μM solution in a 30 ml volume can be created by adding 6 μl of a 10 mM solution to 29.94 ml of fishwater. However, this would introduce a very high, momentary gradient inside the dish when pipetted, which might irritate the fish and could impact their future responses. Thus it is recommended to choose more gradual concentrations like 5 ml of a 12 μM solution to 25 ml of fishwater.

2.1.3.3. Touch Response Sample Preparation

The thigmotaxis described in section 2.1.3.2 renders the required physical stimulation unfeasible due to the larvae being positioned too close to the walls to allow for an unobstructed touch motion. Additionally, the well plates used for the touch experiments are subject to an optical distortion effect due to their smaller size and the surface tension of water basically forming a concave like lens. All this makes detection and stimulation of the fish almost impossible, but can luckily also be solved with the same technique of adding an inert agarose ring. To prepare a 12-well plate for a touch response experiment the individual wells are filled with 2 g of the already introduced 0.5%(w/v) agarose solution. Once cooled and solidified, a ring is cut with yet another cutter tool. The remaining ring has a diameter of 15.5 mm which leaves sufficient room for the fish to still move freely. The tool is shown in figure 2.5.



(a) CAD drawing of cutter



(b) 3D printed cutter on a well plate

Figure 2.5: Cutter tool for 12-well plates with smaller dimensions than the tool designed for the larger petri dishes in figure 2.3.

2.2. Digital Technologies

In order to realize projects like this, numerous technological tools like programming languages, IDEs, software libraries and data transfer protocols are utilized. With Microsoft Windows PCs still being the de facto standard for personal computers, the development was focused on the Windows 7 environment. There are various ways to create stand-alone applications on Windows by for example using the popular IDE Visual Studio and its object-oriented programming languages C++ and C# or by using other frameworks like QT or GTK+. For more low level operations like sensor readings or signal processing, discrete microprocessor units in the form of Arduino boards were used. Data analysis was performed

mostly in Matlab with its powerful, already built-in routines and scripting capabilities. In order to create special hardware on a 3D printer the 3D design and modeling was done with the help of the Autodesk Inventor suite.

2.2.1. C# and the .NET Framework

To produce applications that can be used on almost every Windows Computer and give them easy-to-use Graphical User Interfaces, the Microsoft .NET framework was used. This framework is based on the Common Language Runtime (CLR) and allows the use of multiple supported programming languages in one final application via a process called just-in-time compilation. On compilation an application is only compiled to the so-called Common Intermediate Language (CIL) which results in a portable execution file that is then executed by the CLR during runtime. This is similar to Java based applications that also rely on intermediate and CPU independent instructions. The result is the “Write Once Run Anywhere (WORA)” concept with which the users do not need to compile the application for each of their target computers. Instead, only the execution file needs to be present. It also allows classes from different languages to be used together, as the CLR takes care of combining them.

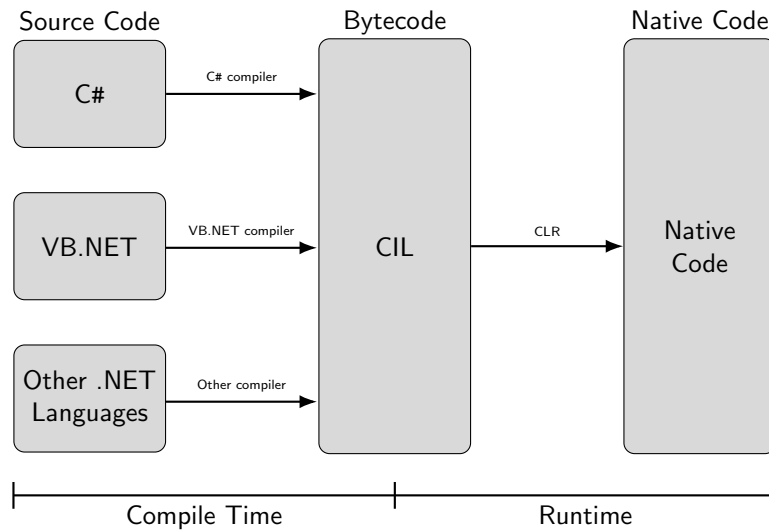


Figure 2.6: Flowchart illustrating the Common Language Runtime that allows just-in-time compilation and with it the simple transfer of compiled applications between systems.

Code generated by the supported languages is typically referred to as managed code. Managed code has the obvious disadvantage that the work done by the CLR takes additional time and thus applications are not as fast as if native code was used. However, in most scenarios and with modern computer hardware this is becoming less and less of an issue.

C# was developed along the .NET framework in mind and is a highly optimized general-purpose object-oriented programming language. The European Computer Manufacturers Association (ECMA) approved C# as a standardized programming language in 2003 [72].

The most popular IDE for C# is arguably Microsoft Visual Studio [73]. It supports multiple programming languages and the code editor offers a large amount of functions for efficient and comfortable usage like syntax highlighting and code completion. It is the de facto standard IDE for any .NET development. Its designer feature allows the creation of the applications' GUIs. Depending on the chosen .NET GUI concept the application is built on there are different paradigms that need to be considered. For .Net applications there are mainly two libraries that can be used for GUI creation. The traditional one is the use of Windows Forms, which was introduced together with the .NET framework itself in 2002 and has been adopted by numerous developers. Its successor was introduced in 2006 along the .NET framework 3.0 and is called Windows Presentation Foundation (WPF). The main difference between the two is the way they connect the actual GUI with the underlying code. WPF GUIs are based on a language derived from XML which is called the Extensible Application Markup Language (XAML). This allows the separation of graphical elements from the code and also allows the definition of data bindings right in the XAML files. The simpler Designer feature and robust technology often favors the use of Windows Forms for standard applications.

2.2.1.1. External C# Libraries and Frameworks

When developing applications that are supposed to incorporate various interfaces, hardware and functionalities, it is often recommended to rely on already existing solutions from either the open-source community or industrial companies. Especially hardware businesses like for instance camera manufacturers like Ximea and Nikon usually offer SDKs in order to allow software developers to use their products in various projects. But besides the mere implementation of proprietary hardware, there are also numerous libraries and frameworks available which help to add specific functionality into more general software projects. Image or video processing for example is a highly complex topic that requires sophisticated algorithms. Luckily there are a number of different open source libraries freely available to use. Sometimes, however, the desired library is only available in a different programming language. The solution to this can be so-called wrappers. These are software packages that offer access in the desired language to functions written in another. The Nreco Video converter for example encapsulates the FFmpeg library while offering .NET access to it.

AForge.NET is an open source C# framework [74] that offers numerous features for digital image processing and computer vision. The inbuilt methods allow the use of various image processing routines and filters like black and white conversion or inversion just as well as object detection. Its development stopped in 2013 and was inofficially replaced by Accord.NET [75].

A useful library to generate videos in the avi file format from the raw images received from the cameras was found in SharpAvi. It is able to process the individual images asynchronously and can store them as files or for example MemoryStreams. MemoryStreams are built-in C# objects that can store data in memory. Instead of directly writing to disk the contained object is written into the memory of the computer, thus eliminating the creation of unwanted files that cause unnecessary read and write processes. This is especially helpful with modern SSDs that have only a limited number of write cycles the underlying NAND flash can endure before degrading. The addition of being able to use streams in the official version of SharpAvi was introduced after showing the personal implementation to the developer via a pull request on github. Unfortunately a major limitation in C# has been a general maximum object size of 2 GB even in 64 bit systems. This was changed with .NET in version 4.5 that allows the use of larger objects for the first time. However, implementation might not always be trivial and thus other alternatives to circumvent this limitation have to be used. A direct drop-in replacement for the standard MemoryStream-class is the MemoryTributary-class. It splits the data into multiple segments, effectively increasing the maximum object size.

After recording a video the resulting data is often supposed to be encoded in order to decrease the final file size. This is especially true with high-resolution or high frame rate recordings as the uncompressed data would use up significant space. A common tool to encode video files is the cross-platform toolbox FFmpeg. It incorporates numerous codecs, file types and formats and is used in many popular projects like the VLC media player or Google Chrome. The FFmpeg video encoder does not offer direct access to its methods in C# which is why it has to be used either via an external commandline process or the Nreco Video Converter wrapper.

To be able to use advanced audio functionality additional libraries are also required. One popular solution is the open-source library NAudio that allows developers to interface with the audio hardware connected to the computer by creating, decoding, converting and recording audio streams.

External libraries are distributed by either actual source code or as already compiled “.dll” files. Dynamic Link Library files are a method of offering the ability to share code, data or other resources across applications. This increases modularity as a DLL can be used as an integrated part by an application but can also be updated or replaced independently from it. The Windows operating system offers its functions for example via DLLs for applications to use like the KERNEL32.DLL that contains many low level functions for memory or process management. These files offer access to their content and are fundamentally similar to the well-known “.exe” files. The major difference is that DLLs cannot be executed by themselves and need an overarching “.exe” file to access their content.

Table 2.3: External C# libraries and frameworks that have been used to implement various functionality.

Name	Description
Ximea Camera SDK [76]	Ximea’s camera API
Nikon Instruments SDK [77]	Nikon Instruments’ camera API
AForge.NET [74]	Open source computer vision library
Accord.NET [75]	Open source .NET machine learning framework with audio and image processing libraries
SharpAvi [78]	Open source .NET library for creating AVI format video files
MemoryTributary [79]	Alternative to .NET’s MemoryStream, eliminating limitation of only allowing maximum size of 2 GB
FFmpeg [80]	Open source cross-platform command line toolbox to manipulate, convert and stream multimedia content
Nreco Video Converter [81]	FFmpeg .NET wrapper
Naudio [82]	Open source .NET audio library

2.2.2. Matlab

Matlab is a proprietary software environment that was originally developed to allow matrix computations like their eigenvalue calculation without having to resort to lower level programming languages like Fortran. Its first official release was in 1984 under the newly founded company Mathworks with 9 major software releases since then. The update cycle was established to be twice a year with the most current version being 9.2 with its release name 2017a. Today Matlab is mainly used in scientific disciplines like engineering or

economics for numerical computations, data visualization and image processing. Numerous built-in functions enable researchers to apply sophisticated algorithms to their data. Matlab uses its own scripting language for the development of executable instruction sets that can be stored as a sort of text file for repeated use. The development of GUIs and standalone applications is also supported, although the Matlab runtime still needs to be installed in order to use them. The runtime is a set of libraries that are crucial for the execution of the code when no Matlab installation is present.

2.2.2.1. External Matlab functions

Mathworks offers a forum-like community that allows the exchange of code pieces, algorithms or full applications. The Mathworks File Exchange is a valuable resource for finding potential solutions for missing functionality. Also numerous solutions have been published that are based on Matlab but extend the range of capabilities to a variety of topics like data mining [83] or zebrafish analysis [66]. For the development of the tools and pipelines in the following chapters some of the available solutions have been incorporated or improved. The chosen solutions are shown and their function briefly explained in table 2.4.

Table 2.4: External Matlab solutions and tools that have been used to implement additional functionality.

Name	Description
<code>rdir</code> [84]	Recursive directory listing
<code>sigstar</code> [85]	Adds significance bars and asterisks for plotting
<code>sort_nat</code> [86]	Sorts strings in more natural order
<code>dispstat</code> [87]	Enables overwritable message outputs to the commandline window
PIMP [66]	PMR Individual Motion Plot Extractor
SciXMiner [83]	Sophisticated Data Mining Toolbox

The use of an external function to enable a recursive directory search was made redundant in newer Matlab versions (R2016b and later) that support wildcard characters natively. The `sigstar` function is helpful when plotting statistical analysis data that should be emphasized by showing significant differences between groups. With Matlab resorting to a (for humans) often unnatural sorting style of strings with digits, the `sort_nat` function can be used instead. Instead of putting numerical values like 1 and 10 next to each other, the natural order will be to order the single digit numbers first, just like how humans would do it

instinctively. Dispstat offers a convenient way of displaying progress data by allowing the overwrite of expired information directly in the Matlab command window. The PIMP-tool is a sophisticated application for automated analysis of video data of zebrafish to extract numerical data on their motility. It was originally developed by Rüdiger Alshut and its usability as well as accuracy was improved in the course of this work on the PMR system. In order to enable the automated analysis of the other zebrafish behaviors (namely vibration and touch response) the SciXMiner was used to provide powerful capabilities for time-series analysis and tracking in the Matlab environment.

2.2.3. Arduino

Arduinos are small, low-cost PCBs with an added microcontroller and other peripheral structures like additional memory or accessible GPIO pins. Their low cost and ease of use make them popular control units for various electronic sensors and other equipment like relays or LEDs. There have been multiple versions released that differ in their range of functions, size, price, speed and memory. Most of the boards use 8 bit microcontrollers like the ATmega168 or ATmega328. But there are exceptions like the Arduino DUE that was introduced in 2012 and uses a 32 bit SAM3X8E.

The controllers can be programmed via a custom Software IDE which makes the upload of the so-called sketches straight forward. In order to run logic on the microcontroller, C-based sketches need to be uploaded. In its minimal form the sketch consists of just two function calls which are illustrated in figure 2.7.

- `setup()` – runs once on startup of the controller and is used to initialize variables, define outputs and establish connection with peripheral devices.
- `loop()` – the loop method is called repeatedly after the setup was successful and contains the main logic. It will continue running until the board is powered off.

Only one sketch at a time can be used as the memory is overwritten on each new upload. Arduinos can be considered to be of a much lower level abstractness compared to more elaborate computation platforms like Raspberry Pi for example. There is no need for an operating system with the Arduino boards basically just offering more comfortable access to the raw microcontroller functionality.

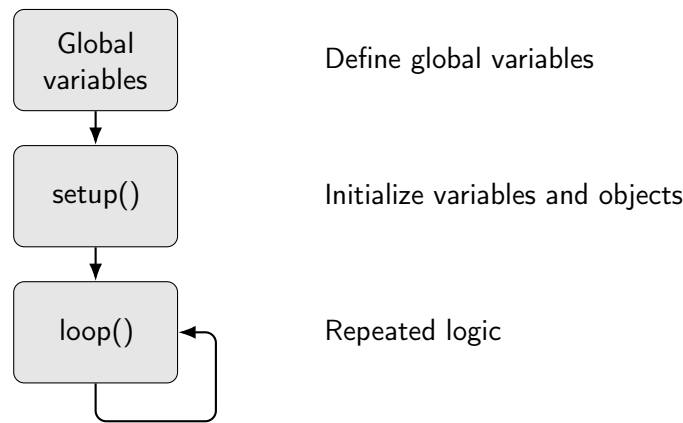


Figure 2.7: Flowchart of the base structure of an Arduino Sketch. Globally used variables are defined outside of the two main functions. The setup is then used to initialize variables or set pin modes as it is only run once on powerup. The following loop function is repeatedly called and is used to manage the actual task the Arduino is supposed to carry out.

2.2.3.1. Data Transfer Protocols

A common transmission method for digital data is to send each individual bit one after the other. This sequential data transfer is called serial communication and is used in many situations to connect components with each other. The advantage is that, compared to parallel connections with multiple wires for each parallel channel, the cable and ports do not need to be unnecessarily complex. Many popular standards use serial communication like as the name implies every Universal Serial Bus (USB) device, PS/2 mouse or keyboard. Historically the RS-232 standard has often been referred to as the reference serial connection and was once a standard port on almost every PC. It was defined by the Electronic Industries Association (EIA) in the 1960s and allowed simple communication with peripheral devices like modems, printers, storage media and others. Per its definition the RS-232 standard is based on a Universal Asynchronous Receiver Transmitter (UART) that uses voltage levels between ± 15 V. A UART is the actual logic interface responsible for sending and receiving serial data while RS-232 is the standard that defines the signal between two connected devices in terms of which voltage, pinouts and connectors should be used. Today the once widespread RS-232 D-sub 9 connector has been replaced by the more general purpose and faster USB port and usually needs some converter dongle to be used with modern PC hardware. However, due to its simplicity, UARTs and RS-232 are still used in many industrial applications and instruments when low-speed is not of concern. Data is transmitted in form of packets whose format is not dictated by the official standard. A typical packet could consist of one start bit, eight bits for the actual data and one stop bit to indicate the end of a packet.

There are also some settings that allow for customization in for example the transfer speed and error detection. The baud rate setting indicates the transfer speed in bits per second while the parity is used to detect data corruption. This communication is often used in combination with the American Standard Code for Information Interchange (ASCII) character encoding to transfer text based commands.

Arduinos offer a number of different communication standards and protocols. The most prominent one is their USB port with which they can communicate with a PC via a UART based serial port that uses a Transistor-Transistor Logic (TTL) voltage between $\pm 5\text{V}$ depending on the board that is used. The officially recommended baud rate to use with classical UART devices is between 9600 and 115 200 bit s^{-1} . To communicate with other peripheral devices, however, Arduinos can also use other bus systems with each having their own advantages and shortcomings. Their main difference is the complexity to set them up and the data transfer rates they offer.

I²C is one such data bus and was designed and developed in the early 1980s by Philips Semiconductors to connect the numerous ICs in their TV sets. Until then the conventional transfer methods relied on distinct connections between each component, which resulted in crowded or larger than necessary PCBs. This problem was solved by establishing a new bus that relies on just two wires: a data (SDA = signal data) and clock line (SCL = signal clock) as illustrated in figure 2.8.

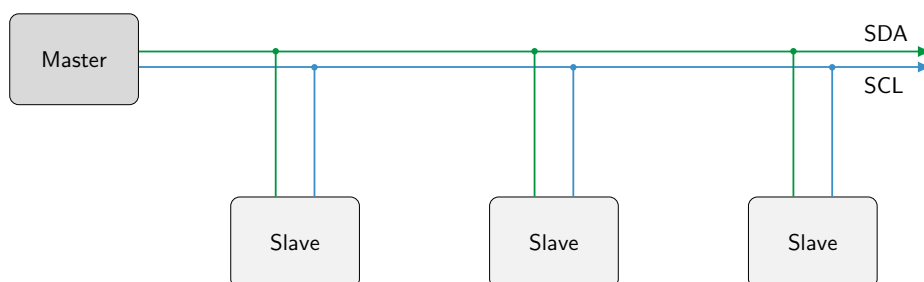


Figure 2.8: Flowchart representing the I²C bus architecture.

With the simplified wiring scheme comes additional data overhead to compensate for the necessary addressing of the slave devices. Each device needs to have a unique address to be able to be selected and the data collected. Usually the address registers come preprogrammed from the factory, but they can be changed to allow usage of multiples of the same device to be connected to a single master. However, this also leads to a limited transfer speed of usually either 100 kbps in standard and 400 kbps in fast mode.

The Serial Peripheral Interface (SPI) is a four wire bus that gets rid of addressing overhead by having a discrete “slave select” signal line. However, it is not capable of bidirectional data transfer on a single line and as such relies on separate input and output wires (MOSI = Master output/slave input, MISO = Master input/slave output) in combination with a signal clock (SCLK). In figure 2.9 a typical SPI bus configuration is shown with a single master and three slave devices. The slaves are selected via the discrete slave select (SS) pins and otherwise share the clock as well as the data lines.

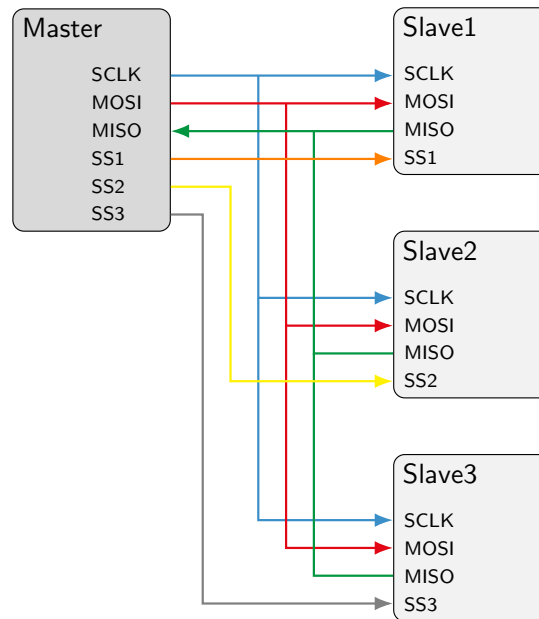


Figure 2.9: Flowchart representing the SPI bus architecture.

The transferred data does not have to conform to a predefined structure which allows for high-speed data transfer in the MHz range. Therefore, SPI is a popular protocol for applications where only a small number of slave devices are connected and high-speed is beneficial. With Arduinos having numerous unused and programmable pins the use of the SPI standard can easily be realized even if a number of slave devices is supposed to be used.

2.2.4. Computer-aided Design and 3D Printing

Creating physical objects from a raw source material usually requires at least some drawings or another form of visualization. Historically this could only be done manually by skilled designers on paper until computers could be used to simplify this task. A rapid rise in computing power since the 1960s led to a dramatic increase in the capabilities for digitally designing, modeling and even simulating new parts or systems. Initially limited to only 2D representations, there was a large demand for more complex and intuitive 3D CAD systems.

The company Autodesk has established itself as one of the major providers of elaborate software packages for design, engineering and even for entertainment purposes. Its Inventor suite is a popular application for the creation of 3D digital prototypes and was used for all design work in the development of the aforementioned systems.

Today almost anyone can design and produce personalized parts with the help of modern manufacturing technologies such as 3D printing. All that is needed is a digital model and one of the many readily available 3D printers. There is a countless number of manufacturers and models of 3D printers on the market today, but they all follow the same fundamental principles. 3D printing, being an additive technology compared to the more traditional subtractive technologies like milling, basically consists of a baseplate on which the desired model is then printed layer by layer. The thinner these layers can be created the higher the resulting quality will be but at the same time the print duration will usually increase. There are a number of different techniques that can be used such as Stereolithography, Laser sintering or fused filament fabrication. In Stereolithography a liquid photo-polymerizing resin is solidified by selectively shining a focussed light source (usually a laser) on it. A movable baseplate moves the solidified object away from the light source so that new layers are formed until the object is complete. Laser sintering takes a different approach by selectively heating a material powder until it melts and a new layer is formed. This way even metals can be processed. The most common technique, however, is the use of a thermoplastic when doing fused filament fabrication. An extruder heats the thermoplastic close to its melting point, so that it can then be deposited layer after layer to form the desired shape. There is a wide variety of usable materials like acrylonitrile butadiene styrene (ABS), Nylon, polylactic acid (PLA) or glycol-modified polyethylene terephthalate (PETG). They differ in strength, flexibility, durability and ease of use. All 3D printed objects in this work have been printed on a Stratasys uPrint printer with ABS as thermoplastic.

2.2.5. Data Compression

With modern video recordings being of high-resolution, in color and oftentimes of high frame rates as well, the amount of data that is captured is astounding. If the information of every individual pixel would be stored on device without any form of compression, the available space would be exhausted with just minutes of video. A typical smartphone for example records at a 1920x1080 resolution in color and reaches 60 frames per second. In an uncompressed colordepth of 24-bits per pixel this would lead to a storage demand of roughly 373 MB s^{-1} . With a storage space of 32 GB the device would be completely filled

with just 86s of video. Sharing this data in a private network, over the internet or even via a physical connection would then also be highly cumbersome.

This is why image data has historically been compressed in order to decrease file sizes and free valuable storage space. Compression utilizes the fact that real-life data often suffers from statistical redundancy with information being repeated unnecessarily often. In an image for example not all pixels will change their color and intensity from one frame to the next, so instead of storing every state individually one might store the state once and keep it for whatever number of frames it does not change. This compression step alone can reduce the size significantly and would still allow a perfectly identical reproduction of the initial data. An attempt like this is, therefore, referred to as lossless compression, since no data is lost and every bit of original information can be recovered.

Lossy compression takes this one step further and exploits also the human visual perception of colors and brightness levels. For example popular image formats like JPEG rely on the fact that humans don't notice differences between hues of color like they would for brightness variations. Additionally there is a varying sensitivity in the perception of entire color ranges, with our eyes being more sensitive towards green than they are to blue and red. High frequency changes in intensity values can oftentimes also be omitted as we can usually not recognize them very well. For the human eye the resulting data is often indistinguishable from the original, which is why this technology has been successfully used in television broadcasting standards like NTSC or PAL. Such a compression is also used in many other aspects of our daily lives and not limited to just image data. One famous example would be the digital audio compression format MP3. It works similarly to the just described image compression as it also removes unnecessary parts of the original data in a way that is based on limitations of the human auditory perception. The result will then again be a compressed audio file that is nearly indistinguishable from the original data when listened to.

For digital video some separate de-facto standards have been established that allow highly efficient transmission of video data over the internet or other data connections. The MPEG-4 Part 10, Advanced Video Coding (MPEG-4 AVC) or H.264 standard has become one of the most widely used standards for video compression with various internet streaming services as well as television broadcasts like DVB-S or DVB-T relying on its efficiency. It was introduced in 2003 and only recently succeeded by the High Efficiency Video Coding (HEVC) or H.265 standard. However, due to its long availability the H.264 standard is still more broadly supported by various software applications like video players. For this

reason H.264 was chosen to compress any potential high frame rate video recordings in the course of this work. As actual encoder x264 was used in form of its implementation in the FFmpeg platform. H.264 relies on a combination of the above mentioned principles to achieve lossless as well as lossy compression on image sequences.

2.2.6. Computer Hardware Setup

In order to build the systems that are described in the following chapters, several high-performance computers needed to be built. To guarantee smooth usage, fast data storage and analysis a capable CPU, high-speed USB3 ports, a sufficient amount of memory as well as a fast storage device were necessary. Building the computers from individual parts allowed the usage of only the parts that met the requirements while neglecting unnecessary options. Three identical computers were built with the parts listed in table 2.5.

Table 2.5: Overview of the equipment that was used to build PCs capable of the high-speed camera connections and execution of the applications to control the individual screening systems. Only freely available, consumer grade hardware was used to allow for cost effective systems.

Description	Name
4x3.2 GHz CPU	Intel i5-6500
M2 SSD	Samsung SM951-NVMe 256GB
DDR4 Memory	G.Skill Value 4 DIMM Kit 16 GB
Mainboard	MSI Z170A PC Mate

Especially important were the USB3 ports that allowed for large data transfer rates so that the cameras could be used to their full potential as well as the fast SSD to make data storage of large files quick and easy. With inbuilt audio capabilities there was no need for additional dedicated sound hardware. The same was true for the graphics card, with the i5 CPU already having one built-in that was perfectly capable of displaying the required information to the screen. To speed up video encoding or data analysis it is possible to upgrade to a dedicated graphics card in the future that can then be utilized for computations, but this seemed unnecessary at the time and has proven to work fine without.

3. Photomotor Response

Early stage zebrafish show characteristic behavioral features at stages between 30 and 42 hours post fertilization (hpf) when exposed to a short and bright light flash. This so-called Photomotor Response (PMR) is a reaction of the nervous system of the fish and can be used as a marker in screenings for neuroactive chemicals. PMR was first described by Kokel et al. in 2010 [32]. They were able to show that a short light flash, lasting about one second, applied to eggs that were kept in the dark, causes an increased motor activity lasting for around 5-7 s. Exposing the eggs to a second light flash within 10-15 s of the first flash, however, results in no visible additional motion activity of the embryo. Consequently, the PMR is characterized by three significant temporal phases that are also visualized in figure 3.1: (1) The basal movement phase in the absence of a light stimulus, (2) The excitation phase corresponding to the zebrafish motion after the application of the light stimulus and (3) The refractory phase where the embryos show no response to a second stimulus.

The exact mechanisms responsible for PMR are still unclear, although it has been shown to be a non-visual response with opsin-based photoreceptors in the hindbrain of the embryo that are controlling this behavior [33].

The PMR is scalable to standard 96-well plates and thus offers the potential to examine a variety of different neuro-active compounds parallelly. This could ultimately be used for the screening of potential analgesics, anti-depressants or other medical drugs and to quickly determine their influence on the nervous system of vertebrates. To allow for statistically significant results, however, a large number of embryos need to be screened, translating to a lot of manual, labor-intensive and time-consuming steps. This is why an automated approach for high-throughput PMR screens needed to be developed that minimizes the exposure of the fish to undesired excess light while at the same time eliminating the mentioned tedious steps. By combining automated sample handling in form of the 96-well microtiter plate preparation with a microscope-based automated image acquisition and system control as well as computational video analysis and data visualization the first high-throughput PMR solution was introduced that ensures minimal human intervention

and can achieve several thousand individual readouts per day on a single system. The following sections are based on [70] and explain the implementation and usage of the system in more detail plus show the results for the screening of a novel neuroactive compound library.

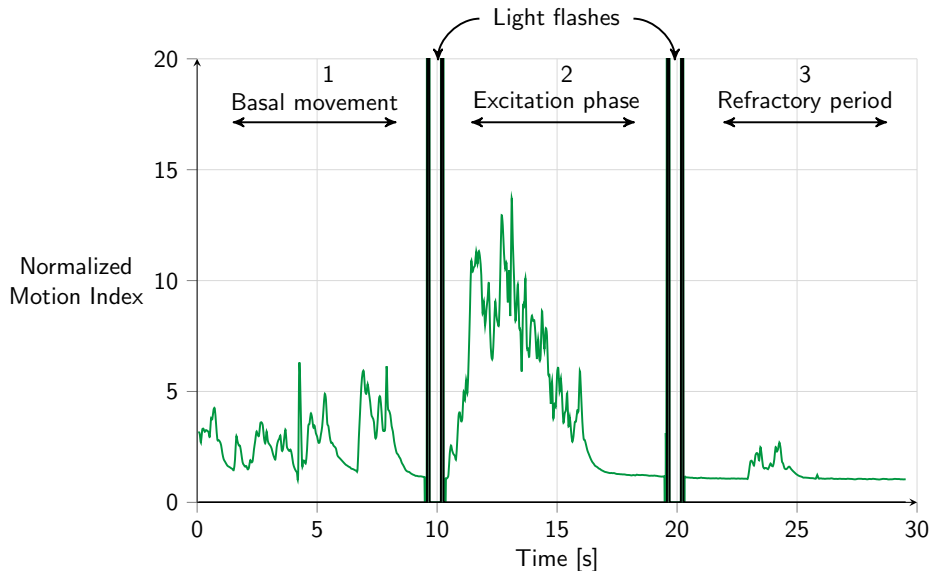


Figure 3.1: PMR control behavior showing the average motion index of 10 embryos. A higher motion index indicates more movement. The three characteristic phases are shown with the basal movement phase representing a phase of unstimulated control movement with occasional muscle contractions a developing embryo shows naturally. The excitation phase shows the increase in motion for several seconds after the first light flash. A second light flash is not able to elicit an excitation anymore and the activity is decreased to a level below the basal movement. This refractory period lasts several minutes before the embryos are able to show PMR again.

3.1. Sample Handling

The first step in the PMR experiment is to collect the zebrafish eggs (typically several thousands a day) and sort these eggs to remove coagulated and unfertilized eggs. The remaining fertilized eggs are then incubated at 28.5°C to ensure proper embryonic development. At 24 hours post fertilization (hpf), the embryos are sorted into a 96-well microtiter plate (typically about 14 embryos per well). This is conventionally performed manually under a light microscope thereby exposing the embryos to light for a significant amount of time. This could potentially affect the PMR behavior and also be very manually intensive depending on the number of plates that need to be prepared. To overcome this problem and reduce manual tasks, a zebrafish sorter robot was developed that is able to work under infrared (IR) lighting conditions invisible to the human eye. Zebrafish embryos

have empirically been shown to be insensitive to IR light [88], which enabled the use of IR light sources to modify and improve an already existing egg sorter robot that was developed in-house [63]. The robot is a camera based system with a pipetting tip that is movable in three dimensions. It is used to take up single eggs from a petri dish and release them into the wells of standard 96-well microtiter plates. To find the eggs that are scattered across the petri dish the camera takes a digital image which is later analyzed to extract the coordinates of a potential single egg. To ensure optimal detection quality a system with IR LEDs with a peak wavelength at 850 nm was required to illuminate the petri dish. The LEDs were mounted directly inside of an aluminum ring to ensure optimal placement and illumination of the petri dish which can be seen in figure 3.2. The aspiration sensor is used to check each egg for coagulation and only allows the transfer of healthy eggs to the well plate.

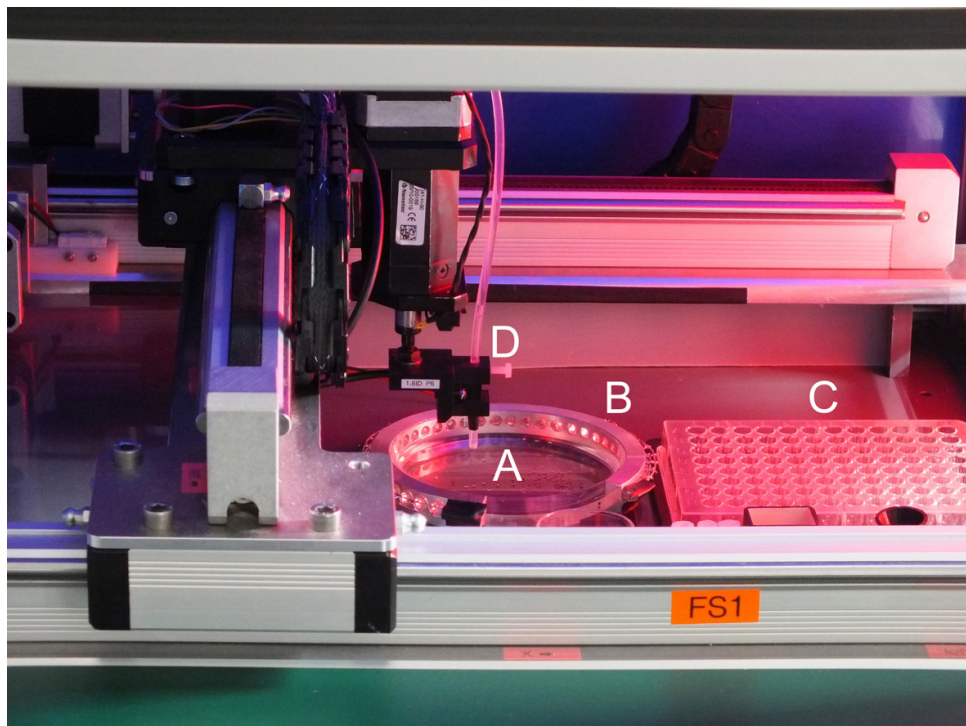


Figure 3.2: Close-up of the egg sorter robot with added IR lighting capabilities. The need for white LED illumination was eliminated and the embryos can thus be sorted without exposing them to excess visible light. A) Petri dish holding the zebrafish eggs B) IR LED ring used to illuminate the petri dish C) 96-well microtiter plate in which the eggs are sorted into D) Aspiration sensor to check for coagulation

3.2. Data Acquisition

After the sample handling, the prepared plate is transferred to a specially designed microscope-based video acquisition system. In order to perform a PMR experiment several methods can potentially be used. Kokel et al. used a system that records well after well in their initial publication, while commercial products like the Viewpoint ZebraBox try to simplify this process and record the entire well plate at once. And even though recording all wells of an entire plate at the same time has obvious benefits in terms of speed and simplicity, it lacks the level of detail one might get from higher resolution images. It is arguable how well an entire well plate can be imaged at once with the currently available resolutions of digital cameras and the optics that are usually used. This is probably why Viewpoint supplies a zoom lens with their PMR add-on that limits the field of view from 96 to 48 wells [53], so that optical distortion of the wells on the periphery of the plate can be avoided that would otherwise render the recordings of those wells unusable. But even at a relatively high 2048x2048 resolution the individual eggs would be hard to distinguish with a theoretical size of just 38x38 pixel/chorion when a total of 48 wells with a center to center distance of 9 mm is recorded. To allow for a more detailed imaging of the embryos, a well by well recording scheme was chosen as the preferred approach. The necessary parts needed to build a system capable of this are a camera that is sensitive towards IR light, IR illumination, a movable stage to move either well plate or camera from well to well, bright white light for the flash and a way to quickly toggle the light on and off. Due to commercially available whole microscope setups that offer most of this functionality out of the box already, the decision was made to modify such a system instead of building one from scratch. However, the control software to integrate all this into an easy to use application was not available at the time.

A Nikon Eclipse Ti-E inverted microscope was equipped with a custom LED ring (as shown in figure 3.3) consisting of a total of 32 Vishay Semiconductors TSHG8200 IR LEDs with a peak wavelength at 830 nm to provide constant IR illumination during the experiment.

The sample plate itself is placed on a motorized stage which can be controlled to move such that each well of the plate is successively in the field-of-view of the microscope. In order to provide the light flash, the microscope was equipped with a controllable shutter and a 100W Halogen bulb. The video recording was done with a Nikon DS-Qi1 monochrome camera with a 1280x1024 pixels resolution at 19 frames per second (fps) connected to a Nikon DS-U3 controller. A CFI Plan Achromat UW 2x objective as well as a 0.55x adapter were used in combination to ensure a sufficiently large field-of-view.

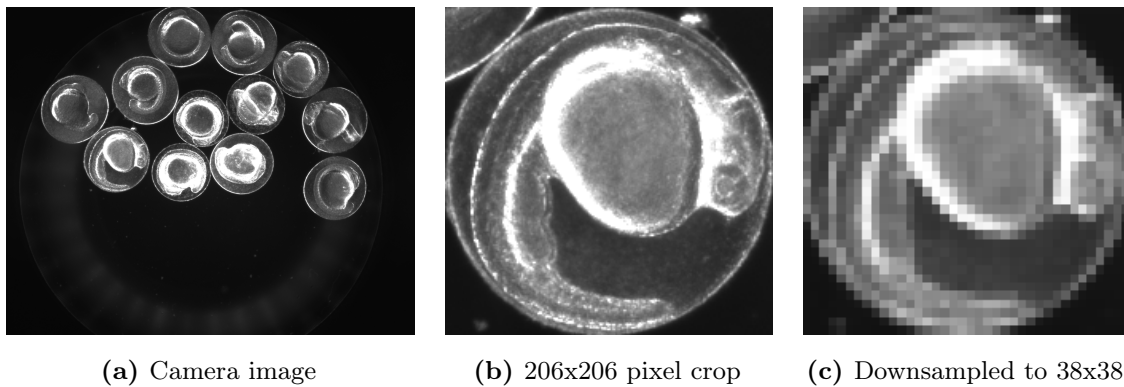


Figure 3.3: Close-up of the IR LED ring that was retrofitted to the Nikon microscope to allow for permanent illumination during a PMR experiment.

As already discussed this allows capturing the individual embryos at a much larger resolution. With a single well being approximately 6.4 mm [89] in diameter a theoretical resolution of 160x160 pixel/chorion is possible.

$$\frac{1024 * 1024 \text{ pixel}}{(6.4 \text{ mm})^2} * (1 \text{ mm})^2 / \text{chorion} = 160 * 160 \text{ pixel/chorion} \quad (3.1)$$

Figure 3.4 illustrates how much of a difference the increased resolution can make, with the low resolution embryo showing significantly less detail.



(a) Camera image

(b) 206x206 pixel crop

(c) Downsampled to 38x38

Figure 3.4: Resolution comparison of chorions between different optical setups to illustrate the differences of single well and multi-well recordings in terms of recordable detail. Single well recordings have much higher detail and allow the analysis of additional endpoints like the presence of a heartbeat or morphological changes if necessary.

The even larger diameter of the chorion compared to the calculated result from equation 3.1 is due to the microscope's magnification causing the well to be larger than the field of view of the camera. Thus, the top and bottom are slightly cropped when the well is

centrally aligned. During the experiments this has not been an issue, however, with the total number of embryos in a well being sufficiently large to be able spare the ones that could potentially be positioned outside the field of view of the camera.

The larger resolution allows for example to check the heartbeat of the embryos to see if they are actually still alive before, during and after an experiment. This was deemed an important information as a toxic effect of chemical compounds should not be confused with an actually non-responding embryo. For raw motion analysis the images could then still be downsampled to a lower resolution if necessary.

By adding a USB controllable power outlet, temperature controlled heating system as well as an opaque housing to avoid ambient light, the usability and durability of the system could be enhanced even further. The system is presented in figure 3.5 and the parts are listed in table 3.1.

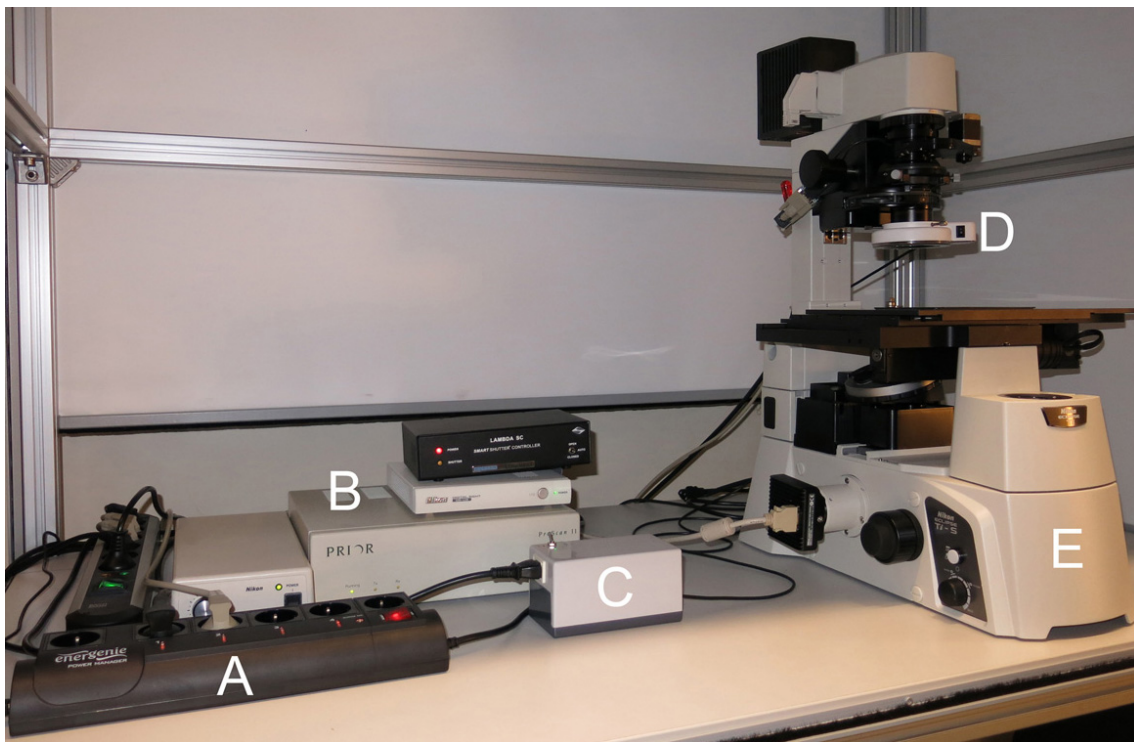


Figure 3.5: Overview of the fully controllable microscope inside a temperature controlled dark housing. A) USB controlled power plug that can be used to prolong the life-time of the light bulb by switching the light on only during an experiment B) Camera, stage, shutter and illumination controllers C) Power supply unit for the IR illumination D) Custom IR LED illumination ring E) Inverted microscope system. The controllable heating system is positioned behind the microscope and not visible from this angle.

Table 3.1: Equipment used to build the PMR acquisition system.

Name	Description
Nikon Eclipse Ti-S	Inverted microscope base
Philips Focusline 7724 12V 100W	Halogen light bulb
Nikon DS-Qi1Mc	Camera
Nikon DS-U3	Camera controller
Nikon Ti-BDTV2	Converter mount with 0.55x adapter
Nikon CFI Plan Achrom UW 2X	Objective
Prior Scientific H117N2TE	XY-table
Prior Scientific ProScan II	XY-table controller
Sutter Instruments Lambda SC Controller	Shutter controller
Sutter Instruments IQ35	Shutter
EWT C120LCD	Controllable heater
Energenie EG-PMS2	Programmable surge protector

The system is controlled using custom software that incorporates the Nikon Instruments Software Development Kit (NISDK) [77]. A .Net Windows Forms application was written in C# in Microsoft Visual Studio 2013. A flowchart is shown in figure 3.6 to indicate the functionality and structure of the application.

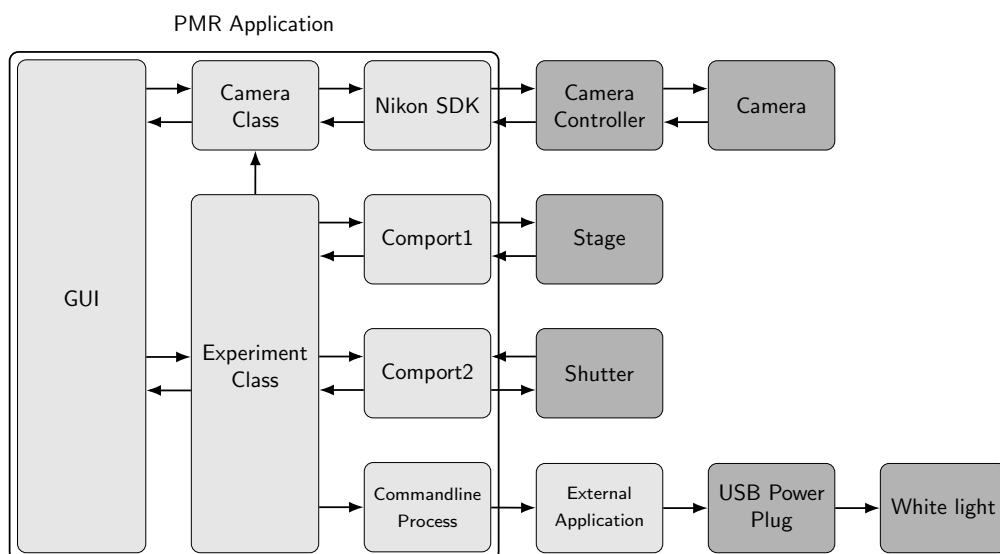


Figure 3.6: Flowchart of the PMR control software. Light gray indicates software objects while dark gray indicates actual hardware the software is communicating with.

The application is designed to control most parts of the hardware like camera, stage and shutter plus it allows the simple configuration of experiments. To setup and start a PMR experiment the user only needs to load a Microsoft Excel file containing the desired experiment settings. Furthermore, there is the possibility to adjust camera settings, light flash exposure time and video duration.

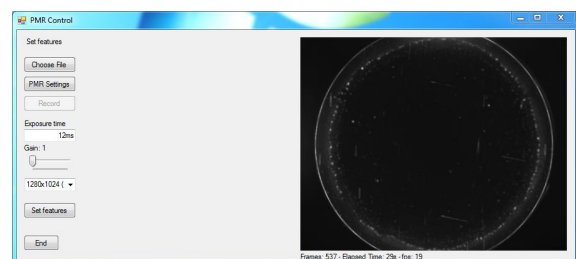
From a technical point of view the application can be considered a hub that incorporates and manages the functionality of the individual hardware parts. A camera class takes care of initializing the camera and of the images that are received via a callback event. Changing camera settings like the exposure time are channeled from the GUI through the camera class to the hardware controller. The camera controller can only be accessed via interop marshalling commands that act as a bridge between the managed code the application is written in and the unmanaged code the Nikon library is supplied in. Luckily they already offer a .NET sample for this that can be easily transferred to other projects. The images are stored as uncompressed AVI files via the Open Source library SharpAvi that writes the images in form of byte arrays to a video stream object that ultimately gets written to disk as the final video file.

The experiment class takes care of the coordination of the remaining parts during an experiment. It controls the stage, shutter and the white light. The stage and shutter both communicate via RS-232 serial ports and a simple ASCII based protocol. Moving the stage is done by sending absolute position values to the stage controller with 9600 baud. The manual [90] lists numerous commands and the structure in which they are supposed to be used. To move the stage a sequence like “G,100,200<CR>” needs to be sent and will return an R character when the communication was successful. “<CR>” is supposed to indicate a carriage return character that terminates the command. This will cause the stage to move to position 100 in x and 200 in y direction. Similar commands are used for the shutter. Here the manual [91] dictates the transfer of decimal, hexadecimal or binary values. Thus, opening the shutter is achieved by simply sending “170” to the controller. Similarly closing only requires the characters “172” to be sent. In order to only supply the white light bulb with electricity when it is actually needed, the light is plugged into a USB controlled surge protector instead of straight to the main power. As there is no control mechanism to toggle the light in this system, the only way to turn it off and on again at will is to toggle the surge protector. There is no direct communication protocol and thus the commands need to be passed through an application that is supplied with the device. This application accepts external commands via command line syntax [92]. A command

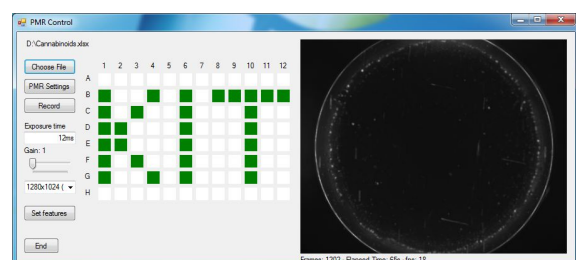
like `"C:\Program Files\Power Manager\pm.exe" -on -Device1 -Socket1"` would turn on Socket1 on the connected device1. With this all the required functionality is implemented and can be accessed from the GUI of the application.

The user is guided through the required steps to start an experiment. The GUI does not allow the recording straight away for example, as crucial information like the wells that should be recorded or where and under what name the files should be stored has not yet been supplied. The "Record"-button will stay disabled until all required metadata has been loaded. The camera's exposure time and gain settings, however, can be changed independently of this. An exposure time of 12 ms and a gain level of 1 has been empirically chosen as default values resulting in good image quality. There is also the option to change the resolution via a pixel binning mode that also increases the camera's sensitivity. However, all performed experiments have been recorded with the standard mode at 1280x1024 pixel resolution. Once the configuration file has been selected, the metadata will be displayed in form of a map of the well plate. By hovering the mouse pointer over a specific well a popup will display the associated metadata. The GUI and its functionality is displayed in figure 3.7 together with an explanation on the individual steps to start an experiment.

On startup the external hardware parts are initialized and a live image from the camera is displayed. Recording functionality stays disabled until a configuration file is loaded via the "Choose file"-button.



Once the configuration is loaded the associated information is used to display a map-like overview of the selected wells. Green indicates selected wells while white ones will not be recorded. The "Record"-button is now clickable.



On clicking the "Record"-button the experiment is either started immediately or at the specified time of the schedule. Every time the stage arrives at a target well its color will change to blue to indicate the current position.

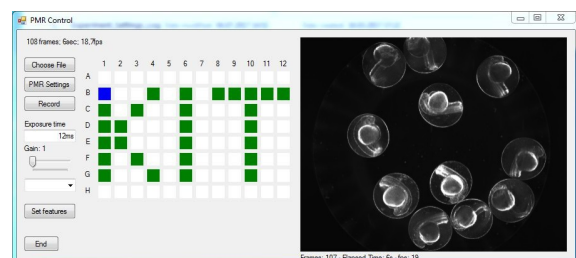


Figure 3.7: Overview of the PMR application GUI and the steps to start a PMR experiment.

It has to be emphasized that the focus for the software application was to make it accessible to researchers with various backgrounds. This means that setting up and starting a PMR experiment was designed to be as intuitive as possible with only a small number of settings and buttons that already recommend sensible values as defaults.

The Excel file required to load the metadata is given in form of a template that can be easily modified before each experiment. The well contents need to be entered and the wells selected. A cell-referenced representation makes this trivial and includes immediate feedback via a similar map like overview as in the application's GUI. Figure 3.8 shows the file that was used to generate the snapshots from figure 3.7 with random well contents.

Figure 3.8: Excerpt of the interactive PMR config file used to define well contents and other meta data like exposure time and age of the embryos. The file is used to tell the PMR application which wells are supposed to be recorded and how to name the corresponding videos depending on the well content. It also allows for recalibration of the well positions by supplying the well coordinates the motorized stage should move to.

With PMR being observable when the embryos are between 30 and 42 hpf and the fertilization typically happening in the mornings, the time of day an experiment can be performed at coincides with evenings and late nights. Also the successful execution of the PMR experiment relies on minimal human disturbance as zebrafish are easily startled by extraneous sound and vibrations [29]. To enable the user to set the experiment up to run time-displaced, the system was designed with a time based schedule and the possibility to check on the PMR imaging platform remotely via remote connections to the control computer.

The PMR settings window in figure 3.9 gives the user a number of options to adjust the default values to suit the intended experiment.

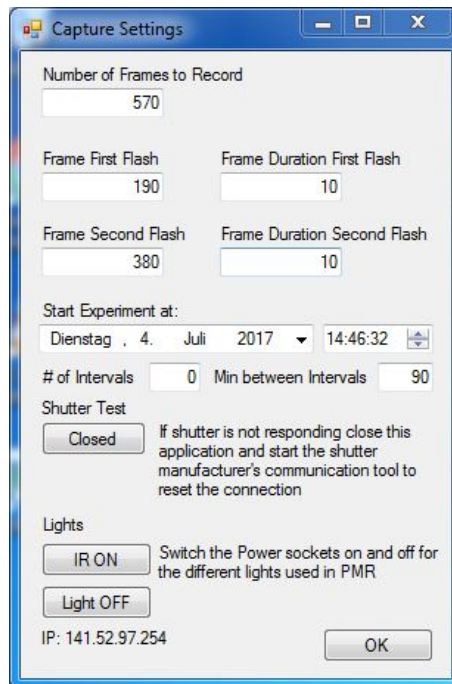


Figure 3.9: Detailed view of the settings section of the PMR application. It allows the adjustment of various parameters like the total video duration or the time points and duration the light is flashed. A timer feature allows the scheduling of experiments in terms of start time and repeats. With this the user can freely choose when an experiment should be performed and how many repeats are to be recorded at a chosen interval duration. Once set the system performs the PMR experiments without requiring the presence of the user. In case of a desired remote login the IP address of the current connection is required for the remote desktop connection which is why the IP address is also displayed to the user in the application itself.

With a frame rate of 19 fps and the established protocol lasting 30s the total number of frames to record was set at 570 as default. Similarly the light flashes are set to occur after 190 and 380 frames respectively. A programmed light flash duration of roughly half a second has shown to be sufficiently large to elicit a robust response. It has to be kept in mind that the shutter itself causes an intrinsic delay due to the digital signal needing to be processed and the actuation of the mechanical shutter taking time as well. Using a frame based counter instead of the time to measure the durations leads to perfectly synchronized videos between wells that can then be easily compared with each other frame by frame. The date and time picker objects underneath the recording settings can be used for a delayed start of the experiment and also repeat it for a defined number of times at a desired time interval. Once a recording is started the system will check and wait if the start time was set to the

future until that point in time is reached. The number of intervals keeps the recording in a loop that repeats the experiment after the set time and exits once the number of intervals has been reached. The IP address at the bottom can be used to remotely log into the computer to check the status of the system. The live preview is still fully functional when logged in remotely, allowing a detailed view on the status of the experiment without the need to be physically present.

3.3. Data Analysis

For video analysis, custom software [33, 66] was used and modified to better suit the framework conditions relating to our high-throughput photomotor response platform. This included the implementation of a recursive file search so that entire folder structures could be loaded and analyzed as well as improvements in the egg detection by including a weighting algorithm and removal of for this system unnecessary normalization steps during the motion index calculations. The graphical user interface of the “PMR Individual Motion Plot Extractor” (PIMP) can be seen in figure 3.10.

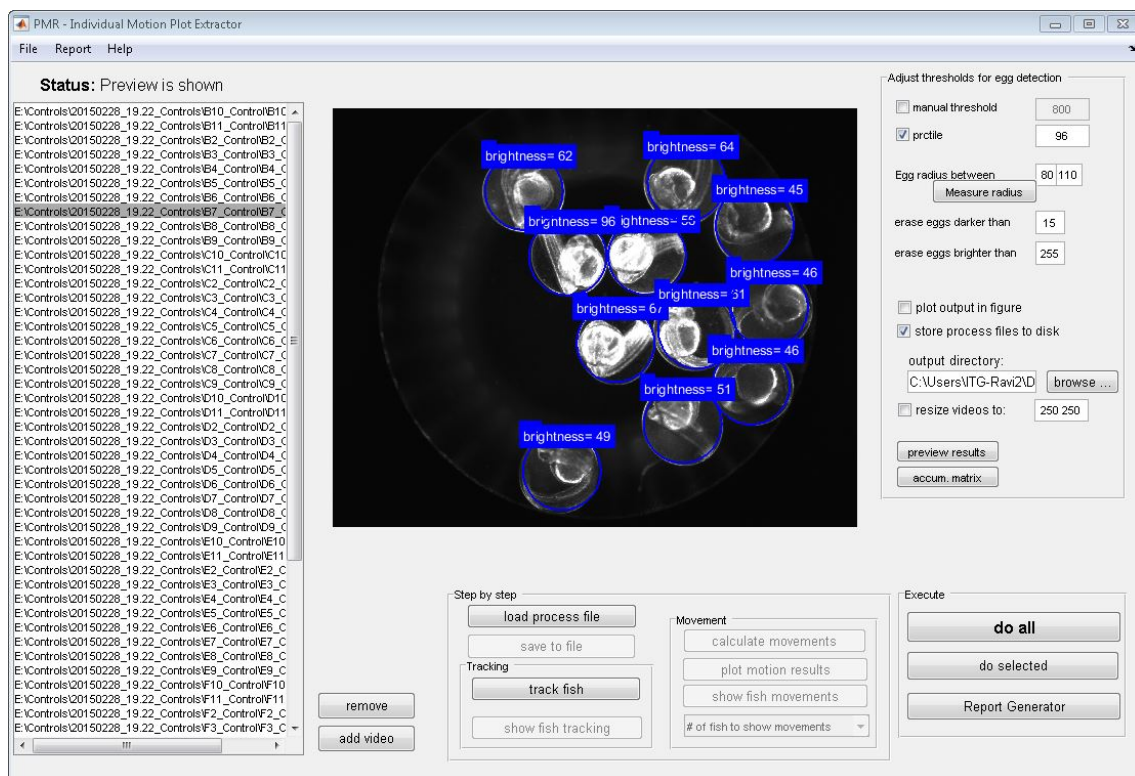


Figure 3.10: Overview of the GUI of the data analysis tool showing detected eggs in the preview window with additional detection information (mean brightness) of each egg. The tool allows the adjustment of detection parameters like the expected egg radii and threshold values.

The underlying analysis algorithm first detects the eggs in each video and afterwards evaluates a motion index representative of the movement of the embryos in that video. A typical analysis can now be started by loading an entire experiment folder containing all video files of that specific experiment. This was done by adding a recursive directory search with a file filter for AVI files that returns a list of all video files in the specified folder. By including subfolders in the search only the main result folder needs to be selected in order to get a list of all video files that are contained in it.

A preview window assists in adjusting parameters for the egg detection to suit the conditions in the video. There are a number of editable parameters like detection thresholds, probable egg radii and cut-off values to reduce wrong detections. Automatic resizing of the video files allows for an increase in processing speed and can be adjusted to the users' needs. The chosen settings will be applied and the motion index representing the movement of every single embryo is then calculated for all loaded videos. The resulting score is saved as a separate file next to each video file for later usage and visualization.

The actual tool relies on several methods to incorporate the described functionality. Egg detection is based on a Circular Hough transformation that is applied on the gradient field of an image. The resulting potential circle centers can be visualized in an accumulation matrix as shown in figure 3.11.

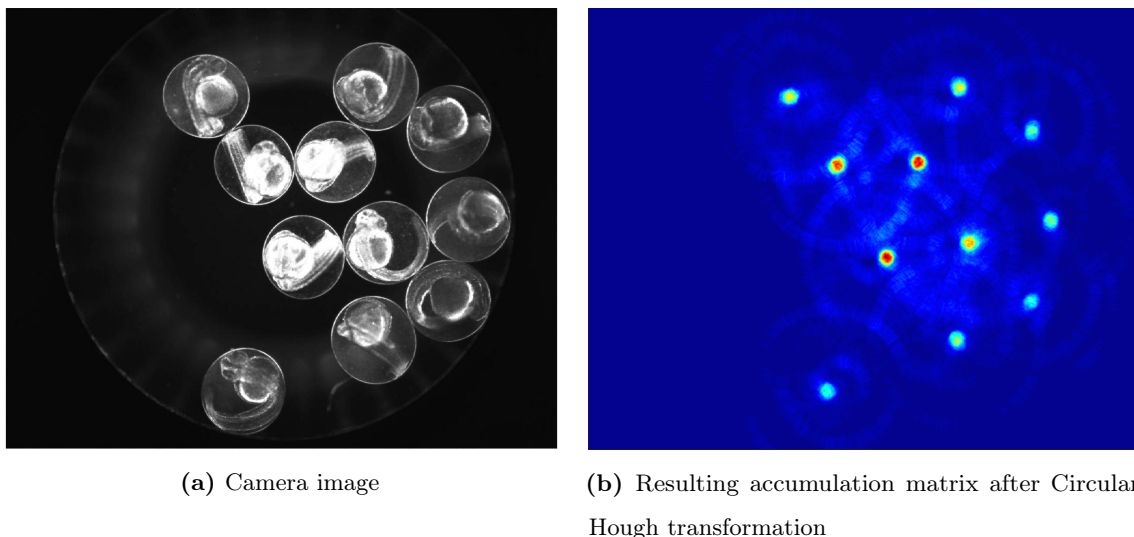


Figure 3.11: Illustration of the accumulation matrix as result of a Circular Hough transformation performed on the source image on the left. The resulting matrix is shown in a heatmap format with the potential circle centers being colored depending on their calculated probability values. In this example all embryos are detected as circles with no false detections.

The matrix is a representation of the statistical probability for each pixel to be the center of a circle. This is calculated by allowing pixels with a high gradient (ideally the outside of a circle) to “vote” on pixels on a circular path around them with the same diameter as the circle that is searched for. Figure 3.12 shows a simplified representation of this with a single circle whose center is then labeled as a red point.

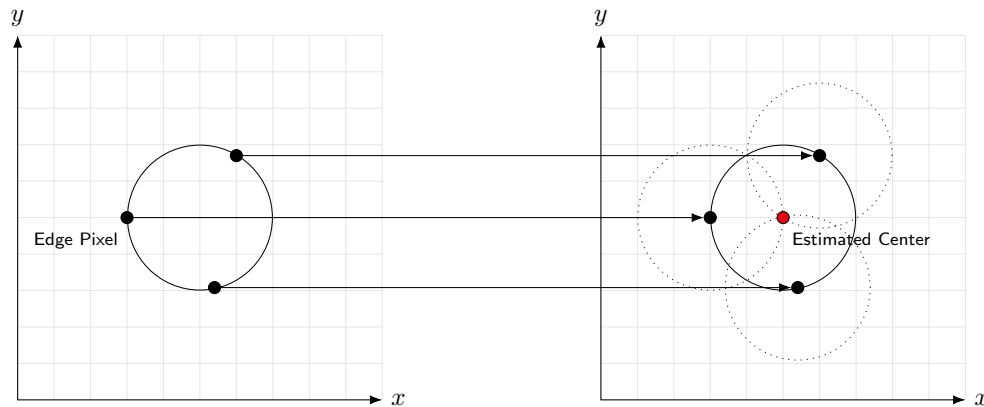


Figure 3.12: Schematic showing the principle of how Circular Hough transformations estimate the probability of circle centers for a fixed radius. It can be visualized as points on the circumference of the source circle building a heatmap of probability values by counting the number of intersections of circles drawn around them. A circle center will accumulate more intersections at its position than any other point.

Ultimately this will cause the votes to accumulate faster at the actual circle center than the surrounding areas. This can be seen in figure 3.11 with blue indicating a low number of votes while red indicates a very strong probability of the point being a circle center due to the high number of votes. A crucial parameter is the circle diameter that is searched for. If this is not exactly known a range might be supplied that causes the analysis to become a three dimensional task. The accumulation matrix now needs to be calculated for every possible diameter in the range and then the most probable centers are selected out of that group.

Depending on the detection threshold values the Hough transformation does not always detect every egg and due to the circular shape of the embryo tail inside the chorion and the multiple embryos in a well there is also the possibility of over detecting the number of circles. To reduce these issues, a weighting algorithm was developed that can be more sensitive as it only takes the most probable circle centers into account and erases the erroneous detections. This is based on the principle that there cannot be a circle center inside the area of another one as the embryos can only be placed next to each other and not overlap. By

looping through the candidates of the potential center locations in the accumulation matrix, starting with the most likely one, the region surrounding the circle center is replaced by a blank space that overwrites any too closely neighboring false detections. This is then repeated until the threshold level is reached which indicates the remaining probabilities to be too low to be taken into account.

Such a weighted detection result is shown in figure 3.13 with the detected circles being labelled according to their probability levels.

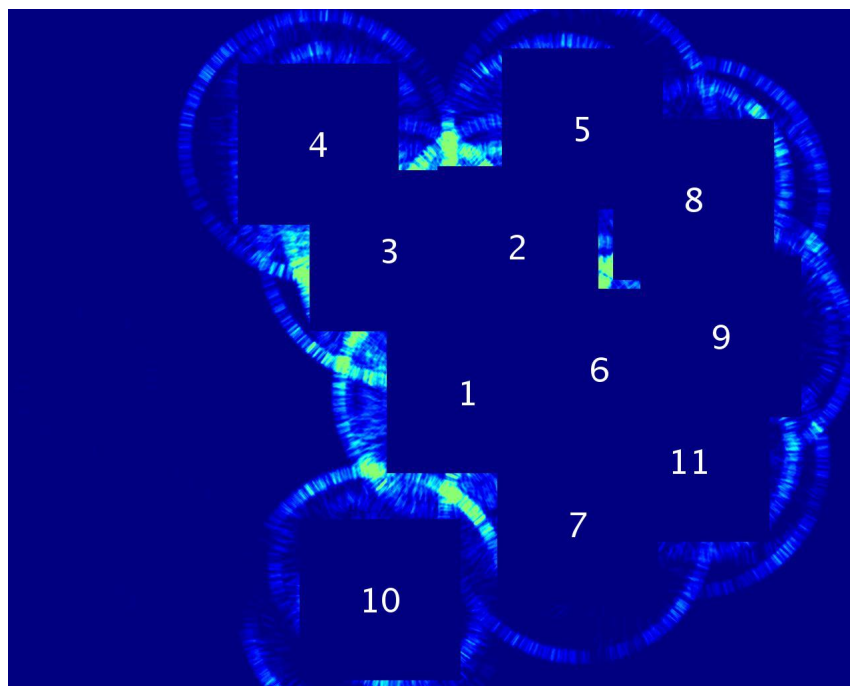
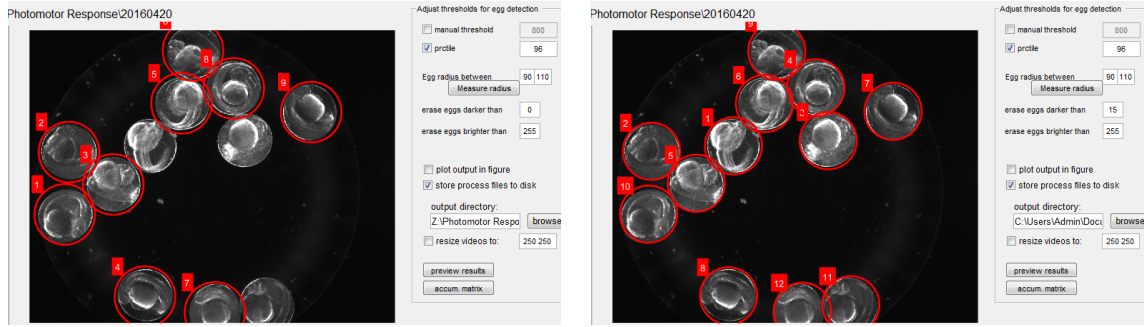


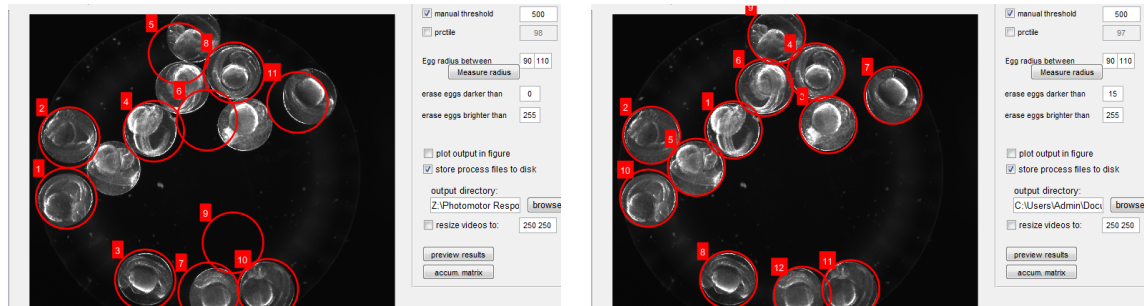
Figure 3.13: Weighted Circular Hough transformation accumulation matrix for motion index calculation for PMR. The detected circle centers are successively removed from the accumulation matrix until a threshold is reached by resetting their values. This is done in order to reduce false detections that could be positioned inside the chorion of an already detected embryo.

In figure 3.14 the benefit of this approach over the published method is shown by visualizing the egg detection on a random result video. It is obvious how the new algorithm improved the detection as it is able to find all the visible eggs with the same threshold values. The effect becomes even larger when suboptimal detection thresholds are used, proving that the new algorithm does also make the detection more robust as it is less prone to failed or erroneous detections in case the threshold is not set correctly.



(a) Results for traditional egg detection when using a dynamic threshold

(b) Results for new weighting algorithm when using a dynamic threshold



(c) Results for traditional egg detection when using a manual threshold

(d) Results for new weighting algorithm when using a manual threshold

Figure 3.14: Comparison of the detection results between the traditional and newly established egg detection algorithms. For a dynamic threshold the traditional algorithm detected 9 out of 12 eggs while the weighting algorithm found all eggs correctly. In case of a suboptimal manual threshold false positives show up and only 7 eggs are detected correctly. The weighting algorithm is much more robust and results in all eggs detected correctly even when the threshold is not optimal.

Once the initial positions of the embryos are found the next step is to track their locations over the duration of the video. This is done via a template matching procedure that has proven itself to be quicker than a continuous circle detection on every frame and will result in time-series data for each individual egg in a rectangular ROI. To convert motion into a numerical value it can be assumed that a change in consecutive frames can only be caused by a moving object. The change due to motion is observed to be significantly larger than that due to image noise and the ROIs of two consecutive frames are, therefore, subtracted to extract the amount of change. The resulting value then has to be normalized by the number of pixels inside the ROI. Normalization is necessary to compensate for varying video resolutions and differing egg sizes while still returning comparable motion indices. A masking step before the actual frame differencing ensures that no neighboring eggs have an

effect on the resulting score. With a rectangular ROI there would otherwise be a potentially large source of error. Figure 3.15 shows how much of a corner area is susceptible to be allocated by a neighboring egg.

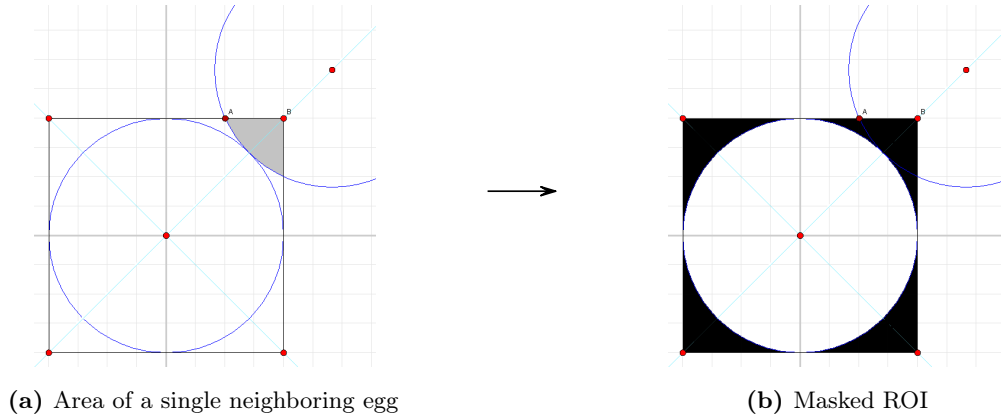


Figure 3.15: Illustration of how the square ROIs for the circular embryos need to be masked in order to not account for movement of neighbouring embryos in the motion index calculation.

The area when all four corners are allocated by an egg can be calculated to be almost 20% of the actual object area. With the chorion not always being perfectly circular this area can potentially be even larger. Therefore, without a masking step the motion index score could be heavily influenced by embryos surrounding the ROI. The masking causes all pixels inside the ROI but outside the actual embryo to be set to 0 and thus have effectively no weight in the following calculation for the motion index. The score is in principal calculated according to the sum of absolute differences as shown in equation 3.2. $M_{i,e}$ represents the motion index and $I_{i,e}$ is the cropped image at frame i for embryo e with its individual grayscale pixel intensity values between 0 and 255. In this case normalization was based on the total number of pixels in the current image section $N(I_{i,e})$.

$$M_{i,e} = \frac{\sum_x \sum_y |I(x,y)_{i,e} - I(x,y)_{i-1,e}|}{N(I_{i,e})} \quad (3.2)$$

This motion index calculation is visualized in figure 3.16 by showing how the number of changed pixels influences the score with two examples from two separate time points in a PMR video. The one from the basal movement phase shows no obvious movement of the fish with it being positioned similarly in both frames. The calculation thus yields a low motion index score as only a small number of pixels changed in between frames. This is different for images from the excitation phase where the embryo is rapidly moving and changes its position inside the chorion. This causes the calculation to result in a high motion index due to the large number of pixel values that have changed.

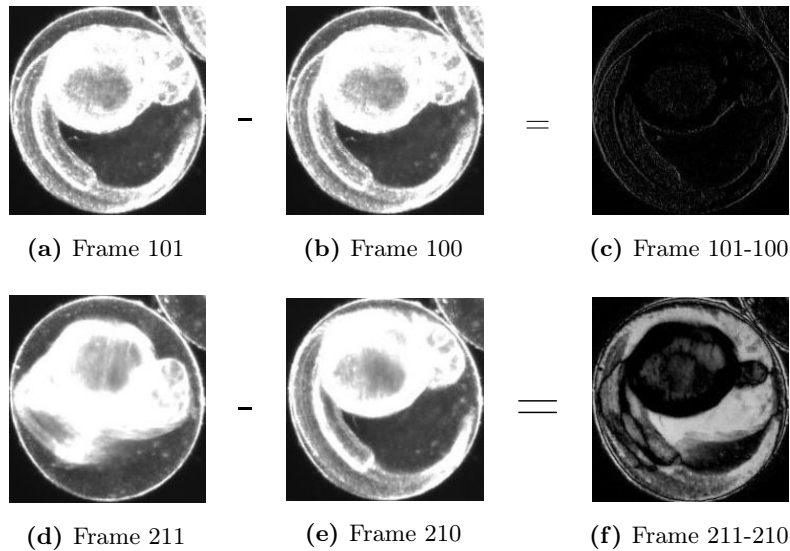


Figure 3.16: Illustration of frame differencing for motion index calculation. In a-c almost no change is visible between frames so the frame difference will result in a low score. d-f show a lot of movement with many pixels changing which will result in a high score.

The actual tool also includes a number of filters and normalizations that are put in place to smoothen the results and make them more immune to noise or artifacts. However, during the addition of the weighting algorithm some seemingly counterproductive normalization factors were removed due to them causing unwanted behavior during the motion index calculation. Figure 3.17 shows two graphs of the motion index scores of chemically treated embryos with an altered PMR. Both have the scores for the same video but one shows the results for the traditional calculation and the other the improved implementation.

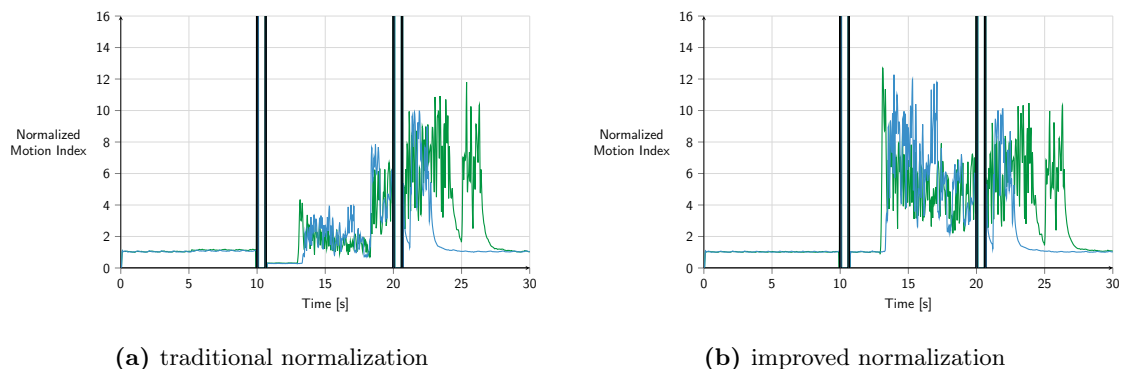


Figure 3.17: Comparison of the normalization between traditional and improved version. The traditional version shows a sinking baseline and an abrupt increase in the score values. A manual observation also verified this defect with no reason for the unstable behavior being visible and the improved normalization representing the expected behavior more closely.

In the traditional algorithm there is an obvious defect in the normalization with the baseline sinking after the first light flash and abruptly increasing again during the delayed movement phase without the embryos actually behaving differently at that point in the video. By simply removing this normalization step a much more uniform and true representation of the embryos' movement could be achieved.

An automated tool like this makes the analysis of large data sets manageable. All the user has to do is select the folder that contains the videos that should be analyzed and set the necessary values for robust egg detection so the tool can work on every file automatically. However, during the development of the PMR pipeline it became clear that using the GUI is actually unnecessary most of the time as the settings values stay the same for a particular optical setup and thus there is no need to manually set them time and time again. Due to this, the underlying analysis functionality was extracted from the GUI application and put in a single function that can be called with a selection of parameters. This also allows the external start of an analysis by utilizing the Matlab option to have it start from the command line and directly start working on a supplied function call. Thus, the PMR application was equipped with an analysis loop that gets activated once an experiment with all its repetitions is finished. The loop will start several Matlab instances simultaneously to speed up the analysis process so that the results will already be waiting for the user instead of first having to start the analysis manually. The number of Matlab instances can be set according to the available RAM and CPU cores. In this case a maximum of four parallel processes was found to be optimal, utilizing all cores of the CPU while still having sufficient RAM available so that no paging was required. On the computer that was used this resulted in the analysis duration for a full plate with 96 videos to be reduced to just 58% of the time it took for the analysis to complete on a single instance of the manual tool. With this, the flowchart from figure 3.6 has to be extended to what can be seen in figure 3.18 with the Matlab analysis added as an additional object that is accessed via a command line process.

The Matlab analysis takes care only of the raw extraction of numerical values for the motility of the embryos. In order to use this data in statistical comparisons between various conditions, however, an additional tool was developed that allowed the identification of various parameters such as the quartile values for each phase, mean values, maximum and minimum values as well as the sum of score values. Depending on the research interest, new parameters can easily be implemented as the result structure is generated dynamically and stored as a separate file for later visualization.

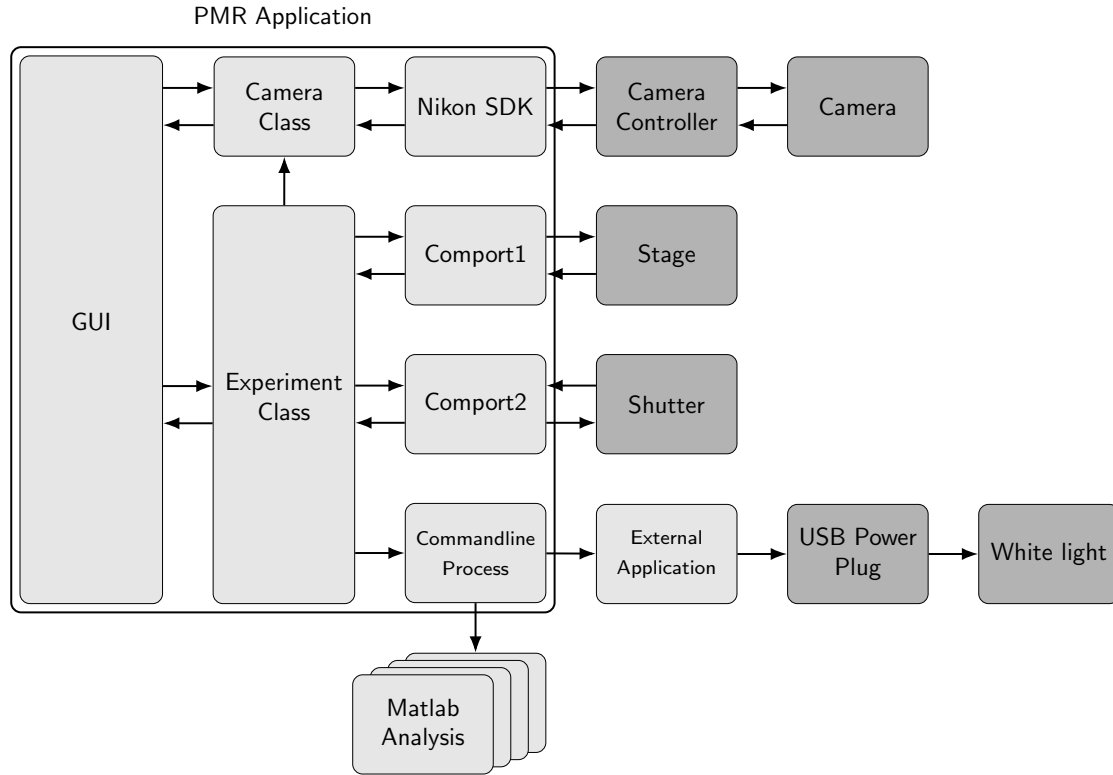


Figure 3.18: Flowchart of the final PMR application that includes analysis of the resulting videos by implementing a command line process loop that manages multiple Matlab instances.

One objective during the development was to be able to directly group results from wells with identical content in order to eliminate the manual sorting of data. Based on the same recursive file listing as the updated PIMP application, the tool was equipped with a grouping algorithm based on a regular expression search pattern. The file names of the result files in a folder are analyzed, compared and the files grouped accordingly. The left list in figure 3.19 shows a list of all the detected individual result files while the list in the middle displays the extracted groups contained in the list of files. The list on the right can be used to exclude eggs that show only low motion index scores from the analysis. This was used for debugging purposes to have the option to eliminate immobile embryos as they could often be defined as malformed or retarded which could render them unsuitable for consideration in the visualization. In the second step the tool extracts the motion index score of all the individual eggs of a group and stores them in one large matrix.

Because subtle effects like heartbeat, camera noise or sometimes even floating compound precipitations were observed to change the baseline level of the motion index, an additional normalization step was introduced. An average over the lowest non-zero values gives a dynamic normalization factor that is adjusted for every embryo individually and normalizes the score to a uniform baseline with value one.

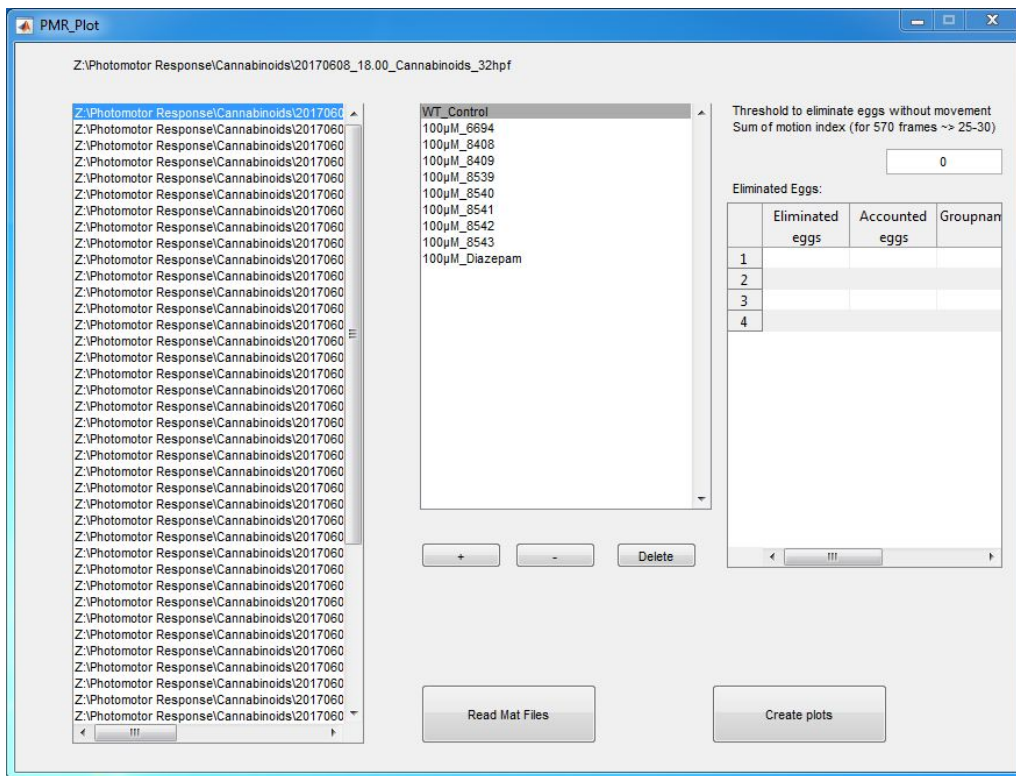


Figure 3.19: PMR score analysis tool that is used to visualize the results by grouping results of similar well content together based on their naming scheme and can then perform ANOVA analysis as well as heatmap creation. Left column: individual result files. Middle column: extracted groups. Right column: list used for debugging purposes to eliminate potentially coagulated eggs based on their low motion index.

By finding the light flashes, the tool is then able to split the score into its three phases and extract several statistical parameters like the average score in the phase or the number of peaks and so on. The results are stored and the scores are plotted in a heatmap format for visualization like the ones in figure 3.20. By selecting a “reference” group in the tool, it can also be used for direct statistical comparisons. A proof of concept was implemented that performed ANOVA analysis between every group and the “reference” group for the first and third quartile values of the motion index for a collection of 7 phases similar to the barcode values shown by Kokel et al. [32]. However, for the screening of cannabinoids this array of 14 values appeared to be unnecessarily complex and did not allow the simple categorization that was required. Therefore, a simpler yet for the intended purpose of categorization sufficient group of parameters was established in the sum of the normalized motion index scores. By using only the sums of each phase per embryo the comparison of the compounds’ effects could be based on a total of just three values that can be visualized in boxplots that also give information on the statistical variance in the population.

3.4. Validation Screens

To evaluate the system a number of pilot experiments were carried out with neuroactive compounds that have already proven [32] effects on the PMR. Once the system was validated and the usage protocols established, it was immediately used to support researchers from the ComPlat-group at KIT by screening a compound library consisting of novel, synthetically produced cannabinoid-like structures for which the effect on living systems was unknown.

3.4.1. Initial Validation Screen

Isoproterenol is a β -adreno-receptor agonist that is supposed to cause an increase in motor activity over the entire PMR experiment duration. Converse effects can be caused by the dopamine-receptor agonist Apomorphine. Apomorphine increases the reaction time to the light flash by several seconds. The expected behavior could be reproduced and validated with the developed system, which robustly handled the high-throughput experiments. Figures 3.20 to 3.23 show some of the results of the various PMR validation screens.

The line plots show the motion index curves for candidates from an individual well over the 30 s time period. For better visualization heatmaps are used that show one embryo per row, as line plots would otherwise get too crowded with the overlays covering some of the results. Brighter colors in these heatmaps represent higher motion indices with the light flashes being presented as white lines. The graphs visualize the expected behavior for control conditions and neuroactive compounds very well. While the control shows a drastic increase in motion almost immediately after the first light flash (just like what is to be expected from figure 3.1), the Isoproterenol causes a lasting increase over the entire time frame that is independent of the light flashes. Apomorphine delays the response for several seconds which causes a shift to the second light flash and even into the refractory period. Diazepam (also called Valium) is known to have a calming effect. This is perfectly represented in the PMR results as the embryos show no response to the light flashes and stay immobile. The remaining motion index can be assigned to noise from the camera or heartbeat for example. It has to be noted though that PMR suffers from a large variance in the sample population, with not all embryos responding the same at all times. Variance is a known issue when dealing with behavior since variation in the genome as well as developmental differences are vital for all living organisms [93] and thus inherently present even in siblings of the same strain. Only by using a large enough number of samples, can the true effect be described with the required certainty. For this reason a sample size of at least 50 embryos was chosen for any future screens.

3.4.2. Cannabinoid Library Screen

The ComPlat-group at KIT focuses on the collection, storage and sharing of compounds that have been created in various research projects. They specialize in solid phase synthesis to create novel compounds that directly address research questions in cooperation with biologists and other collaboration partners. One of the projects led to the accumulation of a library of cannabinoid like structures. However, there is no information on how these compounds act on a living system, what their effect might be and how well they could perform as medical drugs. With cannabinoids being a neuroactive compound class that targets specific receptors in the central nervous system that affect neurotransmission, it is important to find out more about their mechanisms and how they can be improved. Ultimately the effect on the human nervous system is supposed to be determined, however, to give a first indication on the activity of the compounds on a living organism a test with zebrafish is the most feasible way.

The endocannabinoid system plays an important role in a well-functioning human body. It is involved in some of the most fundamental mechanisms like learning and memory, energy balance, the regulation of appetite, stress and emotions as well as inflammation [94]. There is evidence that multiple receptors are involved in the signaling cascades [95], with CB1 and CB2, however, being the two predominant G protein-coupled receptors. While CB1 is mainly expressed in neuronal structures, CB2 receptors are mostly located in immune cells [96]. The typical effect a cannabinoid like Δ^9 -THC has on a living system like mice is the presence of at least one of the four responses in the mouse “tetrad” assay which includes analgesia, sedation, catalepsy and hypothermia [97]. Testing of the neuroactivity of novel compounds could, therefore, be done with a mouse model. But as already described in chapter 1 mice are uneconomic when a large number of tests has to be done. With more than 250 compounds in the ComPlat-library an alternative approach was found in zebrafish. Since CB1 starts to appear in the fish after 24 hpf [98] a zebrafish assay at a later age can be performed. With PMR occurring between 30 and 42 hpf and its potentially large number of observable specimens in a 96-well plate format, it was chosen as new approach for cannabinoid compound analysis.

A total of approximately 250 cannabinoid like compounds and derivatives were tested with at least five repeated wells per compound. This results in the analysis of roughly 50 to 70 embryos per compound to increase statistical accuracy. The compounds can be categorized into two classes of base structures from known cannabinoids. They are shown in figure 3.24 together with examples of how the structures were modified to synthesize novel derivatives.

Around 47% of the tested compounds showed an effect on the behavior of the fish compared to untreated wildtype. In close collaboration with ComPlat, 19 of the compounds were chosen for more intensive studies in terms of a dose response due to their interesting chemical structures. The naming scheme of the compounds was chosen to be obfuscated on purpose to prevent any bias during the analysis. Therefore, a seemingly random numbering was used with a three to four digit number as identifier. Data was acquired in the scope of a supervised bachelor thesis at the KIT [99]. Five distinct patterns were identified that the responses could be categorized into. Figure 3.25 shows these patterns in the heatmap format plus the result for known and commercially available cannabinoid HU-210. HU-210 is said to be magnitudes more potent than naturally occurring THC when tested on pigeons and rats [100].

A range of effects can be observed with the most striking difference being the overall level of activity especially in the excitation phase after the first light flash. While compounds like x8140 show a response that is very similar to the untreated wildtype control, patterns like x8144 can best be described as causing a decrease in PMR while x8246 could be classified as completely eliminating any movement activity. The heartbeat was checked on these animals to guarantee only living embryos are contributing to the resulting data. A seemingly scattered movement is caused by x5745 with random bursts of activity over all phases. Another distinct response can be enforced via x4398 that causes the embryos to respond to the second light flash just like they did to the first. Instead of going into a refractory phase they seem to stay highly sensitive to the light flashes. Out of the 250 tested compounds this was the only one that showed this behavior. Commercially available HU-210 shows a decreased activity in the PMR at the chosen concentration of 100 μ M, possibly indicating that the expected PMR behavior for established cannabinoids is the general activity reduction. However, this is only a theory and needs to be tested with further experiments. One approach could be the use of a cannabinoid receptor antagonist that could selectively block the cannabinoid receptors and keep them from being activated by the cannabinoid-like compounds. If the effects are still observable then, this would mean that the patterns cannot be attributed to the endocannabinoid system but some unknown secondary pathway.

A dose response screen was performed to find out more about the potency of these compounds. To be able to eventually identify the residues and side chains that might be responsible for a certain effect, a group of 19 compounds was selected due to the differences in their structure. Six concentration steps were chosen at 1, 10, 30, 50, 70 and 100 μ M respectively.

The results are shown in a boxplot format, taking into account the statistical variation of every individual embryo. Green boxes indicate the basal movement while red represents the excitation phase and blue the refractory period. The motion index scores were summed in these phases and the summation results then used as data for the boxplots.

Overall the effect on the PMR correlated very well with increasing concentrations. While no effects could be observed at a low concentration of 1 μM they usually increased at higher concentrations. This was especially obvious with drastic effects like the ones caused by x8246 or x5745 that are shown in figure 3.26 together with x8140 that got classified as similar to wildtype and shows similar responses on every concentration step. It is also true for x4398, where an increase in activity in the refractory phase is visible above a 50 μM concentration.

3.5. Conclusions

The first fully automated and remotely controllable system was developed that allows for high-throughput screening of the photomotor response in zebrafish. The platform was established and could already be extensively validated in various screenings. It consists of an automated sample handling stage (via the egg sorter robot), imaging (via the scheduled or remotely controllable microscope-based system), data analysis and visualization and offers a number of noteworthy differences to previously published or commercially available systems. With this the usage of PMR in zebrafish could be improved substantially by making it more robust, more versatile, cheaper, easier to use and more convenient:

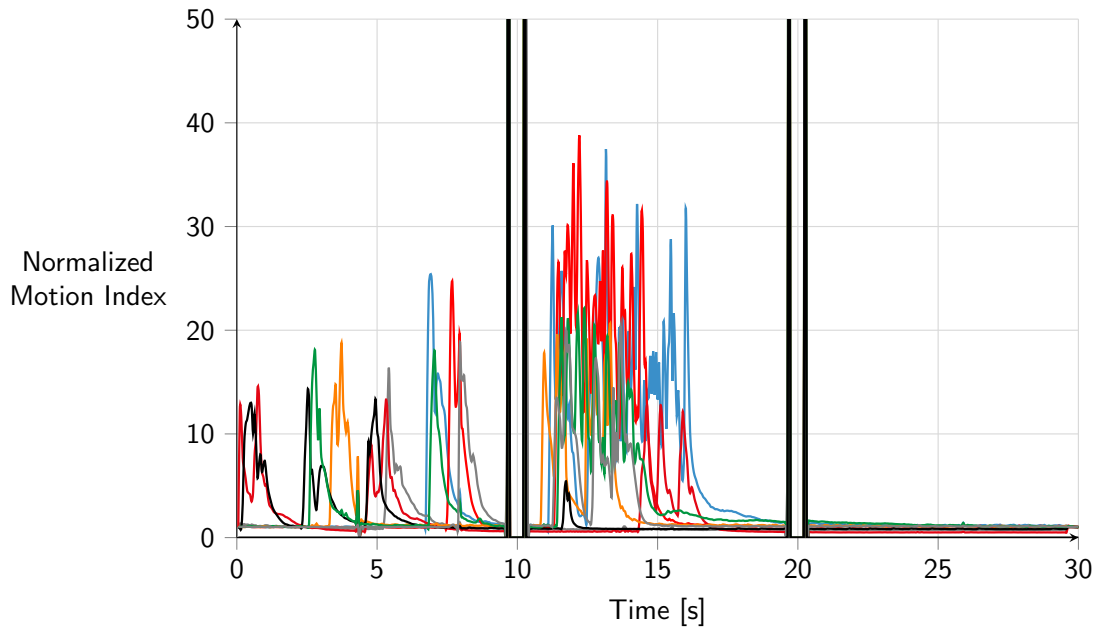
- Fully self-developed and independent control software requires only the hardware to be bought to build a functioning PMR microscope. External software packages are either open-source or available free of charge from the manufacturer and are usually already included when buying the hardware. This enables researchers to easily set up PMR as a new tool in their labs without having to pay unnecessary fees for the control software.
- An effective LED illumination ring was described that can be used to retrofit IR capabilities to almost any microscope.
- Higher resolution allows the subsequent use of the recorded videos for additional analysis in terms of morphological changes or other behavioral endpoints like heartbeat. With this the embryos can be analyzed more detailed than on other PMR hardware.

- An improved egg detection was implemented for the motion index calculation that proved to be more robust to threshold changes than the originally devised method.
- Direct integration of the analysis tool in the control software requires less user interaction and makes the system even easier to use.
- A tool for advanced result analysis and visualization was established that can group results according to their content.
- The system includes scheduling capabilities and was built to be fully remotely controllable. This significantly improves its usability for the recording of multiple time points and allows experiments to be performed without human presence.

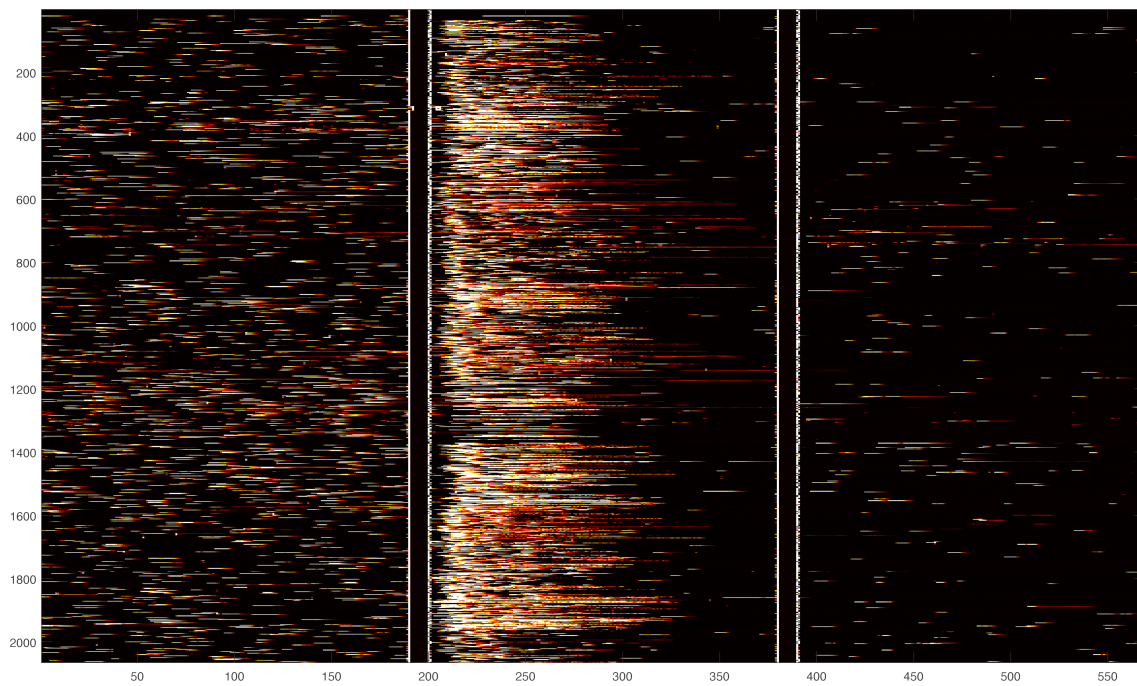
Table 3.2 gives an additional summary of the features of the two prominent systems and illustrates the improvements that have been achieved with the development in this work. The proposed system was successfully used in pilot screens, providing good results in terms of reliability and robustness of the platform. A comprehensive screen for novel cannabinoid-like structures was performed that was already able to offer new insight into the neuroactivity of said compounds. In the future this platform can easily be used for the characterization of other neuroactive and psychotropic compound libraries as well as genetic mutants.

Table 3.2: Overview of the feature sets between the originally published system by Kokel et al. [32], Viewpoint’s ZebraBox and the proposed system from this work [70].

Feature	Kokel et al.	ViewPoint ZebraBox	Marcato et al.
Automated sample handling	-	-	Egg sorter robot
Base equipment	Standard microscope	ZebraBox with add-on module	Standard microscope
Recording method	Well after well	Multiple wells simultaneously	Well after well
Camera resolution	≈450x450	2048x2048	1280x1024
Remotely controllable	-	?	✓
Scheduling ability	-	-	✓
Independent and free software	-	-	✓
Analysis pipeline	✓ [66]	✓	✓ [66] with improved egg detection

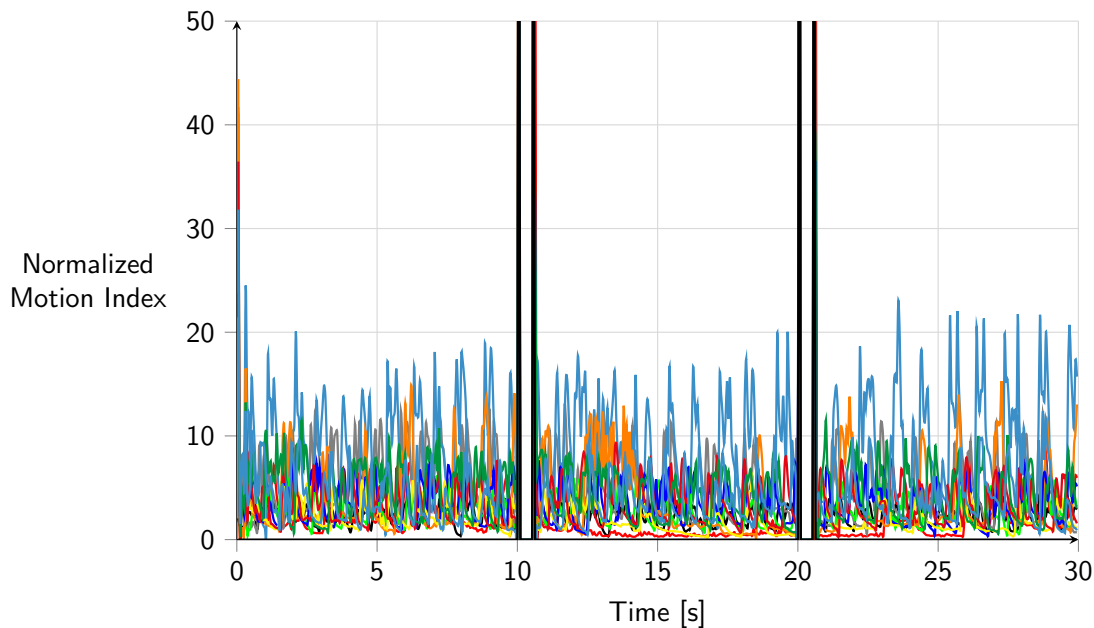


(a) Wildtype control (without neuroactive compounds) in a line plot of a single well

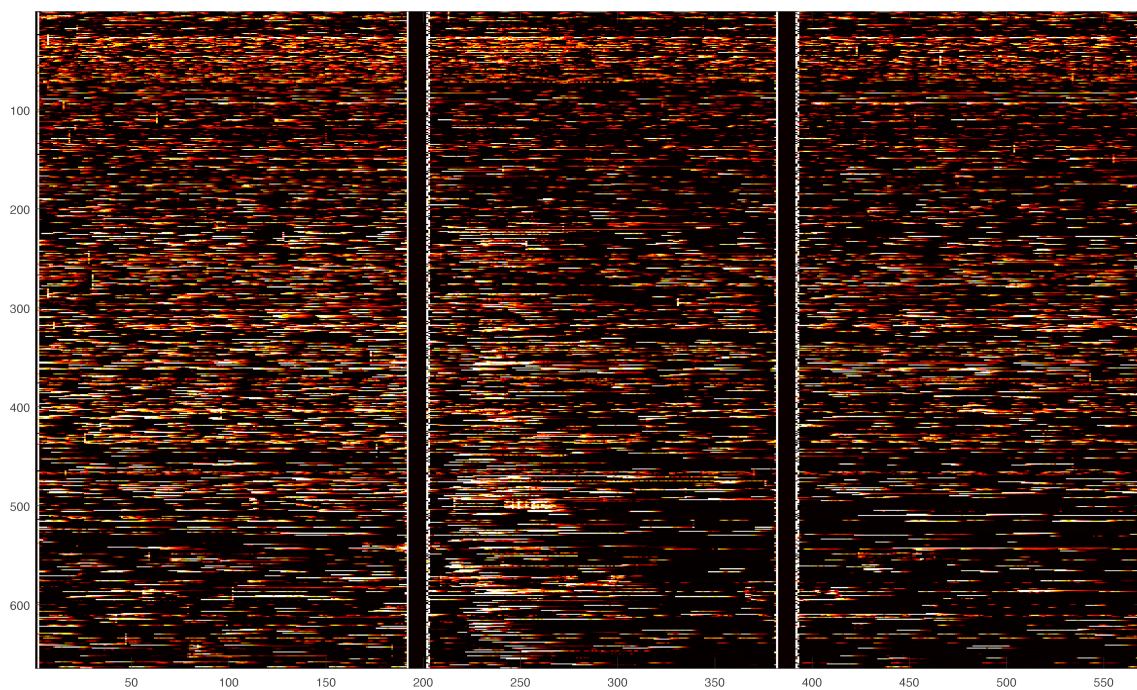


(b) Heatmap visualization for WT data from multiple wells. Each row represents an individual embryo.

Figure 3.20: Results of the PMR validation screen showing the effect various neuroactive compounds at a concentration of $100\ \mu\text{M}$ have on zebrafish embryos. The WT control shows a drastic increase in motion almost immediately after the first light flash. In graph (b) the motion indices of more than 2000 individual embryos from several experiments are shown. Brighter colors in the heatmaps indicate movement with higher motion indices.

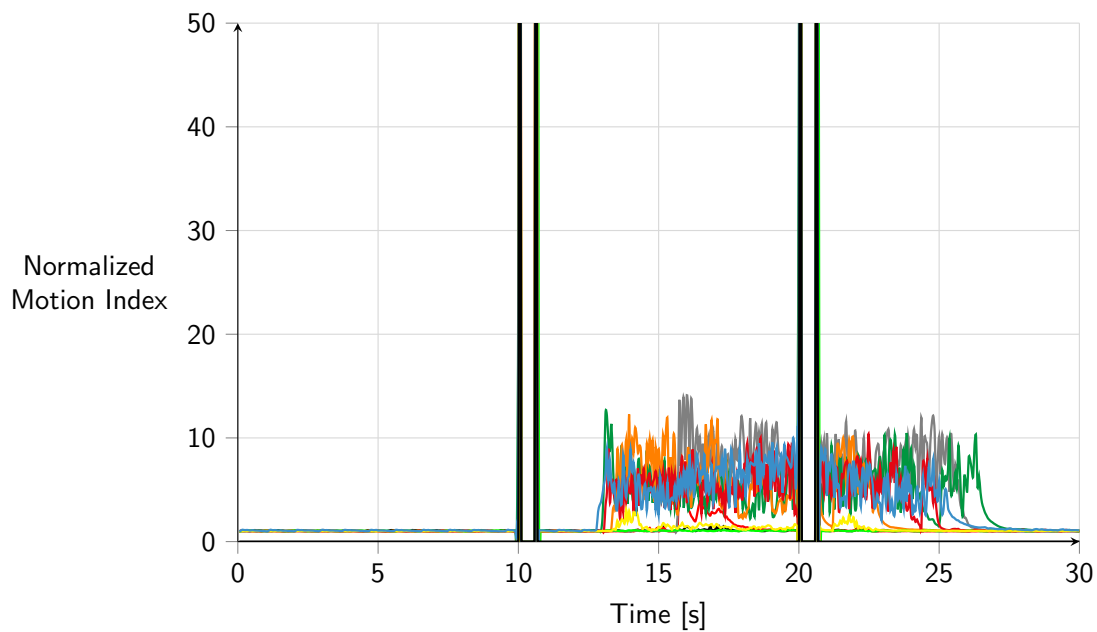
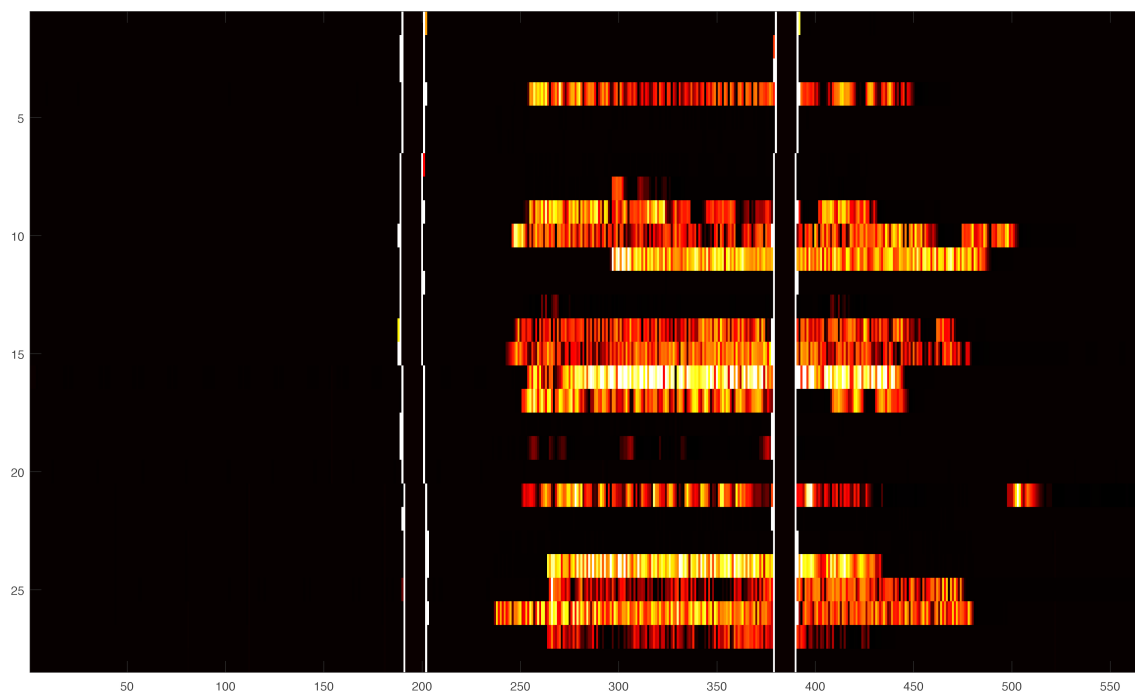


(a) 100 μ M Isoproterenol



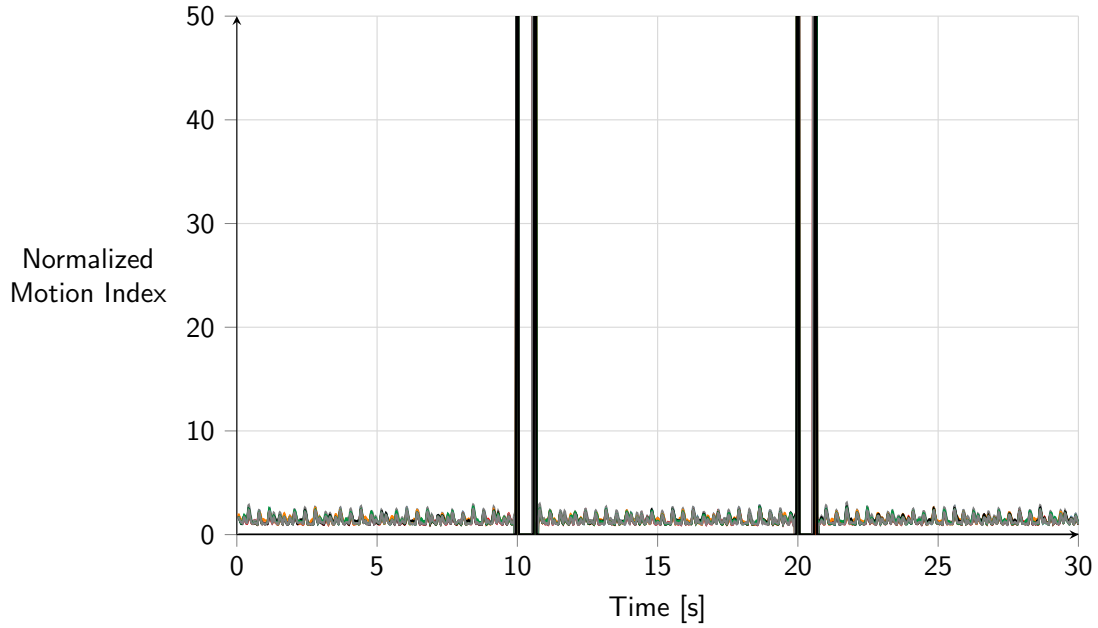
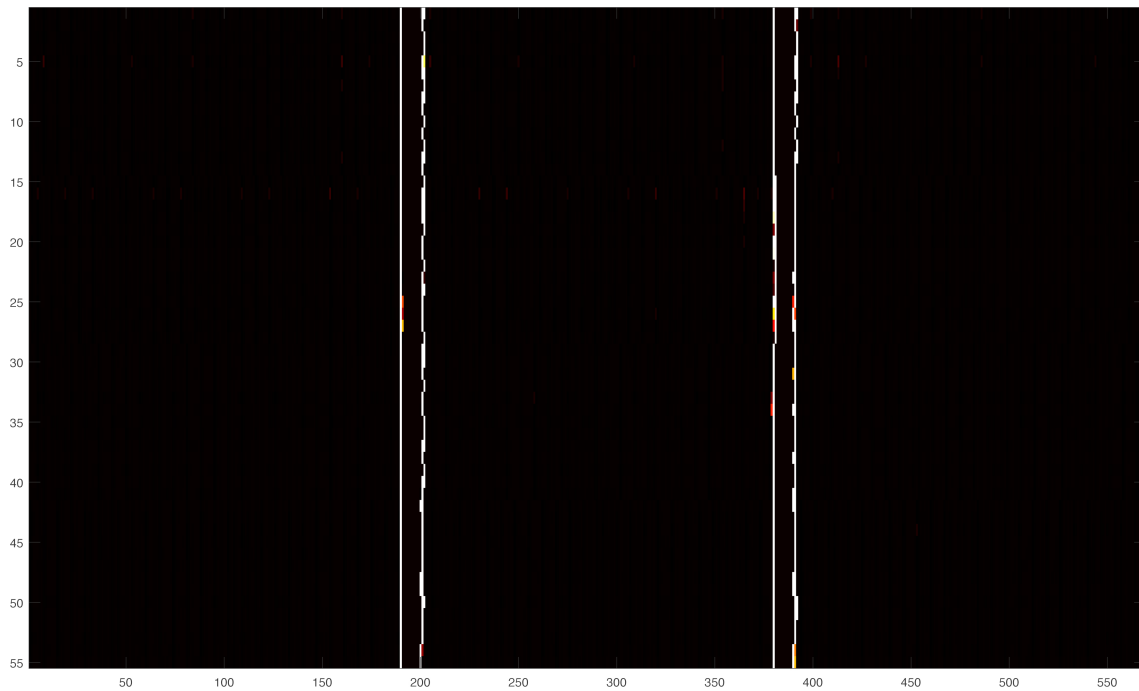
(b) Heatmap visualization for Isoproterenol data

Figure 3.21: Results of the PMR validation screen showing the effect various neuroactive compounds at a concentration of 100 μ M have on zebrafish embryos. Isoproterenol causes a lasting increase over the entire time frame. (b) shows the results for more than 600 individual embryos from multiple experiments. This is due to Isoproterenol being chosen as a positive control when screening other compounds. Brighter colors in the heatmaps indicate movement with higher motion indices.

(a) 100 μ M Apomorphine

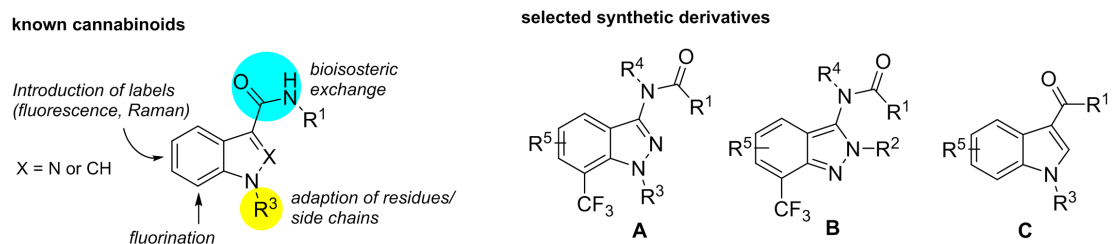
(b) Heatmap visualization for Apomorphine data

Figure 3.22: Results of the PMR validation screen showing the effect various neuroactive compounds at a concentration of 100 μ M have on zebrafish embryos. Apomorphine delays the PMR but causes a prolonged excitation. Brighter colors in the heatmaps indicate movement with higher motion indices.

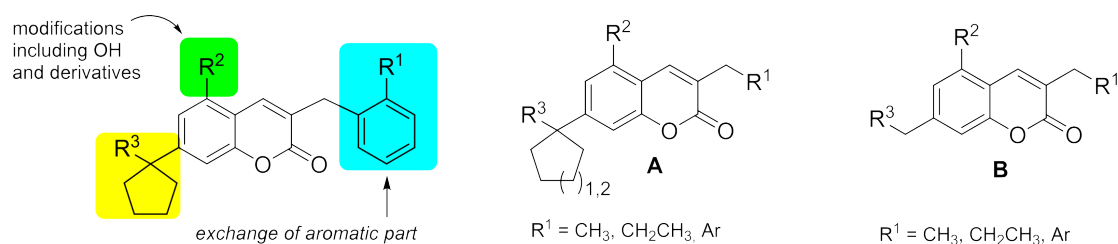
(a) 100 μ M Diazepam

(b) Heatmap visualization for Diazepam data

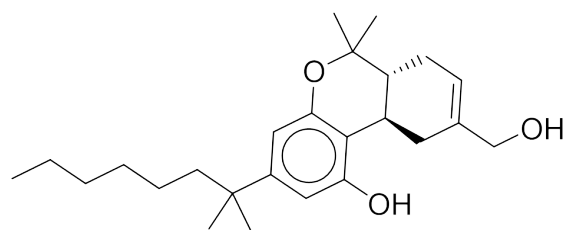
Figure 3.23: Results of the PMR validation screen showing the effect various neuroactive compounds at a concentration of 100 μ M have on zebrafish embryos. Diazepam calms the embryos down so that no movement is observable anymore. The small peaks in the line plot are most probably due to image noise and subtle movements like heartbeat. Brighter colors in the heatmaps indicate movement with higher motion indices.



(a) Compound class I (indazoles and indoles): structural adaptations of chemical library members in comparison to literature known cannabinoids (left), structures of the three main core components (right).



(b) Compound class II (coumarins and chromenes): structural adaptations of chemical library members in comparison to literature known coumarin-based cannabinoids (left), structures of the two main core components (right).



(c) known compound HU-210 of class II

Figure 3.24: Illustration of the two general compound classes investigated in this study and how their derivatives are synthesized. The commercially available known cannabinoid HU-210 is shown as an example for compound class II. Images courtesy of Dr. Nicole Jung (Karlsruhe Institute of Technology).

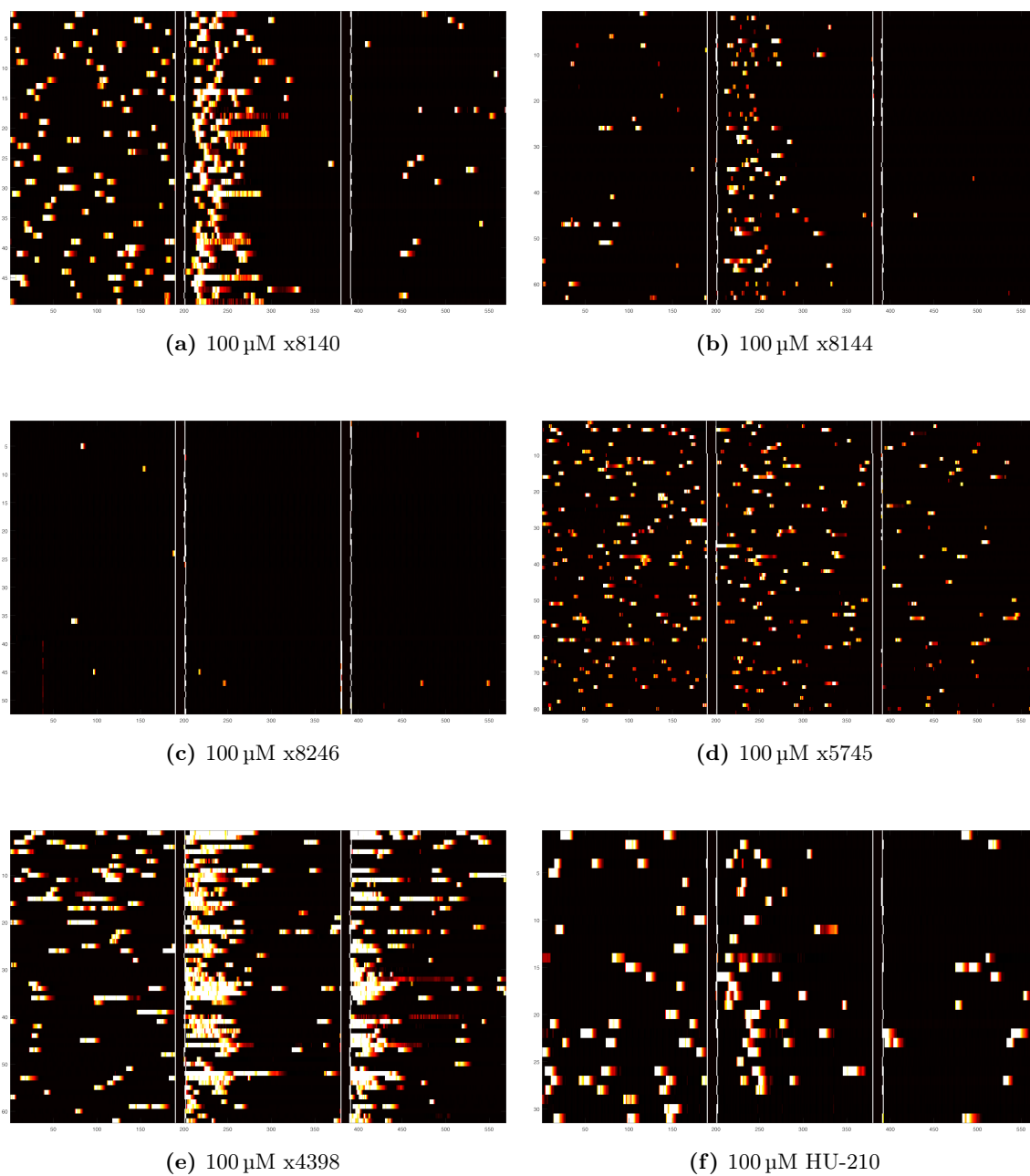
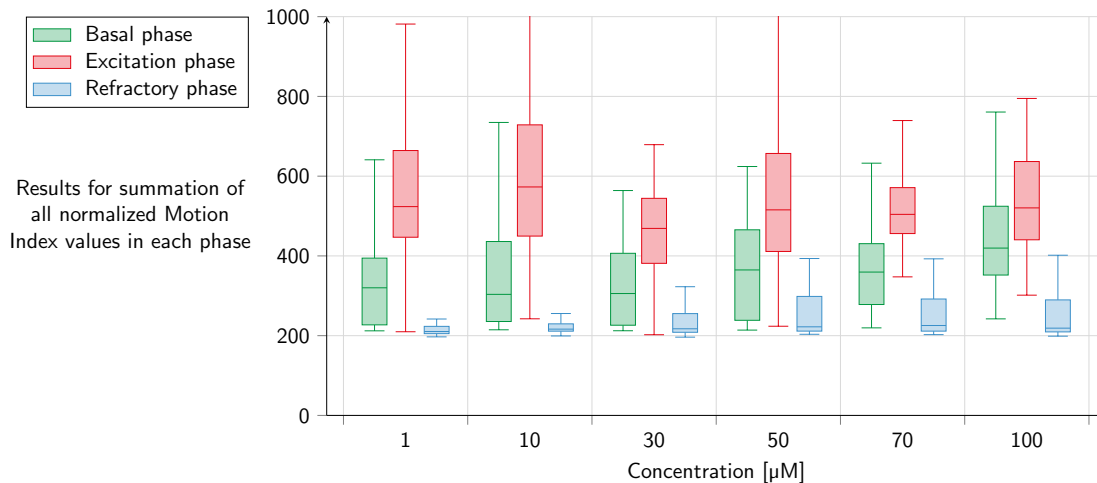
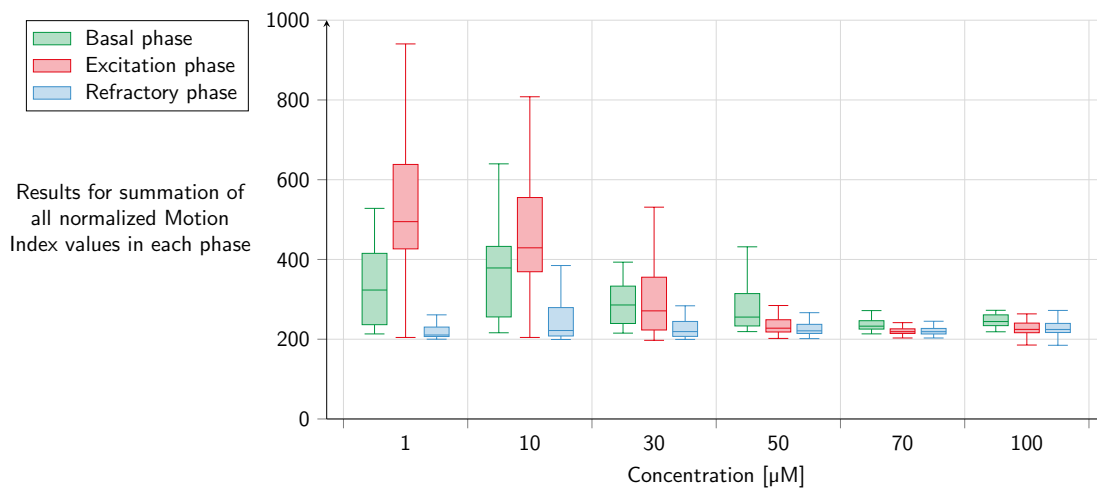


Figure 3.25: PMR results for selected cannabinoid compounds at 100 μ M concentrations. x8140 resembles the untreated WT while x8144 shows a large decrease in PMR. x8246 has an even stronger effect with almost no observable activity. x5745 was categorized to have a scattered movement with seemingly random bursts of activity in any of the phases. x4398 shows a so far unique behavior with seemingly hypersensitive embryos that also react to the second light flash. Commercially available compound HU-210 was tested as a reference compound and shows a reduced PMR. The axes are the same as in the previous heatmaps in figures 3.20-3.23 with variations in the number of tested embryos on the y-axis between the graphs.

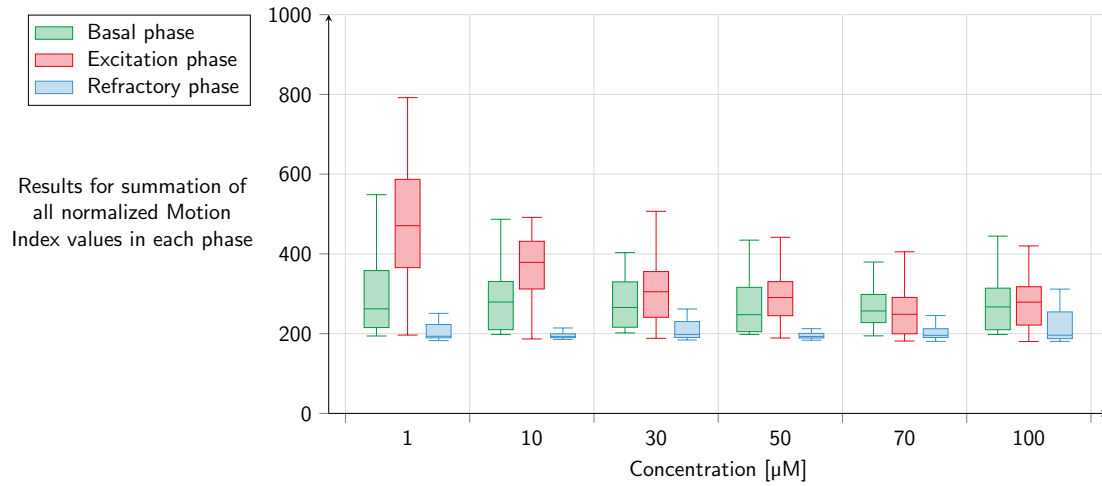


(a) x8140 is WT like

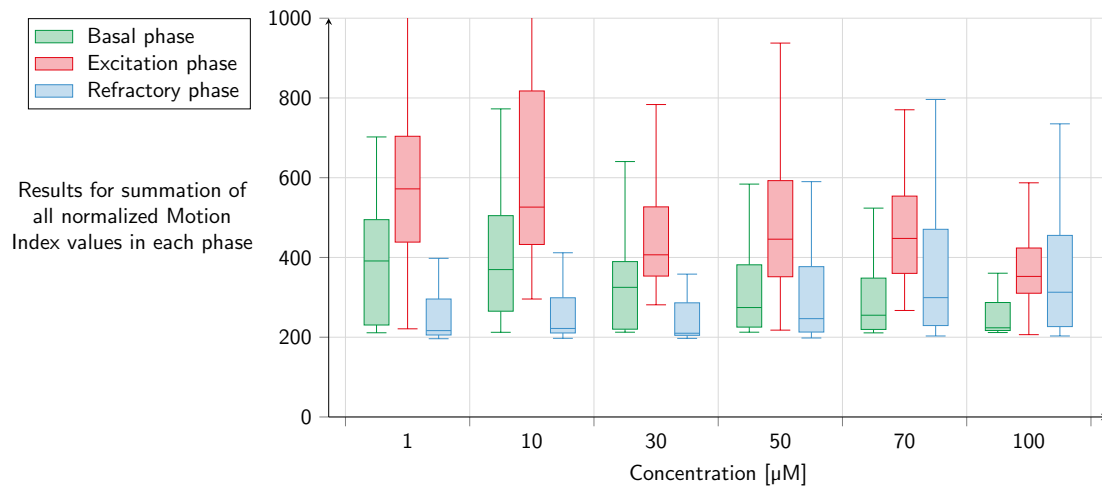


(b) x8246 shows no PMR

Figure 3.26: PMR results for selected cannabinoid compounds at different concentrations ranging from 1 to 100 µM. The motion index values are summed up for each embryo and each of the phases resulting in three values per embryo. The basal movement is shown in green, the excitation phase is in red and the refractory phase is given in blue boxplots. For WT-like compound x8140 the values seem similar on all concentration steps. x8246 on the other hand shows the decrease in activity in all phases with increasing concentration to a basically complete lack of motion at concentrations of 70 µM and above. Subfigures (c) and (d) are shown on the next page.



(c) x5745 causes scattered movement



(d) x4398 causes a PMR also to the second light flash

Figure 3.26: Continued from previous page. x5745 was categorized as having a scattered movement which is represented by a decrease in summation values at higher concentrations. x4398 causes a PMR to the second light flash as well which is visible in the increase for the refractory phase.

4. Vibrational Startle Response

Startle responses are fast, involuntary reactions to threatening stimuli. These can include sudden light flashes, loud noises or unexpected vibrational sensations which indicates that startle aims at threat avoidance, requiring an immediate fight or flight like behavior in order to prevent bodily harm. It has been studied for many classes of vertebrates like mammals [101], fish as well as amphibians [102] and usually manifests in a rapid muscle contraction with latencies smaller than 13 ms [62]. Even though the underlying reflex is by definition involuntary, the intensity of the response can be increased by exposing the animal to fear [103] or pain [104] and can also be decreased by providing anxiolytic compounds [105]. Experiments with rodents typically utilize so-called stabilometer chambers [106], while humans are most commonly analyzed via their eye-blink reflex [107]. In zebrafish, larvae start to show behavioral responses to stimuli like vibration and sound after approximately 4 dpf [108]. Additionally, the responsible neuronal pathway is said to be relatively simple [109] and mainly dependent on the large Mauthner neurons [110] located in the hindbrain of the fish. With Mauthner neurons typically present only in fish and amphibians the question might arise on how their role can be translated to mammals and how especially humans can benefit from experiments targeting them. However, it has been hypothesized that the Mauthner cells' fundamental motor control mechanisms extend to mammals and that they could allow for insights into functionally analogous networks there [111]. This means that a better understanding of pathways involving Mauthner cells could support research towards cures for for example neurological disorders in humans [112].

The most noticeable manifestation of a Mauthner mediated response in fish is the so-called C-bend - a characteristic movement where the head bends all the way to the tail forming a C-shape like posture as presented in figure 4.1. Here the fish is shown in its resting position on the left and during the C-bend in the middle. It usually ends with a counter-turn and a burst like swimming movement away from the initial position [113].

With a behavior this robust and easily observable it is easy to realize the potential applications in screenings for neuroactive compounds as well as genetic modifications.

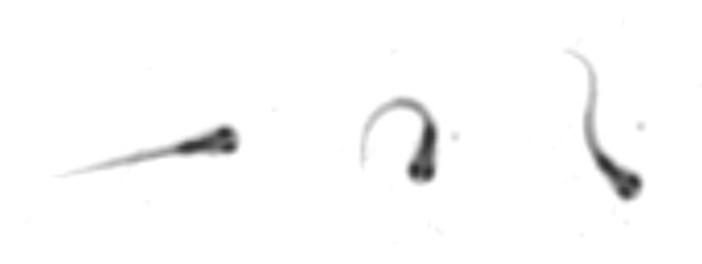
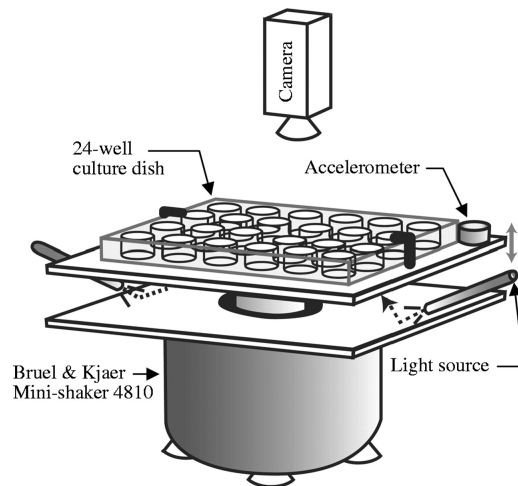


Figure 4.1: Illustration of a typical C-bend in zebrafish. The larva is shown in its resting position on the left and then in its bend form in the middle. Ultimately the larva propels itself away from its original position.

4.1. State of the Art

In water, and for such a small object like a zebrafish larva, a differentiation between an acoustic and a vibrational excitation is almost impossible. Unlike with humans where sound is transported over the air and other vibrations are typically sensed mechanically via the rest of the body, for zebrafish the two effects can be considered to be virtually the same. In zebrafish research there is, therefore, no true consensus on how the startle response is supposed to be described correctly and both methods are combined in the terms escape or startle response [29]. This is why previously built systems tend to be quite similar in their fundamental excitation methods no matter if they target acoustic or vibrational pathways in the larvae. There have been a number of studies on the startle response so far in which several methods of excitation have been described, ranging from scientifically questionable manually applied stimuli [114] to using expensive high-tech equipment [115, 62]. These studies most often rely on a vibrational stimulus as it is relatively easy to apply to a large area of multiple wells at the same time, all while being evenly distributed over the target area or volume. The specialized vibrational exciters used in these studies are based on a solenoid mechanism with an electromagnetic coil and a permanent magnet, causing a shaft to move up and down as soon as an electric current is applied. In figure 4.2 such a shaker and how it was modified to be used for zebrafish analysis is presented. The sectional drawing illustrates the working principle with an electromagnetic coil in a permanent magnet. More recently alternative ways of excitation have also been published [110, 61, 116]. In these the stimulus is indirect and non-directional by exposing the larvae to the sound of hi-fi speakers and relying on the produced sound waves to induce vibrations in adjacent dishes and well plates.

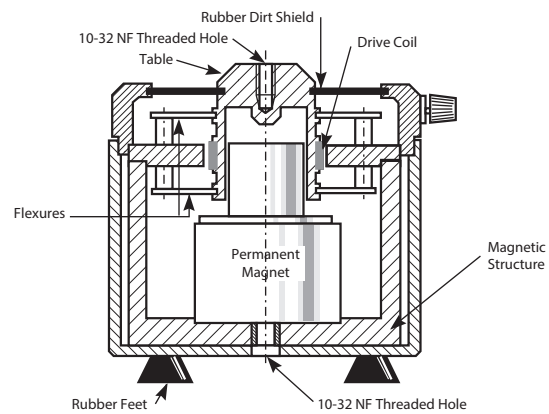
Generally there appears to be an increasing interest in utilizing the escape response in zebrafish with the PubMed database showing that more than 60% of all search results for the term “zebrafish startle” have been published between 2011 and 2017.



(a) Shaker setup used by Zeddies et al. [115]



(b) Mini Shaker 4810 [117]



(c) Sectional drawing [118]

Figure 4.2: Overview of the mini shaker by Brüel & Kjær that was used in other studies on the vibration response in zebrafish. An example of an imaging setup is given as well as a sectional drawing illustrating the electromechanical mode of operation. Images: a) reproduced by kind permission of The Company of Biologists, b) and c) courtesy of Brüel & Kjær.

However, a true high-throughput solution that can be used in not just highly specific genetic but also in chemical screens has yet to be found. This is why this work aims at providing a solution to make startle response experiments with zebrafish simpler and more affordable while ensuring accurate and precise excitations.

4.2. System Requirements

The stimulation methods of the already described systems in the previous section have limitations that can render them unsuitable for the type of high-throughput screening most researchers are aiming for today. Despite the specialized shakers providing accurate and precisely measurable stimuli, they require a substantial monetary investment. A shaker

plus amplifier can be priced at approximately 7000€ for just a single set. As the fish need enough time to habituate on the shaker before it is recommended to conduct an experiment [61], the only way to reach a higher throughput is by parallelizing the setup with multiple shakers, which would drive the cost up even further. The cheaper alternative systems based on indirect excitation on the other hand do not allow a proper characterization of the signal the larvae actually experience. This makes comparisons between systems impossible and could include unforeseen side effects. This is why direct excitation should be preferred over the cheaper indirect variant.

Increasing the throughput with just one of the shown shakers will result in a setup where the camera optics are the limiting factor and only a fraction of the available space can be imaged adequately. This is why setups that tried to mimic the one used by Zeddies et al. were only able to use an area of just 36 central wells of a 96-well microtiter plate due to their limited camera optics [119]. Also it has to be mentioned that the described shakers are specified to be capable of forces up to 10 N - which in earth's gravitational field translates to a weight of approximately 1 kg of movable weight. This appears to drastically exceed the estimation for the weight of the small volumes of fish water necessary for a typical startle experiment, which is expected to be well below 100 g. However, a system comprised of several of these expensive shakers would be difficult to justify without exploring alternative options. Reports of a third excitation option were presented by for example Noldus [47], but no available reviews at the time and obvious limitations due to the design (like only a single point of concentrated stimulus application) supported the development of an alternative system, capable of performing with similar accuracy but at a fraction of the cost of purpose-built equipment.

For this, several key functions were defined as crucial for a well characterized vibrational startle response system:

- Direct excitation resembling the one by dedicated vibrational exciters
- Parallelization with multiple shakers to increase throughput while still allowing habituation
- Low cost compared to traditional systems
- Full characterization of and control over achievable accelerations
- High-speed camera recordings to capture fast movements
- Automated analysis pipeline to cope with large amounts of data

4.3. Setup

The system was first conceptualized from the hardware side to be able to then tailor the software to the used components. For a working system solutions for sensors, cameras and exciters had to be found.

4.3.1. Accelerometer

In order to characterize the individual vibrational pulses applied to the system, a suitable sensor is crucial. Luckily with modern applications in robotics and smartphones, accelerometers are readily available in various designs and sensitivities. With the information in [62] an acceleration of 144 m/s^2 is recommended to be used. This equates to a G-Force value of around 14.7 g. The described pulse is a 500 Hz single sine wave cycle, which leads to a signal duration of 2 ms as shown in figure 4.3. Even though other pulse durations are also published (e.g. 24 ms [119]) the short pulse was preferred due to the minimal water displacement while still working reliably on the proposed system.

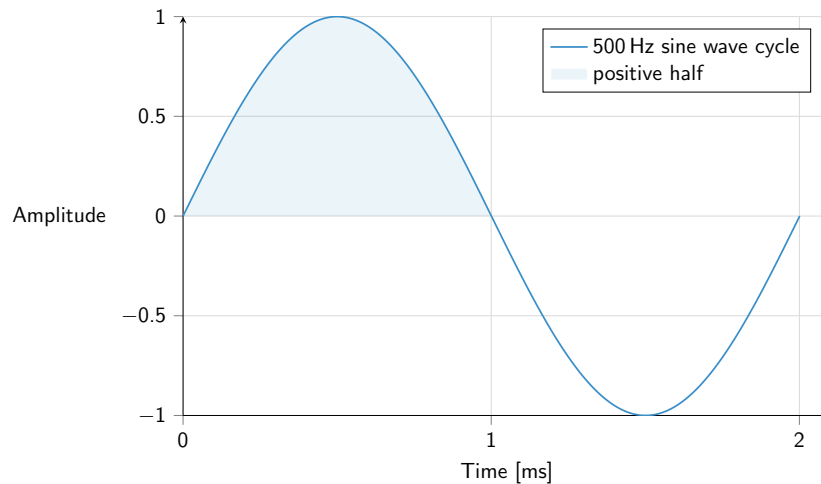


Figure 4.3: 500 Hz signal pulse lasting 2 ms used by Burgess et al. [62] for their startle response analysis as pre-pulse. The amplitude can be adjusted to the desired value and will result in the level of acceleration.

Since the signal is applied for only the fraction of a second the sampling rate needs to be correspondingly high. The Nyquist rate is considered to be the measure for the minimal sampling rate a sensor needs to have in order to be able to fully reconstruct the frequency of the original source signal from the measured sample points. It is given as

$$f_{\text{sampling}} \stackrel{!}{>} 2f_{\text{signal}} \quad (4.1)$$

with f_{sampling} being the desired sampling rate as to be able to reconstruct the signal's

frequency f_{signal} . In this case the accelerometer would need a sampling rate of at least 1000 Hz for when a continuous signal with a frequency of 500 Hz is used. Due to the brief signalling time however, an even higher sampling rate is necessary.

This leads to two conditions the accelerometer needs to fulfill in order to be suitable for the task at hand. Its sampling rate needs to be higher than 1000 Hz and it needs to be able to measure G-Force values of ± 15 g. Other beneficial characteristics are a light weight as to not falsify measurements due to its own inertia, small size so that it can be mounted properly and easy to use communication protocols that do not require proprietary hardware and drivers.

Table 4.1 shows a selection of available accelerometers that can be bought on already assembled breakout boards. The Analog Devices ADXL345 (shown in figure 4.4) was chosen as the preferred sensor for this task due to its sensing range, high sampling rate and the digital data bus systems SPI or I²C. Luckily it is a popular sensor used in numerous robotic projects worldwide, which leads to high availability and low cost of less than \$20.

Table 4.1: A selection of available accelerometers with different characteristics. Out of this list only the ADXL345 fulfilled all requirements and was therefore chosen to be used for the development of the vibration system.

Type	G-Force Range [g]	Sampling Rate [Hz]	Output Type
ADXL335	± 3	50	Analog
ADXL337	± 3	1600	Analog
ADXL362	± 8	400	SPI
MPU-6050	± 16	1024	I ² C
ADXL326	± 16	3200	Analog
ADXL345	± 16	3200	SPI, I ² C
LIS331	± 24	1000	SPI, I ² C
ADXL377	± 200	1600	Analog
ADXL193	± 250	400	Analog

To read the sensor data, a dedicated microcontroller unit is essential. In this case Arduino microcontrollers were chosen due to their convenient implementation, low price and high availability. Because the supply voltage of the raw sensor is only allowed to go up to 3.6 V, a logic level converter has to be used if the sensor is supposed to be connected to a 5 V

microcontroller. Due to this limitation, a 3.3V Arduino DUE (as shown in figure 4.5) was chosen. This specific Arduino has the additional benefit of being equipped with a relatively fast 84MHz CPU compared to the other Arduino boards and offers the functionality of a native USB-serial port on the SAM3X CPU.

This native port is capable of much higher data transfer rates than the usual USB-to-TTL Serial chips used on similar boards.

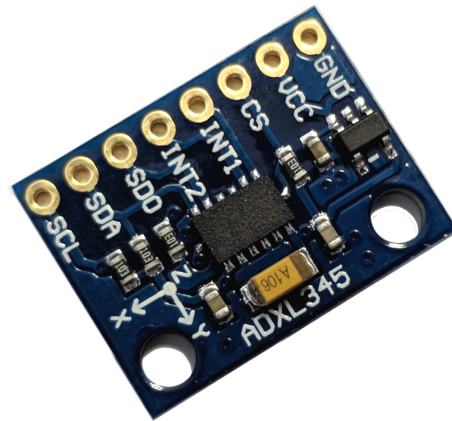


Figure 4.4: ADXL345 on a breakout board with accessible pinouts for simple implementation in various setups.

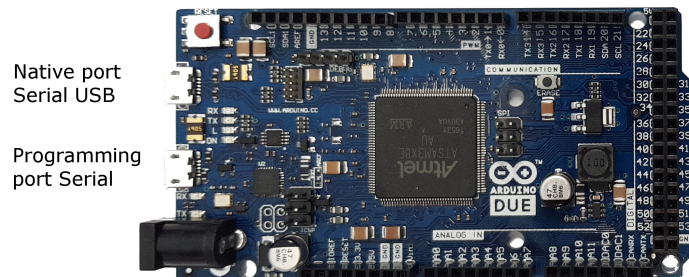


Figure 4.5: Overview of an Arduino DUE with both Serial Ports labeled. The native serial port allows for much higher data transfer speeds than the standard programming port on most Arduino boards. This is required in situations when sensor data at a high sampling rate is supposed to be transmitted.

To connect the sensor to the Arduino two digital transfer systems can be used, namely the SPI or I²C data bus systems. However, according to the ADXL345 data sheet [120], the use of I²C in fast mode achieves a maximum sampling rate of only 800 Hz. For this reason the SPI protocol has to be used in order to fully utilize the sensor's capabilities and reach the necessary bandwidth.

4.3.1.1. Accelerometer calibration

The sensors come precalibrated from the factory to give proper results for most use cases. To be used in the vibration system, however, the calibration is repeated, resulting in offset values that can be hardcoded to adjust the sensor readings. For calibration a special Arduino sketch is used and the accelerometer is placed on a flat surface. The sketch measures the applied force and averages over a specified time frame. This has to be repeated for every axis - with each axis properly aligned to the earth's gravitational pull. With this the sensor axis can be calibrated to 1 g. At a 13 bit resolution in the ± 16 g range the conversion factors between sensor values and g-forces is 0.0039 g/bit or 256 bits/g as shown in equations 4.2.

$$\frac{16 - (-16)}{2^{13}} = 0.0039 \quad \text{and} \quad \frac{2^{13}}{16 - (-16)} = 256 \quad (4.2)$$

The ADXL345 does offer registers to store calibration offsets that are directly used by the MCU for the output calculation. However, they will get reset to default values on every power cycle. To bypass this, the offset values are stored on the controlling unit and are used to adjust the acceleration values after receiving them from the sensor and before sending them to the main computer.

4.3.1.2. Implementation

To seamlessly integrate the Arduino into the main application on the controlling computer a serial connection over USB is used. Usually this type of connection transmits the data in the form of strings and needs to be established at a predefined transfer speed. This ranges from 9600 bps to upwards of 256 kbps. To make sure that the data coming from the sensor is distributed evenly, a timestamp is to be submitted with each sensor reading. For high accuracy this is done with microsecond precision, resulting in a several bytes long integer value. A single sensor reading is therefore comprised of around 10 bytes of timestamp data, three delimiters and up to 12 bytes of the four digit sensor values. These 25 bytes at the maximum sampling rate of 3200 Hz result in a required minimum transfer speed of 800 kbps, with the serial transmissions relying on sending start and stop bits for every byte and thus the conversion factor also being a factor of 10 instead of the usual 8. For most serial port implementations this is far from their recommended performance. Luckily the Arduino DUE has a second native USB port that can be used for serial communication at the rate the USB port itself is specified for, which reaches several thousand kbps easily. This way the communication itself is sufficiently speeded and any remaining optimizations can be done to the underlying code the Arduino is programmed with.

The sensor values are extracted by checking registers and reading their stored values. Accessing such a register is usually done with “digitalWrite()” commands to initiate and end an SPI communication packet. However, the standard command in the Arduino environment is not optimized for performance and is relatively slow. In high performance applications like display refreshing or fast sensor reading this can become a bottleneck. To guarantee optimal and stable performance a “digitalWriteDirect()” command was implemented that bypasses the numerous uncritical instructions in the standard function and accesses the specified pin directly.

```
static void digitalWriteDirect(int pin, boolean value)
{
    if(value)
        g_APinDescription[pin].pPort -> PIO_SODR = g_APinDescription[pin].ulPin;
    else
        g_APinDescription[pin].pPort -> PIO_CODR = g_APinDescription[pin].ulPin;
}
```

Figure 4.6: C code for direct pin manipulation on Arduino DUE. This allows much higher trigger speeds that are required when communicating with external sensors for example.

A benchmark can show how drastic of a difference this optimization can already make: Doing 1000000 on and off pin status changes takes 4.255s on average when using the standard function, while the optimized version takes 0.072s - an improvement by more than 98%. Even though this is not crucial for the sole purpose of reading the sensor values, it allows additional calculations to be done without sacrificing performance.

4.3.2. Vibrational Exciter

The most important part of the vibration system is arguably a suitable exciter that is capable of delivering the desired frequency of 500 Hz with large enough amplitudes of up to 16g and durations of just 2ms. A number of ways to generate vibrations were considered ranging from simple solenoid based systems to motors with counterweights. However, solenoids appeared to not work predictably enough, with most of them using only simple springs to apply their reset force instead of relying on a defined electromagnetically controlled method. Vibrational motors that can be found in most mobile phones allow only a single point of stimulus transfer which would lead to an unevenly distributed signal on the plate. Also they do not have the necessary control mechanisms in order to apply specified frequencies easily without the need of additional sensory hardware. Furthermore

vibrational transducers used in car hi-fi systems appeared to be a viable option at first, but due to their size and weight they were not capable of delivering the desired stimulus parameters and are typically used in lower frequency applications. Smaller versions were capable of delivering the needed frequency, but their lift was too small to reach the desired g-Forces. Ultimately, testing off-the-shelf hi-fi speakers showed to fulfill all the required specifications and are remarkably similar in their construction and mode of operation to the purpose built vibrational exciters. Figure 4.7 shows the speaker that was chosen and a sectional view to illustrate the general working principle of acoustic speakers. There is an apparent structural resemblance to the exciter in figure 4.2 with a similar electromagnetic coil in a permanent magnet generating the vibrations.

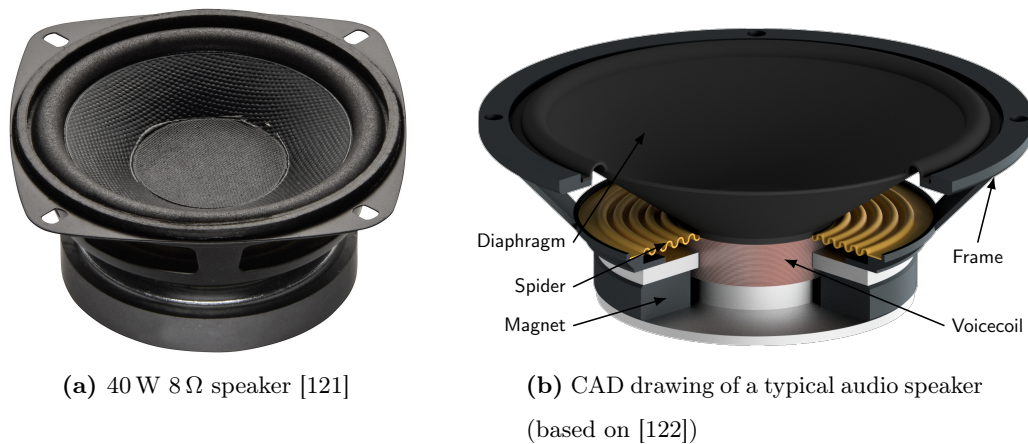
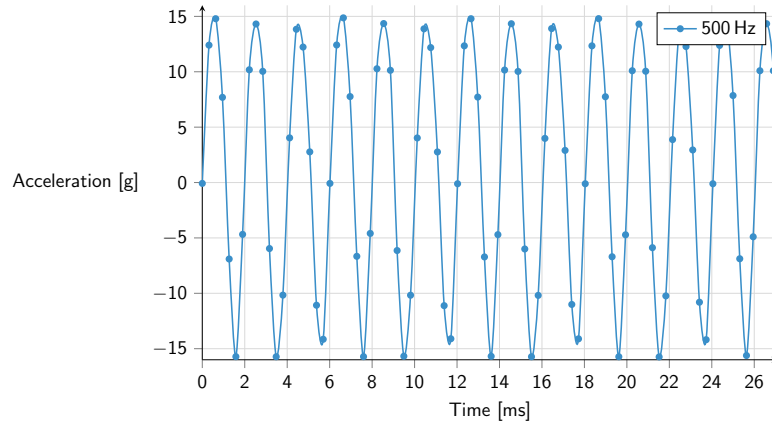
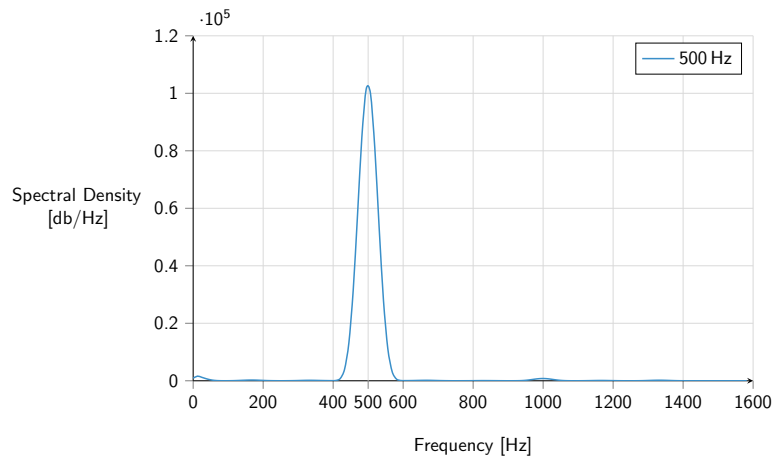


Figure 4.7: Overview of the proposed acoustic speaker and a sectional view that visualizes the general working principle of a speaker. Image a) courtesy of Conrad Electronic SE.

In order to truly evaluate whether a generic acoustic speaker can be used for the deliberate application of a vibrational stimulus to a petri dish filled with water, the speaker’s characteristics had to be analyzed first. By measuring the acceleration for a constant 500 Hz tone, the oscillation behavior of the speaker proved to stay well-defined even though the accelerometer got attached to the membrane and caused additional weight to be moved. A Welch’s power spectral density estimation of the recorded signal shows a distinct peak at solely 500 Hz (with some expected remnant at its harmonics at 1000 Hz), which strengthens the observation that the speaker does indeed output the correct frequency even with the additional weight mounted to it. The results are plotted in figure 4.8 with the data points from the accelerometer being connected with an interpolated line. The spectral density was calculated via Matlab’s built-in “pwelch” function using the same accelerometer readings.



(a) Accelerometer data for a constant 500Hz sine wave tone applied to the vibrational test setup including a petri dish filled with 5ml of water



(b) Power spectral density analysis of the mentioned 500Hz tone

Figure 4.8: Analysis of the frequency characteristics of the speaker measured with the accelerometer. The acceleration values caused by a 500 Hz tone are plotted together with an interpolation line. A power spectral density analysis is done on this data and shows a distinct peak at the desired frequency indicating that the speaker does not significantly change its characteristics when an additional weight in form of the petri dish holder etc. is mounted to it.

For the actual system, however, only a short 2 ms pulse is supposed to be used instead of a constant tone. After empirical testing that is in part shown in figure 4.9, it was found that using a 1 ms pulse results in a shorter transient oscillation phase without omitting any negative acceleration phase. Effectively the acceleration does pass through both positive as well as negative acceleration when a 1 ms pulse is applied as it would for a 2 ms. Therefore, the 1 ms pulse was considered to be the option of choice.

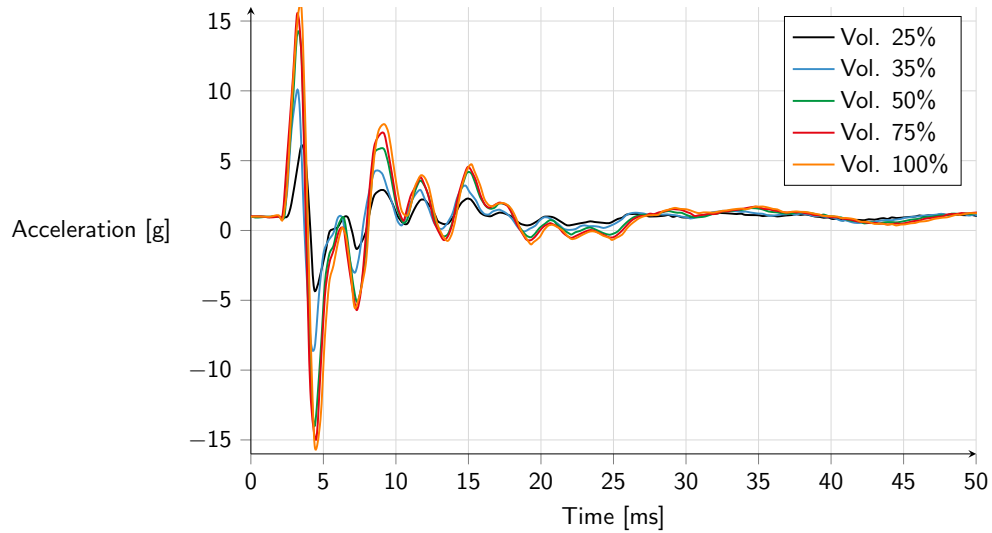


Figure 4.9: Overlay of accelerometer data for several 1 ms 500 Hz pulses at different volume levels. The graph emphasizes how well the resulting acceleration can be adjusted by simply setting the volume level appropriately.

Now that the speaker was shown to be a viable alternative to specialized exciters it had to be modified so that actual zebrafish can be tested on it. Therefore, a lightweight petri dish holder had to be created first. To do so, a CAD model was designed and 3D printed in ABS plastic with the design shown in figure 4.10.

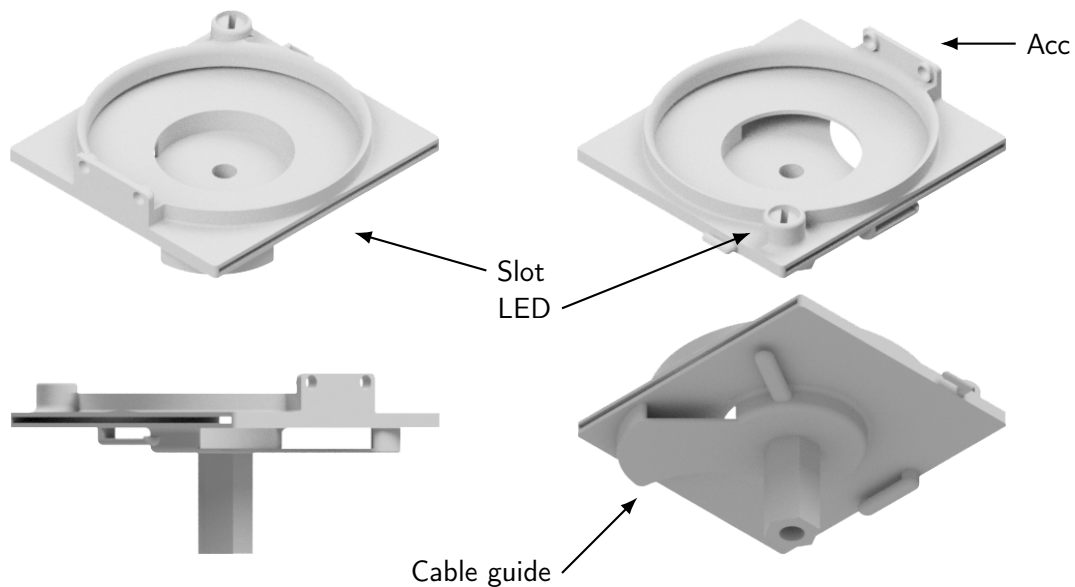


Figure 4.10: Overview of the petri dish holder design from various angles. It includes a slot for the backlight to be mounted in, a fixture for the accelerometer and guides for the required cabling. A platform allows mounting of a signal LED. The recessed center is for a locknut that secures the holder to the speaker via a bolt that is epoxied to the speaker membrane.

It features mounting holes for the accelerometer as well as guides for the cable management and enough space to mount it to the speaker by a bolted joint. It is designed to hold a 60 mm wide petri dish in a slight press fit to allow quick changes of dishes without any tools or complicated mechanisms. The dish size was chosen to be large enough to give the larvae plenty of space for their swimming motion at an observable density of around 20 larvae in a single dish.

This holder is fixed to the flat dust cap in the center of the membrane via an M5 bolt that is bonded with epoxy resin to the speaker. To guarantee good alignment while the resin is curing, a bolt holder was made that can hold the bolt in place and is fixed to the speaker itself tightly via bolted joints on the two opposite corners of the speaker housing. A ready to use speaker and the bolt holder design is shown in figure 4.11.

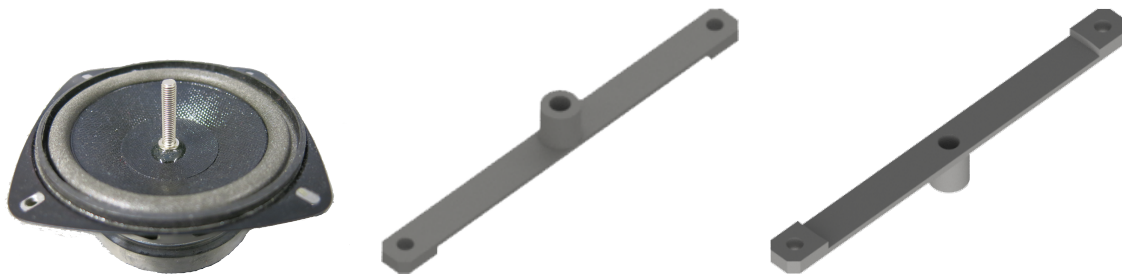


Figure 4.11: Bolt holder design for improved alignment while bonding the mounting bolt to the speaker membrane. The bolt is held in place by the central through-hole and the recess allows for a tight fit to the membrane circumference. The holder is mounted diagonally so that it can be fixed to the speaker's mounting holes for the time the epoxy is curing. The result is shown on the left with the bolt firmly attached to the membrane so that the petri dish holder can be mounted to the speaker.

With lighting playing an important role for any imaging system, a suitable illumination setup also had to be found. For high frame rate recordings the exposure time has to be very short, ranging from just several microseconds to 1-2 ms. This makes bright lighting crucial. Best results when recording delicate objects like zebrafish can usually be achieved with background lighting. This usually guarantees high contrast between object and background and makes detection of the fish easier as well as the observations more accurate. Uniform backlight illumination is, however, not trivial to achieve, especially considering the weight and size concerns for a vibrational setup like this. The solution was found in commercially available smartphone backlight illumination sheets that are marketed to be used for screen repairs. With diagonal sizes between 4 to 5 inches they are capable of covering the area of the entire 60 mm petri dish, are purpose built for uniform light distribution and high efficiency,

are thin and lightweight plus they are mass produced which reduces cost significantly. With voltage requirements between 12 to 18 V DC, they can also be easily hooked up to standard DC power supply units.

The illumination units used here fit 4.7 inch phone displays and generate light via 12 white SMD LEDs embedded on the three pin connector's side of the sheet. A sample is shown in figure 4.12 including measurements to illustrate the size and thinness. Single white LEDs are typically operated at between 2.8 and 3.4 V and at a current of ≈ 20 mA up to several A in case of high-performance ones. For 12 LEDs this would mean that a $12 * 3 \text{ V} = 36 \text{ V}$ PSU is necessary. However, the 12 LEDs are actually connected with two independent sides in parallel with six LEDs each. This then only requires half the voltage and allows the operation at 18 V. The three pin connector has a GND, GND, +18 V pinout. Adding such a lighting setup to the petri dish holder completed the vibrational exciter setup.

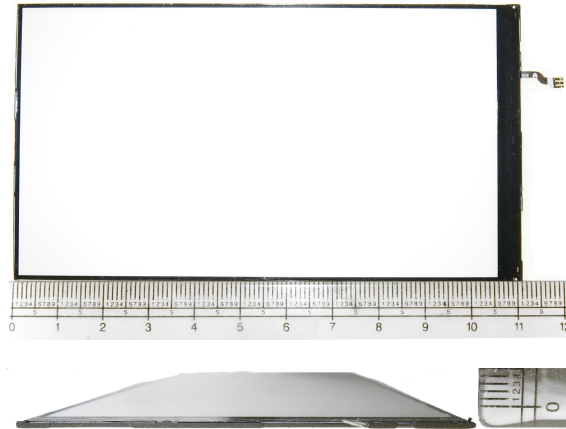


Figure 4.12: An exemplary backlight illumination sheet for an iPhone 6 that is perfectly suited for a bright and uniform yet lightweight illumination solution. The sheet has 12 white SMD LEDs that are connected with two parallel arrays of 6 LEDs in series each.

Ultimately the total weight of the added parts was measured to be well below 40 g including the actual zebrafish and water. In table 4.2 the individual weights are shown with a resulting total weight of only ≈ 32 g. Such a low weight ensures that the speaker can indeed move the zebrafish in the intended manner as the entire holder including the lighting has to be moved together with the membrane when a pulse is applied.

The entire setup was placed on an optical table in order to minimize external vibrations and allow precise alignment. To fixate the speaker to the table a holder was printed that surrounds the permanent magnet tightly and can be bolted to the table via the standardized hole pattern as demonstrated in figure 4.13.

Table 4.2: List of the individual parts of the petri dish holder and their individual as well as total weight.

Equipment	Model	Weight [g]
Petri dish holder	Custom designed	8.17
LED sheet	iPhone 6	6.82
LED	5 mm LED	0.3
Accelerometer	ADXL345	1.67
Bolts and nuts		6.12
Petri dish	ϕ 60 mm + 5 ml water	9.04
Total		32.12

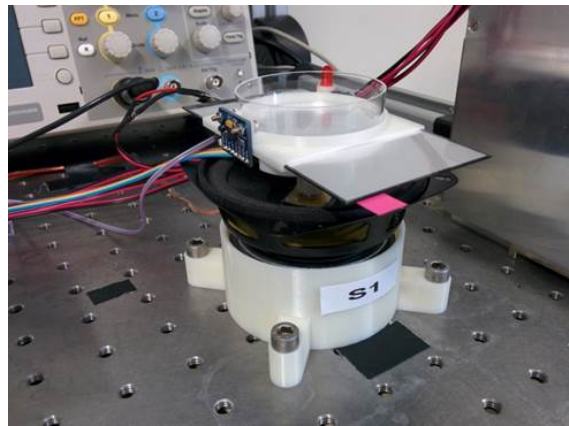
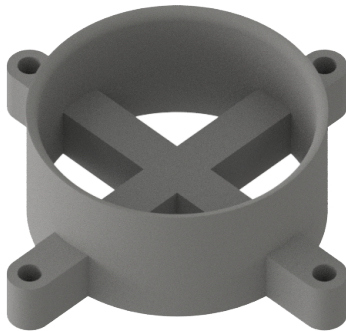


Figure 4.13: Design of the speaker base to mount it to an optical table and a close-up image of the assembled vibrational exciter setup with the speaker and mounted petri dish holder.

With the actual exciter assembled and characterized, a solution for the image recording pipeline had to be found. The goal was a single camera that can be used to image multiple exciters at high frame rates. Since the C-bend is a behavior happening in milliseconds, the recordings need to be at around 1000 fps or better in order to capture the larvae's movement. Otherwise the time between images would be larger than the time the larvae moves. Thus a high speed XIMEA MQ013MG-ON USB 3 camera was chosen. The camera is capable of delivering 1280x1024 pixels at 210 fps. This can be increased significantly, however, by reducing the number of pixels and limiting the field of view. With a round petri dish the field of view was artificially limited to a square at a 480 by 480 pixel resolution. This is still large enough, so that the individual larvae can be detected with the entire petri dish in the image and results in a frame rate of \approx 1000 fps.

To record multiple exciters a motorized linear axis was chosen. This allows the camera to be moved from one exciter to the next or in any order imaginable. Precise positioning with high repeatability was made possible by using a stepper motor to drive this in combination with a Nanotec SMCI33 stepper motor controller. A belt driven linear axis was used with a length of 1 m. Such a length allowed the use of five exciters next to each other with sufficient space between them so that no cross-excitation could be observed. This was tested with the individual accelerometers that did not register any vibrations when neighboring speakers were actuated. The camera was mounted to the stage by a number of 3D printed brackets and a metal bar with which the camera could be moved freely up and down to find and adjust the optimal distance between the camera and the larvae. Figure 4.14 shows the full setup with five exciters and the camera mounted to the motorized linear axis.

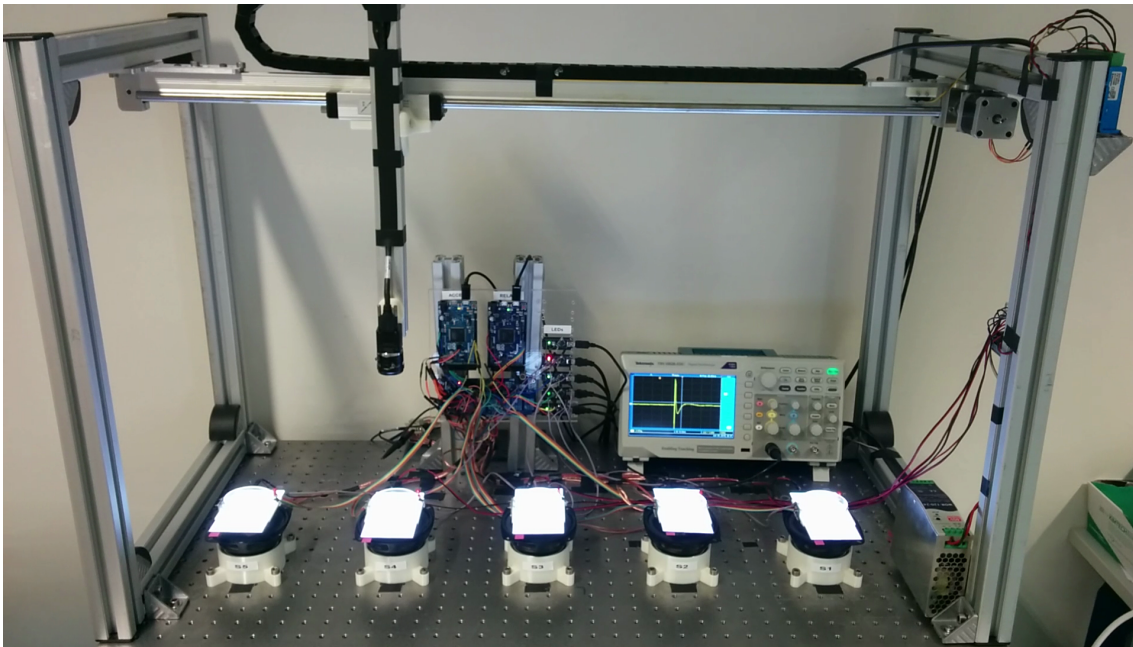


Figure 4.14: Overview of the final system assembly with five vibrational exciters and the movable camera. The oscilloscope is connected to the amplifier output to measure the electrical signal for the vibrational pulse. The Arduinos control the Accelerometers as well as the relays and signal LEDs.

Using multiple exciters also required a solution to deliver the electrical signal to each of them. Multiple amplifiers and signal sources seemed unnecessarily complex and expensive. One of the main advantages of using acoustic speakers as vibrational exciters is that the standard audio output ports on a computer are already perfectly suited as signal sources and compatible amplifiers are also readily available. However, each of the speakers is supposed to be actuated independently of the others since with the chosen recording setup

only one of them can be imaged at a time. This functionality was implemented by using a relays module that is controlled by a dedicated Arduino microcontroller. The speakers are all connected in parallel to a single mono amplifier but each of the signal lines passes through a usually closed relays. Only the one set to be active is then opened and allows the current to flow through the relay to the speaker. Because of concerns regarding the signal quality after the amplification, a Pro-Ject Amp Box Mono was chosen as amplifier. One advantage of this is also that the amplifier does not have distinct volume controls like most consumer products do. This eliminates user errors down the line when the amplification levels could otherwise be changed at will or by accident.

Another point to consider is how the exact time point of the vibrational pulse application can be made usable in the analysis later on. Ideally the video itself would contain an optical indication of when the pulse was applied in order to measure what is called the latency of the larvae. The time it takes for the larvae to move after the pulse was applied can be an important indicator for the activity of chemical compounds and their potency. To measure this duration, however, a start point has to be reliably determined. For this, a signal indicator was added to the exciters via an LED that gets triggered by a third dedicated Arduino. The Arduino's analogue pin is connected to the second channel of the stereo output signal and measures the voltage continuously at a rate of roughly 10 000 Hz. When a pulse is given the voltage rise is detected and once a threshold is reached the Arduino will turn on all the LEDs for exactly one second. This way there will be a precise visual indication directly embedded in the recorded video frames as to when the signal was applied. A simplified wiring diagram is presented in figure 4.15 showing the Arduino controlling the relays as well as an Arduino Nano for voltage measurement and LED switching.

Because the analogue input pin voltage is limited to a range from 0 to 5 V a voltage divider is used that allows the measurement of even higher values than 5 V without damaging the microcontroller. When connected to the signal line before the amplification the voltage will stay well below this value, however, the voltage could also be measured after amplification when it can reach a maximum of 24 V. Because of the time critical task of triggering the LEDs, another code optimization was implemented that is similar to the replacement of the standard `digitalWrite()` function when reading the accelerometer values. When triggering the five LEDs one after the other via individual function calls for each of them, the first and last LED might be turned on (or off) at slightly offset time points. However, by directly manipulating the port registers all LEDs can be triggered at exactly the same time with a single function call.

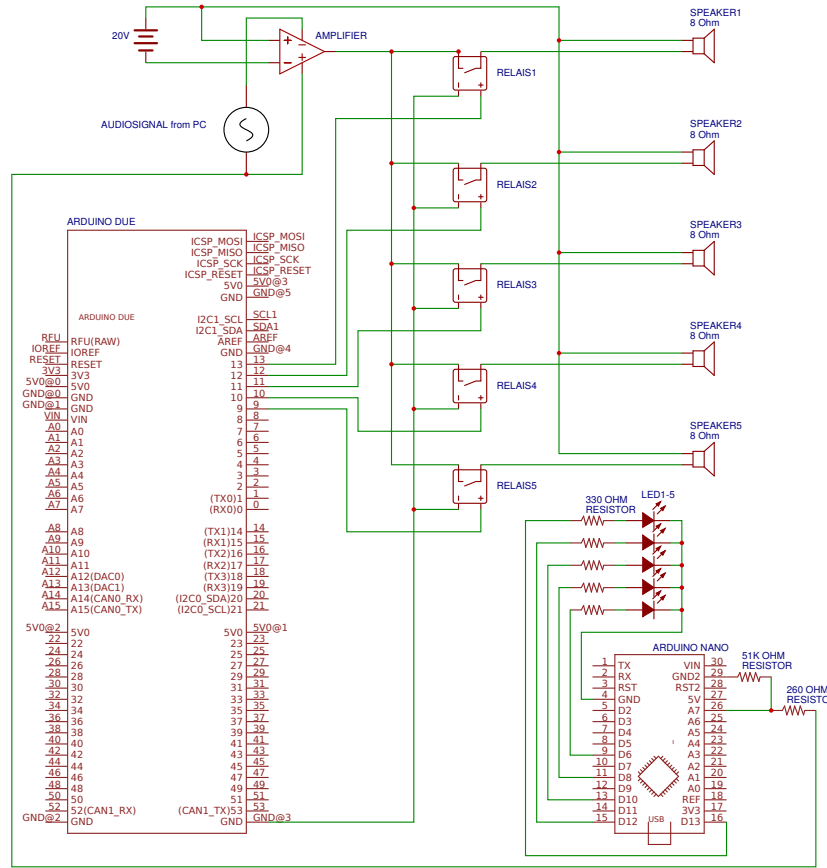


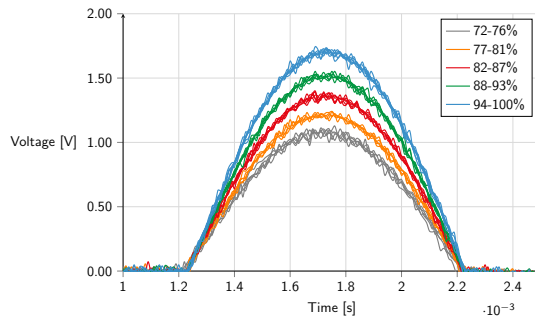
Figure 4.15: Wiring diagram for relays and signal LEDs. The Arduino DUE controls the five relays with only one being open at a time and thus closing the circuit to the amplifier for only the corresponding speaker. The Arduino Nano measures the signal voltage and turns the signal LEDs on for one second once a threshold is reached. A voltage divider allows for safe voltage sensing without overloading the analogue pin.

The pins on the Arduino Nano are grouped into ports B (digital pin 8 to 13), C (analog input pins) and D (digital pins 0 to 7). For the chosen wiring this means that two different ports had to be used since pin 6 belongs to port D instead of port B like the other four. However, the use of two ports was considered to be a significant improvement for the synchronization between the LEDs anyway.

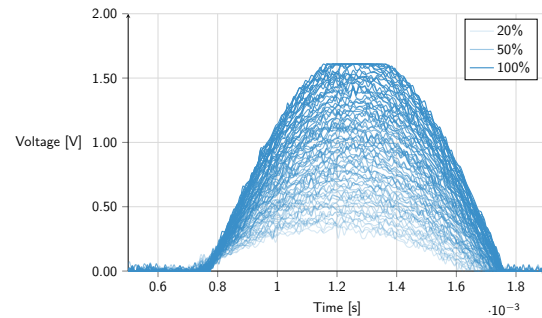
4.3.3. Exciter Calibration

With the accelerometer calibrated to 1g, the actual object acceleration at varying power levels also needs to be adjusted. To do this, each speaker was equipped with petri dish holder, backlight, sensor and a petri dish with 5 mg of water. The setup was thus identical to the one that was going to be used in the final experiments. In a first step the output levels from the computer as well as the amplifier were measured to get an idea of how volume changes affect the actual output voltages. To do this a Tektronix TBS1052B oscilloscope

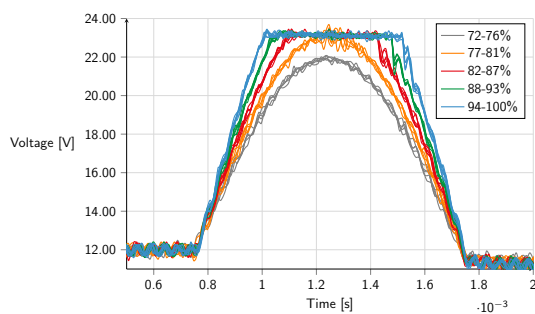
was connected to the output at the computer's audio port and in a second step to the output after amplification. The oscilloscope's data was extracted using a custom C# application accessing the Tektronix SDK. The reason for this is that the excitation can be controlled by two independent approaches with so far unknown characteristics. One is the audio output volume setting on the operating system level and the other the chosen amplitude level during the digital signal generation. Initially the signal generation was planned to be set to a constant value and only the audio output volume settings were supposed to be adjusted accordingly. This would minimize the number of variable factors involved and simplify the control algorithms. The audio output volume can commonly be controlled in individual percentage steps from zero to 100%, which is why the voltage at every single percentage point was measured. Surprisingly, the output voltage proved to not increase linearly with every percentage point but only step-wise as it can be seen in figure 4.16a.



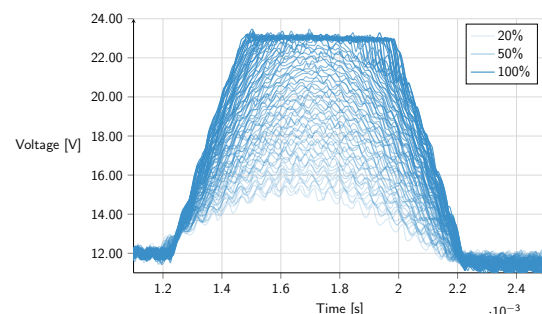
(a) Voltage for various audio output percentage levels with the digital source signal at constant amplitude



(b) Voltage levels at a constant 70% audio output level but varying source signal amplitudes



(c) The same conditions as in (a) but measured after amplification



(d) The same conditions as in (b) but measured after amplification

Figure 4.16: Voltage levels for various output volumes before and after amplification. The operating system volume as well as volume via the generated signal amplitude were measured. The operating system volume seems to not behave gradually but increase in discrete steps. This reduces the level of control over the resulting acceleration. By keeping the operating system volume fixed but changing the signal amplitude, a much finer control over the resulting voltage can be achieved.

The numerical percentage values in these graphs indicate either the operating system audio level or the digital source signal amplitude. For easier interpretation the signal amplitude is shown as percentage of the actual integer values ranging from 0 to 65535 with 65535 being the maximum number the unsigned 16bit integer can represent that is used for the digital signal generation. The signal is dynamically computed by a custom written generator function using the open source .NET audio library Naudio. Its computation is presented in figure 4.22 with simplified pseudo code that shows the dynamic calculation depending on the desired frequency, volume and duration.

For the operating system audio level there are clearly visible bands in which the output voltage stays nearly constant and then jumps to the next one once the according percentage is reached. This obviously stays true after amplification of the signal as well. Keeping the output level at a fixed value and changing the amplitude of the source signal ultimately allowed for much finer control over the output voltages and thus the vibrational excitation in the end. There are no visible bands but a homogenous increase in voltage with increasing signal amplitude. The floating baseline after the amplification at 12 V is due to the way this particular amplifier works with a 0 V to 24 V range instead of a -12 V to +12 V range around a 0 V baseline.

Now that the digital variation of the source signal proved to be the better approach, the resulting vibrational excitation could be determined. To do so the signal amplitude itself was dynamically adjusted and a constant operating system volume was set for each speaker so that the entire sensitivity range of the accelerometer was utilized. The values were found by administering a pulse with increasing amplitude every three seconds and recording the maximum peak value the accelerometer detected. This was repeated numerous times and the peak values compared with each other. However, this approach resulted in a large variation within the collection of values for each repeat. Puzzling at first, this can be explained by the still relatively low sampling rate of the accelerometer. Because the sampling rate is limited to 3200 Hz, the time in between samples is 0.3125 ms. At a signal duration of just 1 ms, this leads to the actual maximum value of the excitation not necessarily being captured every time but possibly some lower values left or right of the maximum being recorded. To compensate for this a more comprehensive calibration step was performed. The excitation in each speaker was measured repeatedly 100 times for each amplitude level and only the maximum value considered as the actual peak value. Giving the speaker sufficient time in between pulses ensured that they could return to their resting position and individual pulses did not contaminate succeeding ones. With 3 s in between pulses the calibration

of five speakers with 100 repeats at 100 volume levels took ≈ 41 h. Because of the offset values for 1 g the maximum output values at 16 g also varied by these values. In order to get uniform numbers, a normalization was done by dividing each speaker's data point with its maximum value and multiplying it with 16. The conversion between raw accelerometer readings and actual acceleration was assumed to be linear over the entire range.

Figure 4.17 shows the almost perfect linear correlation between amplitude and achieved acceleration. The graph shows the measured acceleration for increasing signal amplitudes for each of the five speakers. For each speaker the predefined output volume level is shown in the legend with either 50% or 60%. Changing this value would change the slope of the resulting lines. By fitting linear trendlines through the data points, each speaker was assigned its own calibration curve. With this every desired acceleration can be specifically chosen to be used in an experiment. The visible variation between the speakers themselves is most probably due to differences in the mounting positions of the petri dish holder. Since they were attached by hand, slight variations are to be expected. Deviations in manufacturing and varying magnet strengths for example could also cause this. However, since this can be compensated for via the right volume settings it was not considered to be an issue.

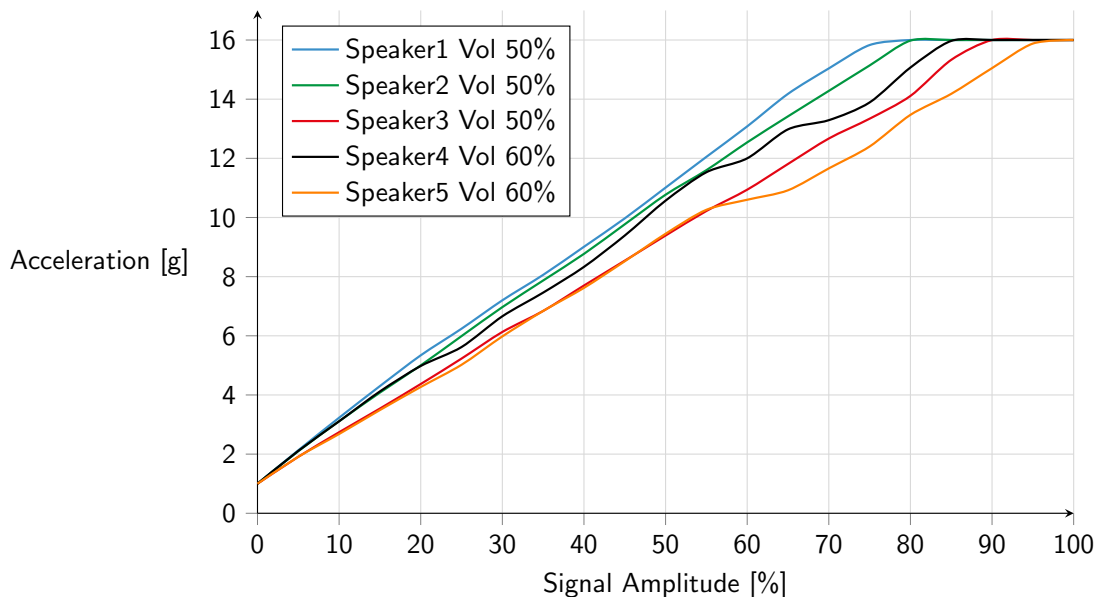


Figure 4.17: Results for the speaker calibration. The operating system volume was fixed and the signal amplitude adjusted in one percent increments between 0 and 100%. The stagnant level of 16 g is caused by this being the maximum value the accelerometer can measure.

4.4. Software

Having the hardware set up, the next critical step was the development of software capable of integrating all the necessary features into one application. To record the startle response in zebrafish larvae with the presented hardware, a number of individual functionality needed to be included. Next to an intuitive GUI the application needed to be able to communicate with two Arduinos, motor controller, camera, encoding tools as well as do audio signal generation. The flowchart in figure 4.18 shows how the application was ultimately structured and which modules are communicating with each other. The application was again created in C# with the Windows Forms GUI class library. It is mainly divided into two main classes that are responsible for the GUI and to take control over what is necessary for a single experiment. Specialized subclasses then manage the individual hardware parts and report back to the main classes.

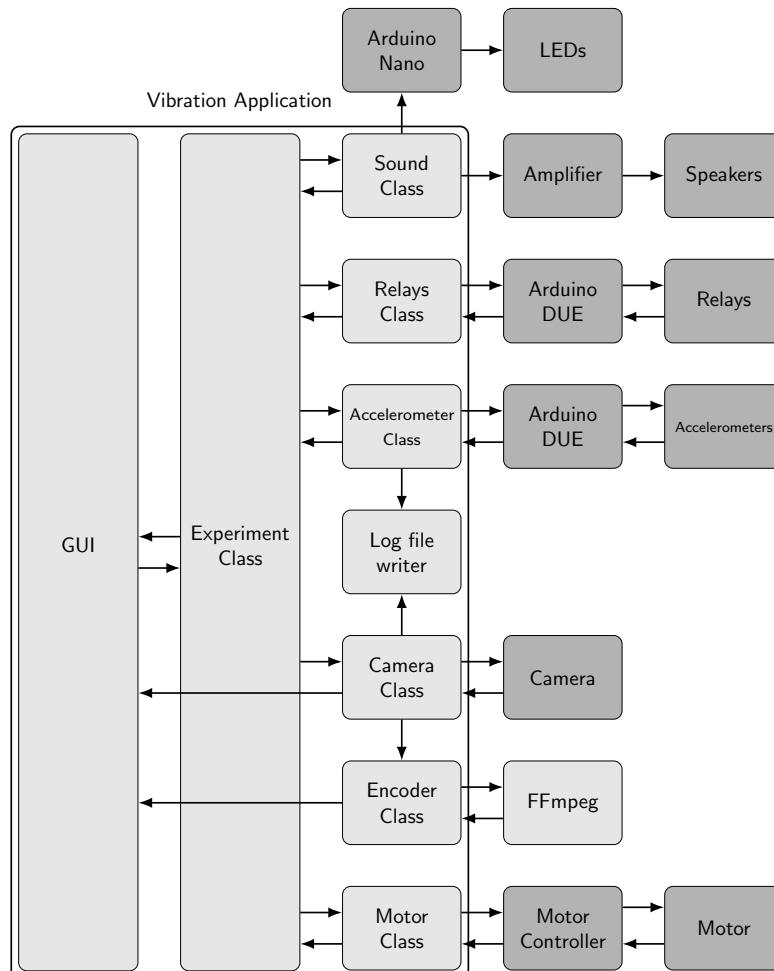


Figure 4.18: Flowchart of the vibration system control application. Light gray indicates software objects while dark gray indicates actual hardware the application is communicating with.

The GUI in figure 4.19 presents a prominent live image from the camera to the user and also allows direct control over the camera positioning and various camera settings like the exposure time or gain. An info box tells the user about additional information like the status the system is currently in and metadata like the mode the camera is currently in. Notably once an experiment is started a second window will appear and give visual feedback on the settings that were chosen for this particular experiment.

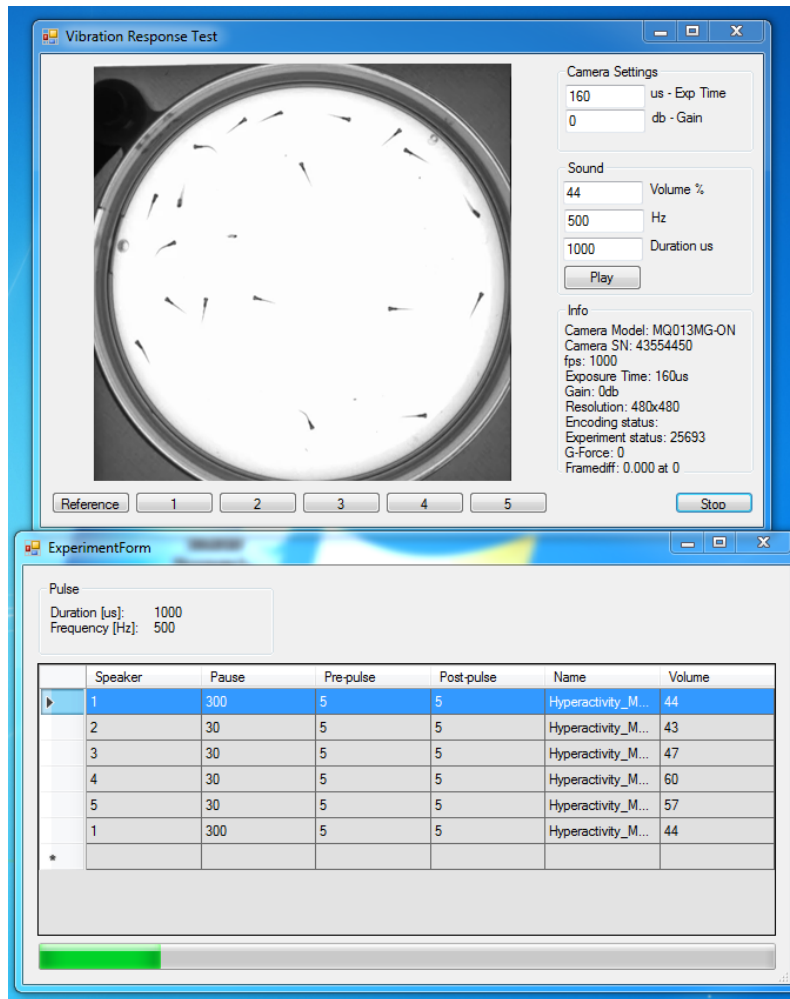


Figure 4.19: Overview of the vibration system application's GUI showing both the main window with the live preview at the top as well as the status window of the currently running experiment at the bottom.

An experiment is started by loading a predefined Excel sheet like the one presented in figure 4.20 that contains the actual settings and parameters that are used during an experiment. The user can specify the speakers that are supposed to be used in any desired order. The list of these planned excitations is in theory endless and only limited by the Excel row count. For each of the excitations a wait time can be set that represents the time the system will wait at a certain position before starting the recording. This is useful in situations

when for example an experiment should be repeated some time later or the larvae are given a certain amount of habituation time in between pulses. The user can also define the duration of the actual recording duration before and after the pulse is applied. By changing this value the resulting video would include more or less of the neutral swimming activity. Arguably the most important settings are regarding the pulse duration, its frequency and the resulting acceleration settings. The system allows full control over the final acceleration, with the user choosing the acceleration g-force values and the spreadsheet then dynamically calculating the corresponding volume settings according to the predefined calibration curves and their linear trendline functions. These functions are included in the sheet and can be changed if needed as when a speaker would require to be replaced for example.

Speaker	Pause before recording [s]	Recording duration pre Pulse [s]	Recording duration after Pulse [s]	Desired Acceleration [g]	Resulting Volume	HW Volume Name
1	90	2	2	14	66	WT
2	10	2	2	14	69	WT+Propofol1x
3	10	2	2	14	78	NFPS
4	10	2	2	14	74	NFPS+Propofol1x
5	10	2	2	14	84	NFPS+Propofol2x
1	900	2	2	14	66	WT
2	10	2	2	14	69	WT+Propofol1x
3	10	2	2	14	78	NFPS
4	10	2	2	14	74	NFPS+Propofol1x
5	10	2	2	14	84	NFPS+Propofol2x
1	900	2	2	14	66	WT
2	10	2	2	14	69	WT+Propofol1x
3	10	2	2	14	78	NFPS
4	10	2	2	14	74	NFPS+Propofol1x
5	10	2	2	14	84	NFPS+Propofol2x
1	900	2	2	14	66	WT
2	10	2	2	14	69	WT+Propofol1x
3	10	2	2	14	78	NFPS
4	10	2	2	14	74	NFPS+Propofol1x
5	10	2	2	14	84	NFPS+Propofol2x
1	900	2	2	14	66	WT
2	10	2	2	14	69	WT+Propofol1x
3	10	2	2	14	78	NFPS
4	10	2	2	14	74	NFPS+Propofol1x
5	10	2	2	14	84	NFPS+Propofol2x

Figure 4.20: Overview of the vibration experiment configuration file. The yellow color indicates fields the user can freely change and that are then extracted by the application to perform the experiment as defined.

With the information embedded in this configuration file, the experiment class will then manage the individual parts of the system. The experiment is designed as a loop with the length of the number of entries in the configuration file. A visual representation is given in figure 4.21. For each entry the loop will go through a number of steps in order to perform the intended excitation. First of all, the operating system volume is unmuted and set to the predefined value. Only afterwards can the relays open and physically connect the speaker to the amplifier. The reason for this is that programmed unmuted or volume changes cause an unwanted electrical pulse that can already cause an excitation in the larvae. Unfortunately this pulse is so low in its amplitude that it can only be audibly

verified. Measuring the voltage before and after the amplification with an oscilloscope as well as measuring the resulting acceleration does not show a distinct signal that can be distinguished with certainty from the static signal noise. Single peaks in the accelerometer readings indicate a maximum value of just ≈ 1.28 g. However, it has been observed that the larvae occasionally respond to this pulse already. One solution was to keep the relays closed while setting the volume, so that the pulse is physically hindered in reaching the speaker and thus does not disturb the larvae.

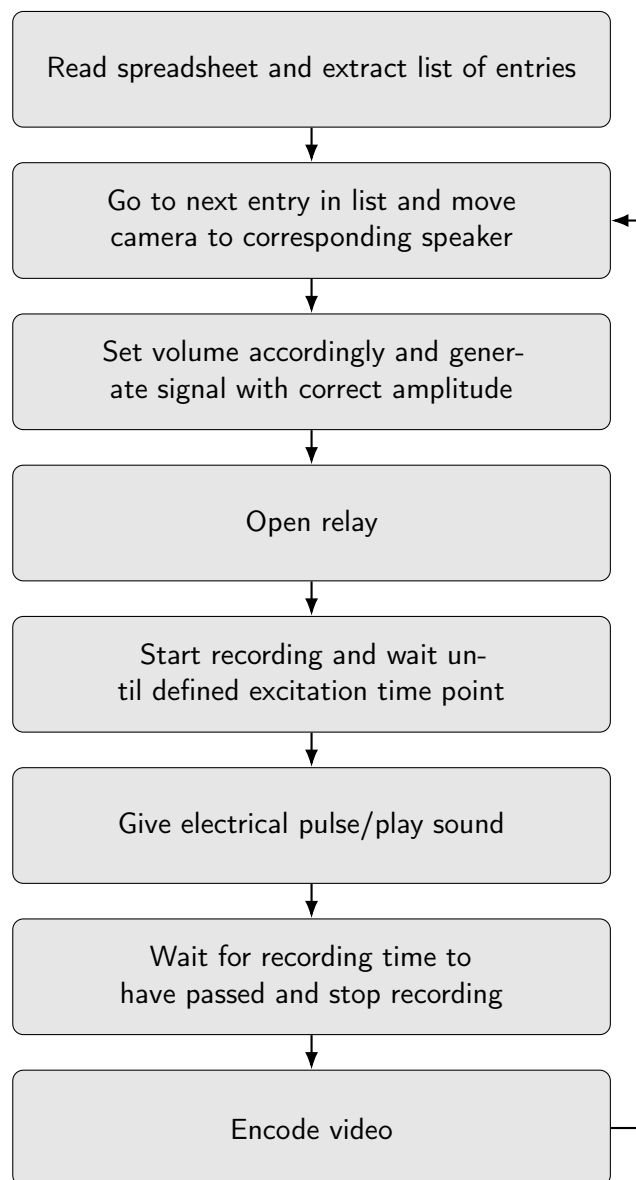


Figure 4.21: Flowchart visualizing the steps that are executed in order to perform a vibration experiment. The experiment will loop through the speaker positions for the values that have been defined in the configuration file and will stop once all listed positions have been approached.

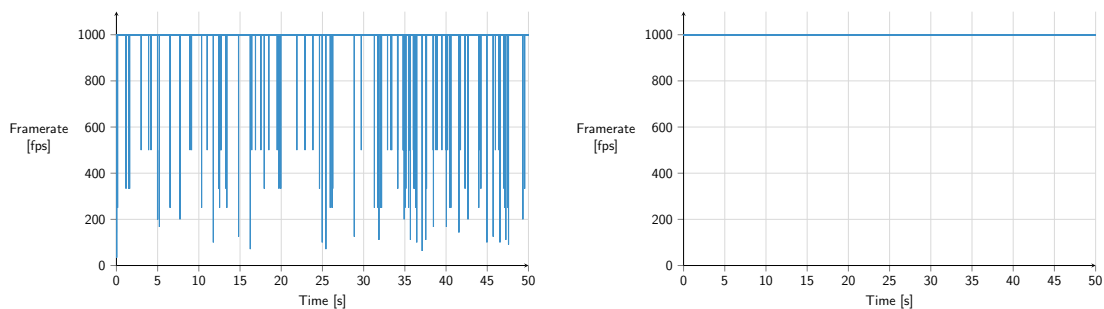
To generate the electrical signal pulses, sinusoidal waves of the desired length and amplitude are generated and output via the soundcard of the computer. The signal is created with 96 000 samples per second at 16 bit per sample using a digital wave function which is shown in figure 4.22 in the form of simplified pseudo code. For the performed experiments a 500 Hz pulse with 1 ms in duration was chosen, effectively utilizing only the positive half of a full sine wave period. The volume is given as percentages and converted into an unsigned integer to adjust the signal amplitude accordingly. Signal duration is calculated by converting the supplied duration in micro seconds to the total number of samples via the sampling rate. Afterwards the created signal is used to play the corresponding sound on the speakers.

```
int volume = Signal.Volume; //volume given in percentage between 0 and 100
volume = volume/100*65535; //value is converted to range 0 to 65535
int samplesPerSecond = 96000;
int sampleNumber = samplesPerSecond * usDuration / 1000000;
double theta = frequency * 2 * Math.PI / samplesPerSecond;
double amplitude = volume / 2;
for (int sample = 0; sample < sampleNumber; sample++)
{
    short s = amplitude * Math.Sin(theta * sample);
    Signal.AddSample(s);
}
```

Figure 4.22: Simplified pseudo code illustrating how the audio signal is generated and how the desired volume is converted from percentage into signal amplitude.

Another critical part of the vibration system was the integration of the high frame rate camera. In order to record the very fast reaction times and swimming motions, an imaging system capable of around 1000 fps is necessary. The time in between individual frames would then be only 1 ms. However, such a task requires performance optimizations in the way the data is transmitted and read from the camera buffer. This is especially helpful in situations when the resolution of the camera is changed in order to increase the frame rate. According to [123] an increase of the buffer queue size and a decrease of the transport buffer size is necessary to receive all images at high frame rates. This optimization was thus implemented in the initialization routine of the camera before the acquisition is started. To ensure that any dropped frames are handled correctly the timestamp of every recorded frame is logged in a text file next to the resulting video. This way any skipped frames can be easily detected and the analysis can be adjusted accordingly. However, the performance optimization has made the recordings so robust that no skipped frames could be observed

afterwards. In figure 4.23, an analysis of the logged timestamps for two untypically long 50 s recordings with about 50 000 frames each is shown. The momentary frame rate f is calculated as $f_i = \frac{1}{T_i - T_{i-1}}$ based on the timestamps T_i at any particular frame i . Figure 4.23a shows the unstable frame rates due to dropped frames when the optimization is not in place, while figure 4.23b illustrates how stable the frame rate becomes once the optimization is included. Both videos have been recorded on the same computer and only the optimization code snippet has been changed in between the two versions. The duration of 50 s was chosen so that almost all available RAM on the computer was filled and no swap file had to be used. It therefore equates to the maximum recording duration in which a constant 1000 fps at the chosen resolution on the chosen equipment can be guaranteed and exceeds the typical recording durations of just several seconds when doing actual experiments.



(a) Without buffer optimization a total of 385 dropped frames (or 1 for every 130 recorded frames) was registered over the 50 s recording period

(b) Buffer and queue optimization leads to stable frame rate and no dropped frames

Figure 4.23: Analysis of logged timestamps for 50 s recordings at 1000 fps with the frame rate f being calculated as $f_i = \frac{1}{T_i - T_{i-1}}$ based on the timestamps T_i at any particular frame i .

To display the images to the user without the risk of conflicts in the memory management and thread safety, two separate buffers were used: one that gets populated with images in just their raw data form when a recording is activated and another that is solely responsible for holding a single image to display to the user in the GUI. Once this bitmap is displayed, the buffer gets emptied and only then a new bitmap will be added to this buffer. In return the GUI's refresh rate is capped at an artificial 20 fps via an event based timer. The raw data itself is read from the camera in an infinite loop that not just reads the data but also checks for the status of several trigger variables. With this a recording can be started by passing a single bool variable to the camera class. The loop is asynchronously running in its own separate task parallel to the GUI and the other classes. To be able to quickly

convert the raw data in form of byte arrays into bitmaps, some additional information for the bitmap header is necessary. The header holds additional information next to the actual pixel values and usually does not change for a chosen system. Such a conversion can thus be optimized by performing a byte array merge. Directly reading a single frame as bitmap object when the camera is initialized and the application started allows the header information to be extracted in the form of a byte array. The first 1078 bytes of the bitmap object hold the header data which can then be merged with any subsequently generated raw data byte array to form a bitmap object again. Figure 4.24 summarizes this explanation in the form of a flowchart.

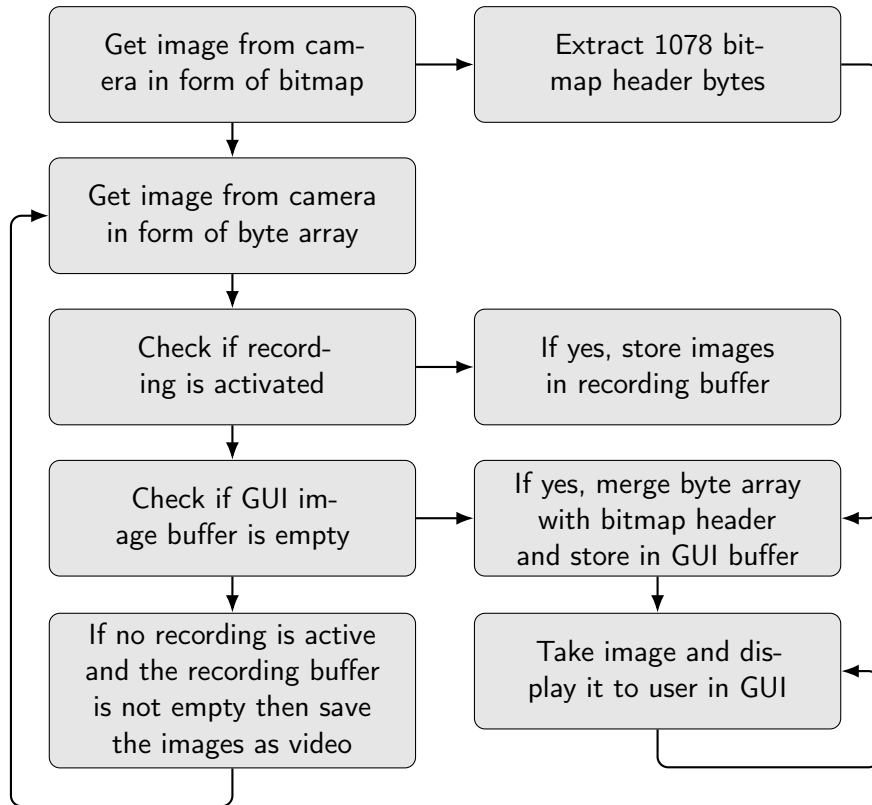


Figure 4.24: Flowchart illustrating the high speed camera recording algorithm and the approach to optimize performance by creating bitmap data only when necessary by merging a byte array holding the bitmap header information with the byte array containing the image information.

4.4.1. Vibration Analysis Tool

In order to reliably analyse the resulting videos of the performed startle response experiments a video analysis tool was conceptualized with and the algorithm then developed by Dr. Johannes Stegmaier and Ravindra Peravali based on [124] and [125]. The software was designed to detect all larvae in a video and then track their movement after the stimulus was applied. This results in numerical readouts that can be used to compare the activity levels

between various experimental conditions. To make this viable for a large number of videos it was implemented in the form of a batch analysis pipeline that reads the result folder's contents and extracts all video files in it. Each video is analyzed and the resulting data is then merged and sorted into one cumulative result file. While doing so, the tool reads and computes parameters like the total number of detected larvae, if they have responded to the stimulus, their travelled distance and more. For the performed experiments the most telling parameter was the percentage of larvae that showed activity after the pulse was applied. Before using the tool's results in actual experiments, however, an analysis of its detection capabilities was performed. 54 pulses with between 23 to 26 larvae each were analyzed manually as well as with the tool to find the percentage of larvae that responded to the stimuli. By calculating the difference in the results of the two methods for each video, an indication of the quality of the automated detection was extracted. Figure 4.25 shows a comparison of the detected activity percentages for the two methods for the entire set of 54 pulses. The manually determined values were considered to be correct with the tool ideally giving the exact same values that would then result in no deviation at all. However, automated tools like this are susceptible to errors and small deviations are to be expected and acceptable when low enough. The presented values show that the tool performs very well and deviates from the manually determined values with a low average of 1.83%, a median value of 1% and first and third quartiles of -1% and 5%.

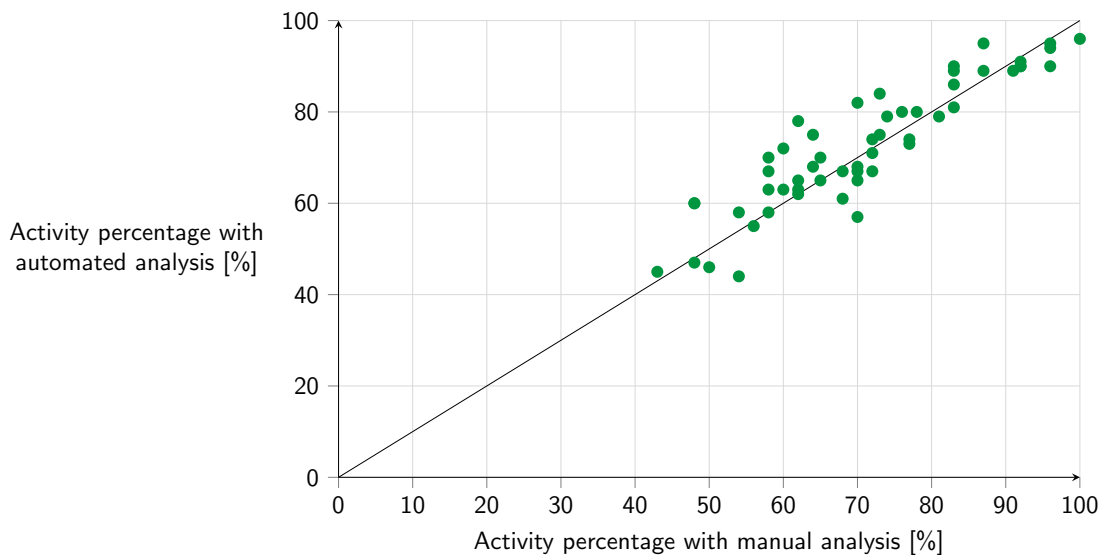


Figure 4.25: The activity percentages for 54 different pulses with between 23 and 26 larvae each are shown. The manual and automated analysis deviate from each other with a low average of just 1.83%, a median of 1% and the first and third quartiles at -1% and 5%. The tool can thus be classified as capable of accurately determining the percentage of larvae that respond to the stimuli.

4.5. Assays and Results

With the system fully set up, the first step was to get an impression of the larvae's reference behavior to vibrational stimuli. There have been earlier studies on the vibrational startle response that generally characterized the development of startle responses in zebrafish [108]. However, the methods used to cause excitation in this study are far from the level of accuracy the proposed system is capable of. In these cases the vibrational stimuli were created by periodically tapping the petri dish with a metal rod which is a highly subjective method and does not take the strength of the stimuli into account. The taps can vary significantly between persons conducting the experiment and even in between taps performed by the same person with manual control not being as precise as a tailored technological solution.

By measuring the percentage of larvae that respond to a defined 1 ms 500 Hz pulse delivering a peak acceleration of 14 g over the course of several days, the development of the vibrational startle response could be determined. The results are shown in figure 4.26 with the average activity percentage for between 26 to 42 recorded pulses for each time point and the associated standard error of the mean plotted in a bar graph. It is clearly visible that the activity increases with age.

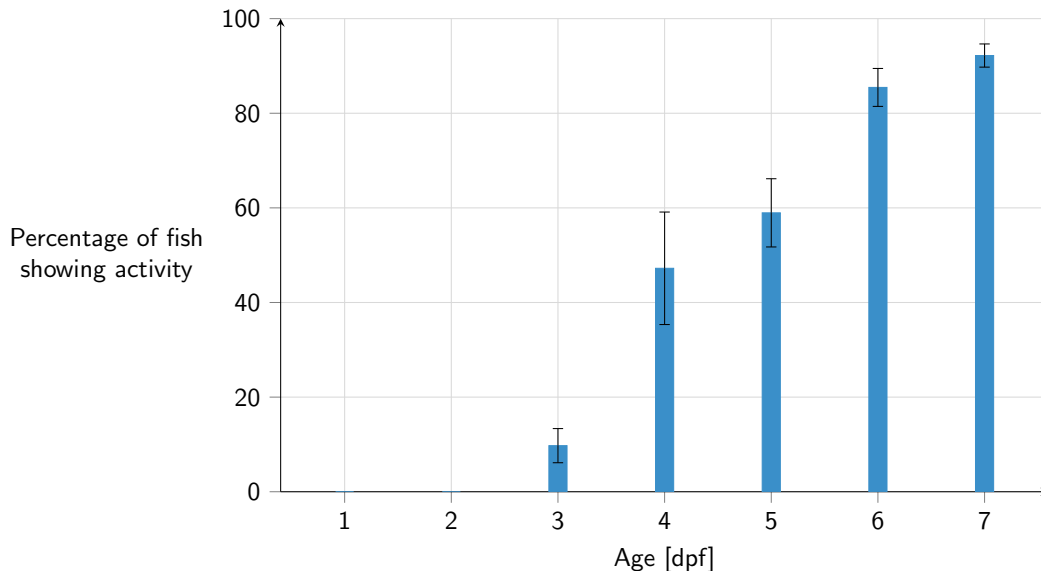


Figure 4.26: The percentage of larvae responding to a 14 g acceleration pulse is plotted for the early developmental stages between 3 and 7 dpf. Day 1 and 2 were not tested as the embryos have not hatched yet. The values are calculated from a collection of between 26 and 42 recorded pulses for each time point. The average is given as well as the standard error of the mean.

For the time points at 1 and 2 dpf no data was collected as the larvae do not hatch naturally at these time points and separate observations showed that there is no detectable activity for vibration this early in the development. This is also confirmed with the low activity at 3 dpf that indicates that the onset of the vibrational startle must happen between 2 and 3 dpf. These results correlate well with the development of the lateral line system and its increasing number of neuromasts [126, 127]. The lateral line development is also most probably responsible for the quite large variation on day 4 and 5 post fertilization due to the drastic developmental changes the larvae are going through and small deviations in the staging potentially having large effects on the activity of the larvae. Conversely, however, there have been reports that excluded the lateral line system as not contributing to the detection of acoustic stimuli [119] even though a similar excitation approach was chosen. One potential explanation could be the different durations and frequencies of the given pulses that cause a separate stimulation of the larvae's inner ear and a successive activation of the Mauthner neurons. At this point no detailed answer can be given on the actual pathways involved, but it is clear that more research is necessary to better understand the responsible mechanisms. Generally, however, the time point at 5 dpf can be considered a viable option to perform vibrational startle response assays with zebrafish as there is a substantial response to the stimuli and it still fulfills the EU regulations on animal experiments [31]. However, vibrational startle experiments can become more unambiguous at later time points with the percentage of active fish rising to levels of around 90% as early as 7 dpf. For the experiments in this work, only fish close to 120 hpf have been considered in order to comply with the regulations if not mentioned otherwise.

Another critical characterization is the sensitivity of the larvae towards the actual acceleration they are experiencing. Therefore, several batches of untreated WT larvae were exposed to accelerations in the range between 4 and 16 g. Their activity percentage is plotted as the mean value and the standard error in figure 4.27. For a finer resolution on the sensitivity this experiment was performed with larvae at a stage between 120 and 130 hpf. The resulting data coincides with the intuitive assumption that an increase in acceleration causes an increased activity. A maximum activity plateau was found at after 14 g for the tested larvae which means that a further increase will not cause an increase in activity anymore. Due to the accelerometer only being able to measure up to 16 g the speakers could not be calibrated for higher values than this, which is why no additional values could be tested. With the activity percentage supposedly being at maximally possible values the acceleration for future screens is recommended to be at least 14 g. Depending on the assay,

however, a decrease in acceleration can be preferred and the best values need to be chosen on a case by case basis. When screening for hyperactivity for example a reduction in the acceleration could help to identify the corresponding phenotypes.

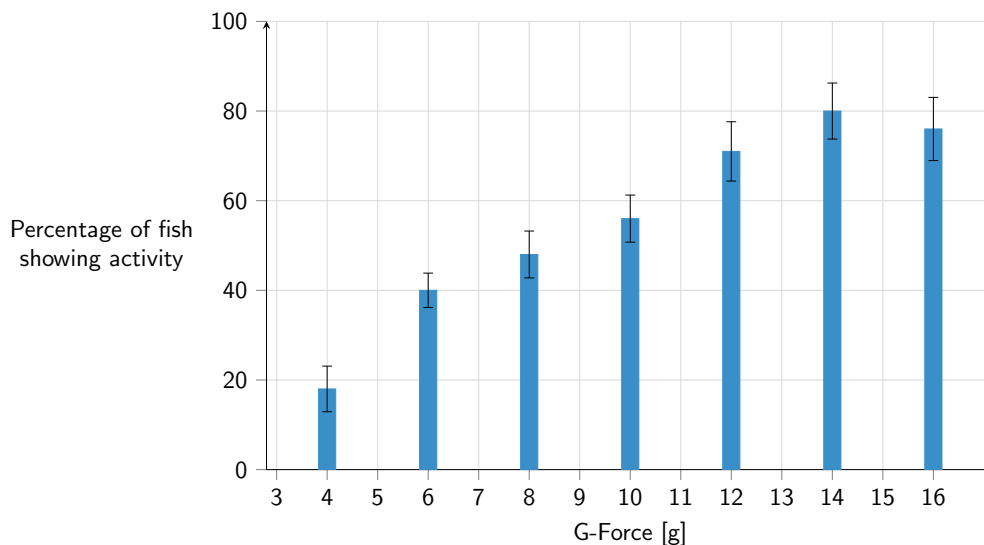


Figure 4.27: Results for a sensitivity analysis of larvae towards different acceleration values. 120 to 130 hpf old larvae were subjected to various acceleration values ranging from 4 to 16 g. An increase in the percentage of moving fish is observable with a plateau after 14 g. The chosen maximum of 16 g is due to the accelerometer having its measurement limit there.

To show the viability of the vibration system as a tool in chemical screens a test for the waking behavior with anesthetic Propofol was performed [128]. Propofol is a powerful drug that is often administered to humans to induce their loss of consciousness in general anesthesia for surgeries. It acts by potentiating either GABAA (γ -aminobutyric acid type A) or glycine receptors that both play an important role in the central nervous system, with them being the major inhibitory receptors in the mammalian brain [129]. Due to their substantive role for the functioning of the nervous system, any nonconformance in the receptor or the substrates can have drastic effects. It has been shown that mutations in the Glycine Transporter 1 for example [130] can cause severe diseases like glycine encephalopathy which can result in life-threatening problems with breathing and muscle movement. Luckily, the zebrafish was shown to be a highly suitable model for the involved pathways [131] so that it can be used in research on this topic. To learn more about phenotypes with mutations in the GlyT1 receptor for example, an important question to answer could be if these mutants do exhibit a delayed emergence when exposed to anesthesia like Propofol. To test this, a phenocopy of a GlyT1 mutant was created by exposing WT larvae to N-Fluorophenyl Propyl Sarcosine (NFPS). NFPS acts as a glycine transport inhibitor that targets the GlyT1

receptor family [132] and basically renders it useless. This way no actual mutant has to be used while still giving indicative results.

A major drawback when working with Propofol is its tendency to interact with materials made out of plastic [133] which can lead to decay and a loss in concentration when used with standard petri dishes [134]. Concentration values are therefore only representing the initial preparation and do not take the potentially decreasing concentration over time into account.

After exposing the larvae to $0.02 \mu\text{l ml}^{-1}$ ($\cong 54 \mu\text{M}$) Propofol for 30 min, an extensive washing was performed by rinsing the larvae in a net usually used for egg collection with fresh fish water for 30 s to guarantee no cross contamination with Propofol traces on the larvae. After the washing procedure the vibration response was recorded every 30 min for untreated WT, WT treated with only NFPS, WT treated with Propofol and WT plus NFPS treated with Propofol. The results are plotted in figure 4.28 with the phenocopied GlyT1 mutants showing a significantly prolonged waking behavior compared to the Propofol treated wildtype.

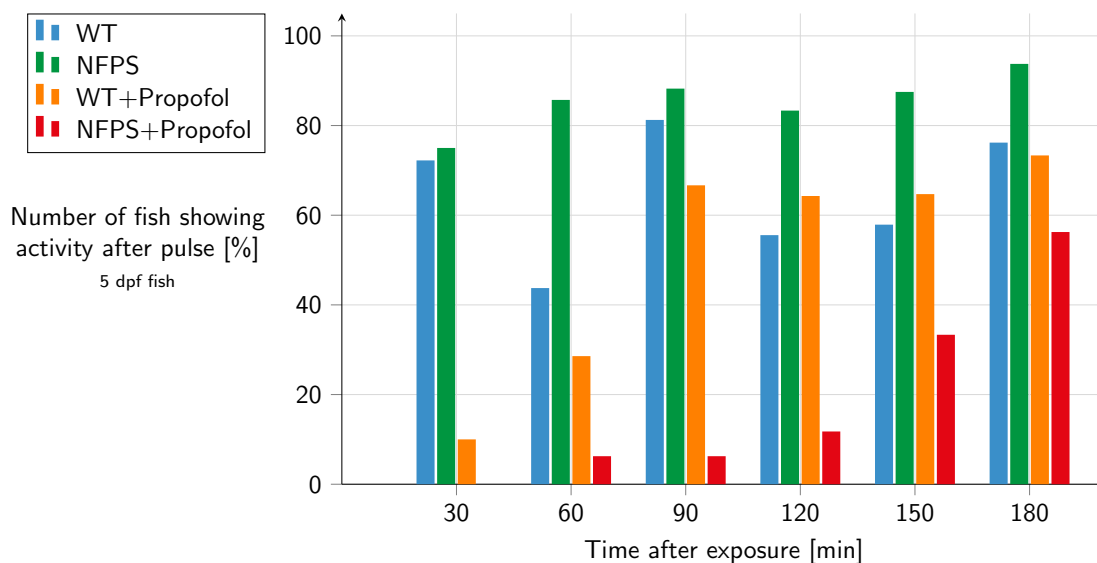


Figure 4.28: Results for the waking behavior of NFPS and Propofol treated larvae. The NFPS+Propofol treated fish show a delayed waking behavior compared to the WT+Propofol samples. The WT and NFPS samples are used as a reference for untreated larvae. A vibrational stimulus of 14 g and 1 ms was used for all recordings.

With the obvious effects the cannabinoids have on the PMR, they were an interesting set of compounds to use on the vibration system in order to verify that this system can indeed be used as a tool in chemical screens as well. For this experiment, four cannabinoids were selected, the larvae then exposed and their behavior recorded on the vibration system.

The results of the automated analysis are shown in figure 4.29 with similar responses to the compounds than what could be observed in the PMR screens. There is an obvious tendency towards a calming effect with a decrease in the percentage of fish that respond to the stimulus compared to the untreated WT.

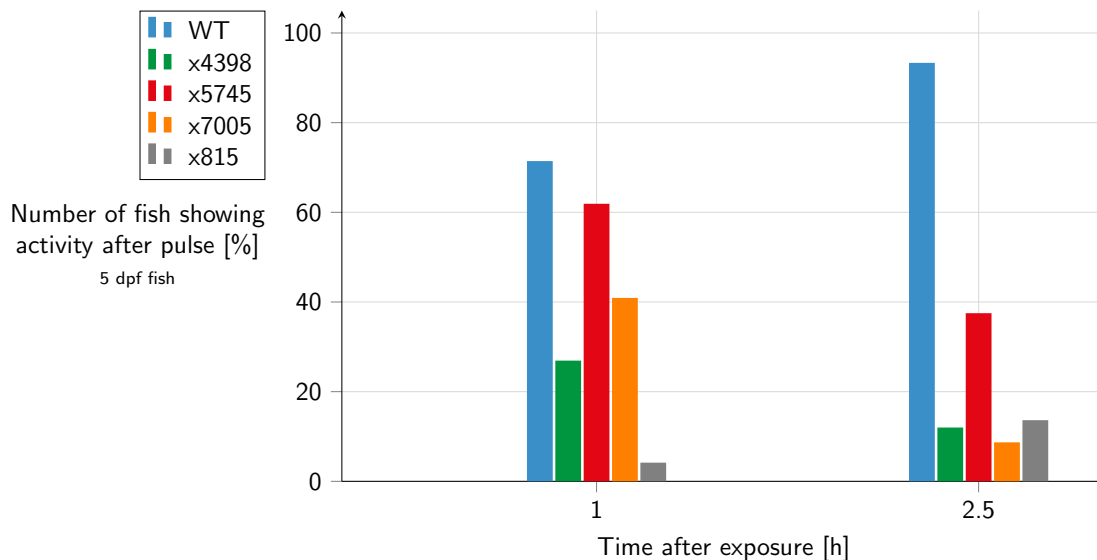


Figure 4.29: Results for the effect chosen cannabinoid compounds have on the vibrational startle response of 5 dpf old larvae at a 100 μM concentration. The cannabinoids seem to cause different results with x4398, x5745 and x7005 showing a decrease in the activity that gets more pronounced with the longer exposure time while x815 on the other hand shows a slight recovery. Generally, a calming effect can be observed with the activity staying below the untreated wildtype for all treated samples. A vibrational stimulus of 14 g and 1 ms was used for all recordings.

The results emphasize how the vibration system can be used for both genetic as well as chemical screens to achieve quick behavioral readouts. Compared to existing solutions that utilize the vibrational startle response this system is based on a simplified excitation method that allows parallelization and ultimately increases throughput to completely new levels. The system's design with multiple exciters that share one common signal source as well as imaging device reduces the hardware requirements and makes the system affordable and easy to set up. Anyone can use the system thanks to the simple GUI that has been developed without the need for commercial solutions resulting in completely independent and free control software.

4.6. Conclusions

By developing a cost-effective yet fully characterized vibrational exciter, a completely new approach to high-throughput startle responses could be realized. Compared to other acoustic and vibrational excitation setups the proposed system is capable of delivering precise stimuli to multiple dishes in relatively fast succession, only limited by user-chosen parameters like pause- and pulse-durations as the time the camera needs to move in between speakers is negligible. This allows the recording of a never before possible number of recorded larvae in a short time. By using multiple exciters in parallel more dishes can be screened as the need for habituation when replacing larvae can be circumvented by recording other samples in the meantime. The chosen number of five exciters can even be extended to further increase the throughput.

By developing an independent software application that incorporates multiple functionalities ranging from high-speed camera recordings to audio signal generation, a fully independent solution was presented that makes the system even more affordable as no external fee-based interfaces need to be used. With an emphasis on a simple GUI, performing sophisticated vibrational excitation experiments is possible at just the press of a few buttons in one central application. A newly developed analysis pipeline also helps coping with the many recordings and resulting large data sets.

A detailed overview over the capabilities of other vibrational systems and how their performance can be compared to the proposed system is given in table 4.3. In summary the proposed system allows precise vibrational startle experiments at a fraction of the cost of comparable systems with a price for all materials of approximately between 1000 to 2000 €. It also simplifies the usage by combining all functionality in one user-friendly control application that also offers convenient features like the ability to plan and schedule multiple pulses over extended periods of time.

The system was shown to work and be beneficial in the characterization of larval behavior as well as chemical screens. It was used to characterize the age dependent development as well as the stimulus sensitivity of the startle response in zebrafish and was verified by testing phenocopied GlyT1 mutants with the help of NFPS towards their waking behavior with the anesthetic Propofol as well as the effect cannabinoids can have on the startle response.

Table 4.3: Overview of the feature sets between several published and commercial systems for the vibrational excitation of zebrafish and the proposed system from this work.

Feature	Burgess et al. [62]	Viewpoint ZebraBox	Roberts et al. [110]	Pantoja et al. [61]	Marcato et al.
Vibrational Exciter	Brüel&Kjær	Modified speaker	Speaker	Speaker	Modified speaker
Excitation direction	Vertical	Horizontal	Indirect	Indirect	Vertical
Recording speed	1000 fps	1000 fps	1000 fps	30 fps	1000 fps
Recordable larvae	25–30	12	24	48	20–30
No pause for habituation due to parallelization	-	-	-	-	✓
Cost-effective	-	-	✓	✓	✓
Variable acceleration at high precision	✓	-	-	-	✓
Scheduling ability	-	-	-	-	✓
Independent and free software	-	-	-	-	✓
Automated analysis pipeline	✓	✓	-	✓	✓

5. Touch Response

Together with light and vibrational startle, the first observable escape behaviors in zebrafish larvae include the response to tactile stimuli after 21 hpf [135]. Touching the head or tail of a larva at this stage causes several rapid coilings, while later stages add swimming episodes to the response. Depending on the location of the touch, different neuronal pathways are involved. Touching the head must be mediated by trigeminal neurons [136] while in the tail only Rohon-Beard neurons are present at this stage of development [137]. With increasing age the touch response becomes more prominent [138] and can be tested on hatched fish after 2 dpf, eliminating the need for manual dechoriation.

5.1. State of the Art

So far this type of experiment has been done solely manually [139, 140, 141, 142, 143] without an automated solution available at all, especially not a high-throughput one. Touching an only 3.5 mm long object is challenging which is why even modern protocols [65, 144] still not only require time-consuming manual steps but also introduce operator dependent variables like force, touch location, or sometimes even usage of anesthetics or fixation in agarose gels. Possible side effects of this like agitation or differences in responses due to varying touching speeds or locations have apparently not been considered in most touch response assays so far but are of great importance in order to fully characterize and utilize the underlying mechanisms [145]. Commonly the performed methods are based on stimulation of individual larvae by hand under a microscope with a thin object like an insect pin or blunt needle. For this the larva needs to be positioned and aligned properly so that it is in the field of view of the used optical setup. This is an obvious limitation when a large number of larvae is supposed to be screened as this is a tedious and slow step that is only necessary because the manual stimulation in a well is nearly impossible to perform by hand without obstructing the view of the camera. This is why developing an automated system to measure touch response not only completes the behavioral analysis pipeline comprised of PMR and vibration, but can also be the first of its kind, allowing unbiased, computer controlled touch experiments with freely movable larvae.

5.2. System Requirements

With no automated solution available at all, an automated system has large potential in simplifying the way touch assays are performed. More specifically the way the actual touch is delivered needs to be improved as the most important step. Manually touching a larva has numerous downsides with it being highly subjective and dependent on the operator. Especially small objects make manual handling and observations difficult, with humans not being able to control their motor functionality precisely enough due to muscle contractions and resulting oscillations. Even though assays like this have been performed successfully manually, the problem is in the number of observable responses per time and the potentially high variance in between stimuli. From a scientific point of view an unbiased automated approach is obviously favorable.

To create such a system several key requirements needed to be fulfilled:

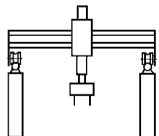
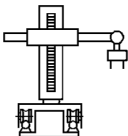
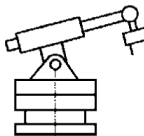
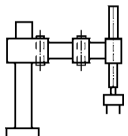
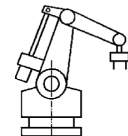
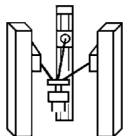
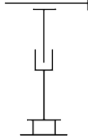
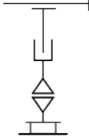




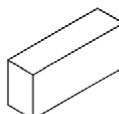





- Touch stimulation needs to be automated to result in repeatable responses
- System should be based on well plate format to simplify handling and increase throughput
- High-speed camera recordings are necessary to capture fast swimming motions
- A variety of users need to be able to use and control the system without supervision
- Best case scenario: Implementation of an autonomous touch functionality that does not require human interaction at all; this would require:
 - Robust object detection via image processing
 - Autonomous pathfinding calculations

With a similar requirement for high-speed recordings there is an obvious overlap with the vibration system. Therefore, already existing experience from the camera system and illumination setup was transferred almost directly and only had to be adjusted slightly. However, the motor setup and image analysis algorithms needed to be developed from the ground up in order to stimulate the larvae in the intended manner, be able to detect them and move the touch mechanism to the defined position autonomously in the first place.

5.3. Mechanical Setup

The most important step in the touch system development was finding and implementing a suitable touch mechanism. An obvious choice could be a robot arm mimicking the human movements in three dimensions, however, such equipment would be expensive and overly complex with unnecessary degrees of freedom. The space a robot can reach is called its work envelope or workspace. Depending on the type of robot the range of its movement can differ between variants. The deciding factors for this are the size and the number of motorized axes. Probably the most common variant is the Cartesian robot in which the axes are aligned orthogonally to each other. This variant is very popular in for example modern 3D printers. But there are alternatives. In table 5.1 several different variants are shown, illustrating the various work envelopes and the mechanical configuration of the individual robot.

Table 5.1: Overview of typical industrial robot configurations according to [146]. Images courtesy of Carl Hanser Verlag GmbH & Co. KG.

Variant	Cartesian	Cylindrical	Spherical	SCARA	Articulated	Parallel
Layout						
Kinematics						
Work Envelope						

The shown variants all have advantages and disadvantages and the most suitable one has to be determined on a case by case basis. SCARA robots for example are the variant of choice for pick and place applications because they operate at high speeds while still being very precise in their positioning. More complex articulated robots are often used in the automotive industry for example, where modern assembly lines take advantage of their ability to move heavy objects or automate processes like welding and painting in for other robots hard to reach places. However, the mechanisms required to control robots like this are far more complex than for the intuitive Cartesian robot. In order to position the other robots in three dimensions the individual motors need to be driven so that the

resulting motion follows the desired path. It is usually much more intuitive to picture such positions in a Cartesian coordinate system than the robots' own coordinate system. Therefore, these positions need to be transformed in order to be able to position the robot correctly. Especially with multiple degrees of freedom this can become quite challenging and computational extensive. For the development of the touch system a simple Cartesian system seemed to be the option of choice because of their low-cost and relatively simple controls. By mounting two belt driven linear axes together in a 90° angle, the movement in the 2D plane could be achieved. To move up and down (to allow moving from well to well in a well plate) a linear actuator was used. With this the robot was able to move anywhere on the well plate in three dimensions. With the chosen belt driven axes and the linear actuator the system needs to find the reference positions on every startup. Otherwise the coordinates would be completely off and a correct positioning impossible. The easiest way to implement functionality like this is by mounting end switches to the ends of the axes that get triggered when the stage touches them. The linear actuator, however, translates rotational motion of the motor into linear motion by turning a threaded rod. To be able to find its reference position an end switch needs to be mounted so that the upwards moving rod is able to hit the switch. For this an end switch holder was designed that can be mounted directly to the motor and carries an end switch at its top end. Figure 5.1 shows the designed holder which was then 3D printed.

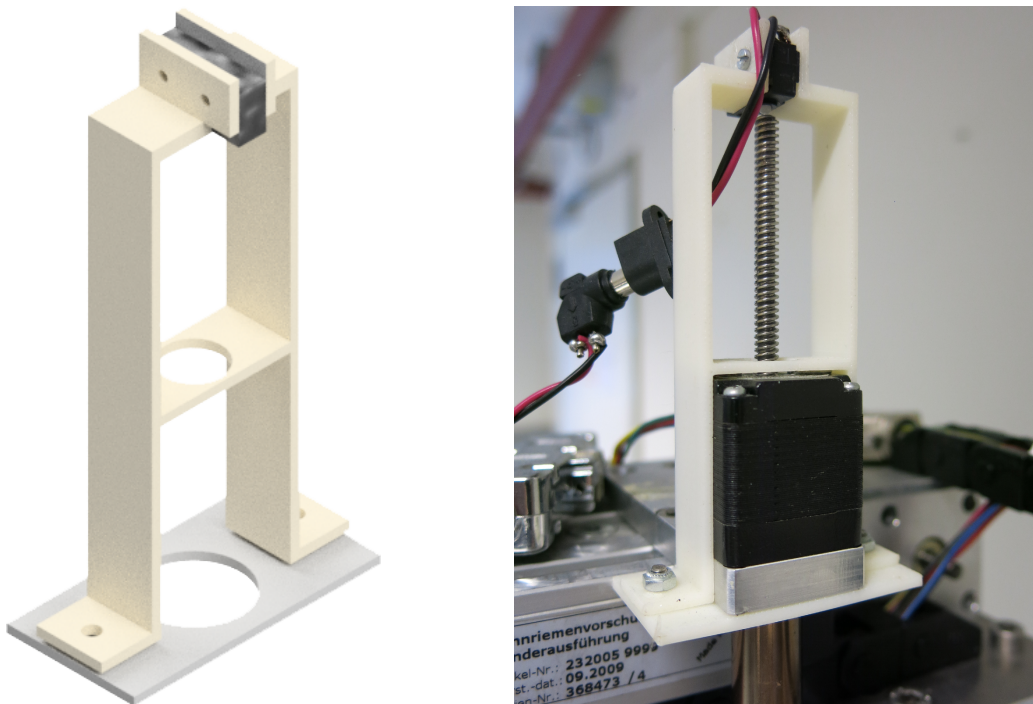


Figure 5.1: Design and printed product of an end switch holder for the reference position of the linear actuator controlling the needle position in z direction.

As the actual tool to touch the larva, it seemed reasonable to use a thin needle-like object as this is already the method of choice in the manual assays as well. This needle can then be lowered into the well and cause the startle response by touching the fish. With three degrees of freedom, two potential methods of performing the touch come to mind. For one the needle could be moved outside of the water and be lowered on top of the larva until it touches it. This would require sensitive sensors to keep the needle from piercing the larva though. In initial testing it could also be observed that the needle breaking the surface tension of the water causes a substantial amount of water displacement. As this can interfere with the results of the experiment by accidentally stimulating the larva to move, the second option was preferred. For this the spring-loaded needle was lowered to the bottom of the well where an end switch senses the barrier and retracts just so far as to not scrape the well bottom. In figure 5.2 the needle head pressing against the spring loaded end switch inside the holder is shown.

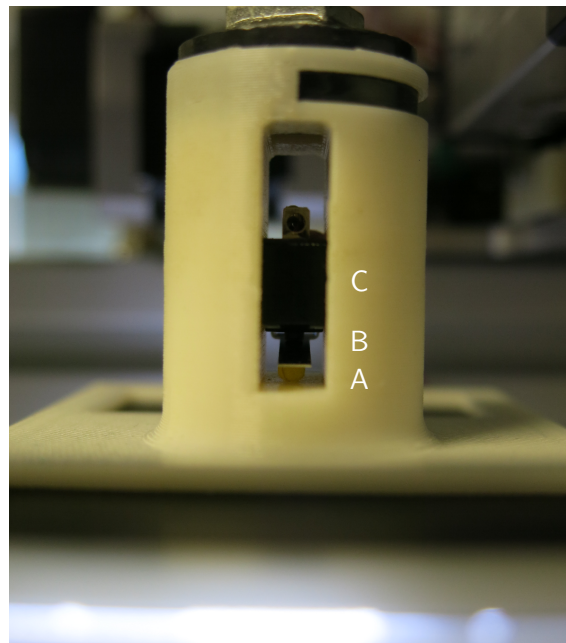
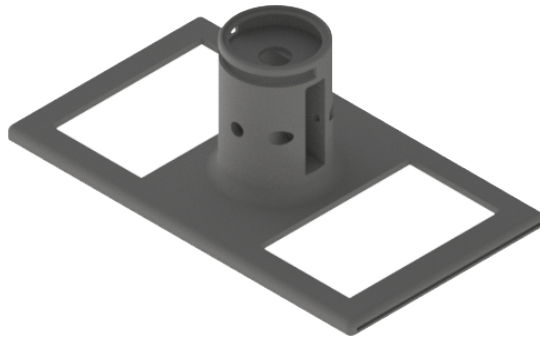


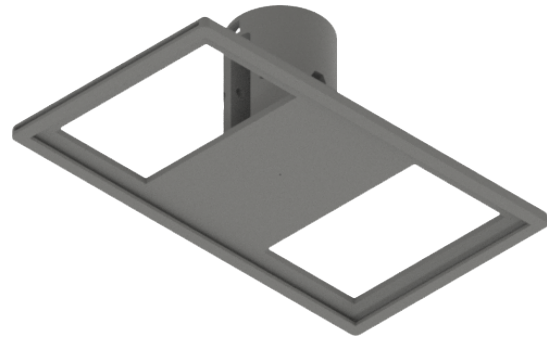
Figure 5.2: The round needle head (A) inside the holder presses against the spring (B) of the end switch (C). At contact with the bottom of the well the end switch is activated, the movement stopped and the needle retracted until it hovers slightly above the well bottom. This is a crucial safety feature and helps to even out small height deviations in the plate. This way the needle finds its end position dynamically and no calibration is necessary.

Moving the needle sideways in the 2D pane, the larva can then be touched with the side of the needle which is blunt enough as to not cause any harm. When moving the immersed needle there is also some water displacement observable, but only to minor extents. In

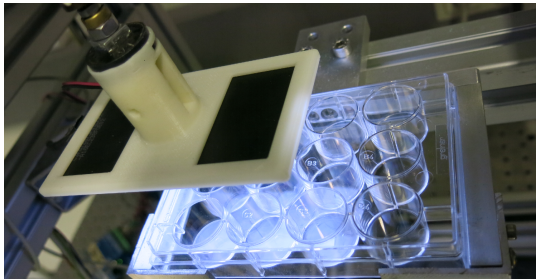
figure 5.3 the model for the proposed needle holder is shown. As needle a stainless steel household pin was used as its thick end keeps the spring-loaded and loosely inserted tip from falling out of the holder. The needle is fitted through a small hole in the center of the holder and an end switch is mounted above it. When pressure is applied so that the needle is forced upwards, the end switch will recognize this. It also features a similar slot for the same backlight illumination sheet than the vibration system. This sheet is punctured so that the needle can travel through.



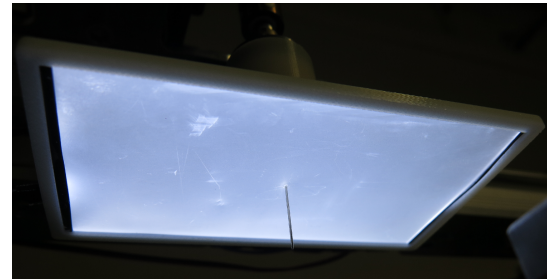
(a) Angled view from the top on the needle holder



(b) Angled view from the bottom - the hole for the needle is manually drilled after printing to ensure the correct diameter



(c) Mounted needle holder above a 12-well plate



(d) Needle holder with backlight and needle

Figure 5.3: Overview of the needle holder design for touch experiments from various angles. The slot is used to mount the backlight illumination sheet. The slot on top is to hold a circular magnet that allows toolless detachment of the holder from the motor. A spring loaded microswitch is mounted inside the channel that holds the needle to sense the point of contact with the well bottom.

When testing the system it became clear that moving around a rigid holder like this can cause serious problems when the motor axes are falsely positioned. Once lowered into the well the needle will crash into the side walls if moved too far in one direction for example. This can potentially break the needle, the holder, the well plate or even the motor axes. To make the system safer the mount was designed to be easily detachable via a magnetic

connector as shown in figure 5.4. This does not only allow the holder to break off the motor axis without damaging anything but also results in the opportunity to quickly change between mounts in case any future modifications require redesigned ones or completely new functionality is supposed to be implemented on the same system. A round magnet was inserted into a socket and a corresponding second magnet then permanently fixed to the linear actuator. In case of user error or system malfunctions this will prevent major damage to the system.

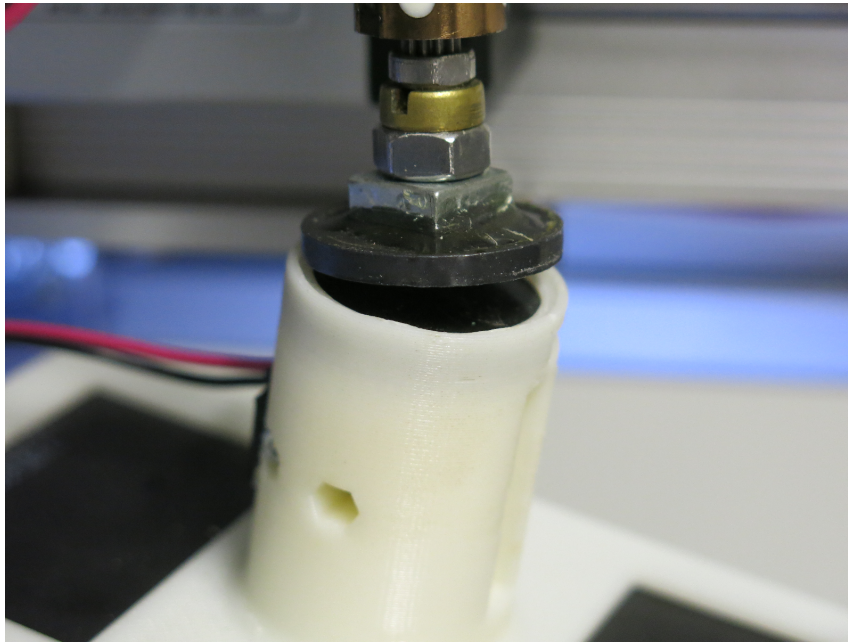


Figure 5.4: The needle holder is connected to the linear actuator via a magnetic connection to guarantee detachment if the needle would be moved too far to the sides. It also allows a quick and toolless exchange of the entire holder. Two round magnet discs are mounted to attract each other with one being fixed to the actuator and the other being embedded in the needle holder.

For imaging the same high-speed camera as in the vibration system was used. This also allowed reusing the required software class which speeded up the implementation. However, the mounting position of the camera was not as trivial to determine as with the vibration system. With the needle being required to enter the well from the top, the only option to see what is happening is by recording from the bottom looking up. Therefore, the camera has to be positioned on the opposite side of the touch mechanism. To minimize additional hardware needs, one option would be to fix the camera to the two dimensional motor axes of the touch holder. This would then lead to the camera being moved synchronously to the upper stage at all times and the needle always appearing centered in the image. However, this design has multiple drawbacks. First of all the camera mount would need

to be angled and bent around the well plate in a C-like shape. This can be considered to be a form of spring already which will inevitably cause oscillations when moving the stage. Such unpredictable camera movements would render subsequent analysis steps very difficult, with the larvae potentially appearing to be moving even though they are not. Secondly, a movable camera would also result in the field of view not being focused on the inside of the well at all times. If the touch stimulus was applied at the border of the well, only half of the well would actually be captured by the camera with the other half showing irrelevant parts of the well plate. With the larva swimming away from the position where the stimulus occurred this could mean that the larva cannot even be tracked over its entire swimming motion. For these reasons an additional 2D motor axes system was added on which the camera was then mounted. This allows the camera to be positioned independently of the upper stage holding the touch mechanism. Due to the available camera objectives and because a longer distance between object and camera increases the depth of field, the camera was mounted with a negative offset in height relative to the moving stage utilizing the space in a reused cube out of aluminum profiles. The camera holder presented in figure 5.5 shows this offset with the actual camera mounting holes being positioned on a downwards facing extension.

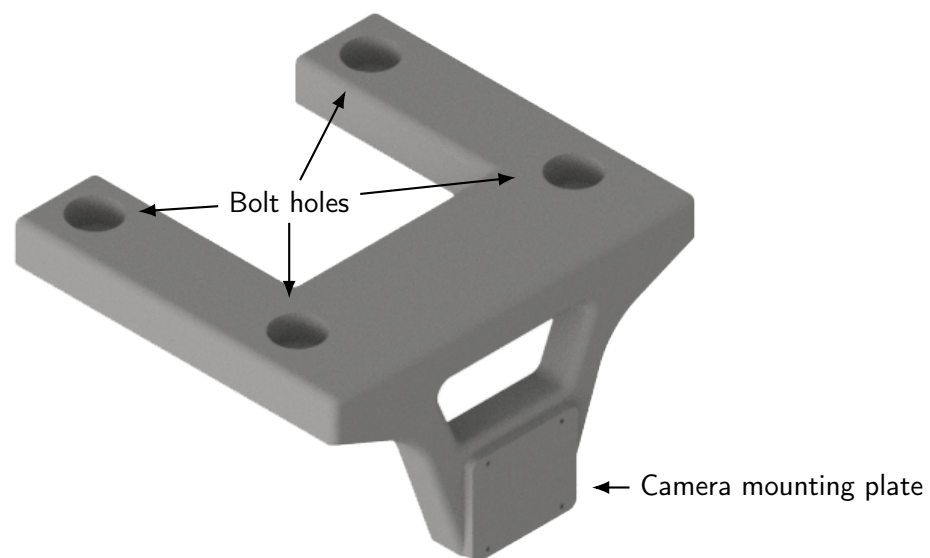


Figure 5.5: Design of the camera holder for touch experiments that is mounted to the movable stage via four bolts on the top and negatively offsets the camera on the side of the stage so that the distance between well plate bottom and camera increases.

The chosen motorized axes relied on stepper motors to drive them. Stepper motors are one type of electric motor next to other variants like DC or servo motors. They are very popular for applications that require precise positioning as they allow for an intrinsic position control

due to the way they are controlled. As their name already implies, they operate in discrete steps by using an alternating current in opposing coils. Every time a current is applied the motor will spin by one step and change its position by a specific angle the motor is built for. One popular configuration for example would have one step cause 1.8° of rotation. Each of these motors has to be controlled by a dedicated stepper motor driver. With the five motors in use five Nanotec SMCI33 motor drivers were used and connected to the PC in order to make them controllable from the computer. Multiple of these drivers can be connected in parallel via a single cable and can be identified in software via a configurable identifier integer. This allows the use of a single serial port in the software to communicate with all of them. Each of the drivers can be connected to additional rotary encoders on the motors to allow for closed-loop position control. In contrast to open-loop position control the added encoders ensure that the controller gets feedback whether the motor actually travelled the number of steps it was supposed to. Otherwise the motor could introduce positioning errors when there is excessive inertia or if the motor stalls for example. However, this is usually only an issue when the motors are moving at high speeds or undergo rapid directional changes when carrying heavy loads. The use of encoders proved to not be necessary as the added weight by the needle holder is well below 500 g and no sudden directional changes are to be expected. The completed hardware setup with needle holder, well plate and movable camera stage is shown in figure 5.6.

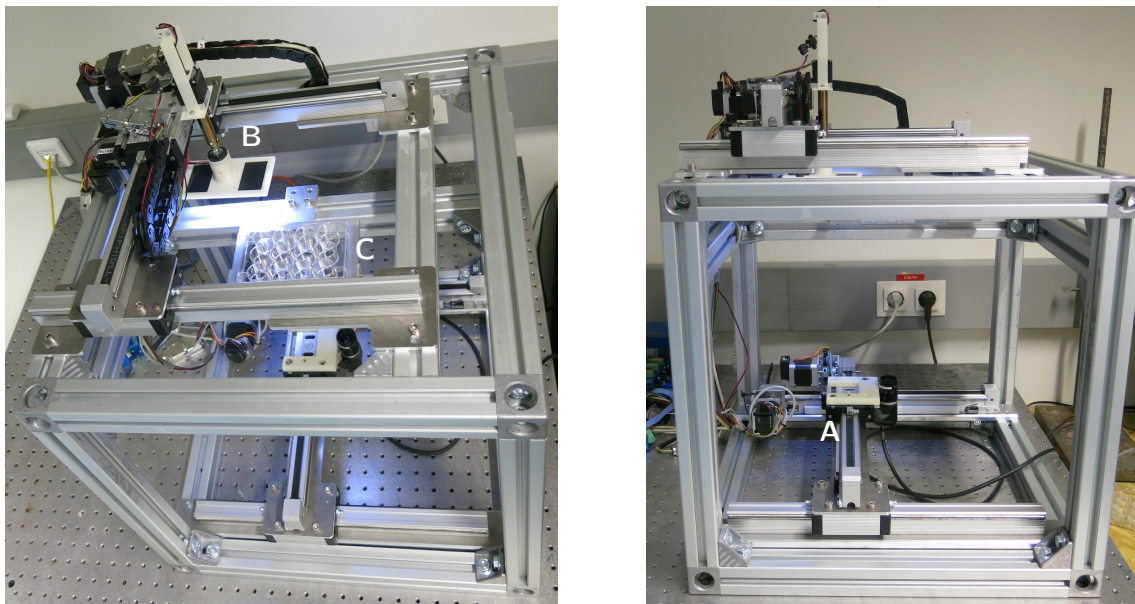


Figure 5.6: The entire touch system occupies only little space. The frame was built using aluminum profiles and houses the movable camera system at the bottom (A) and the touch mechanism on the top (B). A custom tray holds the 12-well plate between the camera and needle (C).

5.4. Software

With five motors, a high speed camera plus a real-time image processing pipeline the controlling application needed to be able to handle all this robustly and stay performant. Since so far no real time video analysis had to be performed while the system was running, this posed entirely new challenges in terms of handling the data streams and even though the camera is the same on both vibration and touch system, a completely different approach for the software development was required. Additionally, the image processing pipeline increased the complexity of the UI with potentially multiple image sources. For this reason, the application was written not with the previously used Windows Forms framework but the newer Windows Presentation Foundation framework.

This allowed for a clean separation of data logic and UI with its more sophisticated data binding approach via the MVVM pattern. Data binding makes updating the UI much simpler as the individual controls do not need to be updated manually anymore once their value changes. Binding the text displayed in a button for example to a string does not require manually updating this text again, instead it will be automatically updated once the string is changed. Another advantage of the WPF framework is that the GUI can be designed solely via XAML markup. This further separates the UI from the logic parts. Downsides of the MVVM pattern include the more complex structure which can be overkill for small applications. Also the readability and debugging of the code become harder with the increased use of declarative data binding instead of imperative, procedural programming methods. In applications, however, that update the GUI frequently like in the live preview of a camera the MVVM pattern can be really helpful. Figure 5.7 shows the flowchart for the developed application based on the MVVM pattern. It is obvious that the GUI is separated from the logic via the ViewModel class. All other components are then controlled via their own dedicated subclasses and update the variables in the ViewModel accordingly.

The GUI of the application is shown in figure 5.8 with the live preview on the left and a number of controls on the right that are used to move the individual axes manually on button or key presses or send the needle holder to a specific well automatically via a well plate locator field that displays the currently visited well with a colored marking. Choosing a well will move the touch mechanism as well as the camera to the associated positions and once arrived the needle will be lowered to the bottom of the well.

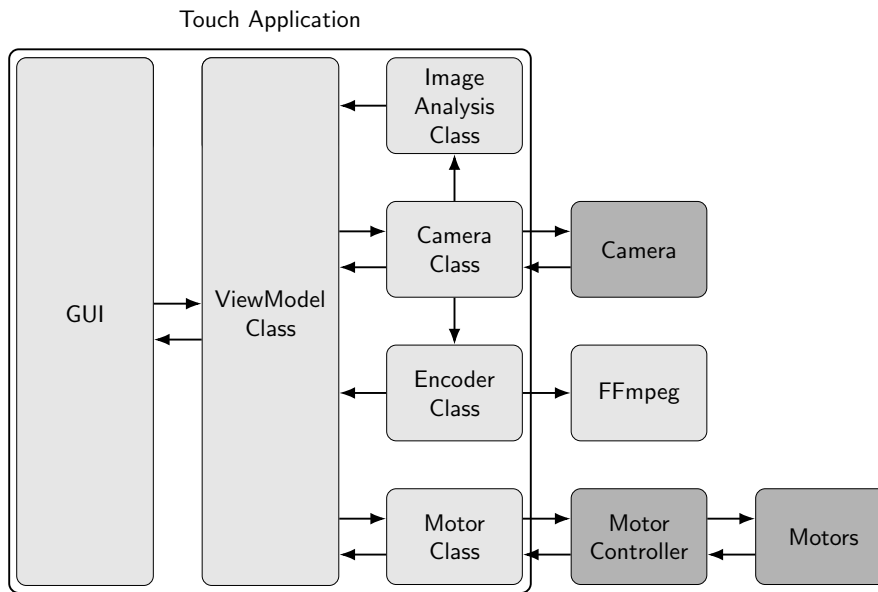


Figure 5.7: Flowchart of the touch system control application. Light gray indicates software objects while dark gray indicates actual hardware the application is communicating with.

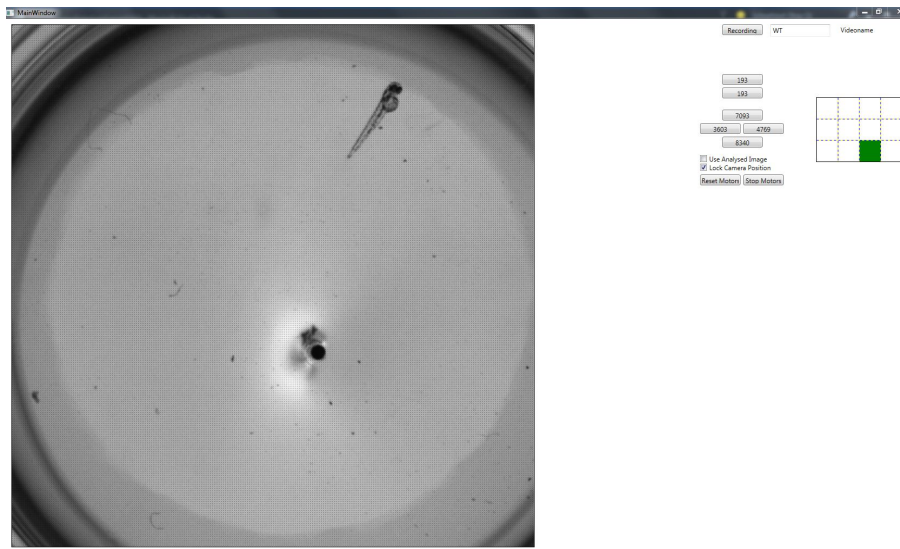


Figure 5.8: The touch system's GUI with the camera's live preview on the left and motor control buttons on the right. The well plate locator enables the user to choose a well on the well plate which will then cause the touch mechanism and camera to move to the associated positions. Once arrived the needle will be lowered to the bottom of the well and is ready to be used to touch larva. The mosaic pattern in the image is due to the camera having a Beyer filter and only the raw pixel values being displayed.

One of the main objectives was to develop a method to move the touch mechanism not just horizontally but also diagonally. Moving the needle diagonally is an important functionality to be able to touch the larvae no matter their orientation. With a 2D Cartesian motor axes system, however, the two independent motors need to be driven at exactly the right speed to be able to cause a precise diagonal movement. One way this is typically done is by using an external controller acting as a central clock that then gives signals for each stepper motor in a clock/direction mode. When using an orthogonal system and one central controller like this any diagonal line can be interpolated by using Bresenham's line algorithm [147]. This algorithm is commonly used to determine discrete steps on a hypothetical grid that approximate a straight line between two points. In case of stepper motors the calculated steps directly represent the steps the motors should do. More complex curves would need to be divided into smaller straight sections and could then also be approximated this way. With the hardware at hand, however, such an approach would have required additional items in terms of the clock controller. The Nanotec stepper motor drivers are capable of directly executing predefined sets at any desired speed, a function that can be utilized to circumvent the need for an external controller. The controllers can store up to 32 sets in its EEPROM. In this case the first 10 are reserved for basic operations like moving between wells and finding the reference positions. Since a diagonal line is achieved by adjusting the relevant speeds on each axis accordingly, a different approach to controlling steps like with Bresenham's line algorithm can be to precompute the required speed components for each of the axes and have the motor controllers then move the motors continuously with the right settings afterwards. A set is comprised of multiple values that need to be set before it can be stored in the EEPROM.

The most relevant EEPROM values are:

- The positioning mode which was set to be absolute, relative or a reference run.
- The travel distance that specifies the number of steps the motors should move
- The initial step frequency specifies the speed the motors start spinning with
- The maximum step frequency specifies the maximum speed the motors will reach after acceleration
- The resulting acceleration a can be defined in Hz/ms with the supplied value x needing to solve $a = \frac{3000}{\sqrt{x}} - 11.7$
- The same applies to the brake ramp

- The direction of rotation can be used to switch between forward and reverse operation when using relative positioning
- A useful feature is the ability to concatenate sets by specifying the set number of the next set
- Between two concatenated sets a pause can be defined that the controller waits before continuation

There are a number of additional settings [148] that have, however, not been used for this work like for example limiting the maximum jerk when accelerating or braking.

Figure 5.9 illustrates the diagonal movement computation by showing a schematic of a diagonal line between points A and B that represents the line the needle is supposed to travel to get from A to B at a defined velocity of v_{total} . Instead of calculating the individual steps and their offset, all that needs to be done in this case is to compute the velocity components in x and y direction. On an orthogonal grid this can easily be done by using the Pythagorean theorem to divide v_{total} into v_x and v_y based on the distances $d_{total} = \overline{AB}$, $d_y = \overline{AC}$ and $d_x = \overline{CB}$. In this case v_x will be substantially larger than v_y as the motors need to move a larger distance in x-direction in the same time as in y-direction. By doing so the resulting velocity v_{total} can be defined to be constant, which translates to the touch stimulus on the larva being the same no matter how the motors have actually moved. This is a crucial step to ensure consistent stimuli and high reproducibility. The direction the motors need to spin can be extracted from the sign of the distances.

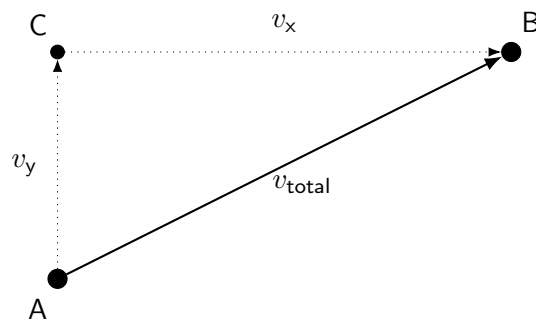


Figure 5.9: Schematic for the speed vector calculation to result in diagonal movement of the orthogonal motor axes.

In order to tell the motors which movements they should actually make two approaches have been realized. The first is a manual mode in which the user can actively and directly control the movement of the needle. This is done by drawing numerous lines on the well visible in the GUI. These then get translated into individual sets for the motors to move, are

stored on the stepper motor drivers and are then initiated on both drivers as simultaneously as possible. To translate the drawn lines into motor coordinates the previously explained speed vector approach is used to determine the speed for each of the motors individually. The number of steps to cover the arbitrarily long lines has to be adjusted depending on the width of the GUI in pixels. For this a conversion factor was established by empirically measuring the correlation between steps and travelled distance in the camera view. The supposed speed can then be calculated like in equation 5.1 depending on the relation of the distance in x (d_x) to the distance in y (d_y) due to the time for each axis movement intentionally being the same with $\frac{d_x}{v_x} \stackrel{!}{=} \frac{d_y}{v_y} \stackrel{!}{=} \frac{d_{total}}{v_{total}}$. The speed is supposed to be only given as positive values and the direction is then adjusted via the number of steps (n_{steps}) that can be supplied as positive or negative depending on the distance and the conversion factor between pixels and motor steps ($f_{conversion}$).

$$v_x = \left| \frac{d_x v_{total}}{d_{total}} \right| = \left| \sqrt{\frac{v_{total}^2}{1 + \left(\frac{d_y}{d_x}\right)^2}} \right|$$

$$v_y = \left| \frac{d_y}{d_x} v_x \right| \quad (5.1)$$

$$n_{steps \text{ in } x} = d_x f_{conversion}$$

$$n_{steps \text{ in } y} = d_y f_{conversion}$$

In edge cases as when the movement is purely horizontal and does not involve the vertical axis at all the motor driver is supplied with a dynamically precomputed pause that is used to wait for the actual movement to finish. The algorithm for establishing and loading the individual sets to the motor controllers is shown in figure 5.10 in the form of a flowchart.

For the implementation to work reliably it is important to not use acceleration values in the driver sets, otherwise the speed calculations will also need to include the increase in speed over time. With the low weights and slow speeds that were used to move the motors the omitted acceleration was not an issue with the motors neither stalling nor noticeably losing steps.

Next to the semi-automated movement of the needle via manual drawn lines a second method for fully autonomous touch stimuli was developed. Based on an image analysis pipeline the needle and larva are detected, their detected coordinates used to find an optimal path for the needle to arrive at the tail of the larva and the needle then moved accordingly. Figure 5.11 lists the required steps in order to find the needle and larva in the image.

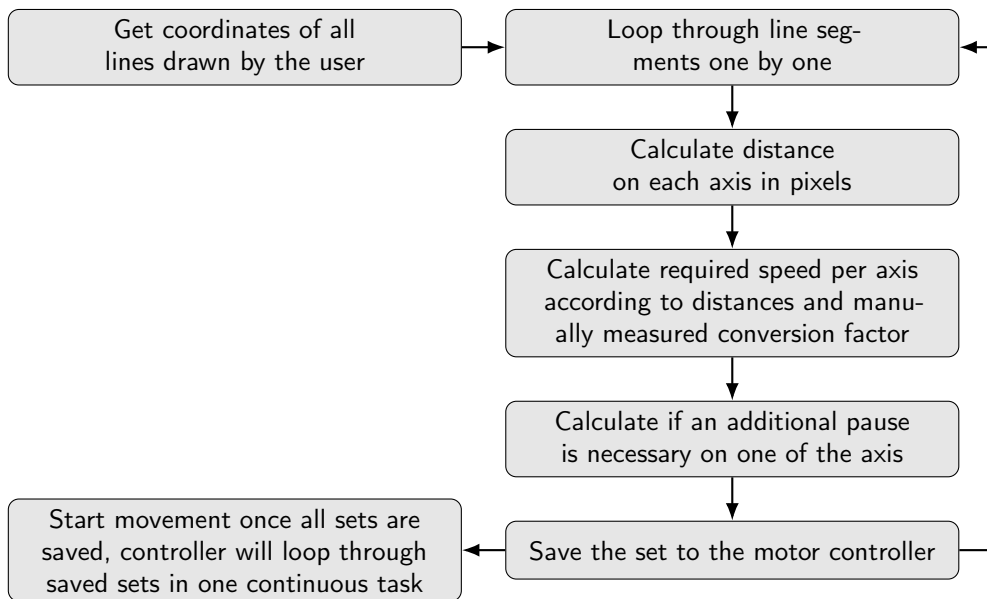


Figure 5.10: The touch system’s 2D movement algorithm. A manually measured conversion factor is used to translate the coordinates according to the size of the GUI window. The user drawn lines are translated into sets for each of the motor controllers to allow diagonal movements. For this the speed for each motor is calculated according to the Pythagorean theorem as seen in figure 5.9.

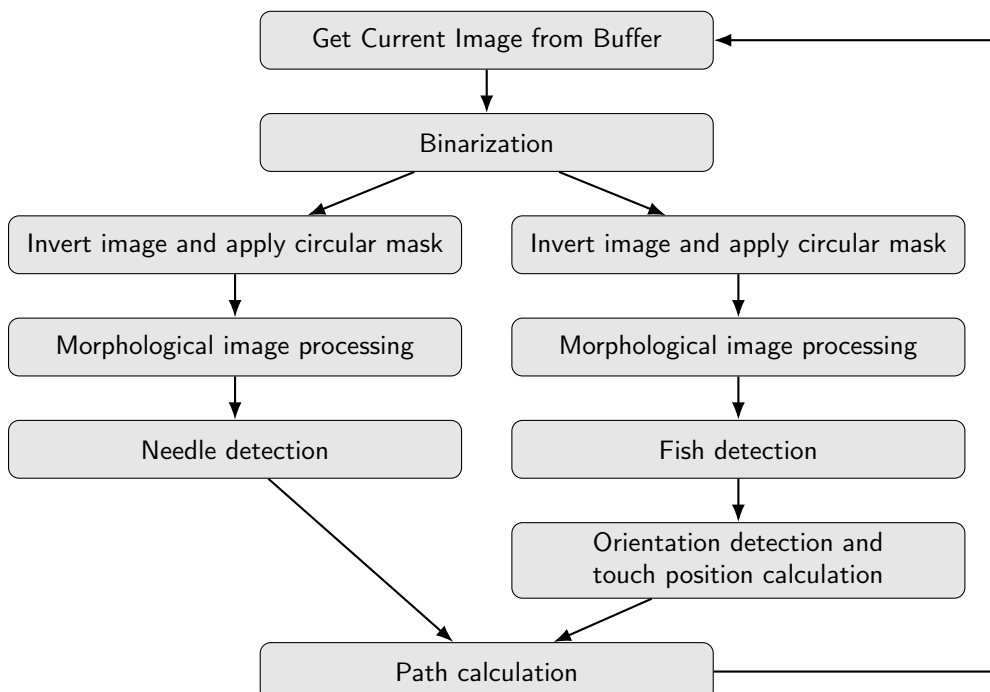
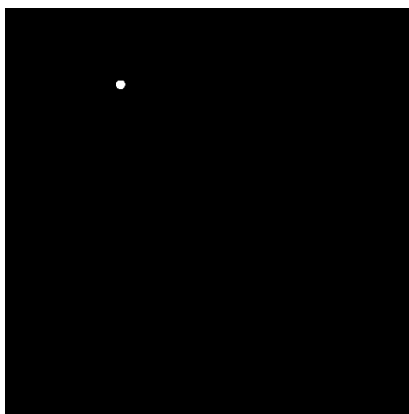


Figure 5.11: Flowchart of the touch system’s object detection algorithm. The image is preprocessed with two separate binarization threshold values before the objects are detected via blob detection. The larvae’s orientation is determined and the optimal path from needle to larvae then calculated. The path is updated multiple times per second as quickly as the computer is able to.

The entire algorithm runs in a continuous loop parallel to the camera which leads to the path being updated almost instantaneously. When activated this mode uses the images from the GUI image buffer and applies several image processing operations from the AForge framework to the grayscale image. Since no color details are necessary for this operation the first step is a binarization to convert the image into a black and white image with only the two pixel values 0 for black and 1 for white. For the built-in blob detection function to work the image needs to be inverted afterwards so that the background is black and the objects white. For performance improvements the image is also masked with a black circular ring on the outside that limits the search area to the actual well and removes the well wall and well plate from the field of view.

For a more robust detection of the needle, two different binarization thresholds have been used. The needle has proven to always be the darkest object in the image so a very low binarization threshold removes any unwanted artifacts and results in the detection of just the needle's circular tip. This was especially helpful because the water surface curvature around the needle caused a halo like effect that made a robust detection of the needle troublesome. However, the larva would not be visible anymore with only this binarization so a second, higher binarization threshold had to be used in order to detect the fish separately. The image quality was further improved for better detection results by morphological image processing operations. A 3x3 erosion and dilatation filter and an additional filling step up to a hole height and width of 20 pixels are performed to get rid of background noise and unwanted particles. In figure 5.12 the processed images for each of the two thresholds are shown.



(a) Low threshold for needle detection



(b) High threshold for larva detection

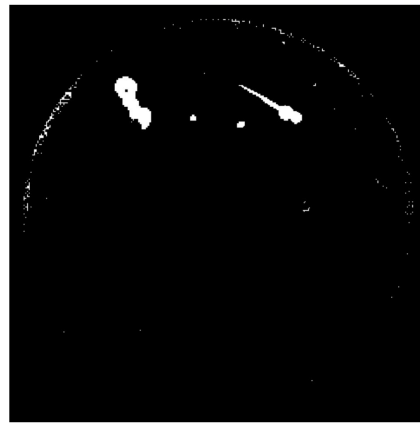
Figure 5.12: Effect the two thresholds have on the binarization. The low threshold allows robust needle detection where virtually all other objects and noise are eliminated. A higher threshold is then used to detect the larva according to its size and slender shape.

These thresholds are subjective to the camera and lighting conditions and need to be empirically defined for the imaging setup - a slider in the GUI lets the user reconfigure the value for the larva detection if necessary. The needle detection on the other hand appeared to be so robust that no reconfiguration by the user was ever necessary.

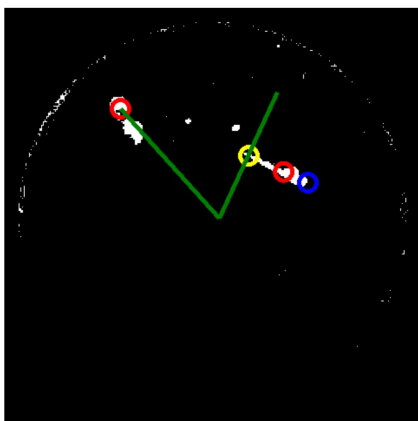
The resulting path is visualized in an overview in figure 5.13. A raw camera image is shown together with the binarized version used to detect the larva according to its size and shape. For better visualization the pathfinding results are also shown with the center of gravity in the needle as well as the larva being shown by a red circle. The larva's head and tail position are also detected and indicated by blue and yellow circles. Finding an optimal path between needle and tail position is based on the shortest distance between the needle and a point perpendicular to the larva's tail position.



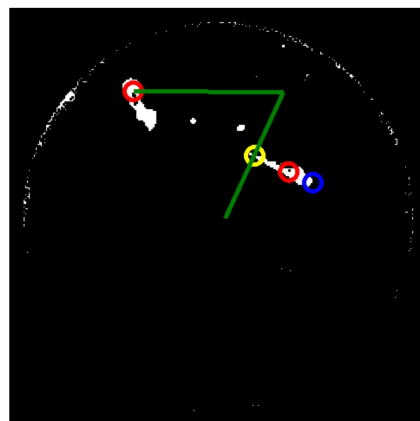
(a) Raw camera image



(b) Image after binarization



(c) Image with detected objects and drawn path



(d) Adjusted path depending on needle location

Figure 5.13: The touch system's object detection pipeline detecting the needle and larva position and calculating the shortest path that results in an orthogonal touch on the tail of the larva.

In a geometric view the planned pathfinding can be visualized as in figure 5.14 with an orthogonal coordinate system that has a large circle representing the well, the detected needle and the detected larva as objects in it.

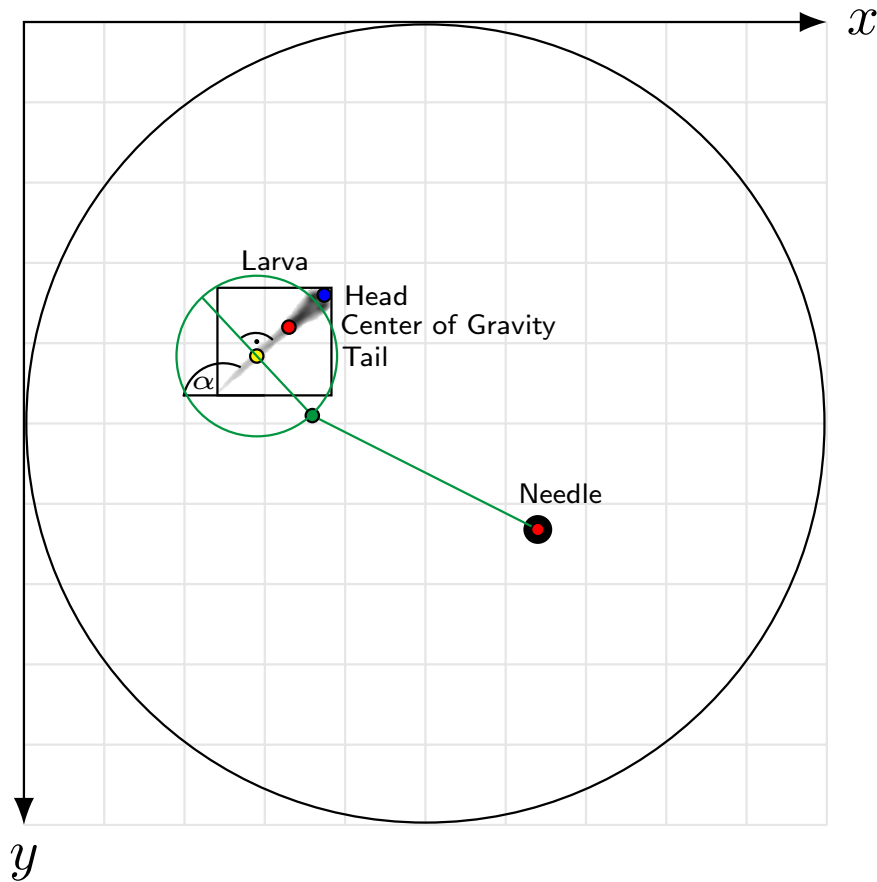


Figure 5.14: Schematic illustration of the geometric elements that are used to calculate the optimal path the needle should be moving to touch the larva at its tail with an orthogonal motion. The needle's and larva's centers of gravity are detected via blob detection. Afterwards the angle α is calculated using the second order central moments. With this the normal equation can be established and the two opposing points on a circle around the larva can be found. The one with the shortest distance to the needle is preferred as long as it is positioned inside the well. The motors can then be moved between the three points, which results in an autonomous touching of the larva.

The shortest path the needle could take is directly to the larva and then continue the movement through it to guarantee a touch stimulus. However, this would result in random touch locations and touch angles depending on the orientation of the larva. For example the path to the center of gravity could go through the head of the larva first which would cause unwanted stimuli. A better approach is to settle on a set of rules to make a touch as uniform as possible. In this case it was decided in agreement with biologists from the Institute of Toxicology and Genetics (ITG) at KIT that a touch should be applied not to

the head but only to the tail of the larva. For the angle an orthogonal touch was chosen that has the needle always move towards the tail in a 90° angle. In theory any other angle could also be implemented depending on the desired experimental conditions. However, in such a case additional complexity needs to be introduced, as the direction from front to back or back to front might play a role as well. At an orthogonal motion this can be omitted which is why for this prototype only orthogonal touching was considered. To make the path fully independent of the orientation of the larva, an imaginary circle with a diameter larger than the length of a larva acts as the switching point between general movement towards the larva and orthogonal movement towards the tail.

The pathfinding itself is then based on geometric calculations that involve the normal equation to the larva so that an always orthogonal touch can be guaranteed. In order for the needle to be able to move to the larva a total of three points on the path is necessary. The needle's starting position, the point in which it changes the direction from angled to orthogonal and the end position where the needle should stop moving again. However, there are a number of additional points necessary to establish these coordinates on the path.

First the needle and larva need to be detected. After finding the centre of gravity for both needle as well as larva via blob detection, the angle the larva is oriented at is calculated via its second order central moments. This results in a general orientation of the entire object and does not take into account the head or tail of it. By comparing the centre of gravity coordinates with the coordinates of the centre point of the bounding rectangle the angle of the general orientation can be corrected to give the true orientation of the larva between -180° and 180° . In this case an orientation angle of 0° was set to point in the left direction, 90° up, -90° down and 180° as well as -180° to the right. Once the true rotation angle is available the head and tail positions can be identified. The head is calculated by cropping and rotating the larva's bounding rectangle and identifying the minimum bounding box after the rotation with the head aligned to the left of the coordinate system. Finding the centre of gravity for this newly positioned larva results in the exact distance between the outer head position from the centre of gravity. As position on the tail the larva is supposed to be touched at, a point was chosen that is equidistant from the centre of gravity to the head but in the opposite direction. By changing the distance value the point can obviously be moved to any desired position on the tail and does not have to stay fixed to the currently chosen location. To correct for the initial rotation the points' coordinates are transformed via their corresponding ratios depending on the rotation angle. This is shown in equation 5.2 with $CoG_{larva}^{x,y}$ being the centre of gravity components of the detected larva,

$D_{\text{rotated head}}^x$ being the distance from the centre of gravity to the head of the larva in the rotation corrected minimal bounding box, $P_{\text{head}}^{x,y}$ being the x and y coordinates of the head and tail positions and α being the rotation angle between -180° and 180° . The point of touch on the tail was set to be at the same distance from the $\text{CoG}_{\text{larva}}^{x,y}$ as the head but in the opposite direction.

$$\begin{aligned}
D_{\text{rotated head}}^x &= \text{CoG}_{\text{rotated larva}}^x - 0 \\
P_{\text{head}}^x &= \text{CoG}_{\text{larva}}^x - D_{\text{rotated head}}^x \cos(\alpha) \\
P_{\text{head}}^y &= \text{CoG}_{\text{larva}}^y - D_{\text{rotated head}}^x \sin(\alpha) \\
P_{\text{tail}}^x &= \text{CoG}_{\text{larva}}^x + D_{\text{rotated head}}^x \cos(\alpha) \\
P_{\text{tail}}^y &= \text{CoG}_{\text{larva}}^y + D_{\text{rotated head}}^x \sin(\alpha)
\end{aligned} \tag{5.2}$$

Now that the individual coordinates for the head as well as touchable tail are established, the pathfinding via the normal equation on the tail position can be performed. Using the normal equation 5.3 in its general form for the point on the tail results in equation 5.4 as the slope is given with the tangent of the larva's already calculated orientation angle.

$$n(x) = \frac{-1}{f'(P_{\text{tail}}^x)}(x - P_{\text{tail}}^x) + f(P_{\text{tail}}^x) \tag{5.3}$$

$$n(x) = \frac{-1}{\tan(\alpha)}(x - P_{\text{tail}}^x) + P_{\text{tail}}^y \tag{5.4}$$

In order to find a starting point for the orthogonal motion, the equation 5.5 for a circle with a fixed radius around the tail position must be solved with the normal equation 5.4. This results in equation 5.6 that is solved by two opposing points on the circle around the tail position that represent the closest positions the needle should move to next to the larva before changing its direction.

$$r^2 = (x - P_{\text{tail}}^x)^2 + (y - P_{\text{tail}}^y)^2 \tag{5.5}$$

$$\begin{aligned}
x_{1,2} &= P_{\text{tail}}^x \mp \frac{\sqrt{r^2(\tan^4(\alpha) + \tan^2(\alpha))}}{\tan^2(\alpha) + 1} \\
y_{1,2} &= P_{\text{tail}}^y \pm \frac{\sqrt{r^2(\tan^4(\alpha) + \tan^2(\alpha))}}{\tan^3(\alpha) + \tan(\alpha)}
\end{aligned} \tag{5.6}$$

These coordinates do not have a solution when α is 0 or $\pm 180^\circ$ in which case the larva is oriented in parallel to the x-axis and thus the coordinates can be simply given as constant

in x direction and only shifted in y direction as visible in equation 5.7.

$$\begin{aligned}x_{1,2} &= P_{\text{tail}}^x \\y_{1,2} &= P_{\text{tail}}^y \pm r\end{aligned}\tag{5.7}$$

Once the coordinates for these two points have been established the algorithm needs to choose between them and find the one that is better suited for the current conditions. There are two conditions that need to be considered: (1) The closest point to the current needle location is preferable over the one further away as it automatically means that there will be no unwanted collision with the larva on the way there and (2) the point needs to be located inside the well so that the needle can actually get there without damaging anything. The distance between needle and point can be determined with the Euclidian distance with the smaller of the two distances then indicating the potential point that is located closer to the needle. Afterwards the second condition can be tested by verifying that the chosen point is located closer to the circle centre than the points on the circumference as shown in equation 5.8. If true the path is valid and can be used to autonomously touch the larva.

$$(C_{\text{circle}}^x - P_{\text{closest}}^x)^2 + (C_{\text{circle}}^y - P_{\text{closest}}^y)^2 \stackrel{!}{<} r^2\tag{5.8}$$

5.5. Assays and Results

To characterize the behavior of larvae to a touch stimulus the system was first tested according to the main adjustable parameter: the speed the needle is moved at. The software allows changing the resulting speed in terms of motor steps per second in Hz which translates to the needle travelling at a rate of 0.2876 mm/s for every 1 Hz. As a reasonable range of speeds the values of 10 Hz (2.88 mm/s), 25 Hz (7.19 mm/s), 40 Hz (11.50 mm/s), 60 Hz (17.25 mm/s), 80 Hz (23.00 mm/s) and 100 Hz (28.76 mm/s) were tested and the responses of on average 26 larvae per speed were recorded. Each touch was registered in a binary format depending on whether they responded to the touch or not. The same batch of three day old larvae was used on all speeds to ensure any behavioral deviations in the population are present on every speed. Roughly one hour of resting time was given so that the larvae were able to habituate again and not be affected by previous touches. For this they were put back into the incubator and taken out 10 min prior to every test. The speed of the motors was increased sequentially from 10 to 100 Hz. The results in figure 5.15 show that the speed has only little effect on the overall responsiveness. Only at very high speeds of 23 and 28.76 mm/s all touched embryos responded while the lower speeds still resulted in a robust activity of more than 80%. With increasing speeds the water displacement becomes

more apparent with noticeable waves forming on the surface. For this reason a speed of 25 Hz (7.19 mm/s) was considered to be the default choice to ensure robust activity and only little water displacement without causing an unnecessarily slow needle speed.

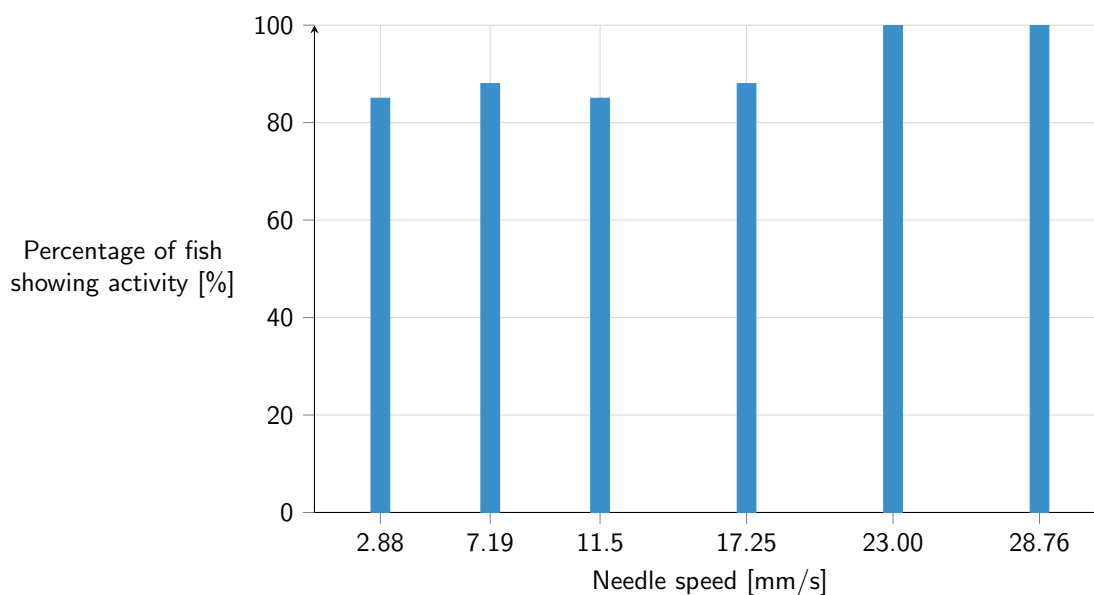


Figure 5.15: Results for the test of various needle speeds on the responsiveness of three day old zebrafish larvae. For each speed the same population of larvae was used and a habituation time of 1 h was given to make sure they are not affected by previous stimulations. The speed has only little effect on the overall activity. High speeds have the downside of causing noticeable water displacement.

The system was further validated by performing a similar screen as with the vibration system. The waking behavior of Propofol treated fish (similar to what was shown for the vibration system) is a perfect use case of the system as it involves characteristics from chemical as well as genetic screens. Using phenocopied GlyT1 mutants by exposing fish to NFPS can be considered a sort of genetic screen as they are made to behave like true mutants. Exposing them to Propofol and analysing their waking behavior is then a typical example for a chemical screen that is not aimed at just drastic morphological changes or toxicity. Larvae were again exposed to 2 μM NFPS at an age of 24 hpf for best phenocopy. After 72 hpf the larvae were exposed to Propofol at a concentration of 0.02 $\mu\text{l ml}^{-1}$ ($\cong 54 \mu\text{M}$). After 30 min they have been washed thoroughly and left on the touch system to habituate for 10 min before starting the experiment. The results are shown in figure 5.16 where a high WT baseline shows the reference behavior for larva at an age of 3 dpf. The WT baseline was recorded on a different day to give a clean reference the screening results can be compared to. The graph clearly shows that NFPS treated fish appear to behave similarly to the

untreated WT with a relatively high and only slightly fluctuating activity. Fluctuations like this can have multiple reasons, the most probable one being that every behavior is intrinsically susceptible to variance as the sample population shows genetic variation with no genotype truly being the same. Just like with PMR this is the reason why multiple touches have to be performed in order to find the true average of the population. With drastic effects these fluctuations become less of an issue. So is the waking behavior for Propofol treated WT clearly visible with a fast increase in the activity after roughly 3 to 4 h. The NFPS treated mutants on the other hand need far more time and did not fully recover even at the latest recorded time point that day.

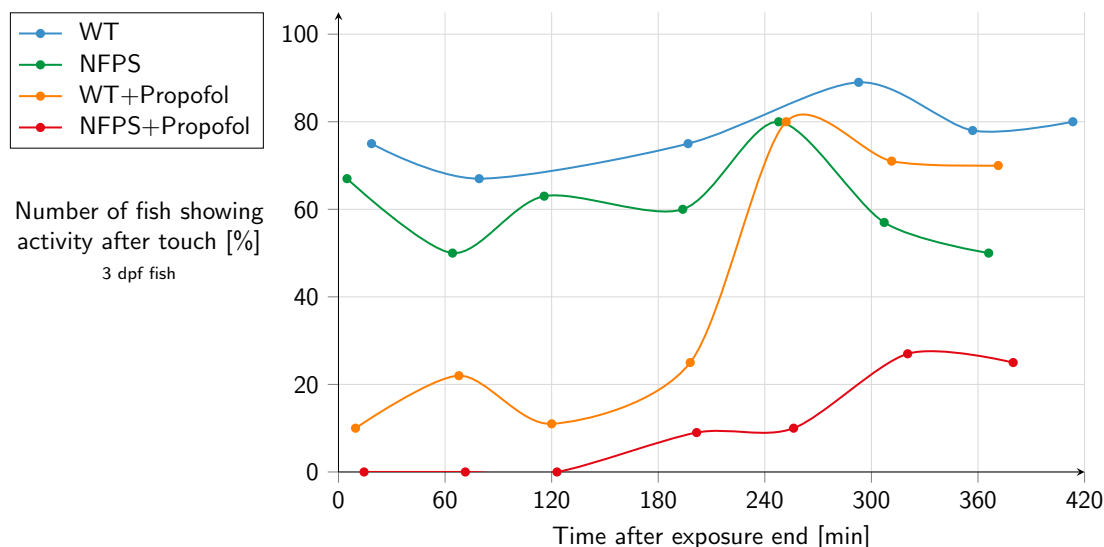


Figure 5.16: Results for the waking behavior of NFPS and Propofol treated larvae. The NFPS+Propofol treated fish show a delayed waking behavior compared to the WT+Propofol samples. The WT and NFPS samples are used as a reference for untreated larvae. The larvae were exposed to $2\ \mu\text{M}$ NFPS at an age of 24 hpf and to $\approx 54\ \mu\text{M}$ Propofol after 72 hpf. The first timepoints were recorded after an exposure duration of 30 min, the subsequent washing steps and 10 min of habituation time on the system.

For the experiment multiple larvae at each time point per condition were touched and their response registered the same way as for the speed analysis. The needle was cleaned with Ethanol when switching from one compound to the next. Between 33 and 41 larvae were touched on each time point resulting in a total number of 254 touches in a single day for this particular experiment. The data acquisition took a total of 123 min which results in a rate of around 2 touches per minute.

5.6. Conclusions

The proposed touch system has been shown to be the first functional automated system to perform touch response assays on zebrafish larvae and is currently undergoing KIT invention disclosure procedures. With a computer controlled touch mechanism in the form of the needle holder, a high-speed camera for high frame rate recordings and even an autonomous object detection pipeline a sophisticated system could be presented. It was shown to work reliably in the initial validation screen, in which the waking behavior of 3 dpf old larvae that have been exposed to the anesthetic Propofol and have been phenocopied to the GlyT1 mutants via NFPS was measured. The resulting data correlated well with the already established data from a vibration experiment with similar exposures.

With a rate of around 2 touches per minute the system was shown to be faster than the currently known protocols that all require manual positioning of the larvae under a microscope and careful manual touching. Especially considering that with conventional protocols a habituation time would be required after pipetting the larvae into the field of view of the camera. Unfortunately no data for the actual rate could be found but with the mentioned considerations a conservative estimate would be that the traditional manual systems need at least double the time to perform a single touch on a zebrafish larva than what the proposed system is capable of.

The system is therefore not only more precise and consistent but also faster than established protocols and can be a true improvement in using the touch response in zebrafish research for more than just small scale assays.

6. Summary and Outlook

In total, three independent systems have been developed that can be used to study behavioral phenotypes in early zebrafish. To do so three characteristic behaviors of developing zebrafish were chosen that can be triggered artificially and that cause measurable responses. Behavior is an increasingly popular field for biological, pharmacological and medical research as it enables much subtler observations than traditional assays that only target morphological changes or toxic effects. Combined with the promising model organism zebrafish this has huge potential for gaining new insights into the fundamental biological processes and how neurological diseases can be treated.

Photomotor Response

A robust imaging and analysis pipeline was developed to measure the photomotor response in 30 to 42 hpf old embryos inside the chorion. By combining automated sample handling, imaging and analysis a convenient solution for high-throughput PMR screens was established. The system is based on an inverted microscope that was modified with additional hardware like the IR lighting solution and was made fully controllable from a host computer via custom software that incorporated the Nikon SDK to record images from the camera. By controlling the movable stage and shutter via their respective serial commands the recording of a PMR experiment with 10 s of basal movement phase, short light flash by opening and closing the shutter, 10 s of excitation phase, a second light flash and 10 s of refractory phase could be implemented. The system records well after well to increase resolution and reduce optical distortion effects. This allows detailed observations of morphological effects as well as other behaviors like heart beat analysis in subsequent steps. A single experiment is configured via an interactive spreadsheet and the software allows scheduling one or even multiple timepoints for recordings without any human presence. The videos are stored as avi files for later analysis that extracts a motion index for every individual egg inside a well. This numerical representation of the movement was then used in further statistical analysis and visualizations. By developing a tool that is able to group results of the same type the analysis was extended to quickly characterize entire data sets automatically.

The PMR pipeline was tested and validated by performing a chemical screen of unknown cannabinoid-like compounds to test their effect on the PMR. More than 250 compounds were tested with a hit rate of effective compounds of around 47%. Some selected compounds were analyzed for their dose dependency in a subsequent step that involved each compound to be tested at 1, 10, 30, 50, 70 and 100 μM . The results were able to show the increasing effect at higher concentrations by establishing a new set of parameters. By using the sum of the motion index in each phase the motion index was reduced to three numbers that represent the behavior in each phase. The screen led the ComPlat group at KIT to gain a better understanding of the relevant molecular structures that affect the activity and potency of cannabinoid-like compounds.

Future improvements to the system could be made by either replacing the sample preparation steps with a completely different approach via the so-called Fish-Microarray [149] or by using a higher resolution camera with a different optical setup so that multiple wells at the same time can be imaged without losing detail or risking distortion. A multi-camera system could also be used to eventually make the movable stage obsolete by covering the entire plate in the field of view of the camera array. This would allow a significant reduction of the processing time from 96×30 s to just 1×30 s. Depending on how time critical the assay is and how high the throughput is desired to be this might be worth the additional investment in multiple cameras. Systems using camera arrays have been successfully used for fluorescent microscopy for example [56] and proved to be viable options when throughput is a concern. The bottleneck in applications like this is then usually the host computer as the bandwidth is limited and multiple cameras generate large amounts of data simultaneously. However, with technology advancing at a rapid pace this is not an unrealistic scenario for future developments. Other improvements could be made by using telecentric lenses that remove the optical distortions at the edges that get introduced with a larger field of view. All in all the imaging setup with its optical configuration appears to offer the best opportunity to improve the system even further.

Vibrational Startle Response

In a subsequent step after the PMR a high-throughput vibrational startle response system was developed. A completely new vibrational exciter based on an acoustic speaker allowed to parallelize multiple exciters and made screening multiple petri dishes possible without having to wait for the habituation of the larvae after handling. The system can be used with only one amplifier due to a controllable relays system that only connects one speaker

at a time to the output of the computer's soundcard. Vibrations are generated by supplying a 1 ms 500 Hz pulse and the acceleration can be controlled via the amplitude of this signal. The speakers were extensively characterized and calibrated by measuring the resulting vibrations via accelerometers. A custom-designed petri dish holder was used to hold the larvae, the accelerometer, a uniform LED backlight illumination sheet and a signal LED. The entire holder was built to be lightweight as to not change the characteristics of the oscillations and was verified to result in the desired pulses. A high-speed camera system was developed that allows recordings of more than 1000 fps in order to capture the fast moving larvae. By moving the camera on a motorized linear axis only one camera is required to record every speaker one after the other.

Custom software was developed that combines communication with camera, relays, accelerometers and motor axis and synchronizes them to form coherent vibration experiments. Using a spreadsheet configuration the experiments can be timed and scheduled and allow recordings of the speakers in every imaginable order. The videos are encoded according to h264 to save valuable disk space as the high frame rates would otherwise create unnecessarily large files. By integrating an externally developed tracking algorithm the analysis of the videos was also automated and resulted in numerical parameters representing the activity of the larvae when exposed to the vibrational stimulus.

The system's capabilities were assessed by performing several screens with zebrafish larvae of various age groups. An age dependent analysis was able to confirm the slowly developing neuronal pathways responsible for the larvae to respond to vibration. Only between 96 and 120 hpf the responses start to occur and can be considered robust to be used for screening at later timepoints. It was also shown that the larvae's activity is highly dependent on the strength of the acceleration with increasing g-forces causing an increase in the activity. By testing the waking behavior of 5 dpf old larvae to the anesthetic Propofol a combination of genetic and chemical screen was performed. WT larvae were exposed to NFPS to achieve a phenocopy of the GlyT1 mutant. As expected a slower emergence could be observed with the NFPS treated larvae not waking up nearly as quickly as the WT ones when exposed to Propofol.

Due to the full control over the hard- and software the system can be adjusted to various other configurations which makes it useful for a wide variety of future projects and changing demands. To get an even better understanding of the vibration response for example the used pulse could be extended to either a longer duration or other frequencies. If necessary the system could also be extended to not just record with a single motorized axis but in

a planar setup to fit even more exciters and increase the throughput further, especially considering the low cost of a single exciter. In the future the system will be used to screen for genetically modified strains such as hyperactivity mutants from the ITG that might show interesting phenotypes at such an early stage. In general the system was proven to be a viable option for a new type of high-throughput screening of developing zebrafish. Other use cases could even result in the system being used in research of other behaviors like sleep or completely different species like the blind cavefish whose navigation relies mainly on vibrations [150].

Touch Response

The third step to complete the behavioral analysis pipeline was the development of the first automated system to measure the zebrafish startle response after touch. To do so an entirely new mechanism was introduced that allows computer controlled movement of a thin needle in the wells of a 12-well plate. A 2D orthogonal axes belt-driven system was used to move the needle sideways in one plane. In combination with a custom designed needle holder that is magnetically attached to a linear actuator to adjust the height and move the needle up and down a completely novel mechanism was proposed to touch larvae. Two end switches detect the well bottom and sense when the needle is fully retracted and ready to be moved between wells. A bottom mounted camera records the images from below the well plate and is positioned via its own independent 2D axes system. High frame rates are achieved by relying on a high-speed USB3 camera as it was already used in the vibration system.

Custom software was developed to enable the user to control all motors and the recording while offering an easy-to-use GUI. The interface makes navigating between wells simple and offers a live preview of the well contents in the view of the camera. Two different modes to touch the larva have been implemented: a manual mode that relies on the user interactively defining a path with a series of line segments and an autonomous mode that is based on an object detection pipeline that is capable of differentiating between needle and larva and then finds the optimal path to touch the larva.

Being the first of its kind, the touch system leaves room for a number of improvements that could result in even more precise, more robust and faster touch assays. With the current motorized axes the stepper motors have a noticeable resolution limit in that one step causes the needle to move quite far in the well. By introducing additional transmission in the form of gearing the individual steps could be changed to result in much finer movements. This

could increase accuracy of the positioning as well as the resulting speed. The currently used diagonal movement calculations based on a speed vector analysis could also be changed to a more traditional motor control mechanism as it is used in CNC routers. For this an external step and direction interface would need to be implemented that controls multiple axes at the same time via a PWM signal. Using a single controller for multiple axes could also result in even smoother movements and allow arcs and circular movements as well.

On the software side the autonomous touching is arguably the most promising feature to result in a truly effortless setup that does not require human involvement to perform the experiments. For this the proposed object detection algorithm needs to be evaluated further. The detection could also be improved by for example restricting the search area for the larva to regions outside of the (at this point in the algorithm already detected) needle ROI. Another feature that could be implemented is the ability to detect not just one larva in a well but multiple by ranking and tracking them. Without continuous tracking of each larva it would not be guaranteed that a larva is touched only once. A completely different approach to the object detection might make this even easier. Machine learning algorithms are becoming more accessible each day and with technology like neural networks [151] this could be incorporated into the existing application to replace the classical object detection with a convolutional neuronal network. A traditional template matching could also be an alternative detection method that might be easier to implement with the existing image processing framework.

For a more detailed readout than the binary activity that was used in this work, an external tracking algorithm could be implemented in the form of a video analysis pipeline. First evaluations look promising with the pipeline giving readouts for additional parameters like latency or the travelled distance. However, the algorithm still needs to be evaluated with a larger data set to assess how robust its detection actually performs and how susceptible it is to noise or other artifacts in the images.

Outlook

By combining the three systems into one comprehensive pipeline, researchers can now use these systems to cover most of the spectrum of excitable responses in early zebrafish in an automated and high-throughput manner. They can benefit immensely from the insights the systems potentially offer by learning more about the involved neuronal pathways and the effects chemical compounds can have on living systems. Instead of only looking into morphological changes and toxicity these systems allow the screening for far more subtle

effects by exploring behavioral differences that are either caused by genetic variation, chemical compounds acting on the neuronal pathways or other effects that alter the motility of the larvae like muscular defects. Using the proposed automated and high-throughput imaging solutions paves the way to completely new assays that were not feasible until now. The minimal need for human interaction, the higher speed and most importantly the high accuracy and precision in the stimuli are crucial points that make these systems valuable tools in research topics humans can directly benefit from.

Bibliography

- [1] A. T. Chinwalla, L. L. Cook, K. D. Delehaunty, G. A. Fewell, L. A. Fulton, R. S. Fulton, T. A. Graves, L. W. Hillier, E. R. Mardis, J. D. McPherson et al. “Initial Sequencing and Comparative Analysis of the Mouse Genome”. In: *Nature* 420.6915 (2002), pp. 520–562.
- [2] A. M. Stewart, O. Braubach, J. Spitsbergen, R. Gerlai and A. V. Kalueff. “Zebrafish Models for Translational Neuroscience Research: From Tank to Bedside”. In: *Trends in Neurosciences* 37 (2014), pp. 264–278. ISSN: 1878108X. DOI: 10.1016/j.tins.2014.02.011. Reprinted with permission from Elsevier.
- [3] E. Bier. “Drosophila, the Golden Bug, Emerges as a Tool for Human Genetics”. In: *Nature Reviews Genetics* 6.1 (2005), pp. 9–23.
- [4] L. I. Zon and R. T. Peterson. “In Vivo Drug Discovery in the Zebrafish”. In: *Nature Reviews Drug Discovery* 4.1 (2005), pp. 35–44.
- [5] W. Driever, D. Stemple, A. Schier and L. Solnica-Krezel. “Zebrafish: Genetic Tools for Studying Vertebrate Development.” In: *Trends in Genetics : TIG* 10 (1994), pp. 152–159. ISSN: 0168-9525.
- [6] P. Haffter, M. Granato, M. Brand, M. C. Mullins, M. Hammerschmidt, D. A. Kane, J. Odenthal, F. J. van Eeden, Y. J. Jiang, C. P. Heisenberg, R. N. Kelsh, M. Furutani-Seiki, E. Vogelsang, D. Beuchle, U. Schach, C. Fabian and C. Nüsslein-Volhard. “The Identification of Genes with Unique and Essential Functions in the Development of the Zebrafish, *Danio rerio*.” In: *Development (Cambridge, England)* 123 (1996), pp. 1–36.
- [7] C. B. Kimmel, W. W. Ballard, S. R. Kimmel, B. Ullmann and T. F. Schilling. “Stages of Embryonic Development of the Zebrafish”. In: *Developmental Dynamics* 203.3 (1995), pp. 253–310.
- [8] A. Vogt, H. Codore, B. W. Day, N. A. Hukriede and M. Tsang. “Development of Automated Imaging and Analysis for Zebrafish Chemical Screens.” In: *Journal of Visualized Experiments: JoVE* 40 (2010).

- [9] G. Streisinger, C. Walker, N. Dower, D. Knauber and F. Singer. “Production of Clones of Homozygous Diploid Zebra Fish (*Brachydanio rerio*).” In: *Nature* 291.5813 (1981), p. 293.
- [10] S. Chakrabarti, G. Streisinger, F. Singer and C. Walker. “Frequency of γ -ray Induced Specific Locus and Recessive Lethal Mutations in Mature Germ Cells of the Zebrafish, *Brachydanio rerio*”. In: *Genetics* 103.1 (1983), pp. 109–123.
- [11] G. W. Stuart, J. V. McMurray and M. Westerfield. “Replication, Integration and Stable Germ-line Transmission of Foreign Sequences Injected into Early Zebrafish Embryos”. In: *Development* 103.2 (1988), pp. 403–412.
- [12] Wellcome Trust Sanger Institute, Hinxton UK. *Zebrafish Mutation Project*. URL: <http://www.sanger.ac.uk/science/collaboration/zebrafish-mutation-project> (visited on 08/06/2017).
- [13] Y.-Y. Huang, S. Neuhauss et al. “The optokinetic response in zebrafish and its applications”. In: *Front Biosci* 13 (2008), pp. 1899–1916.
- [14] G. Gestri, B. A. Link and S. C. Neuhauss. “The visual system of zebrafish and its use to model human ocular diseases”. In: *Developmental Neurobiology* 72.3 (2012), pp. 302–327.
- [15] K. D. Poss, L. G. Wilson and M. T. Keating. “Heart Regeneration in Zebrafish”. In: *Science* 298.5601 (2002), pp. 2188–2190.
- [16] M. H. Mokalled, C. Patra, A. L. Dickson, T. Endo, D. Y. Stainier and K. D. Poss. “Injury-induced *Ctgfa* Directs Glial Bridging and Spinal Cord Regeneration in Zebrafish”. In: *Science* 354.6312 (2016), pp. 630–634.
- [17] R. Spence, G. Gerlach, C. Lawrence and C. Smith. “The Behaviour and Ecology of the Zebrafish, *Danio rerio*”. In: *Biological Reviews* 83.1 (2008), pp. 13–34.
- [18] U. Irion, H. G. Frohnhöfer, J. Krauss, T. Ç. Champollion, H.-M. Maischein, S. Geiger-Rudolph, C. Weiler and C. Nüsslein-Volhard. “Gap Junctions Composed of Connexins 41.8 and 39.4 are Essential for Colour Pattern Formation in Zebrafish”. In: *Elife* 3 (2014), e05125.
- [19] P. Antinucci and R. Hindges. “A Crystal-clear Zebrafish for In Vivo Imaging”. In: *Scientific Reports* 6 (2016).
- [20] Dr. Sarah Zala, Vetmeduni Vienna. URL: <https://www.vetmeduni.ac.at>.
- [21] M. Westerfield. “The Zebrafish Book: A Guide for the Laboratory Use of Zebrafish (*Danio rerio*)”. Eugene, USA: University of Oregon Press, 2007.

- [22] B. L. Bohnsack, D. Gallina and A. Kahana. “Phenothiourea Sensitizes Zebrafish Cranial Neural Crest and Extraocular Muscle Development to Changes in Retinoic Acid and IGF Signaling”. In: *PloS One* 6.8 (2011), e22991.
- [23] C. L. Winata, S. Korzh, I. Kondrychyn, W. Zheng, V. Korzh and Z. Gong. “Development of Zebrafish Swimbladder: The Requirement of Hedgehog Signaling in Specification and Organization of the Three Tissue Layers”. In: *Developmental Biology* 331.2 (2009), pp. 222–236.
- [24] S. J. Moorman. “Development of Sensory Systems in Zebrafish (*Danio rerio*)”. In: *ILAR Journal* 42.4 (2001), pp. 292–298.
- [25] H. Lopez-Schier and J. Pujol-Martí. “Developmental and Architectural Principles of the Lateral-line Neural Map”. In: *Frontiers in Neural Circuits* 7 (2013), p. 47.
- [26] J. Bilotta and S. Saszik. “The Zebrafish as a Model Visual System”. In: *International Journal of Developmental Neuroscience* 19.7 (2001), pp. 621–629.
- [27] S. S. Easter Jr and G. N. Nicola. “The Development of Vision in the Zebrafish (*Danio rerio*)”. In: *Developmental Biology* 180.2 (1996), pp. 646–663.
- [28] Charles River Laboratories International, Inc. *Zebrafish: A Powerful Alternative Model for Developmental Toxicity Testing*. URL: <http://www.criver.com/files/pdfs/pcs/tox/zebrafish-developmental-toxicity-testing-technical.aspx> (visited on 14/06/2017).
- [29] A. V. Kalueff, M. Gebhardt, A. M. Stewart, J. M. Cachat, M. Brimmer, J. S. Chawla, C. Craddock, E. J. Kyzar, A. Roth, S. Landsman et al. “Towards a Comprehensive Catalog of Zebrafish Behavior 1.0 And Beyond”. In: *Zebrafish* 10.1 (2013), pp. 70–86.
- [30] U. Strähle, S. Scholz, R. Geisler, P. Greiner, H. Hollert, S. Rastegar, A. Schumacher, I. Selderslaghs, C. Weiss, H. Witters et al. “Zebrafish Embryos as an Alternative to Animal Experiments—a Commentary on the Definition of the Onset of Protected Life Stages in Animal Welfare Regulations”. In: *Reproductive Toxicology* 33.2 (2012), pp. 128–132.
- [31] European Parliament and the Council of the European Union. “Directive 2010/63/EU of the European Parliament and of the Council of 22 September 2010 on the Protection of Animals Used for Scientific Purposes”. In: *Official Journal of the European Union* (2010), pp. 33–79.
- [32] D. Kokel, J. Bryan et al. “Rapid Behavior-based Identification of Neuroactive Small Molecules in the Zebrafish”. In: *Nature Chemical Biology* 6.3 (2010), pp. 231–237.

- [33] D. Kokel, T. W. Dunn, M. B. Ahrens, R. Alshut, C. Y. J. Cheung, L. Saint-Amant, G. Bruni, R. Mateus, T. J. van Ham, T. Shiraki et al. "Identification of Nonvisual Photomotor Response Cells in the Vertebrate Hindbrain". In: *Journal of Neuroscience* 33.9 (2013), pp. 3834–3843.
- [34] O. TG236. "OECD Guidelines for the Testing of Chemicals Section 2: Effects on Biotic Systems Test No 236: Fish Embryo Acute Toxicity (FET) Test". In: *Organization for Economic Cooperation and Development, Paris, France* (2013).
- [35] T. Braunbeck, B. Kais, E. Lammer, J. Otte, K. Schneider, D. Stengel and R. Strecker. "The Fish Embryo Test (FET): Origin, Applications, and Future". In: *Environmental Science and Pollution Research* 22.21 (2015), pp. 16247–16261.
- [36] D. Staudt and D. Stainier. "Uncovering the Molecular and Cellular Mechanisms of Heart Development Using the Zebrafish". In: *Annual Review of Genetics* 46 (2012), pp. 397–418.
- [37] T. Barros, W. Alderton, H. Reynolds, A. Roach and S. Berghmans. "Zebrafish: An Emerging Technology for in Vivo Pharmacological Assessment to Identify Potential Safety Liabilities in Early Drug Discovery". In: *British Journal of Pharmacology* 154.7 (2008), pp. 1400–1413.
- [38] S. Nasrat, D. Marcato, S. Hirth, M. Reischl and C. Pylatiuk. "Semi-automated Detection of Fractional Shortening in Zebrafish Embryo Heart Videos". In: *Current Directions in Biomedical Engineering* 2.1 (2016), pp. 233–236.
- [39] CELLTREAT Scientific Products, Pepperell USA. *Tissue Culture Plates*. URL: <https://www.celltreat.com/> (visited on 20/06/2018).
- [40] A. Smith. "Screening for Drug Discovery: The Leading Question". In: *Nature* 418.6896 (2002), pp. 453–459.
- [41] R. Peravali, J. Gehrig, S. Giselsbrecht, D. S. Lütjohann, Y. Hadzhiev, F. Müller and U. Liebel. "Automated Feature Detection and Imaging for High-resolution Screening of Zebrafish Embryos". In: *BioTechniques* 50 (2011), pp. 319–324.
- [42] W. Spomer, A. Pfriem, R. Alshut, S. Just and C. Pylatiuk. "High-throughput Screening of Zebrafish Embryos Using Automated Heart Detection and Imaging." In: *Journal of Laboratory Automation* 17 (2012), pp. 435–42. ISSN: 2211-0682. DOI: 10.1177/2211068212464223.

- [43] Noldus Information Technology, Wageningen NL. *DanioVision*. URL: <http://www.noldus.com/daniovision/daniovision-observation-chamber> (visited on 08/06/2017).
- [44] Noldus Information Technology, Wageningen NL. *DanioScope*. URL: <http://www.noldus.com/danioscope/more-about-danioscope> (visited on 14/06/2017).
- [45] Noldus Information Technology, Wageningen NL. *DanioVision Without Lid*. URL: <http://www.noldus.com/daniovision/optogenetics> (visited on 14/06/2017).
- [46] Noldus Information Technology, Wageningen NL. *DanioVision Wellplate Holder*. URL: <http://www.noldus.com/daniovision/new> (visited on 14/06/2017).
- [47] Noldus Information Technology, Wageningen NL. *DanioVision Tapping Device*. URL: <http://www.noldus.com/daniovision/tapping-device> (visited on 08/06/2017).
- [48] Noldus Information Technology, Wageningen NL. *DanioVision Temperature Control Unit*. URL: <http://www.noldus.com/daniovision/daniovision-temperature-control-unit> (visited on 14/06/2017).
- [49] ViewPoint, Civrieux FR. *ZebraBox*. URL: <http://www.viewpoint.fr/en/p/equipment/zebrabox> (visited on 14/06/2017).
- [50] ViewPoint, Civrieux FR. *ZebraBox*. URL: <http://www.viewpoint.fr/app.php/en/p/equipment/add-on-fast-camera> (visited on 15/06/2017).
- [51] ViewPoint, Civrieux FR. *ZebraLab*. URL: <http://www.viewpoint.fr/en/p/software/zebralab> (visited on 14/06/2017).
- [52] Phylonix. *Zebrafish Assays for Drug Screening - Services - Safety*. URL: <http://phylonix.com/safety.htm> (visited on 15/06/2017).
- [53] ViewPoint, Civrieux FR. *ZebraBox PMR Module*. URL: <http://www.viewpoint.fr/app.php/en/p/equipment/add-on-photomotor-response> (visited on 14/06/2017).
- [54] ViewPoint, Civrieux FR. *ZebraBox Vibration Module*. URL: <http://www.viewpoint.fr/app.php/en/p/equipment/add-on-vibration-module> (visited on 14/06/2017).
- [55] R. Mikut, T. Dickmeis, W. Driever, P. Geurts, F. Hamprecht, B. X. Kausler, M. J. Ledesma-Carbayo, R. Marée, K. Mikula, P. Pantazis, O. Ronneberger, A. Santos, R. Stotzka, U. Strähle and N. Peyri eras. “Automated Processing of Zebrafish Imaging Data - A Survey”. In: *Zebrafish* 10.3 (2013), pp. 401–421.
- [56] A. Pfriem. “Modulares Laborrobotersystem: zur Durchf hrung biologischer Hochdurchsatzuntersuchungen”. Berlin, Boston: De Gruyter Oldenbourg, 2017.

- [57] D. Marcato, H. Breitwieser, P. Scheickl, R. Peravali, M. Reischl and C. Pylatiuk. “Beispiele für den Einsatz von Automatisierungstechnik bei der Analyse biologischer Modellorganismen”. In: *at-Automatisierungstechnik* 64.11 (2016), pp. 915–925.
- [58] A. Letamendia, C. Quevedo, I. Ibarbia, J. M. Virto, O. Holgado, M. Diez, J. C. I. Belmonte and C. Callol-Massot. “Development and Validation of an Automated High-throughput System for Zebrafish In Vivo Screenings”. In: *PloS One* 7.5 (2012), e36690.
- [59] D. M. Reif, L. Truong, D. Mandrell, S. Marvel, G. Zhang and R. L. Tanguay. “High-throughput Characterization of Chemical-associated Embryonic Behavioral Changes Predicts Teratogenic Outcomes”. In: *Archives of Toxicology* 90.6 (2016), pp. 1459–1470.
- [60] C. Pylatiuk, D. Sanchez, R. Mikut, R. Alshut, M. Reischl, S. Hirth, W. Rottbauer and S. Just. “Automatic Zebrafish Heartbeat Detection and Analysis for Zebrafish Embryos”. In: *Zebrafish* 11.4 (2014), pp. 379–383.
- [61] C. Pantoja, A. Hoagland, E. C. Carroll, V. Karalis, A. Conner and E. Y. Isacoff. “Neuromodulatory Regulation of Behavioral Individuality in Zebrafish”. In: *Neuron* 91.3 (2016), pp. 587–601.
- [62] H. A. Burgess and M. Granato. “Sensorimotor Gating in Larval Zebrafish”. In: *The Journal of Neuroscience* 27.18 (2007), pp. 4984–4994.
- [63] A. Pfriem, C. Pylatiuk, R. Alshut, B. Ziegner, S. Schulz and G. Bretthauer. “A Modular, Low-cost Robot for Zebrafish Handling”. In: *Annual International Conference of the IEEE Engineering in Medicine and Biology Society*. San Diego, USA, Aug. 2012, pp. 980–983. DOI: 10.1109/EMBC.2012.6346097.
- [64] M. Schutera, T. Dickmeis, M. Mione, R. Peravali, D. Marcato, M. Reischl, R. Mikut and C. Pylatiuk. “Automated Phenotype Pattern Recognition of Zebrafish for High-throughput Screening”. In: *Bioengineered* 7.4 (2016), pp. 261–265. DOI: 10.1080/21655979.2016.1197710.
- [65] T. E. Sztal, A. A. Ruparella, C. Williams and R. J. Bryson-Richardson. “Using Touch-evoked Response and Locomotion Assays to Assess Muscle Performance and Function in Zebrafish”. In: *Journal of Visualized Experiments: JoVE* 116 (2016), e54431–e54431.
- [66] R. Alshut. “Konzept für Bildanalysen in Hochdurchsatz-Systemen am Beispiel des Zebrabärblings.” PhD thesis. Karlsruhe Institute of Technology, DE, 2016.

- [67] B. Reed and M. Jennings. “Guidance on the Housing and Care of Zebrafish”. In: *Southwater: Royal Society for the Prevention of Cruelty to Animals* (2011).
- [68] Martin Lober, Karlsruhe Institute of Technology (KIT). *Vielfalt: Aquarien im Ressourcenzentrum*. URL: <https://www.kit.edu/kit/11477.php> (visited on 25/06/2018).
- [69] J. Graw. “Genetik”. Berlin: Springer Spektrum, Sept. 2005. ISBN: 3540240969.
- [70] D. Marcato, R. Alshut, H. Breitwieser, R. Mikut, U. Strähle, C. Pylatiuk and R. Peravali. “An Automated and High-throughput Photomotor Response Platform for Chemical Screens”. In: *37th Annual International Conference of the IEEE Engineering in Medicine and Biology Society (EMBC)*. Milan, IT, Aug. 2015, pp. 7728–7731. DOI: 10.1109/EMBC.2015.7320183.
- [71] R. Creton. “Automated Analysis of Behavior in Zebrafish Larvae”. In: *Behavioural Brain Research* 203.1 (2009), pp. 127–136.
- [72] European Computer Manufacturers Association. *C# Language Specification*. URL: <https://www.ecma-international.org/publications/standards/Ecma-334.htm> (visited on 27/03/2017).
- [73] P. Carbonnelle. *Top IDE Index*. URL: <https://pypl.github.io/IDE.html> (visited on 27/03/2017).
- [74] A. Kirillov. *AForge.NET Framework*. 2011. URL: <http://www.aforgenet.com/>.
- [75] César Souza. *Accord.NET Image Processing and Machine Learning Framework*. URL: <http://accord-framework.net/> (visited on 28/06/2017).
- [76] XIMEA GmbH, Münster DE. *XIMEA Windows Software Package*. URL: https://www.ximea.com/support/wiki/apis/XIMEA_Windows_Software_Package (visited on 28/06/2017).
- [77] Nikon Instruments, Melville USA. *Nikon Instruments .NET SDK for DS-U3*. URL: <http://www.nisd.net/> (visited on 28/06/2017).
- [78] Vasili Maslov. *.NET Library for Creating Video Files in AVI Format*. URL: <https://github.com/baSSiLL/SharpAvi> (visited on 28/06/2017).
- [79] Sebastian Friston. *.NET MemoryStream Replacement*. URL: <https://www.codeproject.com/Articles/348590/A-replacement-for-MemoryStream> (visited on 28/06/2017).
- [80] FFmpeg. *A Cross-platform Solution to Record, Convert and Stream Audio and Video*. URL: <http://ffmpeg.org/> (visited on 28/06/2017).

- [81] NReco components. *FFMpeg C# Wrapper*. URL: https://www.nreco.site.com/video_converter_net.aspx (visited on 28/06/2017).
- [82] Mark Heath. *.NET Audio Library*. URL: <https://github.com/naudio/NAudio> (visited on 28/06/2017).
- [83] R. Mikut, A. Bartschat, W. Doneit, J. Á. G. Ordiano, B. Schott, J. Stegmaier, S. Waczowicz and M. Reischl. “The MATLAB Toolbox SciXMiner: User’s Manual and Programmer’s Guide”. In: *arXiv preprint arXiv:1704.03298* (2017).
- [84] Gus Brown. *Recursive Directory Listing*. URL: <https://de.mathworks.com/matlabcentral/fileexchange/19550-recursive-directory-listing> (visited on 28/06/2017).
- [85] Rob Campbell. *Sigstar*. URL: <https://www.mathworks.com/matlabcentral/fileexchange/39696-raacampbell-sigstar> (visited on 28/06/2017).
- [86] Douglas Schwarz. *Sort_nat: Natural Order Sort*. URL: <https://www.mathworks.com/matlabcentral/fileexchange/10959-sort-nat--natural-order-sort> (visited on 28/06/2017).
- [87] Kasim Tasdemir. *Overwritable Message Outputs to Commandline Window*. URL: <http://www.mathworks.com/matlabcentral/fileexchange/44673-overwritable-message-outputs-to-commandline-window> (visited on 28/06/2017).
- [88] F. Emran, J. Rihel and J. E. Dowling. “A Behavioral Assay to Measure Responsiveness of Zebrafish to Changes in Light Intensities.” In: *Journal of Visualized Experiments: JoVE* (2008). DOI: 10.3791/923.
- [89] PerkinElmer, Waltham USA. *Dimensions of CellCarrier-96 Ultra*. URL: http://www.perkinelmer.de/lab-solutions/resources/docs/TDS_CellCarrier-96_Ultra_17141.pdf (visited on 05/07/2017).
- [90] Prior Scientific, Cambridge UK. *ProScan II Manual*. URL: <http://www.prior-us.com/files/Proscan-II-Operating-Manual.pdf> (visited on 05/07/2017).
- [91] Sutter Instrument, Novato USA. *Lambda SC SmartShutter Manual*. URL: https://www.sutter.com/manuals/LBSC_OpMan.pdf (visited on 05/07/2017).
- [92] Gembird Europe B.V., Almere NL. *Energenie EG-PMS2 Manual*. URL: http://energenie.com/Repository/7415/EG-PMS2_manual---1c4b8cbf-c53a-464e-88c5-e6240bd0fdbb.pdf (visited on 05/07/2017).

- [93] M. Lange, F. Neuzeret, B. Fabreges, C. Froc, S. Bedu, L. Bally-Cuif and W. H. Norton. “Inter-individual and Inter-strain Variations in Zebrafish Locomotor Ontogeny”. In: *PLoS One* 8.8 (2013), e70172.
- [94] O. Aizpurua-Olaizola, I. Elezgarai, I. Rico-Barrio, I. Zarandona, N. Etxebarria and A. Usobiaga. “Targeting the Endocannabinoid System: Future Therapeutic Strategies”. In: *Drug Discovery Today* 22.1 (2017), pp. 105–110.
- [95] M. Begg, P. Pacher, S. Bátikai, D. Osei-Hyiaman, L. Offertáler, F. M. Mo, J. Liu and G. Kunos. “Evidence for Novel Cannabinoid Receptors”. In: *Pharmacology & Therapeutics* 106.2 (2005), pp. 133–145.
- [96] R. Pertwee. “The Diverse CB1 and CB2 Receptor Pharmacology of Three Plant Cannabinoids: Δ 9-Tetrahydrocannabinol, Cannabidiol and Δ 9-Tetrahydrocannabivarin”. In: *British Journal of Pharmacology* 153.2 (2008), pp. 199–215.
- [97] K. Mackie. “Understanding Cannabinoid Psychoactivity with Mouse Genetic Models”. In: *PLoS Biology* 5.10 (2007), e280.
- [98] C. Lam, S. Rastegar and U. Strähle. “Distribution of Cannabinoid Receptor 1 in the CNS of Zebrafish”. In: *Neuroscience* 138.1 (2006), pp. 83–95.
- [99] A. Hariharan. “Analysis and Characterisation of Cannabinoids Using Photomotor Response in *Danio rerio* Embryos”. Bachelor Thesis. Department of Genetic Engineering, School of Bioengineering, SRM University, Kattankulathur, Chennai, 2017.
- [100] W. A. Devane, A. Breuer, T. Sheskin, T. U. Jaerbe, M. S. Eisen and R. Mechoulam. “A Novel Probe for the Cannabinoid Receptor”. In: *Journal of Medicinal Chemistry* 35.11 (1992), pp. 2065–2069.
- [101] M. Koch. “The Neurobiology of Startle”. In: *Progress in Neurobiology* 59.2 (1999), pp. 107–128. ISSN: 0301-0082. DOI: 10.1016/S0301-0082(98)00098-7.
- [102] A. D. McClellan. “Neurobiology of Vertebrate Locomotion: Proceedings of an International Symposium held at The Wenner-Gren Center, Stockholm, June 17th – 19th, 1985”. In: ed. by S. Grillner, P. S. G. Stein, D. G. Stuart, H. Forssberg and R. M. Herman. London: Palgrave Macmillan UK, 1986. Chap. “Command Systems for Initiating Locomotion in Fish and Amphibians: Parallels to Initiation Systems in Mammals”, pp. 3–20. ISBN: 978-1-349-09148-5. DOI: 10.1007/978-1-349-09148-5_1.

- [103] M. Davis, W. A. Falls, S. Campeau and M. Kim. “Fear-potentiated Startle: A Neural and Pharmacological Analysis”. In: *Behavioural Brain Research* 58.1 (1993), pp. 175–198.
- [104] C. A. Sorenson and N. R. Swerdlow. “The Effect of Tail Pinch on the Acoustic Startle Response in Rats”. In: *Brain Research* 247.1 (1982), pp. 105–113.
- [105] R. L. Commissaris, E. A. Fomum and B. J. Leavell. “Effects of Buspirone and Alprazolam Treatment on the Startle-potentiated Startle Response”. In: *Depression and Anxiety* 19.3 (2004), pp. 146–151.
- [106] M. Domjan. “The Principles of Learning and Behavior”. Wadsworth, USA: Cengage Learning, 2014.
- [107] D. L. Filion, M. E. Dawson and A. M. Schell. “The Psychological Significance of Human Startle Eyeblink Modification: A Review”. In: *Biological Psychology* 47.1 (1998), pp. 1–43.
- [108] C. B. Kimmel, J. Patterson and R. O. Kimmel. “The Development and Behavioral Characteristics of the Startle Response in the Zebra Fish”. In: *Developmental Psychobiology* 7.1 (1974), pp. 47–60. ISSN: 1098-2302. DOI: 10.1002/dev.420070109.
- [109] R. W. Friedrich, G. A. Jacobson and P. Zhu. “Circuit Neuroscience in Zebrafish”. In: *Current Biology* 20.8 (2010), R371–R381.
- [110] A. C. Roberts, J. Reichl, M. Y. Song, A. D. Dearing, N. Moridzadeh, E. D. Lu, K. Pearce, J. Esdin and D. L. Glanzman. “Habituation of the C-Start Response in Larval Zebrafish Exhibits Several Distinct Phases and Sensitivity to NMDA Receptor Blockade”. In: *PLoS One* 6.12 (Dec. 2011), pp. 1–10. DOI: 10.1371/journal.pone.0029132.
- [111] R. C. Eaton, R. DiDomenico and J. Nissanov. “Role of the Mauthner Cell in Sensorimotor Integration by the Brain Stem Escape Network”. In: *Brain, Behavior and Evolution* 37.5 (1991), pp. 272–285.
- [112] H. Korn and D. S. Faber. “The Mauthner Cell Half a Century Later: A Neurobiological Model for Decision-making?” In: *Neuron* 47.1 (2005), pp. 13–28.
- [113] S. Budick and D. O’Malley. “Locomotor Repertoire of the Larval Zebrafish: Swimming, Turning and Prey Capture”. In: *Journal of Experimental Biology* 203.17 (2000), pp. 2565–2579. ISSN: 0022-0949. URL: <http://jeb.biologists.org/content/203/17/2565>.

- [114] S. Chanin, C. Fryar, D. Varga, J. Raymond, E. Kyzar, J. Enriquez, S. Bagawandoss, S. Gaikwad, A. Roth, M. Pham et al. “Assessing Startle Responses and Their Habituation in Adult Zebrafish”. In: *Zebrafish Protocols for Neurobehavioral Research* (2012), pp. 287–300.
- [115] D. G. Zeddies and R. R. Fay. “Development of the Acoustically Evoked Behavioral Response in Zebrafish to Pure Tones”. In: *The Journal of Experimental Biology* 208.7 (2005), pp. 1363–1372. DOI: 10.1242/jeb.01534. Republished with permission of The Company of Biologists Ltd; permission conveyed through Copyright Clearance Center, Inc.
- [116] K. C. Marsden and M. Granato. “In Vivo Ca²⁺ Imaging Reveals That Decreased Dendritic Excitability Drives Startle Habituation”. In: *Cell Reports* 13.9 (2015), pp. 1733–1740.
- [117] Brüel & Kjær, Nærum DK. *Mini-Shaker Type 4810*. URL: <https://www.bksv.com/en/products/shakers-and-exciters/measurement-exciters/mini-shaker-type-4810> (visited on 10/07/2017).
- [118] Brüel & Kjær, Nærum DK. *Mini-Shaker Type 4810 Manual*.
- [119] A. A. Bhandiwad, D. G. Zeddies, D. W. Raible, E. W. Rubel and J. A. Sisneros. “Auditory Sensitivity of Larval Zebrafish (*Danio rerio*) Measured Using a Behavioral Prepulse Inhibition Assay”. In: *Journal of Experimental Biology* 216.18 (2013), pp. 3504–3513. ISSN: 0022-0949. DOI: 10.1242/jeb.087635.
- [120] Analog Devices, Norwood USA. *ADXL345 Datasheet*. URL: <http://www.analog.com/media/en/technical-documentation/data-sheets/ADXL345.pdf> (visited on 22/03/2017).
- [121] Conrad Electronic SE, Hirschau DE. *4.4 Inch SpeaKa 40/80 40 W*. URL: <https://www.conrad.de/de/44-zoll-lautsprecher-chassis-speaka-4080-40-w-8-300236.html> (visited on 19/07/2017).
- [122] P. Vieites, C. Wilk, S. Hardy, A. Salvatti, O. Leonhardt and S. Porter. “Audio Speaker Surround Geometry For Improved Pistonic Motion”. Patent US20160080870 (USA). 2016.
- [123] XIMEA GmbH, Münster DE. *Software Performance Optimization*. URL: https://www.ximea.com/support/wiki/usb3/How_to_optimize_software_performance_on_high_frame_rates (visited on 11/09/2017).

- [124] J. Stegmaier, R. Alshut, M. Reischl and R. Mikut. “Information Fusion of Image Analysis, Video Object Tracking, and Data Mining of Biological Images Using the Open Source MATLAB Toolbox Gait-CAD”. In: *Biomedical Engineering/Biomedizinische Technik* 57.SI-1 Track-B (2012), pp. 458–461.
- [125] J. Stegmaier. “New Methods to Improve Large-Scale Microscopy Image Analysis with Prior Knowledge and Uncertainty”. Karlsruhe: KIT Scientific Publishing, 2017.
- [126] V. Ledent. “Postembryonic Development of the Posterior Lateral Line in Zebrafish”. In: *Development* 129.3 (2002), pp. 597–604.
- [127] D. W. Raible and G. J. Kruse. “Organization of the Lateral Line System in Embryonic Zebrafish”. In: *Journal of Comparative Neurology* 421.2 (2000), pp. 189–198.
- [128] V. Bedell, E. Buglo, D. Marcato, C. Pylatiuk, R. Mikut, J. Stegmaier, W. Scudder, M. Wray, S. Züchner, U. Strähle, R. Peravali and J. E. Dallman. “Chapter Ten - Zebrafish: A Pharmacogenetic Model for Anesthesia”. In: *Chemical and Biochemical Approaches for the Study of Anesthetic Function, Part A*. Vol. 602. Methods in Enzymology. Cambridge, USA: Academic Press, 2018, pp. 189–209. DOI: 10.1016/bs.mie.2018.02.004.
- [129] E. Sigel and M. E. Steinmann. “Structure, Function, and Modulation of GABAA Receptors”. In: *Journal of Biological Chemistry* 287.48 (2012), pp. 40224–40231.
- [130] A. Kurolap, A. Armbruster, T. Hershkovitz, K. Hauf, A. Mory, T. Paperna, E. Hannappel, G. Tal, Y. Nijem, E. Sella et al. “Loss of Glycine Transporter 1 Causes a Subtype of Glycine Encephalopathy with Arthrogyriposis and Mildly Elevated Cerebrospinal Fluid Glycine”. In: *The American Journal of Human Genetics* 99.5 (2016), pp. 1172–1180.
- [131] C. Renier, J. H. Faraco, P. Bourgin, T. Motley, P. Bonaventure, F. Rosa and E. Mignot. “Genomic and Functional Conservation of Sedative-hypnotic Targets in the Zebrafish”. In: *Pharmacogenetics and Genomics* 17.4 (2007), pp. 237–253.
- [132] K. R. Aubrey and R. J. Vandenberg. “N [3-(4'-Fluorophenyl)-3-(4'-Phenylphenoxy) Propyl] Sarcosine (NFPS) is a Selective Persistent Inhibitor of Glycine Transport”. In: *British Journal of Pharmacology* 134.7 (2001), pp. 1429–1436.
- [133] J. Rutherford and G. Milward. “Effect of Propofol on Plastic Components”. In: *Anaesthesia* 60.10 (2005), pp. 1046–1046.
- [134] J. W. Sall and J. Leong. “Stability of Propofol in Polystyrene-based Tissue Culture Plates”. In: *Anesthesia and Analgesia* 117.1 (2013), p. 65.

- [135] L. Saint-Amant and P. Drapeau. “Time Course of the Development of Motor Behaviors in the Zebrafish Embryo”. In: *Journal of Neurobiology* 37.4 (1998), pp. 622–632.
- [136] C. B. Kimmel, K. Hatta and W. K. Metcalfe. “Early Axonal Contacts During Development of an Identified Dendrite in the Brain of the Zebrafish”. In: *Neuron* 4.4 (1990), pp. 535–545.
- [137] J. Y. Kuwada, R. R. Bernhardt and N. Nguyen. “Development of Spinal Neurons and Tracts in the Zebrafish Embryo”. In: *Journal of Comparative Neurology* 302.3 (1990), pp. 617–628.
- [138] V. Carmean and A. B. Ribera. “Genetic Analysis of the Touch Response in Zebrafish (*Danio rerio*)”. In: *International Journal of Comparative Psychology/ISCP* 23.1 (2010), p. 91.
- [139] L. L. Smith, A. H. Beggs and V. A. Gupta. “Analysis of Skeletal Muscle Defects in Larval Zebrafish by Birefringence and Touch-evoked Escape Response Assays”. In: *Journal of Visualized Experiments: JoVE* 82 (2013), e50925–e50925.
- [140] M. Granato, F. Van Eeden, U. Schach, T. Trowe, M. Brand, M. Furutani-Seiki, P. Haffter, M. Hammerschmidt, C.-P. Heisenberg, Y.-J. Jiang et al. “Genes Controlling and Mediating Locomotion Behavior of the Zebrafish Embryo and Larva”. In: *Development* 123.1 (1996), pp. 399–413.
- [141] E. Brustein, L. Saint-Amant, R. R. Buss, M. Chong, J. R. McDermid and P. Drapeau. “Steps During the Development of the Zebrafish Locomotor Network”. In: *Journal of Physiology-Paris* 97.1 (2003), pp. 77–86.
- [142] T. Friedrich, A. M. Lambert, M. A. Masino and G. B. Downes. “Mutation of Zebrafish Dihydrolipoamide Branched-chain Transacylase E2 Results in Motor Dysfunction and Models Maple Syrup Urine Disease”. In: *Disease Models and Mechanisms* 5.2 (2012), pp. 248–258.
- [143] C. Bragato, G. Gaudenzi, F. Blasevich, G. Pavesi, L. Maggi, M. Giunta, F. Cotelli and M. Mora. “Zebrafish as a Model to Investigate Dynamin 2-Related Diseases”. In: *Scientific Reports* 6 (2016).
- [144] J. Giacomotto, A. Carroll, S. Rinkwitz, B. Mowry, M. Cairns and T. Becker. “Developmental Suppression of Schizophrenia-associated miR-137 Alters Sensorimotor Function in Zebrafish”. In: *Translational Psychiatry* 6.5 (2016), e818.

- [145] K. Umeda, T. Ishizuka, H. Yawo and W. Shoji. “Position-and quantity-dependent responses in zebrafish turning behavior”. In: *Scientific Reports* 6 (2016), p. 27888.
- [146] S. Hesse. “Grundlagen der Handhabungstechnik”. München: Carl Hanser Verlag GmbH & Co. KG, 2010.
- [147] J. E. Bresenham. “Algorithm for Computer Control of a Digital Plotter”. In: *IBM Systems Journal* 4.1 (1965), pp. 25–30.
- [148] NANOTEC ELECTRONIC GmbH & Co. KG, Feldkirchen DE. *SMCI33 Programming Manual*. URL: https://en.nanotec.com/fileadmin/files/Handbuecher/Programmierung/Programming_Manual_V2.7.pdf (visited on 22/08/2017).
- [149] A. A. Popova, D. Marcato, P. Ravindra, I. Wehl, U. Schepers and P. A. Levkin. “Fish-Microarray: A Miniaturized Platform for Single-Embryo High-Throughput Screenings”. In: *Advanced Functional Materials* 28.3 (2017), p. 1703486. DOI: 10.1002/adfm.201703486.
- [150] M. Yoshizawa. “Behaviors of Cavefish Offer Insight Into Developmental Evolution”. In: *Molecular Reproduction and Development* 82.4 (2015), pp. 268–280.
- [151] J. Redmon and A. Farhadi. “YOLO9000: Better, Faster, Stronger”. In: *2017 IEEE Conference on Computer Vision and Pattern Recognition (CVPR)*. Honolulu, USA, July 2017, pp. 6517–6525. DOI: 10.1109/CVPR.2017.690.

Appendix

A. Arduino DUE Benchmark Code

```
long timestart, timeend; // To store timepoints
int pin = 13;           // pin to be toggled

void setup(){
    Serial.begin(115200);
    pinMode(pin, OUTPUT);
}

void loop(){
    long counter = 1000000; // Number of passes in loop
    timestart = micros();
    for(long i = 0; i < counter; i++){
        digitalWriteDirect(pin, 1);
        digitalWriteDirect(pin, 0);
    }
    timeend = micros();
    Serial.println(timeend-timestart); // Time for direct write
    timestart = micros();
    for(long i = 0; i < counter; i++){
        digitalWrite(pin, 1);
        digitalWrite(pin, 0);
    }
    timeend = micros();
    Serial.println(timeend-timestart); // Time for common digital write
}

static void digitalWriteDirect(int pin, boolean value){
    if(value)
        g_APinDescription[pin].pPort -> PIO_SODR = g_APinDescription[pin].ulPin;
    else
        g_APinDescription[pin].pPort -> PIO_CODR = g_APinDescription[pin].ulPin;
}
```

B. Arduino Nano LED Signalling Code

```

const int AnalogPin = 2; // Pin the audio line is connected to besides GND
int value = 0;           // To store measurement result

void setup() {
  DDRB = B00110101;    // set PORTB (digital 13 to 8) to outputs
  DDRD = B01000000;    // set PORTD (digital 7 to 0) to outputs
  Serial.begin(250000);
}

void loop() {
  value = analogRead(AnalogPin);
  Serial.println(value);
  if(value > 5)        // Empirically established threshold value
  {
    PORTB = B00110101; // Set Pin 13,12,10,8 HIGH
    PORTD = B01000000; // set Pin 6 HIGH
    delay(1000);
    PORTB = B00000000; // Set Pin 13,12,11,10,9,8 LOW
    PORTD = B00000000; // set Pin 7,6,5,4,3,2,1,0 LOW
  }
}

```

C. Camera Recording Loop Code

```

//once initialized run in loop until closed
while (closeCamera==false){
  try{
    //get image from camera as byte array
    myCam.GetImageByteArray(bytelmage, timeout);
    //check if recording is active and not suspended
    //if it is then add image to buffer
    if (Recording == true && SuspendRecording == false){
      RecordingBuffer.Add(bytelmage);
      timestamp = myCam.GetLastImageParams().GetTimestamp();
      RecordingTimestamps.Add(timestamp);
    }
    //check if GUI has used the image from the image buffer
    //if it has then merge bytearray with bitmap header
    //and add to the GUI image buffer
    if (ImageBuffer.Count == 0){
      byte[] merged = new byte[Camera.ImageHeader.Length
        + bytelmage.Length];
    }
  }
}

```

```

    Camera.ImageHeader.CopyTo(merged, 0);
    byteImage.CopyTo(merged, Camera.ImageHeader.Length);
    ImageBuffer.Add(merged);
}
//once recording has stopped save frames to video
if (Recording == false && RecordingBuffer.Count > 0 &&
    Saving == false && SuspendRecording == false){
    Saving = true;

    //move to separate task to not block GUI preview
    Task.Run(() => {
        //create SharpAvi aviwriter
        var aviwriter = new AviWriter(Filepath){
            FramesPerSecond = myCam.GetParamInt(PRM.FRAMERATE),
            EmitIndex1 = true
        };
        var videostream = aviwriter.AddVideoStream();
        videostream.Width = myCam.GetParamInt(PRM.WIDTH);
        videostream.Height = myCam.GetParamInt(PRM.HEIGHT);
        videostream.Codec = KnownFourCCs.Codecs.Uncompressed;

        //Uncompressed format requires to specify bits per pixel
        //set value depending on mode the camera is in
        int videocolor = myCam.GetParamInt(PRM.IMAGE_IS_COLOR);
        int videoformat = myCam.GetParamInt(PRM.IMAGE_DATA_FORMAT);
        if (videocolor == 1 & videoformat == 3)
            videostream.BitsPerPixel = BitsPerPixel.Bpp32;
        else if (videocolor == 1 & videoformat == 2)
            videostream.BitsPerPixel = BitsPerPixel.Bpp24;
        else
            videostream.BitsPerPixel = BitsPerPixel.Bpp8;

        //pass each frame one after the other to the aviwriter
        while(RecordingBuffer.Count != 0){
            videostream.WriteFrame(true,
                RecordingBuffer.Take(), //array with frame data
                0, //starting index in the array
                image.Length //length of the data
            );
        }

        //save timestamps in log file to find lost frames
        //convert double to string

```

```
        File.WriteAllLines(Filepath + "_log.txt",
        RecordingTimestamps.Select(d => d.ToString()));
        //reset values
        aviwriter.Close();
        RecordingTimestamps.Clear();
        Framecounter = 0;
        Saving = false;
    });
}
}
catch(Exception ex){//handle errors}
}
```